UNCLASSIFIED

AD 285 037

Reproduced
by the

ARMED SERVICES TECHNICAL INFORMATION AGENCY
ARLINGTON HALL STATION
ARLINGTON 12, VIRGINIA

UNCLASSIFIED

NOTICE: When government or other drawings, specifications or other data are used for any purpose other than in connection with a definitely related government procurement operation, the U. S. Government thereby incurs no responsibility, nor any obligation whatsoever; and the fact that the Government may have formulated, furnished, or in any way supplied the said drawings, specifications, or other data is not to be regarded by implication or otherwise as in any manner licensing the holder or any other person or corporation, or conveying any rights or permission to manufacture, use or sell any patented invention that may in any way be related thereto.

63-1-1

285037

CATALOGED BY ASTIA
AS AD NO.

U. S. ARMY
TRANSPORTATION RESEARCH COMMAND
FORT EUSTIS, VIRGINIA

TCREC Technical Report 62-21

RESULTS OF STATIC TESTS OF A FULL SCALE, WING MOUNTED, TIP TURBINE DRIVEN LIFT FAN

(December 1960 - April 1961)

Task 9R38-01-020-02

Contract DA 44-177-TC-584

March 1962

prepared by :

GENERAL ELECTRIC COMPANY
Flight Propulsion Laboratory Department
Cincinnati 15, Ohio

ASTIA
RELEASED
OCT 5 1962
TISIA

HEADQUARTERS
U. S. ARMY TRANSPORTATION RESEARCH COMMAND
Fort Eustis, Virginia

FOREWORD

The test data reported herein is the result of more than 50 hours of lift-fan operation in a wing-type inlet static environment. Satisfactory solutions were accomplished for performance losses due to facility interference and inlet separation.

FOR THE COMMANDER:

L. A. FLORO, JR.
Captain, TC
Actg Deputy Commander for
Plans and Programs

APPROVED BY:

JOHN W. WHITE
USATRECOM Project Engineer

Task 9R38-01-020-02

Contract DA 44-177-TC-584

October 1961

RESULTS OF STATIC TESTS OF A FULL SCALE, WING MOUNTED, TIP TURBINE DRIVEN LIFT FAN

Testing Period

December 1960 - April 1961

Prepared By:

GENERAL ELECTRIC COMPANY

Flight Propulsion Laboratory Department

Cincinnati 15, Ohio

for

U. S. ARMY TRANSPORTATION RESEARCH COMMAND

FORT EUSTIS, VIRGINIA

TABLE OF CONTENTS

		PAGE
	LIST OF ILLUSTRATIONS	viii
	LIST OF TABLES	xvii
I.	SUMMARY	1
	Aerodynamic	2
	Mechanical	3
	Environmental	4
II.	TEST VEHICLE DESCRIPTION	5
	Specific Fan Assembly	5
	Forward Frame	5
	Rotor	5
	Aft Frame	5
	Scroll	5
	Exit Louvers	6
	Balance	6
	J85-7 Engine	6
	Diverter Valve	6
	Test Configuration	7
III.	TEST FACILITIES, INSTRUMENTATION AND EQUIPMENT	9
	Test Facility	9
	Facility Modification	9
	Pitch Maneuver Equipment	11
	Diverter Valve Modification	12
	Instrumentation	12
IV.	TEST PROCEDURE AND RESULTS	17
	Test Objectives and Limits	17
	Summary of Test Runs	18
	Test Results	24
	Measurement Accuracies	24
V.	ANALYSIS OF RESULTS	27
	A. General Considerations	27
	J85-7 Engine Performance	27
	EGT Calibration Run	29
	Horsepower Calculation	29
	Ram Drag	30
	Turning Angle	31

PAGE

B. Fan Aerodynamic Performance 32
Fan Internal Performance Development 32
Inlet Flow Angles 38
Fan Efficiency and Power Consumption 39
Fan Efficiency Measurement Accuracy 41
Throttle Characteristics 43
Turbine Efficiency 43

C. Fan System Performance 47
Throttle Characteristics 50
Staggered Louver Performance 51
Fan Transient Aerodynamic Performance 53
Acceleration 53
Deceleration 54
J85 Overspeed 54
Divided Flow Performance 55

D. Fan Mechanical Performance 58
Rotor Blade Stresses 59
Cosine 2θ Mode 59
First Flexural Mode 59
Torsional Mode 60
Torque Band 60
Rotor Stress Response to J85 Throttle - Transients 62
Diverter Valve Transients 64
Pitch Maneuver Loading 65
Stress 65
Deflection 68
Stator Vane Stress 68
Stationary Parts 71
Frames 71
Inlet Baffle 71
Circular Inlet Vane 73
Hardware Temperatures 73
Temperature Cycling 74

E. Environmental Factors 75
Sound Levels 75
Wind Velocity 81

VI. HARDWARE INSPECTION RESULTS 87

Forward Frame and Scroll 87
Rear Frame 88
Rotor 89
Diverter Valve 90
Frame Deflection Test 90

	PAGE
VII. RECOMMENDATIONS	91
VIII. REFERENCES	93
APPENDIX A	95
Table A-1	95
Table A-2	96
Table A-3	97
Table A-4	114
Table A-5	115
APPENDIX B	117
Sample J85 Weight Flow Calculation	117
Reading 108	117
Derivation of Diverter Valve and Scroll Loss Curves and Analysis of Diverter Valve Bleed and Lift Fan Horsepower	119
Fan Weight Flow	124
Table B-1	125
Figures B-1 through B-10	126 - 135
APPENDIX C	137
Figures 1 through 107	137 - 249

LIST OF ILLUSTRATIONS

FIGURE		PAGE
B-1	J85 Inlet Weight Flow versus Bellmouth Static Pressure Difference	126
B-2	J85 Compressor Bleed versus J85 Speed	127
B-3	Full Scale Diverter Valve Losses as a Function of Turbine Discharge Mach Number	128
B-4	Ducting Losses versus Turbine Discharge Mach Number	129
B-5	Turbine Ducting Total Pressure Ratio (Diffuser + Diverter Valve + Scroll, S/N 002) versus Scroll, S/N 002, Flow Function	130
B-6	Turbine Ducting Pressure Loss (Diffuser + Diverter Valve + Scroll, S/N 002)	131
B-7	X353-5 Full Scale Scroll, S/N 002, Flow Function	132
B-8	Ideal Gas Horsepower Function versus Total to Ambient Pressure Ratio	133
B-9	Fan-in-Wing Inlet Weight Flow Calibration Curve (Exit Measuring Duct)	134
B-10	Fan-in-Wing Inlet Weight Flow versus Bulletnose Ambient to Static Pressure Difference	135

LIST OF ILLUSTRATIONS

FIGURE		PAGE
1	View of Fan Installed in Wing Showing Exit Louver Actuation Details	137
2	Differential Exit Louver Actuation - Mechanical Actuation Angle Limits	138
3	Views of Complete Test Vehicle, After Test	139
4	360° Inlet Vane - Outline	140
5	Fan Assembly Showing Inlet Baffle Welded to Forward Frame	141
6	Fan Installation in the Test Facility	142
7	Wing Dimensional Details	143
8	Views of Fan Installation After Removing Facility Walls	144
9	Actuator and Trunnion Support for Pitching Maneuvers	145
10a	Wing at +15° Angle of Attack (Before Pitch Maneuver)	146
10b	Wing at -15° Angle of Attack (After Pitch Maneuver)	146
11	Diverter Valve Actuation Set Up for Split Flow Testing	147
12	Schematic of Instrumentation Planes	148
13	Inlet Total Pressure Rakes Modified for Radial Static Pressure Measurement	149
14	Fan Discharge Sound Traverse Probe and Actuator	150
15a	Diverter Valve Inlet Weight Flow and Fan Turbine Inlet Weight Flow versus J85-7 Speed (Diverter Valve Set for 3.2% Bleed)	151

FIGURE		PAGE
15b	Weight Flow at Diverter Valve Inlet (Station 5.15) and Fan Turbine Nozzle Inlet (Station 5.4) versus J85-7 Speed (Diverter Valve Fully Closed)	152
16a	Exhaust Gas Temperature versus J85-7 Speed (Diverted Flow)	153
16b	Exhaust Gas Temperature versus J85-7 Speed (Straight Through Flow)	154
17	Fan Speed versus J85-7 Speed (Diverter Valve Positioned for Approximately 3.2% Bleed)	155
18	J85-7 Circumferential EGT Profile and Diverter Valve Skin Temperature	156
19	Total to Ambient Pressure Ratio at Diverter Valve Inlet (Station 5.15) and Fan Turbine Nozzle Inlet (Station 5.4) versus J85-7 Speed	157
20a	Horsepower at Diverter Valve Inlet (Station 5.15) and Fan Turbine Nozzle Inlet (Station 5.4) versus J85-7 Speed	158
20b	Power Loss Relative to Diverter Valve Inlet (Station 5.15) versus J85-7 Speed	159
21	Fan Speed and Diverter Valve Inlet (Station 5.15) Flow Characteristics versus J85-7 Speed	160
22	J85-7 Thrust versus Speed	161
23	J85-7 EGT Profile	162
24	Plane 5.15 EGT Calibration Curve	163
25	Fan Speed versus Available Horsepower	164
26	Thrust Correction for Ram Drag Due to Wind	165
27	Actual Turning Angle versus Indicated Louver Angle	166
28a	Summary of Fan Pressure Coefficients	167
28b	Summary of Fan Pressure Coefficients	168

FIGURE		PAGE
29	Bellmouth Lampblack Test Results (No Baffle)	169
30	Bellmouth Lampblack Test Results (360° Baffle Installed)	170
31	Fan-in-Wing Inlet Flow Diagram	171
32	Internal Performance (Facility and Baffle Effects)	172
33	Effect of Wind on Fan Internal Performance (Inlet Vane Plus 180° Baffle)	173
34	Effect of Wind on Fan Internal Performance (Inlet Vane Only)	174
35	Fan-in-Fuselage (X353-5-002) Rotor Inlet Air Angles versus Radius Ratio at Various Throttle Positions	175
36	Fan-in-Wing Rotor Inlet Air Angles versus Radius Ratio at Various Throttle Positions	176
37	Fan-in-Wing (X353-5-002) Rotor Inlet Air Angles versus Radius Ratio as a Function of Circumferential Location	177
38	Comparison of Scale Model and Full Scale Rotor Inlet Air Angles (Fan-in-Wing)	178
39	Fan-in-Wing Throttle Characteristic	179
40	Fan-in-Wing (X353-5-002) Rotor Discharge Pressure Coefficient versus Louver Angle at Various Immersions	180
41	Fan-in-Wing Rotor Discharge Pressure Coefficients at $\beta = 30^{\circ}$ and $\beta = 35^{\circ}$	181
42	Fan Total Thrust Extrapolated to 100% Speed versus Fan Speed	182
43	Total Fan Thrust versus Fan Speed (Fan-in-Wing with Circular Inlet Vane and Exit Louvers)	183
44	Isentropic Horsepower Available at Fan Turbine Nozzle Inlet versus Fan Speed (Fan-in-Wing with Circular Inlet Vane and Exit Louvers)	184

FIGURE		PAGE
45	Total Fan Thrust versus Isentropic Horsepower Available at Fan Turbine Nozzle Inlet (Fan-in-Wing with Circular Inlet Vane and Exit Louvers)	185
46	Total Fan Thrust versus Fan Speed (Fan-in-Wing with Circular Inlet Vane and Exit Louvers)	186
47	Total Thrust Ratio versus Indicated Louver Angle	187
48	Total Thrust Ratio versus Actual Turning Angle	188
49	Vertical Thrust to Total Thrust Ratio versus Louver Angle (Constant Fan Speed)	189
50	Vertical Thrust to Total Thrust Ratio versus Louver Angle (Constant Fan Horsepower)	190
51	Horizontal Thrust to Total Thrust Ratio versus Louver Angle (Constant Fan Speed)	191
52	Horizontal Thrust to Total Thrust Ratio versus Louver Angle (Constant Fan Horsepower)	192
53	Vertical Lift versus Horizontal Thrust at Constant Fan Horsepower and Speed (Fan-in-Wing)	193
54	Schematic - Dual Actuated Staggered Louvers	194
55	Vertical and Horizontal to Total Thrust Ratio versus Indicated Average Exit Louver Angle as a Function of Stagger Angle (Fan-in-Wing with Baffle and No Inlet Vane)	195
56	Total to Total Thrust Ratio versus Indicated Average Exit Louver Angle as a Function of Stagger Angle (Fan-in-Wing with Baffle and No Inlet Vane)	196
57	Vertical and Horizontal to Total Thrust Ratio versus Indicated Average Exit Louver Angle as a Function of Stagger Angle (Fan-in-Wing with Inlet Vane and No Baffle)	197
58	Total to Total Thrust Ratio versus Indicated Average Exit Louver Angle as a Function of Stagger Angle (Fan-in-Wing with Inlet Vane and No Baffle)	198

FIGURE		PAGE
59	Actual and Estimated Transient Performance, J85 Acceleration	199
60	Actual and Estimated Transient Performance, Diverter Valve Switch from Cruise Mode to Lift Mode	200
61	Actual and Estimated Transient Performance, Diverter Valve Switch from Lift to Cruise Mode	201
62	Actual and Estimated Transient Performance, Throttle Chop	202
63	J85 Overspeed	203
64	Comparison - Test Results with Divided Flow Study	204
65	Torque Band Temperatures - Divided Flow Test	205
66	Schematic of Diverter Valve Positioned for Divided Flow	206
67	Torque Band Stress as a Function of Fan Speed (Slow Transients)	207
68	Torque Band Stress as a Function of Diverter Valve Actuation Rate	208
69	Blade Stress as a Function of J85 Throttle Transients	209
70	Maximum Forward Torque Band Tang Stress as a Function of J85 Throttle Transients	210
71	Time to Maximum Blade Stress versus Fan Acceleration and Deceleration Time	211
72	Time to Maximum Stress versus Maximum Blade Stress	212
73	Time to Maximum Blade Stress versus Speed at Maximum Blade Stress (Throttle Transients)	213
74	Maximum Rotor Acceleration as a Function of Slew Rate and Fan Terminal Speed (J85 Power Setting)	214

FIGURE		PAGE
75	Maximum Rotor Acceleration versus Fan Terminal Speed for Various Slew Rates (Derived from Test Data)	215
76	Fan Speed and Rotor Acceleration versus Time as a Function of Diverter Valve Actuation Rate (1700 rpm Fan Terminal Speed)	216
77	Fan Speed and Rotor Acceleration versus Time as a Function of Diverter Valve Actuation Rate (1910 rpm Fan Terminal Speed)	217
78	Fan Speed and Rotor Acceleration versus Time as a Function of Diverter Valve Actuation Rate (2270 Fan Terminal Speed)	218
79	Fan Speed and Rotor Acceleration versus Time as a Function of Diverter Valve Actuation Rate (2450 Fan Terminal Speed)	219
80	Typical Pitch Maneuver Transients	220
81	Predicted and Measured Blade Stress as a Function of Speed and Precession Rate	221
82	Blade Stress Due to Gyro Loading Only and Also Total Blade Stress Due to Combined Loads as a Function of Precession Rate	222
83	Effect of Pitch Maneuver Loading on Blade Stress (at Critical Rotor Speed)	223
84	Change in Axial Clearance (Rotor to Front Frame) During Pitch Maneuvers (3 o'clock Position)	224
85	Rear Frame Stator Stress as a Function of J85 Throttle Transients	225
86	Forward Torque Band Temperature as a Function of Fan Speed and Inlet Configuration	226
87	Hardware Temperature as a Function of Fan Speed	227
88	Hardware Temperature as a Function of Engine Exhaust Gas Temperature	228
89	Static Hardware Temperature as a Function of Exhaust Gas Temperature	229

FIGURE		PAGE
90	X353-5 Sound Pressure Level Measurement (J85-7 Gas Generator)	230
91	Vertical Lift as a Function of Fan Speed and Wind Velocity	231
92	Vertical Lift as a Function of Fan Speed and Wind Velocity (without Exit Louvers)	232
93	Vertical Lift as a Function of Exit Louver Angle and Wind Velocity	233
94a	Lines of Constant Suction on the Under Surface of the Wing (V_p = 0 mph)	234
94b	Lines of Constant Suction on the Under Surface of the Wing (V_p = 5 mph)	235
94c	Lines of Constant Suction on the Under Surface of the Wing (V_p = 15 mph)	236
95	Pressure Distribution on the Fuselage Upper Surface from Full Scale Fan-in-Fuselage Testing at Ames	237
96	Variation of Load Cell Readings and Center of Lift with Forward Speed	238
97	Comparison of Load Cell Data with Predicted Results	239
98	Fan-in-Wing Flow Patterns at Idle Fan Speed	240
99	Lift Loss at Low Flight Speed	241
100a	Radial Rub at 12:00 o'clock Position - Forward Frame Air Seal	242
100b	Axial Rub at 3:00 o'clock Position - Forward Frame Air Seal	242
101	Insulation Blanket Rubs	243
102	Rear Frame Saw Cut Separation	244
103	Exit Louver After Tip Rub	245
104	Torque Band Crack	246

FIGURE		PAGE
105	Carrier Side Rail Cracks - 8X Magnification	247
106	Missing Carrier Shroud	248
107	Frame Deflection as a Function of Rim Axial Load	249

LIST OF TABLES

TABLE	TITLE	PAGE
I	Instrumentation Summary	15
II	Installed Aerodynamic Instrumentation Breakdown by Instrument Planes	16
III	Fan Stress Limits	19
IV	Summary of Test Runs	20
V	Detailed Listing of Test Configurations	21
VI	Running Time and Data Points - 50 Hour Static Fan-in-Wing Test	22
VII	Summary of Lift Fan Operating Time	23
VIII	Effect of Wind on Thrust (Evendale Facility)	31
IX	Thrust at 100% Speed and Design Horsepower for Fan-in-Fuselage and Various Fan-in-Wing Configurations	33
X	Comparison of Internal Characteristics of Fan-in-Fuselage (X353-5-001) and Fan-in-Wing (X353-5-002)	40
XI	Fan-in-Wing Thrust Coefficients	44
XII	X353-5 Turbine Efficiencies	45
XIII	Comparison of Design Objectives and Test Results	49
XIV	Comparison of Fan-in-Wing and Fan-in-Fuselage Thrust Coefficients	52
XV	Stator Vane Stresses at 2250 rpm (Inlet Vane Plus 180° Baffle Installed)	70
XVI	Stator Vane Stresses (Inlet Vane, No Baffle)	72
XVII	Comparison of Near and Far Field Sound Level Measurements	77
XVIII	Fan Sound Power Levels Due to Blade Passing Frequency (Traverse)	78
XIX	Speed Measurement Comparison	80

TABLE	TITLE	PAGE
A-1	Fan Performance Calculation Standards	95
A-2	Definitions and Symbols	96
A-3	Test Results (50 Hour Fan-in-Wing Test - Evendale)	97
A-4	Summary of Test Transients	114
A-5	Narrow Band Analysis of Fan Exit Sound Pressure Level Traverse (Fan Speed 2565 rpm)	115
B-1	Turbine Ducting Pressure Loss Curve Calculations	125

I. SUMMARY

Contract DA 44-177-TC-584 with the Army requires that, in addition to bimonthly technical progress reports, comprehensive reports of major phases be prepared and submitted to the contracting officer. Previous reports submitted under this requirement are:

X353-5 Fan Design Report, May 1960.

TREC 60-42 Phase I Test Results[a]: Static Tests, Fuselage Mounted X353-5, August 1960.

TREC 61-15 Phase II Test Results[b] (Partial): Wind Tunnel Tests, Fuselage Mounted X353-5, 3 Volumes, April and October 1961

This is the required report for another major portion of Phase II Contract work based on results of static tests of 53 hours duration conducted on the X353-5 mounted in a 10% thick wing. All testing was performed at the contractor's plant at Evendale, Ohio. The report includes:

- Descriptions of the test vehicle, facility, instrumentation and equipment (Sections II and III).
- Test procedures and results (Section IV).
- Analysis of test results, conclusions and discussion of any problems encountered (Section V).
- Hardware inspection results (Section VI).
- Program recommendations (Section VII).

---

[a] Reference 1

[b] Reference 2, 3, and 6

The basic test data for every test point are tabulated in Appendix A. A few items of summary follow:

Fan operating time	52 hours, 51 minutes
Data points recorded	554
Range of variables tested:	
Fan speed	0 to 2640 rpm (100%)
Exit louver angle:	
Vector ($\beta_1 = \beta_2$)	-15° to +44°
Stagger ($\beta_s = \beta_2 - \beta_1$)	0° to 30° stagger angle
J85 engine speed	0 to 16,840 rpm (102%)
Diverter Valve temperature	Maximum of 1400°F
Diverter Valve slew rate	1 to 13 seconds
Pitch maneuver:	
Angle of attack	-15° to +15°
Angular velocity	0.37 and 0.52 rad/sec.
Divided flow (fan/J85)	0/100, 25/75, 50/50, 75/25, 100/0 - nominal settings
Throttle transients	1, 5, 10 and 60 seconds
Wind velocity	0 to 17 miles per hour

Analyses of the results are presented in considerable depth defining fan hover performance out of ground effect and variations with low wind velocities, comparing performance of various exit and inlet configurations including a repeat of the fuselage inlet tested during Phase I work, interpreting transient performance resulting from throttle changes, diverter valve actuations and pitch maneuvers and identifying the fan noise characteristics. A few items of performance conclusions are listed below:

Aerodynamic

- A 360° circular inlet vane is required to prevent bellmouth separation.
- At 100% fan speed the measured lift was 7050 pounds; the maximum horizontal thrust was 3842 pounds (β = 37.5°).

- The lift augmentation ratio was 2.88 based on J85-7 bulletin performance of 2450 pounds thrust.
- Nominal recirculation effects were: J85 inlet 1° to 3°F and fan inlet 1° to 4°F.
- Roll-yaw control capability can be provided by staggering the exit louvers; at 100% fan speed thrust control of 6610 ± 440 pounds is obtainable.
- Gradual conversion from the lift mode to cruise mode can be accomplished using separately actuated diverter valve doors.
- Fan acceleration response was better than predicted primarily because of better than guarantee J85 acceleration performance.
- Fan efficiency was about 1% better than for the fuselage mounted configuration and turbine efficiency was essentially unchanged in spite of variations in clearance and the absence of the turbine tip shroud seal for this testing.

Mechanical

- The wing inlet has changed only the cosine 2θ resonance mode stress in the rotor which ranged from 130% to 180% of the fan-in-fuselage level depending on acceleration rate through the critical speed.
- Combined blade loadings including maneuver loads require increased dovetail strength to meet design flight specifications.
- Rotor stresses were highest during decelerations.
- The best transients from a rotor and stator stress standpoint were the fastest.
- Four torque band tangential cracks were found after 53 hours of testing. This was an expected result based on previous experience with this particular design which is being replaced.
- Hardware inspection after disassembly showed no other significant deficiency and the hardware was generally in excellent condition.

Environmental

- At 200 feet distance the fan noise level was 99 db.
- There was a variation in fan thrust and power absorption with low wind velocity; at constant power the thrust was reduced 1.5% to 2.5% by wind velocities of up to 15 m.p.h.

II. TEST VEHICLE DESCRIPTION

The contractor-owned X353-5 fan, serial number 002, was used for all testing discussed in this report. The fabrication and assembly of the X353-5 are detailed in reference 1 (pages 3 through 52).

SPECIFIC FAN ASSEMBLY DETAILS

Forward Frame:

Cold clearance of the air seal in this frame was set at 0.091 inches which reduces to zero at 100% speed (calculated). This is an approximately 0.050 inches closer clearance setting than for previous X353-5 testing (reference 2 and 3) and about 0.100 inches closer than for initial X353-5 testing (reference 1).

Rotor:

Assembly incorporated a torque-band identical with that used for tests described in reference 3 which shows a history of crack incidence.[a] Periodic monitoring of this part between test runs via dye penetrant inspections was incorporated in the test plan.

Aft Frame:

Turbine tip shroud seals were not installed. The rear air seal clearance was 0.160 inches which is the same as used in Fan 001 (references 2 and 3).

Scroll:

The scroll (S/N 002) was the only component which had been in prior service; it was used in buildups 2 and 2A of Fan 001 (references 1 and 2) for 19 hours, 56 minutes of testing.

---

[a] Assembly was completed prior to completing reference 3 tests indicating this torque-band cracking.

Exit Louvers:

The louvers were installed as two separately actuated sets. The β_1 set consisted of every other louver (seven total), beginning with the forward louver, and was operated by an external push rod. Yokes bridging the aft frame major strut connected the louvers with the push rod and permitted louver closure to 50°; however, two total pressure rakes installed on the rear frame limited louver closure to 44°. The other seven louvers (β_2) were actuated by an internal push rod in the major strut as provided in the original design.

This arrangement (see Figure 1)[a] incorporated louver staggering capability and is a test arrangement only. The physical limits of actuation are as shown in Figure 2.

BALANCE

Rotor component parts were selectively located based on moment weights. Static balance of the assembled rotor by adding weight to prevent rotation in "frictionless" mounts required 88.5 grams at 11.5 inches radius (retainer ring bolt circle). This balance was checked in a dynamic balancing machine and no changes were required.

J85-7 ENGINE

The fan was powered by J85-7 engines during the entire test program. Engine serial number 235-003 was used for the initial four runs. Runs 5 through 26 were conducted using engine S/N 235-004.[b]

DIVERTER VALVE

A diverter valve was used to duct the J85 gas to the fan and was obtained from the Air Force (contract AF 33(600)-40862). This valve S/N 001 was tested previously under this Air Force contract for 31 hours and was completely disassembled, inspected and reassembled for this program.

---

[a] All figures are presented in Appendix C.

[b] Engine change was to balance accumulated operating time so that both could be scheduled for periodic inspection at the same time.

TEST CONFIGURATION

Views taken of the complete test vehicle after testing was concluded are shown in Figure 3. The circular inlet vane pictured was not installed until Run 19. This is an item of nonflight hardware of solid stainless steel weighing 101 pounds. The 360° vane, see Figure 4, has a constant airfoil section with a 5 inch chord and is crowned to match a NASA 65-210 series wing upper surface contour (fan centerline located at 40% chord). It is 58 inches in diameter and was installed in three segments. Each segment attached to the fan front frame struts at the vane ends and additional support was made to the bellmouth opposite the minor strut.

During Runs 5 through 22, various extents (from 360° to 180°) of forward air seal baffling were employed to guide turbine-to-fan gas leakage. A view of this type of baffle is shown in Figure 5; it was welded to the bellmouth skin and overlapped the air seal. There was, however, adequate clearance retained between the rotor leading edge and the end of the baffle as indicated by the sketch below:

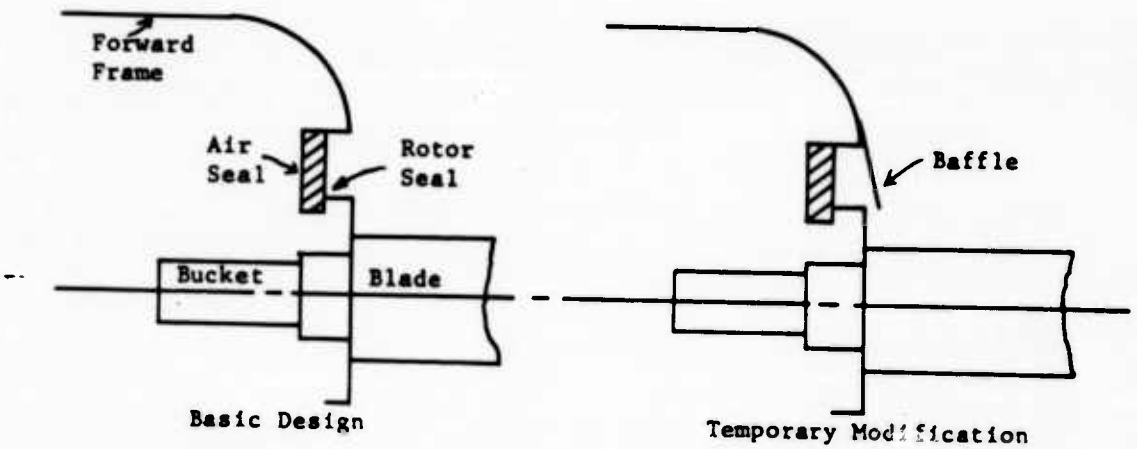

The baffle was a temporary modification and was not retained in the final configuration. The per cent annulus area blockages for the different lengths of baffle were:

Baffle Length (deg.)	Annulus Area Blockage (Per cent)
360	3.78
280	2.94
230	2.41
180	1.89

III. TEST FACILITIES, INSTURMENTATION AND EQUIPMENT

TEST FACILITY

A description of the Evendale facility used for this testing is contained in reference 1 (pages 59 through 68).

All but two of the twenty-six runs were conducted as a fan-in-wing installation so the thrust frame was modified to include a wing leading edge, trailing edge and tip. A wall was installed at the wing root to simulate a fuselage for this semi-span test arrangement. The wing structure was contoured to a NASA series 65-210 airfoil shape.[a] Wing skins were not installed on the underside.

Figure 6 shows the installation. The wing is untapered with a chord of 144 inches and aspect ratio of 2.32. The fan centerline is located at the 40% chord line and is one fan diameter from the wall simulating the fuselage; the fan is mounted between the wing spars and occupies 50% of the wing chord between 15% and 65% chord. Figure 7 shows these dimensional details.

The fuselage inlet duct used during test Runs 11 and 12 and the exit throttling system used in test Runs 11, 13, and 14 are described in reference 1. The exit measuring section was used without the throttle plate in Runs 12 and 25.

FACILITY MODIFICATION

The surrounding personnel protection wall of the facility is ten sided; two of the sides are hinged doors which were opened and closed during test as an additional variable when it was suspected that the fan was pumping considerable quantities of secondary air through the facility

[a] Modified slightly on the underside to mate with the lift fan.

annulus. This was done for both the fan-in-wing and fan-in-fuselage configurations. The following differences in thrust were measured:

Fan-in-wing	2% increase in thrust with doors open
Fan-in-fuselage	3 1/2% to 4% increase in thrust with doors open

At the same time, 35 static pressure elements were monitored on the underside of the wing (these are indicated in Figure 7). By extrapolating these pressure data to apply to the entire wing area, the forces implied were as below:

Fan-in-wing	Implied down force on wing due to static pressure distribution
Doors closed	6% in thrust
Doors open	5%
	Δ = 1% vs. 2% measured
Fan-in-fuselage	
Doors closed	6% in thrust
Doors open	1%
	Δ = 5% vs. 3 1/2% to 4% measured

Based on this analysis and other velocity data taken near the wing, it was felt necessary to remove as many of the remaining facility walls as possible to break up the apparent pumping action of the fan-in-wing installation since just opening the doors was not effective. The modified facility is shown in Figure 8. As will be shown in the section on Analysis of Results, this resulted in an apparent thrust increase of about 3%[a] over that measured with just the facility doors open. The data tabulated

[a] There was a simultaneous inlet modification which contributed to this thrust change to an unknown degree.

above indicated that the fan-in-fuselage configuration would not have required this facility change, probably because the inlet in this case was 2 feet above the facility walls and did not provide as effective an ejector system. The 6% thrust deficiency noted in the fan-in-fuselage configuration with the doors closed can not be assumed to have been present during the original fan-in-fuselage performance runs during Phase I of the contracted work (reference 1). At that time, the wing leading and trailing edges, tip and sealing skins were not employed. These items represent approximately 75 square feet of wing surface. An estimated correction to the original test data was investigated, however, based on the pressure measurements made in the current program that apply to the sections of the wing that were installed originally (about 55 square feet of surface). This amounted to 60 pounds at 2450 rpm or about 1% in thrust.

Previously, the Fan 001 performance has been quoted as below:

Evendale Testing	Thrust at 100% N_F
Fan 001 (6% bellmouth without inlet vanes)	7000 pounds
Ames Testing	
Fan 001 (23.5% bellmouth with circular vane)	7050 pounds

The 1% or 70 pounds correction to the Evendale (reference 1) data, if applied, would therefore bring this in closer agreement with the Ames result; however, the variation is within the thrust measurement accuracy.

PITCH MANEUVER EQUIPMENT

In order to accommodate dynamic tests which affect the rotor as a one-per-rev gyroscopic precession excitation, the thrust frame was fitted with adapters to enable rapid pitch transients. Pivot trunnions were fabricated to replace the load cell supports for the wing and a 3000 psi

hydraulic actuator was connected to the wing behind the pivot line to control the wing angular velocity. Special valving was arranged to limit deceleration rates. Figure 9 shows details of the actuator and trunnion support. Figures 10a and b, show the wing in the limiting $\pm 15^{\circ}$ angle of attack positions.

DIVERTER VALVE MODIFICATION

For test Run 24 (divided flow test), the hydraulic actuator was replaced by two electric screwjacks to actuate the doors separately. Figure 11 shows the screwjack and position indicator locations (refer to Figure 3 for details of normal actuator arrangement).

INSTRUMENTATION

Refer to reference 1 (pages 69 through 90) for a general description of fan instrumentation.

J85 discharge measurements were made in a plane which is two inches aft of the diverter valve forward flange. This station is referred to as station 5.15 and has an annulus area of 154 square inches. Plane 5.1 (J85-7 turbine discharge) annulus area is.148 square inches. A schematic of instrumentation planes is shown in Figure 12.

New instrumentation included:

1. Seven underwing static pressure rakes and four facility velocity probes were installed to provide facility effect data. Figure 1 shows some of the underwing rakes (Figure 7 shows all the locations). The absence of wing skins was considered to be a second order influence in these pressure measurements.

2. Twenty-four thermocouples were installed on the fan inlet screen in lieu of plane 10.3 total temperature rakes which were removed when the circular inlet vane was installed.

3. Four plane 10.3 static pressure rakes (Figure 13) were manufactured from existing total pressure rakes and installed for several runs.

4. Twelve static pressure probes were mounted on the rear frame stators in four radial locations to measure stator discharge static pressure. They were identified as $P_{s\ 11.0}$ since the sensing elements were located aft of the stator edge.

5. Four six-element total temperature rakes were installed in plane 6.0 (cruise nozzle). These were used in test Run 24 to calibrate the plane 5.15 total temperature rakes.

6. A traverse of the fan discharge annulus was made for calculating sound power levels with a piezo-electric sensing element (Atlantic Research-type BC-33 blast pressure probe). The traverse was made 15 1/2 inches below the blade trailing edges as shown in Figure 14. Actuator travel was 20 inches which was sufficient to traverse the annulus. Because of the stream noise generated on the probe it was not a suitable arrangement to yield an octave band analysis, however, determination of the noise level contribution due to blade passing frequency (first and second harmonic) was accurate. The recording setup is sketched below.

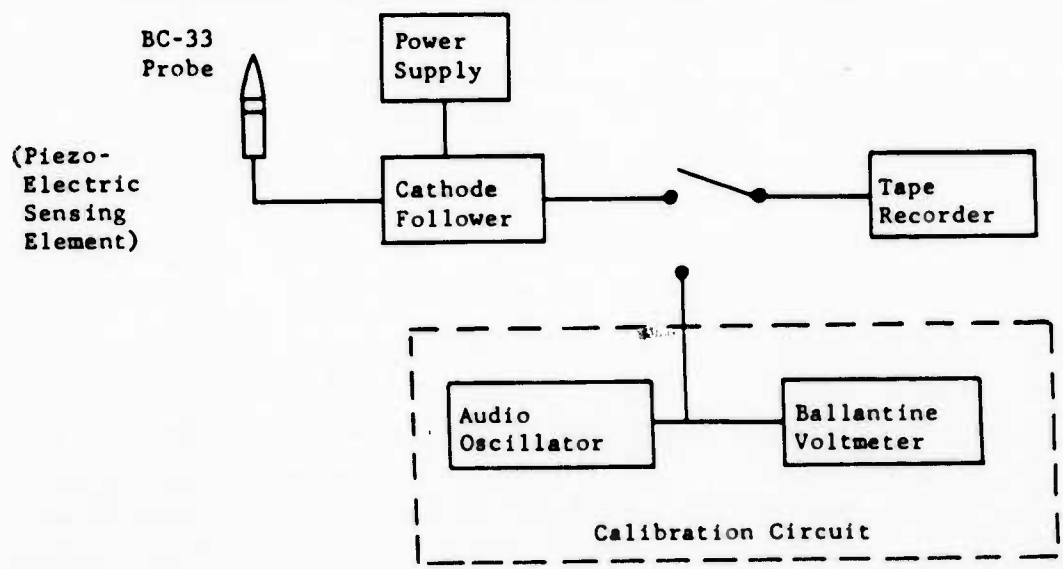

The pressure probe was calibrated (up to 10 kc) in an anechoic chamber by comparing its sensitivity with that of a previously-calibrated microphone. A calibration signal was put on the tape before and after the test with an audio-oscillator. Frequency response of the tape recorder was checked before and after the test.

A narrow band analyzer, 3% band width, was used to reduce the tape. This was necessary due to the noise generated by the wind stream. With the narrow filter, a signal to noise ratio of 6 to 9 db was obtained. The data reduction process is sketched below:

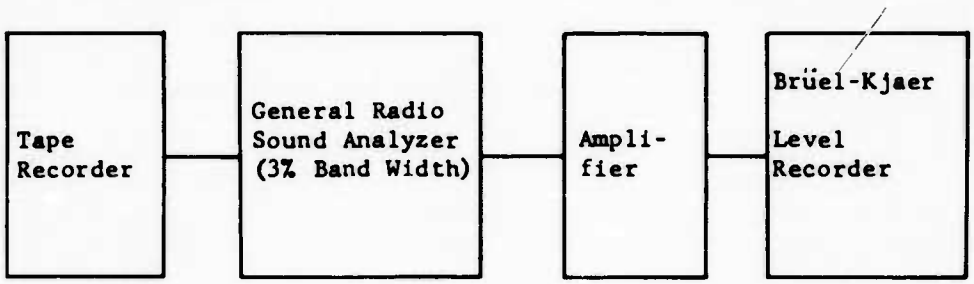

For each fan speed, the first and second harmonic frequencies were determined accurately. The narrow band analyzer was then tuned to each frequency, in turn, and the tape played through the entire traverse (the sound pressure levels (SPL) being recorded on a previously-calibrated B-K level recorder). All SPL data were corrected for recorder response, probe response and all data reducing equipment response. A correction was also made for the slight error introduced by the background noise.

The data were also reduced using 1/3 octave filters, yielding excellent agreement with the narrow band analysis. The reduced traverse SPL data were then used to calculate the sound power levels (PWL) of the first and second harmonic at each speed.

Tables I and II give a summary of all instrumentation included in this test program.

TABLE I

INSTRUMENTATION SUMMARY

Item	Quantity[a]
Aerodynamic Pressures	275
Aerodynamic Temperatures	122
Operating Pressures (fuel, oil, starter air, hydraulic & slipring air pressures)	8
Mechanical Temperatures:	
Non-Rotating (diverter valve skin, J85 bearing, lube oil, wing skins, slipring bearing, fan bearings, exit louvers, stator vanes, and scroll)	64
Rotating (torque band, shaft, carriers, and buckets)	23
Rotor Strain Gages	34
Stator Strain Gages Vibratory	4
Exit Louver Strain Gages	15
Frame Strain Gages:	
Vibratory	0
Steady State	3
Vibration Pickups	12
Speed Pickups	5
Position Indicators	6
T O T A L	571

[a] The numbers shown are maximum installed instrumentation, and were not necessarily all read at one time.

TABLE II

INSTALLED AERODYNAMIC INSTRUMENTATION BREAKDOWN

BY INSTRUMENT PLANES

Plane	Description	P_t	P_s	T_t	Other
2.0	J85 Inlet	0	4	4	0
5.15	Diverter Valve Inlet	21	3	12	0
5.4	Scroll Arms	12	0	0	0
5.45	Turbine Rotor Inlet	0	0	0	0
5.5	Turbine Rotor Exit	8	0	0	3[a]
6.0	Cruise Tailpipe	0	4	24	0
10.0	Fan Inlet Screen	0	0	24	0
10.2	Deep Bellmouth Throat	0	8	0	0
10.3	Fan Rotor Inlet	21	36	24	0
10.6	Fan Rotor Exit	24	0	34	6[b]
11.0	Fan Stator Discharge[c]	48[d]	22[e]	0	0
-	Underwing Static Pressures	0	35	0	0
-	Facility Velocity Probes	6	8	0	0
	T O T A L	140	126	122	9

a. Three P_s pressures installed in inactive arc.

b. Six P_t pressures used to determine flow angles (cobra probes).

c. With rear measuring section installed.

d. Includes two six-element P_t rakes mounted to fan underside for Runs 19 through 25.

e. Includes two dishpan statics, 12 static probes mounted to rear frame stators for Run 10, and 8 static taps in rear measuring section.

TABLE III FAN STRESS LIMITS

Item		Type of Stress	Running[a] Stress Limit - SA (psi)	Absolute[a] Stress Limit - SA (psi)
Rotor Blade:				
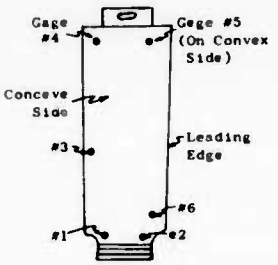	Gage #1 (not installed for this test	First Flexural Vibratory Stress (1850 rpm Speed Range)	8,000	12,500
	Gage #2	First Flexural Vibratory Stress (1850 rpm Speed Range)	3,000	4,700
	Gage #2	Cosine 2θ Vibratory Stress (2080 rpm)	15,800	22,800
	Gage #3	First Flexural Vibratory Stress (1850 rpm Speed Range)	6,500	10,100
	Gage #3	Cosine 2θ Vibratory Stress (2080 rpm)	10,800	15,600
	Gage #4	First Flexural Vibratory Stress (1850 rpm Speed Range)	5,000	7,800
	Gage #5	First Flexural Vibratory Stress (1850 rpm Speed Range)	7,400	11,500
	Gage #6	Cosine 2θ Vibratory Stress Stress (2080 rpm)	15,800	22,800
Bucket		First Flexural Vibratory Stress (800 cps)	10,000	15,600
		First Torsional Vibratory Stress (1540 cps)	7,500	11,700
Disc		All Vibratory Gages	15,000	23,400
Torque Bend		Axial Vibratory Stress	10,000	-
		Tangential Vibratory Stress	10,000	-
Stators[b]		First Flexural Vibratory Stress	10,000	15,600
		Second Flexural Vibratory Stress	8,750	13,600
		First Torsional Vibratory Stress	10,000	15,600

[a] Strain Gage Factor = 20%
Blade to blade stress variation factor = 30%
Blade to blade stress variation factor (cosine 2θ) = 20%

$\lambda = 1.2 \times 1.3 = 1.56$

λ (cosine 2θ) $= 1.2 \times 1.2 = 1.44$

Running stress limit (cosine 2θ) $= \frac{\text{Absolute stress limit}}{1.44}$

Running stress limit (all others) $= \frac{\text{Absolute stress limit}}{1.56}$

[b] Stator stress limits are not confirmed by bench tests.

TABLE IV SUMMARY OF TEST RUNS

RUN NO.	DATE	N_F RPM	β DEG.	PURPOSE OF RUN	CONFIGURATION
1	12/2/60	0	-	Mechanical checkout of J85	X353-5-002 and J85-7-003.
2	12/5/60	Idle-2270	0	Mechanical checkout of fan. Measured seal clearances and rotor yield.	Facility doors closed.
3	12/7/60	Idle-2606	0 to 10	Mechanical checkout and preliminary aerodynamic performance.	Facility doors closed.
4	12/14/60	Idle	0	Smoke and lampblack test.	Facility doors open. Fan inlet screen off.
5	1/17/61	Idle-2250	0 to 44.5	Performance. Exit louver excursion from 0 to +44.5° at 1650 RPM.	X353-5-002 and J85-7-004. Facility doors closed. Fan inlet screen on. 360° seal leakage baffle installed.
6	1/20/61	Idle	0	Smoke and lampblack test.	Facility doors open. Fan inlet screen off. 360° baffle.
7	1/31/61	Idle-1650	0 to 10	Performance. Underwing static pressure survey.	Facility doors closed. Fan inlet screen on. 360° baffle. Underwing static pressure rakes added.
8	2/1/61	Idle-2470	-20 to +45	Performance. Underwing static pressure survey. Staggered louver excursion at 1650 RPM.	360° baffle. Readings 45 - 75: Facility doors closed. Readings 76 - 82: Facility doors open.
9	2/7/61	Idle-2623	-15 to +45	Smoke test. Sound measurement. Performance. Exit louver excursion at 1700 RPM. Three staggered louver points at 2250 RPM.	280° baffle. Readings 83 - 87: Facility doors open. Diverter Valve Opened 2°. Readings 88 -104: Facility doors open. Diverter Valve opened 4°. Readings 105-117: Facility doors closed. Diverter Valve opened 4 1/2°. Readings 118-120: Facility doors closed. Diverter Valve fully closed.
10	2/10/61	Idle-2617	-15 to +45	Smoke test. Performance. Louver excursions at 2250 and 2450 RPM. Staggered louver excursion at 2450 RPM.	280° baffle. Facility doors open. Diverter Valve opened 4 1/2°.
11	2/16/61	Idle-2250	-	Internal performance. Back pressure applied to fan.	280° baffle. Facility doors closed. Removed exit louvers. Installed inlet duct and exit measuring duct. Installed back pressure plate. Inlet screen removed.
12	2/17/61	Idle-2602	-	Internal performance.	280° baffle. Back pressure plate removed. Readings 207 - 216: Facility doors closed. Readings 217 - 223: Facility doors open.
13	2/21/61	Idle-2478	-	Internal performance.	280° baffle. Back pressure plate off. Inlet duct removed. Inlet screen on. Readings 224 - 233: Facility doors open. Readings 234 - 243: Facility doors closed.
14	2/23/61	Idle-2270	-	Internal performance. Back pressure applied to fan.	280° baffle. Back pressure plate on. Four inlet static pressure rakes installed.
15	2/27/61	Idle-2278	-	Performance without exit louvers.	280° baffle. Removed exit duct, back pressure plate and simulated fuselage wall. No exit louvers. Facility doors open.
16	3/16/61	Idle	0	Checkout run (facility modification)	----
17	3/17/61	Idle-2550	0	Pitch maneuver test. 0.35 rad/sec. maneuvers at idle, 1650, 2250, 2450, and 2550 RPM. Measured rotor deflections and stresses.	Fan-in-wing with exit louvers. 230° baffle.
18	3/20/61	Idle-2550	0	Pitch maneuver test. 0.52 rad/sec. maneuvers at idle, 1650, 2450, and 2550 RPM. Measured rotor deflections and stresses.	Fan-in-wing with exit louvers. 230° baffle.
19	3/31/61	Idle-2550	0	Performance.	180° baffle. Inlet vane installed. Facility walls removed. Fan inlet screen on. Exit louvers on. Underwing static pressures installed.
20	4/4/61	Idle-2600	-10 to +40	Performance. Louver excursions from -10° to +40° at 1650, 2250, and 2450 RPM. Staggered louver run at 2450 RPM.	180° baffle. Inlet vane in. 10 mph wind at beginning of test reducing to 2 mph for remainder of test. Underwing statics on.
21	4/5/61	Idle-2600	-10 to +10	Performance. Diverter valve actuations in 3 to 5 seconds at idle, 1650, 1900, 2250 and 2450 RPM. Lampblack applied to fan bellmouth.	180° baffle. Inlet vane in. 12 to 15 mph wind throughout test. Underwing statics on.
22	4/6/61	Idle-2600	0 to +10	Performance. Diverter valve actuations in about one second at idle, 1650, 1900, 2250, and 2300 rpm.	180° baffle. 8 to 10 mph wind throughout test. Underwing statics on. Readings 393 - 406: Inlet vane in. Readings 407 - 437: Inlet vane out.
23	4/10/61	Idle	0	Demonstration run.	Fan-in-wing.
24	4/13/61	Idle-2600	-10 to +8	Performance. Split flow performance. Fan sound power measurements. Straight-through EGT calibration run.	No baffle. Inlet vane in. 0 to 2 mph wind.
25	4/17/61	Idle-2600	-	Internal performance.	Exit louvers removed. Exit measuring section installed. No baffle. Inlet vane in. Underwing statics on.
26	4/19/61	Idle-2550	-15 to +35	Performance. Louver excursions from -15° to +35° at 2250 RPM and 2450 RPM. Accels and decels through cos 2 θ with louvers set at 0, 10, 20, 30 and 35 degrees. Diverter valve actuations at 1650, 2250, and 2400 RPM. Demonstration run for flight research vehicle bidder's conference.	Exit louvers on. No baffle. Inlet vane in. Underwing statics on.
-	4/20/61	-	-	Static load test front and rear frames (9 o'clock deflection).	Fan-in-wing. Inlet vane in.

TABLE V

DETAILED LISTING OF TEST CONFIGURATIONS

Date	Run No.	Reading No. From	Reading No. To	Fan Configuration: Vane	Fan Configuration: Fuselage	Facility Configuration: Doors Open	Facility Configuration: Doors Closed	Facility Configuration: Walls & Ramber Removed	Diverter Valve Setting: Cruise	Diverter Valve Setting: Lift	Diverter Valve Bleed in Lift Position: Fully Closed	Diverter Valve Bleed in Lift Position: ≈ 2%	Diverter Valve Bleed in Lift Position: ≈ 2.5%	Diverter Valve Bleed in Lift Position: ≈ 3.2%	Diverter Valve Bleed in Lift Position: Divided Flow	Exit Louvers: On	Exit Louvers: Off	Fan Inlet Seal Leakage Baffle: No	Fan Inlet Seal Leakage Baffle: 180°	Fan Inlet Seal Leakage Baffle: 230°	Fan Inlet Seal Leakage Baffle: 280°	Fan Inlet Seal Leakage Baffle: 340°	Inlet Screen: On	Inlet Screen: Off	Diverter Valve Actuation: Hydraulic	Diverter Valve Actuation: Electric	Diverter Valve Actuation: Fixed	Back Pressure System: Fan Exit Honeycomb Section	Back Pressure System: With Plate	Back Pressure System: Without Plate	Simulated Fuselage: On	Simulated Fuselage: Off	Gyro Maneuver Setup	J85-7-403	J85-7-404	J85 Engine: Circular	J85 Engine: Inlet Vane
12/2/59	1	1	3	X			X		X		X					X		X					X		X						X			X		
12/5/60	2	4	6	X			X		X		X					X		X					X		X						X			X		
12/5/60	2	7	9	X			X			X	X					X		X					X		X						X			X		
12/7/60	3	10	10	X			X		X		X					X		X					X		X						X			X		
12/7/60	3	11	15	X			X			X	X					X		X					X		X						X			X		
12/14/60	4	16	16	X			X			X	X					X		X						X	X						X			X		
12/14/60	4	17	22	X			X		X		X					X		X						X	X						X			X		
1/17/61	5	23	27	X			X		X		X					X							X	X	X						X			X	X	
1/17/61	5	28	38A	X			X			X	X					X							X	X	X						X			X	X	
1/20/61	6	38B	41	X		X				X	X					X							X		X						X			X	X	
1/31/61	7	42	44	X			X			X	X					X							X	X	X						X			X	X	
2/1/61	8	45	75	X			X			X	X					X							X	X	X						X			X	X	
2/1/61	8	76	82	X		X				X	X					X							X	X	X						X			X	X	
2/7/61	9	83	87	X		X				X		X				X						X		X	X						X			X	X	
2/7/61	9	88	102	X		X				X			X			X						X		X	X						X			X	X	
2/7/61	9	103	104	X		X			X				X			X						X		X	X						X			X	X	
2/7/61	9	105	117	X			X			X				X		X						X		X	X						X			X	X	
2/7/61	9	118	120	X			X			X	X					X						X		X	X						X			X	X	
2/10/61	10	121	189	X		X				X				X		X						X		X	X						X			X	X	
2/16/61	11	190	206		X		X			X				X			X					X		X		X	X	X		X			X	X	
2/17/61	12	207	216		X		X			X				X			X					X		X		X	X	X		X			X	X	
2/17/61	12	217	223		X					X				X			X					X		X		X	X	X		X			X	X	
2/21/61	13	225	233	X		X				X				X			X					X		X		X	X	X		X			X	X	
2/21/61	13	234	243	X			X			X				X			X					X		X		X	X	X		X			X	X	
2/23/61	14	244	280	X		X				X				X			X					X		X		X	X	X		X			X	X	
2/27/61	15	281	288	X		X				X				X			X					X		X		X	X			X		X		X	X	
3/16/61	16	289	289	X			X			X				X		X				X				X		X	X			X		X		X	X	
3/17/61	17	290	296	X			X			X				X		X				X				X		X	X			X		X		X	X	
3/20/61	18	297	302	X			X			X				X		X				X				X		X	X			X		X		X	X	
3/31/61	19	303	309	X				X		X				X		X			X					X		X				X		X		X	X	X
4/4/61	20	310	377	X				X		X				X		X			X					X		X	X			X		X		X	X	X
4/5/61	21	378	392	X				X		X				X		X			X					X		X	X			X		X		X	X	X
4/6/61	22	393	406	X				X		X				X		X			X					X		X	X			X		X		X	X	X
4/6/61	22	407	437	X				X		X				X		X			X					X		X	X			X		X		X	X	X
4/10/61	23	-	-	X				X		X				X		X		X						X		X				X		X		X	X	X
4/13/61	24	438	449	X				X		X			X			X			X					X		X		X		X		X		X	X	X
4/13/61	24	450	453	X				X		X	X					X			X					X		X		X		X		X		X	X	X
4/13/61	24	454	462	X				X	X	X					X	X			X					X		X		X		X		X		X	X	X
4/13/61	24	463	479	X				X		X					X	X			X					X		X		X		X		X		X	X	X
4/13/61	24	480	491	X				X	X						X	X			X					X		X		X		X		X		X	X	X
4/13/61	24	492	498	X				X	X	X					X	X			X					X		X		X		X		X		X	X	X
4/17/61	25	499	523	X				X		X					X	X		X	X					X		X		X		X		X		X	X	X
4/19/61	26	524	525	X				X		X					X	X			X					X		X		X		X		X		X	X	X
4/19/61	26	526	534	X				X		X					X	X			X					X		X		X		X		X		X	X	X

TABLE VI

RUNNING TIME AND DATA POINTS - 50 HOUR STATIC FAN-IN-WING TEST

Run	Speed Range - N_F, %						Temperature Range - $T_{t\ 5.15}$, °F						DATA POINTS
	0-24	25-49	50-74	75-89	90-100	TOTAL	0-599	600-799	800-899	900-999	1000-1200	TOTAL	
1	0	0	0	0	0	0	0	0	0	0	0	0	3
2	0:03	0:24	0:44	0:03	0	1:14	0	0	0	1:14	0	1:14	6
3	0:03	0:20	0:04	0:15	0:05	0:47	0:03	0	0	1:38	0:20	2:01	6
4	0	0:43	0	0	0	0:43	0	0	0	0:43	0	0:43	7
5	0:03	0:25	0:50	0:02	0	1:20	0:03	0	0	1:15	0:02	1:20	16
6	0:02	1:13	0	0	0	1:15	0:02	0	1:13	0	0	1:15	4
7	0	0:26	0:06	0	0	0:32	0	0	0:26	0:06	0	0:32	3
8	0:09	0:28	1:40	0:51	0:12	3:20	0:04	0:09	0:24	1:40	1:03	3:20	38
9	0:16	1:01	0:52	0:59	0:22	3:30	0:08	0:08	0:49	1:04	1:21	3:30	38
10	0:06	0:50	0:38	1:35	1:30	4:39	0:03	0:03	0:50	0:38	3:05	4:39	69
11	0:04	0:22	1:07	0:21	0	1:54	0:02	0:26	1:05	0:21	0	1:54	17
12	0:04	0:25	0:16	0:09	0:14	1:08	0:02	0:02	0:25	0:16	0:23	1:08	17
13	0:06	0:44	0:13	0:18	0:11	1:32	0:03	0:03	0:44	0:13	0:29	1:32	19
14	0:06	0:27	1:00	0:30	0	2:03	0:03	0:03	0:49	0:38	0:30	2:03	37
15	0:02	0:13	0:11	0:08	0	0:34	0:01	0:01	0:13	0:11	0:08	0:34	8
16	0:01	0:09	0	0	0	0:10	0:01	0:01	0:08	0	0	0:10	1
17	0:04	0:59	0:22	0:16	0:16	1:57	0:03	0:03	0:57	0:33	0:21	1:57	7
18	0:06	0:28	0:34	0:02	0:10	1:20	0:03	0:03	0:28	0:34	0:12	1:20	6
19	0:02	0:18	0:05	0:04	0:18	0:47	0:01	0:01	0:18	0:05	0:22	0:47	7
20	0:04	0:47	0:54	0:45	2:26	4:56	0:02	0:02	0:47	0:54	3:11	4:56	68
21	0:10	0:36	0:19	0:10	0:44	1:59	0:05	0:05	0:36	0:19	0:54	1:59	15
22	0:08	1:09	0:51	0:52	0:55	3:55	0:04	0:04	1:09	0:51	1:47	3:55	45
23	0	0:10	0	0	0	0:10	0	0:10	0	0	0	0:10	0
24	1:06	1:05	0:49	1:19	1:55	6:14	0:07	0:07	0:54	1:22	3:44	6:14	61
25	0:06	0:33	0:07	0:09	0:39	1:34	0:03	0:03	0:33	0:07	0:48	1:34	25
26	0:06	2:32	0:35	0:50	1:15	5:18	0:04	0:05	2:32	0:38	1:59	5:18	31
TOTAL	2:57	16:47	12:17	9:38	11:12	52:51	1:07	1:39	15:20	14:06	20:39	52:51	554

TABLE VII

SUMMARY OF LIFT FAN OPERATING TIME

	Fan, S/N 001					S/N 002	Total
	B/U #1	B/U #2		B/U #3		B/U #1	Both
Speed Range	Even.	Even.	Ames	Ames	Total	Even.	Fans
0 - 24%	5:02	4:08			9:10	2:57	12:07
25 - 49	2:43	7:23	5:08	4:10	19:24	16:47	36:11
50 - 74	9:52	5:57	12:01	16:43	44:33	12:17	56:50
75 - 89	1:29	2:11	3:08	1:06	15:49	9:38	36:39
90 - 100				7:45		11:12	
TOTAL HOURS	19:06	19:39	20:17	29:44	88:56	52:51	141:47
Temp. Range							
0 - 599°F	8:20	5:09			13:29	1:07	14:36
600 - 799	1:57	1:49		5:05	9:01	1:39	10:40
800 - 899	7:49	7:04	:28	15:17	30:39	15:20	45:59
900 - 999	1:00	4:39	14:22	1:21	21:22	14:06	35:28
1000 - 1200		:57	5:27	8:01	14:25	20:39	35:04
TOTAL HOURS	19:06	19:39	20:17	29:44	88:56	52:51	141:47
DATA POINTS	71	66	348*	439*	1024	554	1578

*Not including basic airplane data with fan off.

variables were evaluated:

Fan speed	0 to 2640 rpm (100%)
Exit louver angle	
Vector ($\beta_1 = \beta_2$)	-15° to $+44^\circ$
Stagger ($\beta_s = \beta_2 - \beta_1$)	0° to 30° stagger angle
J85 engine speed	0 to 16,650 rpm (101%)
Diverter valve temperature	Maximum of $1400^\circ F$
Diverter valve slew rate	1 second to 13 seconds
Pitch maneuver	
Angle of attack	-15° to $+15^\circ$
Angular velocity	0.37 and 0.52 rad/sec.
Divided flow (fan/J85)	0/100, 25/75, 50/50, 75/25, 100/0 - (nominal)
Throttle transients	1, 5, 10 and 60 seconds
Wind velocity	0 to 17 miles per hour

TEST RESULTS

Test results are all tabulated in Appendix A. Fan performance calculation standards are presented in Table A-1. Definitions and symbols are listed in Table A-2. Table A-3 contains all data points obtained in the test program. Table A-4 is a compilation of transient testing. The following items are direct readings: fan speed (N_F), exit louver angles (β_1 and β_2), engine speed (N_{J85}) and exhaust gas temperature ($T_{t\ 5.15}$). The other items were converted from direct measurements by use of formulae listed in the calculation standards, Table A-1.

MEASUREMENT ACCURACIES

Accuracy of data was affected during test runs by fan reingestion; fan speed and thrust became unsteady and varied as much as 50 rpm. Both speed and thrust were steady when there was no reingestion (speed variance was 10 rpm or less). This reingestion was a facility effect and occurred during adverse wind conditions, turbine discharge air blocked by the test control building being blown back across the inlet.

load cell calibration obtained during thrust frame setup indicates that about 70 pounds should be added to the measured thrust at 100% speed. This correction factor has not been included in the results, however, because the static calibration may include friction and binding which would not occur when the fan is running. In order to improve resding correlation between thrust and speed, thrust readouts were photographed and a simultaneous marker identified the exact speed on the transient speed recorder; manometers were also simultaneously photographed. Speed correction for final performance runs was based on temperatures read from 24 thermocouples attached to the fsn inlet protective screen. These were monitored on a digital recorder using a 5 second scan time.

V. ANALYSIS OF RESULTS

A. GENERAL CONSIDERATIONS

J85-7 Engine Performance:

The performance of the J85-7 engine is presented in Figures 15 through 22.

Turbine discharge bleed was required to provide the total effective area necessary to maintain exhaust gas temperature at military speed. Bleed was accomplished by positioning the diverter valve doors slightly open from the full diverted position. The amount of bleed was determined as shown in the sample calculations in Appendix B and is illustrated in Figure 15a. Figure 15b indicates the leakage when the valve doors are fully closed. Engine weight flow at the diverter valve inlet is calculated from engine bell-mouth measurements corrected for compressor bleed, eighth stage seal leakage and fuel flow; the flow at the fan nozzle is calculated from known diverter valve and scroll losses and the scroll flow function. A sample calculation and appropriate curves for this are also shown in Appendix B.

The effect of bleed on exhaust gas temperature is shown in Figure 16a. Note the difference in average gas temperature between the two engines at the same speed. Gas temperature as a function of speed is also plotted for the straight-through mode in Figure 16b (engine S/N 004 only). The reason for the discrepancy in EGT characteristic in the lower speed region is not known. The change in the fan-engine speed relationship with bleed is shown in Figure 17. 100% fan speed (2640 rpm) was obtained at 100.4% engine speed with the 3.2% bleed setting. Figure 17 also shows the effect of adding the inlet vane for Runs 20 through 26; fan power absorption has increased resulting in higher engine rpm per fan rpm. Checks of engine weight flow and discharge pressure

as a function of speed for both early and late runs show identical results indicating no engine deterioration during test.

Figure 18 shows the relationship between diverter valve skin temperatures and EGT. Hot spots at the top and bottom were evident but 100% fan speed was attainable without exceeding the diverter valve limits. Later model J85 engines incorporate an improved combustor configuration which greatly reduce the wall temperatures so this will not be a problem area.

Total pressure and horsepower at stations 5.15 and 5.4 are shown as a function of engine speed for the 3.2% bleed setting in Figures 19 and 20a. Total pressure points at station 5.4 are calculated from the station 5.15 total pressures based on losses previously obtained (see Appendix B). The change in J85 discharge effective area for straight-through and diverted flow is reflected in the $HP_{5.15}$ curves in Figure 20a. Using $HP_{5.15}$ (diverter valve positioned for approximately 3.2% bleed) as a base, Figure 20b was generated to show the corresponding power losses for the diverted flow $HP_{5.4}$ and for the straight-through flow $HP_{5.15}$.

A summary of the J85-7-004 discharge conditions as measured during this testing is presented as a function of engine speed in Figure 21. Fan speed is also included and all parameters are based on the 3.2% bleed setting of the diverter valve.

The magnitude of the differences which existed between the two J85-7 engines is shown in Figures 16a and 22. Engine J85-7-004 produced more thrust and horsepower per rpm, but it operated at a higher temperature level and necessitated diverter valve bleed. Horizontal thrust with a diverter valve and test tailpipe is presented in Figure 22.

EGT Calibration Run:

A series of straight-through test points was taken during Run 24 to obtain a correction factor for the average EGT measured at plane 5.15. Four six-element temperature rakes were installed 56 inches behind the J85 turbine discharge (plane 6.0) in the straight-through leg. The exhaust gases are more thoroughly mixed and the temperature spread from element to element is reduced considerably. Figure 23 is a plot of the EGT profiles at stations 5.15 and 6.0.

The correction to apply to EGT is shown in Figure 24. All curves in the report incorporate the effect of this correction including weight flow at station 5.4 and horsepower. The tabulated data in Appendix A, however, were not corrected so that this listing retains the data in an unadjusted form.

Horsepower Calculation:

Available horsepower at station 5.4 (fan turbine nozzle inlet) is calculated from conditions at station 5.15 (gas generator turbine discharge where the annulus area is 154 square inches). A sample calculation of this iterative process is shown in Appendix B.

Most of the fan testing was done with the diverter valve doors held open to bleed about 3.2% of the weight flow. For this condition, it was assumed that loss through the diverter valve (or interactions with the scroll) remained the same as for the fully closed condition. This appears to be an incorrect assumption because the calculated horsepower at station 5.4 is higher with the diverter valve doors set for 3.2% bleed. The difference between curves (1) and (3) in Figure 25 represent the available power difference due to 3.2% bleed plus any unaccounted-for power losses in the system. The unaccounted-for losses are equivalent to the difference between curves (2) and (4). These additional power

losses with the diverter doors set for 3.2% bleed may be a result of:

1. Decrease in $P_{T\ 5.4}$ due to increase in turbulence from re-positioned diverter valve doors.

2. Decrease in $T_{t\ 5.4}$ below the $T_{t\ 5.15}$ value due to bleeding higher temperature gas from the outer wall.

Since nearly all of the data taken were with the diverter valve doors set for 3.2% bleed, the horsepowers from curve (2), Figure 25 are used in this report. For a given system, it is not of particular significance to know the precise distribution of available horsepower between the fan, bleed and ducting requirements; however, in system design, such knowledge is necessary in order to obtain optimum performance. Identification of the apparent additional power losses is anticipated in the fan-in-wing wind tunnel test program; from the limited data taken during this testing with the diverter valve doors fully closed, indications are that the horsepower requirement at the diverter valve inlet ($HP_{5.15}$) will then be shown to be decreased 2 1/2% to 3 1/2%. Proper sizing of fan scroll areas with J85 engine characteristics will eliminate the need for inefficient bleed configurations and this would result in a net gain in system efficiency rather than just a redistribution of power requirements.

Ram Drag:

Ram drag effects due to wind were included in horizontal thrust and actual turning angle calculations whenever it was clear that the wind velocity was quite constant. It is not possible to determine the exact wind velocity due to gustiness. Wind velocity and direction recorded in Table A-3 in Appendix A are average conditions approximately at the time of performance data recording.

Figure 26 shows the effect of wind velocity on horizontal thrust. With a wind velocity of 15 m.p.h. west directly at the leading edge, a horizontal thrust correction of + 365 pounds should be applied when the fan is operating at 100% speed (534 lbs/sec. flow). Therefore, on a windy (± 15 m.p.h.) day in the Evendale outdoor test facility, horizontal thrust, total thrust and actual turning angle variations will occur at 100% fan speed as shown in Table VIII.

TABLE VIII

EFFECT OF WIND ON THRUST (EVENDALE FACILITY)

β (deg.)	Wind Velocity (m.p.h.)	Wind Direction	Horizontal Thrust (lbs.)	Total Thrust (lbs.)	$\Delta \beta_V$ (deg.)
0	15	East	- 365	0	- 3
0	15	West	+ 365	+ 20	+ 3
10	15	East	- 363	- 60	- 3
10	15	West	+ 363	+ 80	+ 3
20	15	East	- 354	- 130	- 3
20	15	West	+ 354	+ 150	+ 3
30	15	East	- 334	- 190	- 2 1/2
30	15	West	+ 334	+ 210	+ 2 1/2

Turning Angle:

With the facility walls up, the actual turning angle, β_V, for the fan-in-wing varies from 1° greater than the physical angle, β, at $\beta = 0^\circ$, to 5° greater at $\beta = 45^\circ$. Figure 27 shows the relationship with all data corrected for zero wind velocity. The β_V correction in Table VIII for wind must be applied in addition to this calibration.

The actual turning angles measured before the facility walls were removed varied in the same manner but the difference between actual and indicated angle was greater (see Figure 27). The reason for this difference is due to a facility effect on the lift measurement (see Section III). There was no facility effect on the horizontal thrust based on comparisons of J85 thrust with the walls up and with the walls removed for the same J85 speed in the cruise mode.

B. FAN AERODYNAMIC PERFORMANCE

Fan Internal Performance Development:

Internal performance is represented by the pressure rise developed at the rotor discharge. Since this is expressed in terms of the difference between total pressure rise developed at this plane and ambient pressure, the inlet losses are included in the performance. The pressure rise non-dimensionalized with tip speed squared gives a pressure coefficient which is roughly proportional to thrust. Table IX and Figures 28a and 28b show the calculated pressure coefficients and measured thrusts for the configurations tested compared with fan-in-fuselage results.

The first fan-in-wing configuration tested exhibited poor rotor tip performance. This can be seen by the difference in tip pressure rise for this configuration relative to the fuselage configuration in Figure 28a. Also, horsepower absorption and thrust were considerably reduced. Smoke and lampblack tests were conducted to further identify the problem. At idle fan speed, clear evidence of bellmouth separation along the active arc of the fan occurred, Figure 29. These figures show separation starting near the 6 o'clock strut in the active arc and carrying slightly beyond the other end of the active arc to about the 10 o'clock position. This is consistent with the counter clockwise rotation (forward looking aft).

TABLE IX

THRUST AT 100% SPEED AND DESIGN HORSEPOWER FOR FAN-IN-FUSELAGE AND VARIOUS FAN-IN-WING CONFIGURATIONS

Configuration	Thrust at 100% Speed (lbs.)	Percent Improvement	Estimated Thrust at Design HP (lbs.)	Estimated Fan Speed at Design HP (%)	*Rotor Discherge Pressure Coefficiant $\Psi_{10.6}$
Ames:					
Fan-in-fuselege (X353-5-001), 23.5/6% bellmouth with curved vane end exit louvers.	7050	-	7190	101.0	-
Evendele:					
1. Fen-in-fuselege (X353-5-001), 6% bellmouth, no inlet cescede, with exit louvers.	7000	-	7140	101.0	0.365
2. Fen-in-fuselege (X353-5-002), 6% bellmouth, 280° beffle, no inlet cescede, fecility doors closed, no exit louvers, with exit meesuring duct.	6700	-	6830	101.0	-
3. Fen-in-wing (X353-5-002), 6% bellmouth, no beffle, no inlet vens, facility doors closed, with exit louvers.	5640	-	6150	104.5	0.306
4. Seme es (3), with 360° baffle.	6100	8.2	-	-	-
5. Same as (4), Fecility doors open.	6200	9.9	6355	101.8	-
6. Fen-in-wing (X353-5-002), 6% bellmouth, 280° beffle, no inlet vens, fecility doors closed, with exit louvers.	6200	9.9	6460	102.1	0.340
7. Seme es (6), with fecility doors open.	6275	11.3	6535	102.1	0.340
8. Fen-in-wing (X353-5-002), 6% ballmouth, 180° baffle, no inlet vens, facility walls removed, with exit louvers.	6405	13.6	6490	100.7	0.343
9. Fan-in-wing (X353-5-002), 6% bellmouth, 180° baffle, with circular vene, facility walls removed, with exit louvers.	6810	20.9	6850	100.3	0.370
10. Fan-in-wing (X353-5-002), 6% ballmouth, no baffle, with circular vens, fecility walls removed, with exit louvers.	7050	25.0	7020	99.8	0.378

* Corresponds to 100% speed condition.

To study this problem, model fan tests were conducted with the General Electric 26 inch fan which aerodynamically is a scale of the X353-5; the full scale fan performance deficiency was reproduced by simulating the turbine leakage air using a helium-air mixture to correspond to the density of hot gas. This leakage air was directed into the 26 inch fan through a 360° tip manifold and could be shut off completely. Without leakage air simulated, scale model bellmouth separation did not occur. This indicated that the inlet was marginal and required additional turning control or at least leakage air control. Additional tests of the scale-model fan fitted with a 360° inlet baffle were successful in redirecting leakage air and avoiding bellmouth separation. This fix was then applied to the full scale fan as described in Section II. Figure 30 shows the active arc portion of the fan after lampblack and test investigations. There was no indication of bellmouth separation; the black region at the baffle weld is a local flow disturbance due to the weld irregularity. This modification resulted in a thrust improvement of over 10%, however, to equal fan-in-fuselage results (Reference 1), a 24% improvement was required.

The problem apparently was that in order to draw flow into the full inlet, very high velocities (on the order of 700 ft/sec.) occur on the bellmouth because of the high level of bellmouth suction pressure required to turn the flow. This is illustrated by the fan-in-wing inlet flow diagram, Figure 31. Based on this flow analysis, the high velocity air near the bellmouth wall must diffuse to a rotor entrance average velocity of 435 ft/sec. Since this much diffusion is marginal for stable air flow, separation was easily caused by the leakage air entering the fan stream at the lower end of the inlet bellmouth, being directed slightly forward and radially inward. Installing the baffle served to prevent separation, but, of course, could not reduce the high bellmouth velocity; therefore, the flow stability was still marginal. Some of the thrust deficiency

with the baffle configuration comes directly from the baffle blocking the fan annulus; this amounted to approximately 3.8% of the area. For a given through-flow velocity, the thrust is directly proportional to area and the rotor in the region directly under the baffle is physically prevented from working. Another effect (of the high velocity) is the reduction in power absorption in the rotor tip region because of more negative incidence entering air angles. Table IX shows this effect by comparing the thrust at constant speed with the thrust at constant power. This shows that a large percentage of the thrust deficiency without the baffle could have been recovered by overspeeding the fan about 5% to absorb the available power. With the baffle, the power absorption was greatly increased and would have required only about 1.6% overspeed. Since the fan-in-fuselage case itself required 1% overspeed to absorb design power, the remaining thrust deficiency (6450 relative to 7140 pounds) must have been due to the combination of blockage and reduced fan efficiency.

Continued scale model testing indicated that more improvement in performance could be obtained by adding a circular inlet vane and removing the remainder of the baffle.[a] Removal of the baffle was not done until some tests were run with the vane and baffle combination because there was a lack of certainty that the scale-model fan would simulate the full scale fan in terms of leakage and leakage effects on performance. The improvement due to the vane is apparent in Figure 28a. Further improvement was obtained by removing the remainder of the baffle (Figure 28b). The final test configuration internal performance was an improvement of 25% over the original wing performance and was slightly better than fuselage performance of X353-5-001 for static conditions and $\beta = 0°$.

[a] The blockage area variation with baffle configuration is given in Section II.

Adding the bellmouth vane, which acts as a lifting surface whose force is directed towards the bellmouth lip, relieved the bellmouth lip static pressure and thereby reduced the bellmouth maximum velocity. In the sketch below a plot of maximum bellmouth velocity squared[a] versus depth of the boundary layer retains the same shape but at a higher pressure level; the vane, therefore, provided the same pressure gradient for turning the flow. The effect of the vane is also shown schematically in terms of the boundary layer static pressure:

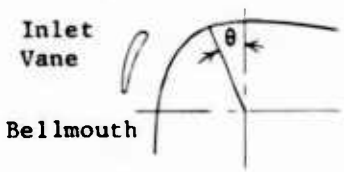

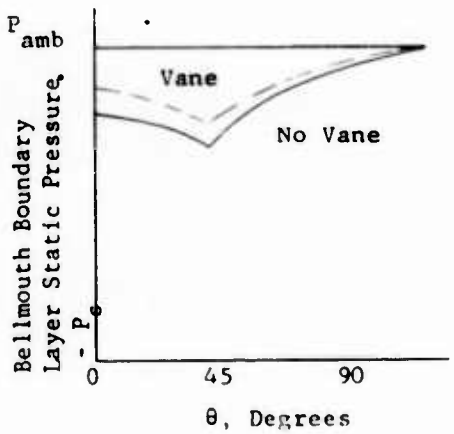

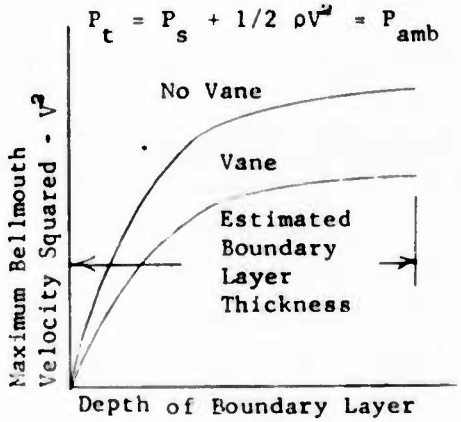

[a] Used as a measure of static pressure change.

The effect of the facility walls on internal performance is shown in Figure 32 which is a comparison of pressure coefficient for the fan-in-wing with the walls up and with the walls removed. A simultaneous reduction of the extent of the baffle from 280° to 180° was made when the walls were removed. Tip performance in the inactive arc for the "walls down" case was poorer, apparently because the baffle had been removed in the region. The pressure coefficients derived from the rakes in the active arc region were higher than in the previous csse and there were also higher peak pressure coefficients measured by the inactive arc rakes. This resulted in a higher overall pressure coefficient for the 180° baffle configuration apparently due to reduced blockage and in spite of poorer tip performance in the inactive arc; approximately 1% thrust increase can be attributed to the approximately 1% increase in pressure coefficient. The thrust, however, increased over 3% as shown in Table IX and the difference is attributed to removing the facility walls (see Section III).

During the testing, wind directed at the wing leading edge was found to have an effect on measured thrust and this is discussed later in this section of the report. There was, however, also an indication of a change in fan internal performance due to the wind which is shown in Figure 33. The difference in pressure coefficients measured for nearly still air snd 10-15 m.p.h. wind cases implies about 2 1/2% thrust reductions at the higher velocity. Figure 33 also shows that this chsnged performance is attributable to poorer pressure profiles st the wing leading edge rake locations. Figure 34 compares two sets of data at different wind conditions for the finsl configuration and an improvement is again noted as the wind velocity is reduced, being primarily an increase in pressure coefficients measured near the leading edge. It should be noted that in quoting the finsl configuration pressure coefficient, the data for a high wind case was used. This was done because at low wind velocity the facility control room caused the turbine dis-

charge gas to recirculate into the fan and this made calculation of pressure coefficients less reliable (since they are based on tip speed squared and a slight error in temperature correction could result in a substantial error in pressure coefficient). The overall effect of wind velocity on measured thrust is larger than can be attributed to this change in internal performance as will be discussed later.

Inlet Flow Angles:

Relative inlet flow angles were calculated from rotor inlet static pressure measurements.[a] The data indicate that the performance of the fan-in-wing would be improved by twisting open the rotor tip so as to improve the air-to-blade angle relationship (increased incidence) and absorb more power.

Figure 35 shows the rotor inlet relative air angle for the fan-in-fuselage tests of Run 11. There is a good match of blade angle and relative air angle over the range of throttling. The blade leading edge angle is larger than the design air angle for several reasons: 1) optimum incidence angle is slightly negative for a cambered airfoil; and 2) extra negative incidence was factored into the design to provide stall margin during throttling.

Figure 36 is a similar plot for the fan-in-wing with the exit measuring duct. As predicted by the flux plot, the tip incidence is quite negative for the un-throttled case, while the hub incidence is higher than for the fuselage installation. Improvement in power absorption could be obtained, at the expense of throttle stall margin

[a] Axial flow is assumed and its velocity is calculated from the static pressure measurement assuming total pressure is equal to ambient. The relative flow angle is then obtained from the blade speed and axial velocity.

by twisting open the rotor tip three to five degrees to match the relative air angle.

The relative flow angle variance with circumferential location is shown in Figure 37. Rake C which is in the deep part of the inlet shows the effect of turbine leakage on inlet air angle. Considerable testing has been done on the scale model fan showing good agreement with the full-scale fan. Figure 38 shows inlet air angles for both the full scale and scale model fan without a measuring section. The scale model fan has the inlet vane installed as is evident by the point at the tip.

Fan Efficiency and Power Consumption:

Data from Run 25 was used to obtain the fan efficiency and power consumption. The stage efficiency is 81.2% average and the fan power consumption is 2905 horsepower at 100% fan speed. Comparison of internal characteristics is made with the fan-in-fuselage (X353-5-001) shown in Table X.

No measurements of inlet losses were made for the fan-in-wing tests. The pressure rises are referred to ambient in the wing configuration instead of rotor inlet (plane 10.3) average total pressure as was the case for the fuselage; therefore, the fan-in-wing pressure rise and efficiency include the inlet losses. If the inlet loss is approximated using the 6% bellmouth loss measured by the boundary layer rakes in the fuselage duct inlet, then a fan-in-wing efficiency can be calculated without inlet losses. This loss coefficient is 0.041 based on duct velocity. Converting this to a loss coefficient based on tip speed, it would be expressed by:

TABLE X

COMPARISON OF INTERNAL CHARACTERISTICS OF
FAN-IN-FUSELAGE (X353-5-001) AND FAN-IN-WING (X353-5-002)

	Fan-in-Fuselage X353-5-001 Buildup No. 1 Reading No. 68	Fan-in-Wing X353-5-002 Buildup - No. 1	Fan-in-Wing Relative to Fan-in-Fuselage
[a]Rotor Efficiency, η_R	98.0[b]	100.7[c]	Up 2.7%
[a]Stage Efficiency, η_S	83.0[b]	81.2[c]	Down 2.2%
Flow Coefficient, ϕ	0.597	0.591	Down 1.0%
Pressure Coefficient, $\Psi_{10.6}$	0.372[b]	0.378[c]	Up 1.6%
Pressure Coefficient, $\Psi_{11.0}$	0.314[b]	0.305[c]	Down 2.0%
Fan Horsepower Absorbed - $\frac{HP}{\delta\sqrt{\theta}}$ (at 100% $N_F/\sqrt{\theta}$)	2890	2905	Up 0.5%

[a] Due to the measurement accuracies involved, the efficiency values are more significant as they imply an incremental or percentage change rather than as they identify a specified level, i.e., η_R = 100.7. See discussion of "Fan Efficiency Measurement Accuracy" on the following page.

[b] Referred to plane 10.3

[c] Referred to ambient conditions

$$\text{Loss coefficient based on tip speed} = \bar{\omega}\left(\frac{\text{Annulus Area}}{\text{Duct Area}}\right)^2 \Phi^2 = \frac{\Delta P_{t\ \text{inlet}}}{1/2\ \rho (V_{tip})^2}$$

$$= (0.041)\ (0.84)^2\ (0.59)^2 = 0.010$$

Excluding the inlet loss, fan-in-wing stage efficiency is:

$$\eta_S = \frac{\Psi_{11.0} + 0.010}{\Psi_{11.0}} \quad (81.2)$$

$$= \frac{0.315}{0.305} \quad (81.2) = 83.9\%$$

and the fan-in-wing discharge coefficient ($\Psi_{11.0}$) is 0.315.

A comparison of the fan-absorbed horsepowers which were calculated from fan flow and temperature rise data give further evidence that system horsepower absorption is lower than calculated from J85 discharge conditions for the configuration with the diverter valve positioned for bleed; the fan-in-wing to fan-in-fuselage fan-absorbed horsepower ratio is 2905/2890 = 1.005 as compared to the system horsepower ratio of 4250/4140 = 1.026. Indications are that the fan-in-wing system horsepower absorption should be about the same as fan-in-fuselage horsepower absorption because both the fan-absorbed horsepower and turbine efficiency, as will be discussed later in this section, are essentially the same. The measured power differences between the two configurations would, therefore, have to be due to increased power losses between the J85 engine and the fan turbine inlet, apparently resulting from diverter valve door positioning for bleed.

Fan Efficiency Measurement Accuracy:

The stage efficiency listed in Table X for the fan-in-wing configuration (81.2%) is the mean efficiency from the eleven data

points obtained during Run 25 listed below:

Reading Number	η_s (%)	$N_F/\sqrt{\theta}_{10.3}$ (%)
501	79.9	87.5
505	89.4	100.3
506	80.0	100.8
507	83.1	100.5
508	78.4	101.0
508A	73.4	101.0
511	80.8	101.1
512	83.1	100.6
513	79.7	100.5
519	88.2	99.7
520	77.2	99.6
Mean η_s =	81.2%	

Statistically, there is a 95% certainty that the mean efficiency calculated from any group of eleven data points (for the same configuration and operating conditions) will be within $\pm$ 2.8 points of this value. Part of this tolerance is due to the different temperature measurement setup used. In earlier runs, the temperature rise was read as a local differential temperature between pairs of elements on the inlet and discharge rakes approximately in the same streamline and tended to eliminate any effect of time fluctuation due to any recirculation on local streamline temperature. This also avoided the necessity of applying a recovery[a] correction for the thermocouples since both inlet and discharge were in approximately the same velocity field. In Run 25, all of the inlet temperatures were read individually but not synchronized

[a] For Run 25, a recovery factor of + 0.6 degrees was applied to the discharge thermocouples. The inlet thermocouples were located on the fan inlet screen and required no recovery correction for the low velocity environment.

with specific discharge elements which were also read individually. These data points, however, were obtained with relatively insignificant reingestion which minimized this instrument setup deficiency. The eleven points do not represent an ideal statistical sample which could be overcome only by a greatly increased number of data points but, since there is no legitimate means to eliminate any of the data, all eleven points were used in the calculation of mean efficiency and this represents the best value which can be obtained with the available data.

Throttle Characteristics:

The constant speed throttle line of the wing installation appears flatter and subject to greater flow reduction for a given louver deflection than the fuselage installation (see Figure 39). The flow coefficients for the fan-in-wing with the exit louvers installed are low at $\beta = 0°$ when compared to the fan-in-wing with exit duct installed (0.554 as compared to 0.591).

Table XI compares thrust coefficients calculated from internal measurements and the measured thrust changes as a function of β. These show consistent results.

Figure 40 shows the rotor discharge pressure coefficients (average of four rakes) as a function of radial position and louver setting. The second and third immersion pick up load continuously, but the tip region falls off at 35°. From Figure 41 it is apparent that rake D in the active arc at the trailing edge is the most affected at the tip for the 35° louver position.

Turbine Efficiency:

The turbine efficiency for Fan 002 was calculated to show the effect of removal of the turbine tip seal. Fan 001, Buildup Number 2 is used as the basis of comparison, because scroll S/N 002 was also used in that buildup.

Table XII lists calculated turbine efficiencies for individual test points for both fans. Average of these points give efficiencies of 82.1% for Fan 001 (with seal) and 83.9% for Fan 002 (without seal).

TABLE XI

FAN-IN-WING THRUST COEFFICIENTS

Exit Louver Angle, β (deg.)	Thrust Coefficient, H_T [a]	Per cent Change	Thrust Coefficient, H_T [b]	Per cent Change
0	0.347	-	0.322	-
20	0.337	2.9	0.307	4.7
30	0.313	9.8	0.288	10.5
35	0.296	14.7	0.271	15.8

[a] $H_T = \frac{\Phi^2 + \Psi_{10.6}}{2}$ (see Reference 6)

[b] $H_T = \frac{F}{\rho A_F (V_{tip})^2}$

TABLE XII

X353-5 TURBINE EFFICIENCIES

Reading	Fan 001, Buildup No. 2 (with Seal) Turbine Efficiency	Reading	Fan 002, Buildup No. 1 (without Seal) Turbine Efficiency
41	0.788	202	0.907
43	0.861	203	0.894
44	0.803	204	0.805
45	0.836	205	0.796
46	0.823	206	0.880
61	0.807	209	0.902
62	0.819	210	0.900
63	0.810	211	0.830
64	0.856	212	0.812
65	0.811	213	0.814
		214	0.770
Mean Efficiency =	0.821	219	0.803
		220	0.799
		Mean Efficiency =	0.839

A statistical analysis of the data gives the following results:

1. Any similarly obtained group of ten individual turbine efficiencies will give a mean efficiency of 0.821 $\pm$ 0.014 for Fan 001 with 95% certainty.

2. Any similarly obtained group of thirteen individual turbine efficiencies will give a mean efficiency of 0.839 $\pm$ 0.026 for Fan 002 with 95% certainty.

3. With a difference of 0.018 for the two means, the probability that one mean (for another group of ten individual efficiencies for Fan 001) and another mean (for another group of thirteen individual efficiencies for Fan 002) will differ by 0.018 or more is about 35%.

4. The mean efficiency for all test points (both fans) is 0.832 with 95% certainty that any two groups of test points (ten for Fan 001 and thirteen for Fan 002) will have a mean efficiency within $\pm$ 0.016 of this value.

The turbine tip seal, therefore, has made no detectable difference in the turbine performance but changes on the order of several points in efficiency probably could not be detected.

C. FAN SYSTEM PERFORMANCE

The final test configuration (fan-in-wing with circumferential inlet vane and no baffle) static system performance is shown in Figures 42 to 46. Some major configuration changes were made and environmental effects also were varied, wherever possible, in order to evaluate their effect on performance. The most significant changes are shown in Table IX and Figure 42. Configuration (2) is the initial configuration tested. The deterioration in performance due to bellmouth separation is evident as the fan speed is increased. Performance is better at 50% speed than for configurations (3) and (4) because the initial configuration is not separated at this speed and it has no baffle to reduce its flowpath area and thrust. The facilities effect mentioned earlier (Section III) is evident in the difference between curves (3) and (4) and curves (5) and (6).

7020 pounds thrust at design horsepower[a] for the fan-in-wing final configuration occurs at 99.8% of design speed. This is equivalent to 7050 pounds at 100% speed. During all tests with the facility walls down, the J85 engine inlet operated within 3° of ambient temperature. During Run 26, J85 inlet temperature rise reached 9° for Northeast wind conditions. The fan inlet was within 4° of ambient temperature for all speeds and beta settings, except for conditions of still air or high North winds. With either of these conditions, the turbine discharge air was deflected off the test control room wall back into the fan inlet and the average fan inlet recirculation penalty was approximately 20°F.

Figures 43, 44, 45 and 46 show the average speed, total thrust and horsepower relationships for low wind velocity conditions with negligible recirculation. Figure 46 illustrates the effect of high

[a] Design $HP_{5.4}$ = 4270

wind velocity on thrust. The two curves were obtained by selecting points from a calm day (0 to 3 mph) and a windy day (8 to 15 mph). The 100% speed thrust could be as high as 7150 pounds for a calm day versus 6850 pounds for a windy day. The 7050 pounds thrust given above for the fan performance is actually an average of data taken over a range of wind velocity from 0 to 5 mph and it may, therefore, be slightly pessimistic. This wind influence referred to as "lift-droop" is discussed in detail in part E of this section of the report.

Table XIII is a comparison of fan-in-fuselage and fan-in-wing performance against the objective performance as listed in Reference 7. The columns showing the deviations from objective performance are an attempt to assign the losses to the various components.

The following derivatives were used:

$$\frac{\partial F}{\partial \bar{\omega}_{10.3}} = 0.44; \text{ HP = constant}$$

$$\frac{\partial F}{\partial \bar{\omega}_{13}} = 0.5; \text{ HP = constant}$$

$$\frac{\partial F}{\partial \eta_{\text{fan}}} = \frac{\partial F}{\partial \eta_{\text{turbine}}} = \frac{\partial F}{\partial_{\text{turbine leakage}}} = 0.7; \text{ HP = constant}$$

The results in Table XIII are based on actual data taken. The data were scaled to design $HP_{5.4}$ using the fan laws. The assignment of component performance was based on the following:

1. Fan 002 inlet performance was not measured because the inlet vane trailing edge was below the boundary layer rakes. It was assumed that the fuselage data for a 6% bellmouth, no vanes

TABLE XIII

COMPARISON OF DESIGN OBJECTIVES AND TEST RESULTS

	(1) Estimated Minimum Bulletin Performance	(2) X353-5-001 Fan-in-Fuselage No Inlet Vanes with Exit Louvers	Change in Thrust Relative to Bulletin (1)-(2)	(3) X353-5-002 Fan-in-Wing with Inlet Vane and Exit Louvers	Change in Thrust Relative to Bulletin (1)-(3)
$HP_{5.4}$	4270	4270	-	4270	-
F, lbs.	7430	7140	-290	7020	-410
N_F, %	98.2	101.2	-	99.8	-
$\bar{\omega}_{10.3}$	0.085	0.041	+140	0.041	+140
$\bar{\omega}_{13.0}$	0.040	0.057	- 63	0.057	- 63
η_{Fan}	0.867	0.831	-187	0.839	-146
$\eta_{Turbine}$	0.832	0.832	0	0.832	0
Turbine Leakage, % $W_{5.4}$	1.2	3.5	-120	-	-
Hub Drag, lbs.	0	75	- 75	75	- 75
Turbine Leakage and Unaccountable Losses, lbs.					-266
Unaccountable Losses, lbs.			+ 15		

and the deep duct combination was equivalent to the wing data for a 6% bellmouth and circular vane configuration.

2. Exit louver losses were also assumed to be the same as measured for Fan 001. These losses are based on a comparison of thrust results with and without exit louvers installed (also without exit measuring section).

3. Hub drag is based on static pressure measurements on the rear frame hub from the fan-in-fuselage tests.

4. Turbine leakage was measured for Fan 001 only, by both a heat balance and from a pressure differential using a calculated seal clearance. Fan 002 was not instrumented for leakage data and this item is, therefore, included in unaccountable losses.

5. Fan and turbine efficiencies were calculated for both fans from flow and temperature rise data.

Throttle Characteristics:

Throttle characteristics of the fan-in-wing configuration differ significantly from the fan-in-fuselage configuration[a] as mentioned previously in the section on internal performance; Figures 47 and 48 show the fan-in-wing throttle performance to fall off more rapidly. At negative louver angles fan-in-wing performance appears to be better, however, the available fan-in-fuselage test data in this region were somewhat limited. Figures 49 through 52 show the vertical and horizontal to total thrust ratios as a function of actual and indicated turning angle for both constant speed and constant power operation. These curves were used to derive the total to total thrust ratio curves in Figures 47 and 48.

[a] Fan-in-fuselage throttle characteristics based on Fan 001, Reference 1.

A comparison of thrust coefficients based on pressure and flow coefficients for the fan-in-wing and fan-in-fuselage configuration indicates that a greater flow reduction occurs with throttling for the fan-in-wing case (see Table XIV). Even though the fan-in-wing has a lower flow coefficient at $\beta = 0°$, the thrust coefficient is equal to the thrust coefficient for the fan-in-fuselage because of the higher pressure coefficient. Figure 53 shows the lift versus the horizontal thrust as a function of fan speed and fan horsepower.

The effect of this steeper throttle characteristic on maximum flight speed during transition will be obtained in a later wind tunnel test program. It will be a function of the change in ram drag because of reduced fan flow and any change in angle of attack to account for lift variation as well as the change in vectored thrust.

Staggered Louver Performance:

Figure 54 schematically illustrates the use of dual actuated, louvers for aircraft control power. Various staggered louver settings were tested and the results are shown in Figures 55 through 58.

There is essentially no change in performance between staggered louver settings of $\beta_s = 0°$ and 10°. Beyond 10° β_s, the staggering begins to increase exit louver losses and provides thrust control. The figures listed above give this performance in terms of total fan thrust as well as in terms of horizontal and vertical components as a function of the indicated average exit louver angle setting.

Figures 55 and 56 are plots of staggered louver performance data taken early in the test program prior to installing the circular vane in the inlet. The thrust spoiling characteristic is quite different from that obtained with the inlet vane installed at the higher β_{ave} settings. There is no immediate explanation for this change. Additional data with another inlet configuration (circular

vane plus fixed side vanes) is planned in the forthcoming wind tunnel test program. It will be necessary to review all these data at that time to determine the final thrust spoiling characteristics as a function of β_{ave} and also crossflow. Based on the data taken with the circular vane installed, Figures 57 and 58 increasing the stagger angle at the higher β_{ave} angles (say 30°) does not provide lift modulation but does result in a variation in horizontal thrust.

Lift modulation versus stagger angle is also seen to be a non-linear relationship, therefore, symmetrical force changes require unsymmetrical changes in stagger angle. Based on a lift of 7050 pounds at $\beta_s = 10°$ and $\beta_{ave} = 0°$, to obtain control of 6610 $\pm$ 440 pounds requires a setting of $\beta_s = 22° \begin{smallmatrix} -12° \\ +8° \end{smallmatrix}$.

TABLE XIV

COMPARISON OF FAN-IN-WING AND FAN-IN-FUSELAGE THRUST COEFFICIENTS

Exit Louver Angle, β (deg.)	Fan-in-Fuselage Thrust Coefficient, H_T[a]	Fan-in-Wing Thrust Coefficient, H_T[a]
0	0.348	0.347
20	0.343	0.337
30	0.332	0.313
35	0.319	0.296

[a] $H_T = \frac{\phi^2 + \Psi}{2}$ (see Reference 6)

Fan Transient Aerodynamic Performance:

Fan response in terms of per cent lift is presented in Figures 59 through 61 for several throttle transients and diverter valve actuations. Table A-4 in Appendix A lists all of the transients conducted.

Acceleration:

Actual transient performance for engine acceleration is shown with predicted transient performance in Figure 59. Curve (A) in Figure 59 was obtained by using the J85-5 guarantee level acceleration characteristic, the fan polar moment of inertia and available and required torques from the turbine and fan based on fan design objectives. Curve (B) was estimated similarly except the measured J85-5 throttle response characteristic was used in place of the guarantee performance (1.4 seconds from 70% J85 speed to an engine terminal speed equivalent to 95% fan rpm versus the 5 seconds guarantee characteristic between J85-5 idle and military).

In comparing the actual performance with estimated for the same engine acceleration time shows very close agreement with the actual transient being slightly faster. These data indicate that not only can the fan response be significantly faster than that based on J85 guarantee level performance, but also that fan response with an engine just meeting guarantee performance would be essentially as predicted in Curve (A).

Transient performance is similarly presented in Figure 60 for fan acceleration via diverter valve actuation from the cruise to lift mode. The actual performance obtained for a diverter valve actuation time of 1.32 seconds appears to be significantly faster than estimated and this is probably the result of assuming a longer lag time in diverting air to the fan than actually occurs. This implies that actual performance for a 1 second actuation at military speed will

be somewhat better than the Curve (A) prediction. The only faster actuation data obtained (1.12 seconds) were for a lower fan terminal speed, however, the faster initial fan response is also apparent here.

Deceleration:

Figure 61 shows close agreement between actual and estimated curves for a diverter valve switch from the lift to cruise mode. The measured data do not begin with the same steepness as the estimated due to the inertia of the diverter valve doors. This means that a diverter valve switch at 100% fan lift will result in a curve as steep as the estimated but offset from it by approximately 0.2 seconds. Reducing the switch time from 1.3 seconds to 1 second may reduce this offset slightly.

Fan deceleration via an engine throttle chop is shown in Figure 62 for a 1.6 second throttle movement versus that estimated based on the maximum control operating speed of 1 second. The measured data in Figure 61 is very similar to the estimated 1 second throttle chop results in Figure 62 giving an indication of how the fan will respond to a faster throttle movement than actually tested.

J85 Overspeed:

Engine overspeeds of approximately 3.5% (e.g. from 16,240 rpm to 16,840 rpm) occurred during diverter valve switches. The overspeeds measured are listed in Table A-4. Figure 63 shows a typical oscillograph trace showing engine overspeed for one of the diverter valve switches.

This overspeed is similar to that experienced when the engine afterburner (provided with the J85-5 engine) is shut off and the effective area change causes the engine to follow the normal droop characteristic of the main fuel control. When the diverter valve switch

begins, a larger area is provided and the fuel requirement decreases. The fuel control reduces fuel flow, but it must follow a droop line to do so as shown in the sketch below and some overspeed results.

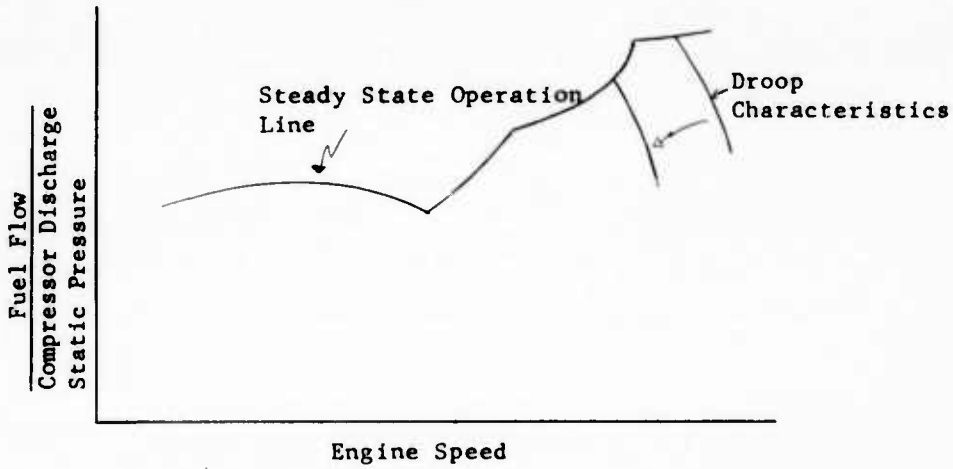

The overspeed and fuel reduction are both evident in Figure 63. When the area begins to reduce as the valve nears its terminal position, the engine follows the droop line back to the steady state operation line. If the system is operated with the diverter valve positioned part way between the terminal position for the lift and cruise modes without altering the door relative positions to maintain a constant effective area, a steady state overspeed condition would exist requiring a throttle position movement for correction.

Divided Flow Performance:

A divided flow test was made to simulate the capability for gradual conversion from the lift to cruise mode of operation. The flow was divided by separately actuated diverter valve doors to direct part

of the engine discharge to the fan and part to the cruise nozzle. In the ideal case the two doors and the fan scroll area and the jet nozzle area would be programmed to change simultaneously in such a manner as to maintain engine back pressure and temperature constant. This is for the primary reason of obtaining the maximum energy gas for driving the fan but as pointed out above would also prevent engine overspeed. For this test each door was moved separately a few degrees at a time. The temperatures were later obtained by determining engine horsepower from fuel flow; temperature then was calculated from this horsepower and measured weight flow and pressure.

Figure 64 shows a comparison of the predicted performance of three approaches to divided flow operation along with actual test data points. The per cent of design fan lift and per cent of engine thrust are plotted versus the per cent of total flow which is delivered to the fan turbine. The upper curves are calculated for the area compensated case which employs variable fan turbine nozzles and a variable jet nozzle to maintain temperature and pressure. The middle curves are calculated for a system with separately actuated diverter valve doors to provide the means for maintaining the engine back pressure and temperature. In maintaining the back pressure by this latter means, there would be increased pressure loss associated with the throttling effects of the doors and the performance would not be as high as obtained with area compensation using variable nozzles. It would, however, be better than performance that could be obtained if no area compensation were provided and back pressure and temperature were reduced because of increased effective area as shown in the lower curves. This third case is accomplished by switching both doors in their same relative position using a single actuation point; a severe drop in thrust and lift results.

The calculations for all the predicted curves assumed no additional

pressure loss for the variations in diverter valve door relative position.

The engine thrust data measured lie above the predicted curve for separately actuated doors because the predicted curve assumed the jet nozzle is flowing full. In the actual case the nozzle is apparently not flowing full; with the diverter valve door acting as the nozzle. This tends to simulate the area compensated case with A_8 variable. Additional pressure losses occur due to the inefficiency of this nozzle and any disturbed flow from the second door. As a result, the test data do not match the optimum performance shown by the upper curve. The scatter which is evident in the thrust ratio points may be indicative of unstable flow conditions in the valve and tailpipe. All data have been corrected to a common $T_{t\ 5.15}$.

Fan lift ratio data measured fall along the predicted curve for separately actuated doors. The flow through the scroll closely simulated the case used in obtaining the middle curve. No effect on lift ratio was expected because of "A_8" being variable instead of fixed. $A_{5.4}$ was not variable and the scroll very probably was flowing full (except for the one test point at 17.2% $W_{5.4}/W_{5.15}$) and corresponded to the conditions assumed for the middle curve for fan lift.

In order to determine the flow split, an iterative calculation process was used to satisfy continuity and energy: $T_{t5.15}$ and fan speed were known; $P_{t5.4}$ was measured in the scroll by only two single element probes, but this was the base point for assuming a value of $P_{t5.4}$; the ideal horsepower $HP_{5.4}$ to satisfy the measured speed was determined from known fan characteristics; from this power, the measured $T_{t5.15}$ and the assumed $P_{t5.4}$, the weight flow was calculated; with the weight flow, the turbine flow function

$W_{5.4}\sqrt{T_{t5.1}}/P_{t5.4}$ was calculated and compared with known fan characteristics versus $P_{t5.4}/P_{amb}$ ratio; new values of $P_{t5.4}$ were assumed and the process repeated until the calculated flow function agreed with known characteristics.

The test results agree very closely with the predicted performance and indicate that the predicted values can be safely used for transition analysis. At high flight speeds and low fan speeds, some judgement will still be required to predict the effect of fan inlet distortion on efficiency.

During low fan speed operation, high torque band temperatures were experienced due to the lack of cooling air pumped by the fan. Figure 65 is a plot of torque band temperature versus flow split and EGT ($T_{5.15}$).

A fan blade resonance was encountered at 975 rpm which had previously been observed in the fan vibration characteristic during engine acceleration to idle speed.

Diverter valve door vibrations did not occur at any of the door positions tested. A schematic of the diverter valve doors set for divided flow is shown in Figure 66 along with a tabulation of the different door positions tested.

D. FAN MECHANICAL PERFORMANCE

Testing of the lift fan system during this 50 hour program included a series of runs to study and evaluate fan mechanical performance for the wing mounted configuration. The tests have provided a definition of fan mechanical characteristics during operation conditions previously unexplored.[a]

[a] Review Section VI-A, Reference 1 for prior static test mechanical performance results.

Rotor Blade Stresses:

Cosine 2θ Mode - The wing inlet environment increased the cosine 2θ mode stress. The effects of the various configurations tested are difficult to analyze precisely, since it has been found that the rate of acceleration through the cosine 2θ mode has a somewhat unexpected effect on the stress amplitude. During most of the testing there was no attempt to use specific acceleration rates or even constant rates of acceleration through the 2θ speed range.

In general, the cosine 2θ stresses were 15,000 to 16,000[a] for the wing configuration with no inlet modification. With the baffle installed, the cosine 2θ stress dropped to 12,000 to 13,000 psi. Removing 80° of baffle appeared to have no effect. For a combination of the 360° inlet vane and a 180° baffle, the cosine 2θ stress appeared to increase slightly to 13,000 to 14,000 psi. With the inlet vane and no baffle, the stress ranged from 11,000 to 15,000 psi depending upon the rate of acceleration through the cosine 2θ speed level. Installation of the fuselage inlet reduced the stress to 8,000 to 9,000 psi, and this is the same stress level experienced with Fan 001 using the fuselage inlet. All of these values correspond to an exit louver setting of zero degrees; the effect of β on stress is discussed with transients.

First Flexural Mode - The first flexural stresses for Fan 002 and Fan 001 were about the same for tests of each using a fuselage inlet. The maximum stress occurred in the 1850 rpm speed region where the first flexural mode is in resonance with an 8/rev excitation. This stress was 6500 psi, or 88.5% of the running stress limit (57% of the absolute stress limit).

---

[a] All stress values are single amplitude unless otherwise noted.

Changing to the wing inlet had very little effect on the first flexural mode stress; at the resonance speed and above, the stress was increased only about 1000 psi.

Torsional Mode - The torsional mode stresses were the same for both fan-in-wing and fan-in-fuselage configurations and the stresses do not appear to have been affected by any of the inlet or baffle configurations used. The torsional mode stress was highest at 2375 rpm excited by a 12/rev component. The level was 6300 psi, or 78% of the running limit (50% of the absolute limit).

Torque Band - Tangential torque band stresses recorded as a function of speed during a slow acceleration and deceleration between idle and 2550 rpm are shown in Figure 67; this closely approximates steady state levels. The torque band design in this test was identical with that employed for the wind tunnel testing reported in Reference 3 which showed crack incidence after 23 hours of operation. Similar cracks appeared in the forward torque band after the ≈ 53 hour program discussed here. Slight cracks in two torque band tabs were noted during zyglo inspection which was also anticipated based on Reference 3 results. The stress levels are consistent with results measured during the Reference 3 testing; no particular significance is attached to the 30 hour difference in operating time before crack incidence which probably reflects the difference in test conditions and operating history between the two programs as well as variations in assembly. The failure analysis presented in Reference 3 applies here.

A design change to correct this problem has resulted in two new configurations, each of which will be demonstrated in future test programs.

Measured torque band stress compared with theoretical was very low.

To illustrate this Figure 68 was constructed as follows:

- The diverter valve actuation rate determines the rotor acceleration rate and this with the rotor polar moment of inertia are used to obtain the torque band force required to drive the rotor. Aerodynamic blade forces are ignored since the acceleration is fast.

- The acceleration was taken from idle to 2600 rpm.

- Three loading cases were analyzed:

  1. tangential - tension only; maximum possible loading (full torque loading carried in torque band).

  2. sinusoidal - one-half tension and one-half compression.

  3. sinusoidal plus admission arc effect - apply ratio of: $\frac{\text{buckets in in-active arc}}{\text{total buckets}} = \frac{199}{324}$ to account for the active arc buckets loading blades directly through tangs.[a]

- The measured tangential stress for accelerations between idle and 2450 rpm was extrapolated for the idle to 2600 rpm case to account for the different acceleration rate.

The force producing the torque required to drive the rotor is necessarily as shown and the low measured stress compared with the possible loading stresses that can be estimated is apparently the result of torque transmission in the inactive arc directly from

[a] A full admission turbine would not require a torque band.

carrier to carrier through torque band attachment bolts and covers rather than via the torque band itself.

Rotor Stress Response to J85 Throttle Transients - Data obtained from a series of timed accelerations and decelerations of the J85 engine between military and idle speeds are presented in Figures 69 through 73. Figures 69 and 70 show maximum blade and torque-band stress levels as affected by J85 acceleration or deceleration time. As pointed out in the discussion on cosine 2θ stress level, time is an important variable in limiting peak stress during transients through the rotor-disc system resonance speed; but primarily during deceleration. During acceleration, the resonance mode stress increases as a function of both increased exit louver angle and increased transient time. The exit louver adds a flow distortion and the transient time affects the residence time in the resonance mode. Deceleration transients show the same effect of increased stress due to increased exit louver setting, however, there is a peak stress for the intermediate transient time of about 5 seconds; either faster or slower decelerations reduced the maximum blade stress level.

Torque-band stresses were not sensitive to β position and were relatively unaffected by acceleration rate. They did exhibit a peak stress response during deceleration similar to the blades, with stresses being highest for a 5 second transient, however, the characteristic was far less pronounced.

In general, the blade and torque band stresses were higher during deceleration than acceleration.

Analysis of the transient recordings showed that the maximum blade stress was attained during approximately the first third of the deceleration transient while, for acceleration, maximum blade stress

occurred during the final half of the transient; also it should be noted that the initial speed is closer to the resonance speed prior to deceleration. This characteristic is shown in Figures 71 and 72.

Figure 73 is included to show that peak transient stresses occurred at a higher fan speed on an acceleration than a deceleration. These data also imply that a very fast transient during deceleration would tend to result in the peak stress occurring at an even lower fan speed which would be desirable (allowable vibratory stress increases as steady-state loadings are reduced).

There is as yet no positive explanation for the difference in blade stress level as the rotor is accelerated or decelerated through the cosine 2θ resonance; however, several speculations indicate this to be a reasonable characteristic. For example, considering the blade Campbell diagram in the sketch below, it can be seen that the exciting force is closer to the resonance characteristic in the speed range above the critical speed than below it. Also, the energy level of the exciting force is higher at the higher speeds. Thus, when decelerating, the conditions appear to be present for a larger exciting force. The possibility of the rotor exhibiting a non-linear "spring constant" characteristic is also a consideration which could influence this phenomenon.

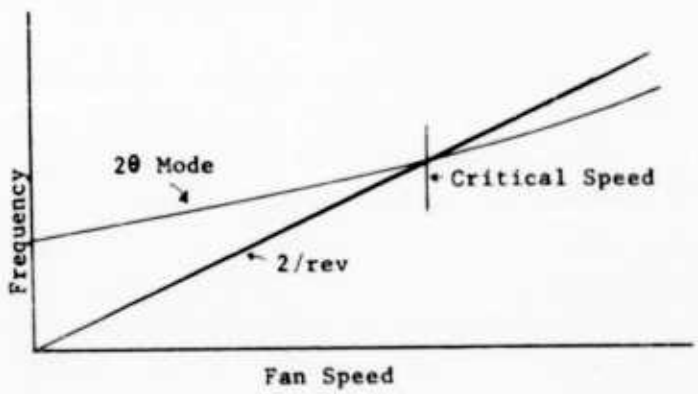

The exact nature of cosine 2θ exciting forces is not known although they may be from at least three sources:

1. Partial arc turbine (impulse entering and leaving the active arc).

2. Pressure distortions from the exit louver system.

3. Aerodynamic distortions at the fan inlet.

Diverter-Valve Transients - A series of runs to explore lift fan rotor behavior during conversion from lift to cruise and cruise to lift modes of operation was also conducted during this test program. Data have been accumulated on critical stress areas at various J85 power levels and diverter valve slew rates to permit extrapolation to full J85 power slew rates as fast as 0.10 seconds. The static test data indicate conversion will not be a problem, however, areas requiring further definition in the wind tunnel are blade and torque band stresses in the rotor system critical modes of vibration (cosine 2θ, cosine 3θ). (Fan-in-fuselage testing has shown that accelerations and decelerations through 2θ do result in an increase in blade and torque band stress levels as the excitation is strengthened by cross flow.)

Review of the transient recordings has been accomplished in considerable detail. Rotor maximum acceleration rate (see Figure 74 and a cross plot, Figure 75) increased as diverter valve actuation time decreased and also was higher for higher J85 power settings (indicated by fan terminal speed); Figures 76 through 79 show the fan speed response characteristics as a function of diverter valve actuation time with acceleration characteristics superimposed. Study of these curves shows the maximum acceleration to occur in the fan speed range between 700 and 1400 rpm. This is favorable

from the standpoint that the acceleration loading of the torque band occurs at a low steady-state stress condition. The fan speed at which maximum acceleration occurred was highest for the highest J85 power settings. The rotor stress characteristics during diverter valve transients were similar to those during throttle transients for the same instantaneous acceleration rates.

Pitch Maneuver Loading:

Stress - Rotor blade stress data from a series of simulated pitching maneuvers on a wing mounted fan have been studied for response to gyroscopic loading. Results include a comparison with analytical studies and predicted overall stress levels incurred by gyro loading during hover. Extrapolation of these data to high flight speeds is reserved until completion of fan-in-wing wind tunnel testing. Maximum gyroscopic loading demonstrated corresponded to a wing pitch angular velocity of 0.52 radians per second[a] with the fan operating at 2560 rpm (≈ 97% speed). Figure 80 is a typical transient recording of important parameters during a maneuver. Previous analyses of conventional turbomachinery indicate that the response is nearly linear with rotor speed for a given precession rate. However, the combination of long, flexible blades and the large tip mass characteristic of the lift fan results in significant deviations from a linear response with speed.

Analysis of predicted gyro effects was made to relate the effective blade dovetail bending moment, $M_{\eta e}$, to the leading edge root stress measured and to the rotor speed and precession rate respectively. $M_{\eta e}$ is an equivalent bending moment acting about the dovetail axis of maximum inertia, and approximates the effects of bending about both axes. Analysis has shown that for

[a] The transient recorder (Sanborn) directly indicated this to be 0.58 rad/sec.; however, differentiation of the wing position record versus time gave the lower value which should be more accurate.

a first approximation:

$$M_{\eta e} = M_{\eta} + 2.7\, M_{\xi}$$

where: M_{η} is the bending moment about the maximum inertia axis

M_{ξ} is the bending moment about the minimum inertia axis

These results are used in conjunction with dovetail strength data to determine permissible maneuver rates.

The accelerating force due to precession is of the form:

$$F_i = 2\, M_i\, \bar{r}_i\, \omega\, \Omega \cos\, \omega_t$$

Where: F_i = axial accelerating force acting on an element - lbs.

M_i = mass of element - lb. sec.^{2}/in.

$\bar{r}_i$ = radius from center of rotation to element - in.

ω = rotor speed - rad/sec.

Ω = precession rate - rad/sec.

t = time - sec.

If the blade is made infinitely flexible, the only resistance to deflection is provided by the centrifugal field which provides resistance proportional to rotor speed squared. To a first approximation the deflection would be of the form:

$$\delta_{axial} = C\, (\Omega/\omega) \qquad \text{where: } C \text{ is a constant}$$

This yields increasing deflection for a given precession rate as the rotor speed is reduced. In the other extreme, a blade having sufficient stiffness to make the centrifugal recovery component of restraint negligible would provide a constant resistance to deflection. In this case, the deflection would be proportional to the driving force and for a given precession rate, the deflection would increase linearly with speed.

The X353-5 system lies between these extremes resulting in the predicted response characteristics shown in Figure 81. This discussion does not include all of the dynamics that were incorporated in the analysis, but gives an insight into the differences between the fan behavior and the nearly linear behavior of conventional turbomachinery.

The test data plotted on Figure 81 is within -4 to +6% of the predicted results. The gyro loading tests have supplied data for two important parameters in fan mechanical design: First, the nonlinearity of stress as a function of rotor speed for constant precession rate has been verified; and second, because the data tend to agree closely with the analysis, extrapolation to higher loading conditions can be made with confidence. Figure 82 is an extrapolation of test data to 1 rad/sec. precessional loading during hover. Lines are shown to indicate existing blade dovetail stress limits; the reduction from absolute[a] to running limits results from the application of a 20% gage accuracy factor and a 20% blade-to-blade variation factor.

Figure 83 shows the magnitude of stress contribution which would result from various precession rates if the fan speed were held exactly at the cosine 2θ resonance speed. The addition of such

---

[a] Based on fatigue test data.

maneuver loadings to other blade loadings at the critical speed would exceed running limits for the rotor dovetail design tested. Modifications of the dovetail are planned which will overcome this deficiency. It is also to be noted that the stress response characteristic is very sharp at the critical speed similar to the shape of the total stress curves in Figure 82 near 2100 rpm; this makes it very difficult to operate precisely at the maximum stress condition because a very small change in speed results in a large reduction in stress. After wind tunnel data is obtained for the fan-in-wing configuration, it will be possible to estimate maximum combined loadings for anticipated flight conditions. Based on data presently available and the new limits of the modified rotor dovetail, preliminary extrapolations indicate sufficient margin to accommodate flight specification maneuver loadings at any transition condition including operation at the rotor critical speed.

Deflection - Figures 100a and 100b show the forward air seal at the three and twelve o'clock positions where the rotor deflected across the face of the seal and removed honeycomb with the torque-band lip. The material removed covered about 250° of arc intermittently and extended as much as 3/8 of an inch axially.

There was no stress or temperature effect indicated during any of these seal excursions.

Figure 84 is a plot of actual and estimated clearance change during the maneuver tests and showed excellent correlation. The maximum clearance statically is 0.700 inches, and the rotor deflection on this basis does not appear to be a problem.

Stator Vane Stress:

The wing inlet configuration increased the stator vane stresses. On the first runs of Fan 002 with no baffle, the vane stresses in-

creased gradually to 10,000 psi at 100% speed. This stress occurred on one vane near the minor strut (3 o'clock). The only other strain gaged vane, 180° away, exhibited quite low stress. The higher stressed stator vane was being excited by separated flow, the type of vibration that produces a rapidly modulating stress. The torsional and flexural modes were always present. At idle speed, the flexural mode was predominate. As speed approaches the vane torsional resonance, excited by the 36 rotor blades at 1980 rpm, the predominant stress changed to torsion. At high speeds, the stress was predominantly flexural.

When the baffle was installed, the vane stress peaked to 4500 psi at the torsional resonance speed, 1980 rpm, decreased to 2500 psi at 2050 rpm and then increased gradually to an average of 5000 psi with frequent peaks going to 6000 psi at 2600 rpm. The type of excitation was still separated flow and because this can result in large vane-to-vane stress variation, four more strain gages were added to vanes on the active arc side of the fan. More testing of this configuration found the vane near the minor strut still highest stressed and also showed vane stress to increase when the exit louvers were at $\beta_1 = \beta_2 = 35^\circ$. The vane stress was modulating with peaks of 12,000 psi. In moving from $\beta_1 = \beta_2 = 35^\circ$ to 40°, the vane stress peaked to 16,000 psi. This stress was primarily in the torsional mode and occurred on the vane near the minor strut. Two other vanes, one at 12 and 4:30 o'clock did not indicate this high stress.

With the inlet vane installed and with 180° of baffle, the stator stresses still increased at 2250 rpm when the louvers were closed as shown in Table XV. For the final configuration with the inlet vane installed and no baffle, the 3 o'clock vane stress at 2250 rpm and 35° β was 14,000 psi and the 4:30 vane stress 6500 psi. At 2450 rpm, the 3 o'clock vane stress increased from 2500 to 6000 psi and 4:30 o'clock vane stress from 3000 to 4000 psi as the louvers were moved from 0° to 35° closed.

TABLE XV

STATOR VANE STRESS AT 2250 RPM
(Inlet Vane Plus 180° Baffle Installed)

Arc β Setting (deg.)	Active 1:30 o'clock Vane (psi)	Active 3 o'clock Vane (psi)	Active 4:30 o'clock Vane (psi)	@ End of Scale 6 o'clock Vane (psi)
0	700	2000	2000	2000
10	700	2500	4500	2000
15	700	2500	4800	2500
20	700	3000	3200	2500
30	700	4000	5500	4000
35	2000	8500	9000	4500

The stress characteristic appears to be due to separated flow excitation near a per-rev excitation of a natural frequency. In this case, the stator vanes are excited at 1980 rpm in the torsional mode by the 36 rotor blades. As speed approaches 1980 rpm, the separated flow stress adds to the per-rev excitation stress. This total stress is not just a vector addition of the two types of vibration since the per-rev vibration aggravates the separated flow condition producing even higher stresses.

The lowest steady-state speed point at which the louvers were closed was 2250 rpm; however, accelerations were made through the 1980 rpm speed range with various exit louver settings. The stator stresses at the torsional resonance speed for these accelerations are shown in Table XVI. These data show the same trend of increasing stress as the louvers are closed. The data also show the trend of lower stress for faster accelerations (see Figure 85). During deceleration, the lowest stress occurred for a five second

transient time at $\beta = 0°$ and for a two second transient at $\beta = 35°$. The stresses in Table XVI are probably not the maximum that would be encountered if speed were held constant at the resonance point since the separated flow type of vibration is a randomly amplitude modulated stress, and the peaks during a transient may not occur at the same time as the resonance.

In general, rear frame stator stresses increase with longer acceleration and deceleration times and with higher exit louver settings. Bench fatigue tests of stator vanes with end conditions as in the rear frame are being conducted to relate these measured values with experimental limits. The effect of cross flow on the stator stress characteristic will be an important result of the fan-in-wing wind tunnel program.

Stationary Parts:

Frames - During this period of testing, the front frame, rear frame and scroll continued to operate without apparent effects from service loads or thermal cycling, and in addition, have demonstrated their ability to limit gyroscopic deflections to design levels (Figure 84).

Inlet Baffle - Several new inlet configurations were tested to improve the wing-installed performance of the fan. Mechanically, these configurations were accomplished by the addition of simple "test-type" components. A 0.030 inch thick sheet metal baffle was fusion welded to the bellmouth skin. Originally, this baffle was installed on the full 360° circumference of the fan and at that time no baffle stress levels above 2000 to 4000 psi (double amplitude) were observed. An 80° arc of this baffle was later removed and at that time, the stress level in the unsupported end of the baffle increased to 6000 to 10,000 psi d.a. This level was below the stress limit for the material used and did not limit the fan

TABLE XVI

STATOR VANE STRESSES
(Inlet Vane, No Baffle)

β Setting (deg.)	Transient[a] Time Sec.	4:30 o'clock Vane psi - SA	3:00 o'clock Vane psi - SA
0	10 - 15	5200	4000
0	5	4500	2500
0	1	3000	2500
10	10 - 15	5700	2500
10	5	6000	2500
10	1	4500	2000
20	10 - 15	8500	4500
20	5	9000	3500
20	1	6500	2500
30	10 - 15	10500	5500
30	5	8200	---
30	1	7700	---
35	10 - 15	11000	13000
35	5	9500	9500
35	1	7500	9000

[a] Acceleration rates are seconds from 1140 to 2450 rpm.

operation. Subsequently, the entire baffle was removed.

Circular Inlet Vane - The circular inlet vane tested (see Figure 4) was a solid stainless steel machined ring bolted into place and exhibited no stresses over 2000 psi during any fan operation.

Hardware Temperatures:

Progressive removal of the inlet baffle resulted in reduction of torque band temperatures. The use of the circular inlet vane (360°) had the effect of raising torque band operating temperature level to that equivalent to 270° of baffle when no vane was used. This amounts to a 50° to 70°F higher operating temperature relative to the fan-in-fuselage configuration. These results are shown in Figure 86.

The temperature characteristics of other rotor parts are shown in Figure 87 as a function of fan speed. These are approximately a linear function of exhaust gas temperature as shown by Figure 88 and all are with design limits. For a 100°F increase in exhaust gas temperature the following temperature rises can be expected:

Component	ΔT/100° EGT
Forward torque band lip	50°F
Blade-carrier pin	36
Rotor shaft	25
Aft torque band lip	15

Other hardware temperature characteristics are shown in Figure 89: exit louver, rear frame stator, forward frame, wing, scroll and scroll and diverter valve mount; it should be noted that there was no skin installed on the under side of the wing.

Temperature Cycling:

Table A-4, Appendix A lists the transient testing accomplished and the time - temperature change experiences for the hardware. Inspection of the hardware at the end of test has not shown any indication of trouble or malfunction due to this transient temperature cycling.

Conclusions which can be derived from the mechanical performance test results are:

1. The wing inlet has affected only the cosine 2θ resonance mode stress which varied from 130% to 180% of the fan-in-fuselage level depending on acceleration rate through the critical speed.

2. Combined blade loadings including maneuver loads require increased dovetail strength to meet design flight specifications.

3. Blade stress behavior during throttle or diverter valve transients is similar:
   - Stresses are highest during decelerations.
   - Deceleration stresses peak for a transient deceleration time of about five seconds.
   - Stresses during acceleration are a function of transient time and power level directly as they affect the residence time in the resonance speed range.

4. Maximum rotor acceleration always occurs at a speed lower than 50% fan rpm for a wide range of transient times and power levels.

5. The best acceleration transients (from a stress standpoint)

are the fastest and those with terminal fan speeds furthest from the cosine 2θ resonance speed.

6. The best deceleration transients (from a stress standpoint) are also the fastest; very slow decelerations (> 10 seconds) would also be favorable for low β settings.

7. Stator stress at high β settings may require additional stator damping particularly if cross flow increases the stress characteristic significantly.

8. Higher EGT's associated with J85-5 engines should not result in exceeding any fan temperature limits.

E. ENVIRONMENTAL FACTORS

Sound Levels:

In Reference 1 sound level measurements were reported based on far field data, 175 feet from the fan. At 90% speed sound pressure levels (SPL) of 97 db and 95 db were recorded for the overall (all octaves) and blade passing frequency noise levels respectively at this distance. This configuration was the X353-5 lift fan powered by facility air heated in a preburner. Considerable leakage air via a labyrinth seal to provide a flexible connection between the fixed air pipe line and the thrust frame was contributing to the overall noise level but the magnitude of this contribution was not measured.

During Run number 5 in this test program near field SPL data were recorded while the lift fan was powered by the J85-7 engine and operated at 100% speed. The microphone was located 11 feet from the engine inlet. The overall noise level at this distance was 126.3 db.

Table XVII compares these data and includes calculated power levels based on all octaves contributing and also for just blade passing frequency contributing.

During Run number 24 a sound pressure traverse was made 20 inches below the fan rotor blade trailing edge using a piezo-electric sensing element (see Section III). Sound data were recorded at 1113 rpm and 2565 rpm at 19 equally spaced stations one inch apart. The results of this traverse are shown in Table XVIII. This is a very accurate measure of fan exit noise level due to blade passing frequency separate from the J85 and fan inlet noise contributions. Three db has been added to the results in Table XVIII to account for the fan inlet which is assumed to be a discrete sound power source and, therefore, an equal contributor to total acoustical power level.[a]

The agreement of all the test data PWL values due to blade passing frequency is excellent. It is probably somewhat coincidental because there are several possible errors in sound measurement that would affect the data:

- measurement accuracy is about $\pm$ 2.5 db
- no humidity corrections were determined for the far field measurements.
- near and far field measurements are likely subject to some directivity.
- far field measurements are influenced somewhat by the presence of the facility personnel shield.
- speeds are not precisely identical.

---

[a] $\frac{PWL_2}{PWL_1} \propto 10 \log_{10} \frac{HP_2}{HP_1}$

TABLE XVII

COMPARISON OF NEAR AND FAR FIELD SOUND LEVEL MEASUREMENTS

Configuration	Measurement Distance (ft.)	1	2	3	4	5	6	7	8	Overall SPL (db)[a]	Overall Source Power Level PWL (db)[b]	Blade Passing Frequency PWL (db)[b]
		Blade Passing Frequency										
X353-5 + Preburner: 90% N_F	175	-	-	89	87	89	94	88	83	97	-	-
100% N_F[c]	175						96.5			98.5	151.3[d]	149.3[d]
X353-5 + J85-7: 100% N_F	10	105	106	110	111	115	123	122	115	126.3	154.3[d]	151[d]

[a] db relative to 0.0002 dynes/cm^2.

[b] db relative to 10^{-13} watts.

[c] Extrapolated from 90% N_F data.

[d] Attenuation assumed only for distance: $PWL = SPL + \left[(10 \log_{10} (2\pi R^2)\right]$

TABLE XVIII

FAN SOUND POWER LEVELS DUE TO BLADE PASSING FREQUENCY (TRAVERSE)

Fan Speed (rpm)	Fan Frequency (cps)	Component	PWL (db re 10^{-13} Watts)	Total PWL (db re 10^{-13} Watts)	
				Exit Only	Exit Plus Inlet Estimated
1113	668	1st Harmonic	124	125	128
	1336	2nd Harmonic	118		
2565	1540	1st Harmonic	143	146	149
	2080	2nd Harmonic	142		

The humidity correction is probably on the order of 1 db at 200 feet (attenuations in the 6th, 7th and 8th octave bands where fans passing frequency is predominate). The far field results given could be considered slightly pessimistic on this basis.

One significant difference noted between far field data obtained with the fan powered by facility air and both the near field and traverse data is that the second harmonic in the latter two cases was a noise source essentially equivalent to the first harmonic. Reviewing Table XVII shows that the second harmonic (7th octave) based on far field measurement at 90% speed was significantly lower (6 db) than the first harmonic (6th octave); Table XVIII also shows this to be the case at 42.5% speed based on traverse data. This leads to the conclusion that the blade passing frequency second harmonic contribution to overall acoustical power level is

not significant except at high fan speeds above 90%. The 100% speed PWL extrapolation for the initial test configuration in Table XVII is therefore probably low by about 3 db.

Sound data were also recorded for the cruise or turbojet mode of operation with the diverter valve set for straight through flow. Figure 90 is a comparison of the noise levels for the turbojet and lift fan modes of operation based on near field measurements. This shows a substantial reduction in noise level in the 3rd through 8th octaves at military speed for the lift fan mode. On the other hand, at idle[a] there is not a great deal of difference except, as can be sensed aurally; the lift fan has a lower low frequency characteristic at idle than the J85. It is not inconsistent with the previous discussion for the 6th and 7th octaves in the lift fan mode at idle to be nearly the same level in Figure 90; in this case, the J85 inlet noise is also involved in the result.

Additional data showing the individual station readings for the traverses is included in Appendix A, Table A-5.

Since the lift fan noise is predominantly high frequency, it will attenuate faster as a function of distance. This will be a significant reduction, at say 1000 feet, on the order of 4 db. This is not a total gain, however, because human reaction to noise is dependent to a large extent on the predominant frequencies and when noise is of high frequency, it is generally more objectionable. Weighting schemes such as the PNdb[b] system penalize the 6th, 7th and 8th octaves quite heavily in determining overall sound level.

---

[a] It should be noted that idle here is ≈ 40% fan rpm since the J85-7 idles at 72% rpm. Fan idle for a J85-5 engine will be ≈ 30 to 35% rpm since this engine version idles at 45% rpm.

[b] Perceived noise level - Bolt, Beranek and Newman, Inc., Cambridge, Massachusetts.

The tabulation below compares the db and PNdb systems of evaluating overall noise levels applied to the lift fan considering relative humidity to be 50%:

Distance from X353-5 Fan (feet)	db	PNdb
10	126.3	140
200	99	112
1000	82.8	94.5

The blade passing frequency pure tone is an accurate measure of fan speed. A comparison of the fan speed implied by the sound measurement data and as measured directly is shown in Table XIX. It is apparent from this table that the 1% to 3% variation in fan speed observed during test on the digital readout can be avoided by averaging the transient oscillograph recording. This was done for all performance data and the table shows that this is very nearly true fan speed.

TABLE XIX

SPEED MEASUREMENT COMPARISON

Reading Number	A. From Sound Measurements* (rpm)	B. From Sanborn* (rpm)	C. From Digital Readout Maximum (rpm)	Minimum (rpm)
438	1113	1105	1118	1089
443	2565	2570	2591	2548

*Average for duration of sound traverse.

Wind Velocity:

During the testing with the facility walls taken down, the variation in ambient wind velocity was found to have an influence on system lift. Since this is an uncontrollable variable, there is a paucity of data; however, there is apparently a lift variation with forward speed such that at very low velocities on the order of 15 feet per second, approximately a 6% loss in lift is experienced; this is recovered at wind velocities of about 25 feet per second.

Vertical lift is plotted in Figure 91 as a function of corrected fan speed and wind velocity with the louvers set at zero degrees. Figure 92 is a similar plot with the exit louvers removed and the exit measuring section installed. Lift is also plotted as a function of exit louver angle in Figure 93 for various wind speeds with all lift data corrected to 100% fan speed. Figures 94a, 94b and 94c show lines of constant suction pressure on the lower wing surface for a nearly constant fan speed and $\beta = 0°$, but for three different wind velocities: 0, 5, and 15 mph. Figure 95 is copied from Reference 3, showing the distribution of static pressure on the upper surface of the fuselage measured in the full scale fan-in-fuselage testing at Ames as a function of velocity ratio, V_p/V_{tip}. In Figure 96 the load cell readings for several different wind cases are shown and the effective center of lift is marked for each case. Figure 97 shows the specific load cell readings as they varied from predicted.

With this variety of data, analysis of the so-called "lift droop" phenomenon has proceeded, although by no means has it been concluded. Figures 91, 92 and 93 show some data scatter which is likely due to reduction of accuracy with gustiness; there is, nevertheless, a lift-droop trend which can be observed. Underwing static pressures are apparently not the cause of this lift loss. In Figures 94a, 94b and 94c the actual reduction in lift was measured

between 100 and 300 pounds, but the variation implied by pressure integration between any two runs (at constant fan speed) had a maximum value of only 50 pounds. A slightly decreased suction is apparent for the 15 mph case over the 5 mph case in the same direction as measured lift is varying, but again, of much less magnitude.

The similarity of Figure 91 and 92 indicates no change in the phenomenon when the measuring duct is installed. (There is an increase in fan momentum lift because of replacing the exit louvers with the exit duct which is not pertinent to this discussion.)

Recirculation was negligible in accounting for any lift loss since both fan and J85 inlet temperatures were within 1°F of the ambient temperature for the test points used in this analysis.

For the 0, 5 and 15 mph wind velocities, the fan rotor discharge total pressure ($P_{t\ 10.6}$) showed no appreciable difference between each case. If a flat speed line is assumed, an expression can be written for the change in fan flow associated with a depressed static pressure at the discharge:

$$(P_{t\ 11} - P_{amb})_1 = K\, W_F^2 \quad \text{(for no underwing suction)}$$

$$(P_{t\ 11} - P_{amb})_2 = K\, W_F^2 + \Delta P_s \quad \text{(with underwing suction)}$$

and

$$(P_{t\ 11} - P_{amb})_1 = (P_{t\ 11} - P_{amb})_2$$

$$\therefore \left(\frac{W_{F_2}}{W_{F_1}}\right)^2 = 1 - \frac{\Delta P_s}{P_{t\ 11} - P_{amb}}$$

ΔP_s is negative and was a maximum value of 0.4 inches H_2O at $(P_{t\ 11} - P_{amb}) \approx 40$ inches H_2O $\therefore \frac{W_{F_2}}{W_{F_1}} \approx 1.005$

Hence, underwing static pressure reduction could be responsible for 1/2% increase in mass flow or a thrust increase of 1% (about 70 pounds). The 0.4 inches H_2O suction used in this calculation was a maximum value; the nominal difference between any two runs was on the order of 0.1 inch H_2O. In addition to the change in flow, there would be a change in plug thrust in the opposite direction which would reduce the effect of wing pressure on fan momentum lift so that for all practical purposes the fan contribution to the measured thrust is independent of the wing underside pressure.

Reviewing the load cell data, it is seen that the center of lift moves slightly forward with increased wind velocity up to about 10 mph as shown in Figure 96. At 13 mph, the center of lift began moving back toward the zero forward speed position. It is apparent from Figure 97 that the loss occurred at the trailing edge load cell with the leading edge lift increasing somewhat. There was also a very slight increase in the tip region.

Smoke studies were conducted at Evendale to give a gross view of the stagnation streamlines bounding the flow into the fan and also the strength of any induced flow streams above or below the wing. A stagnation line was clearly defined on the wing upper surface about one foot from the trailing edge, although it was not possible to quantitatively identify any particular variation in its location with any test variable. (The full-scale results of the fan-in-fuselage at Ames, Figure 101, generally showed an effect of change in upper surface static pressure with forward speed such that the stagnation point shifts slightly.) The sketch in Figure 98 shows qualitatively the air flow patterns viewed which have been recorded on film for the Army Film Technical Progress Report of the Lift Fan Contract DA 44-177-TC-584.

In spite of data scatter, the trend toward a lift loss of about 6% between 5 and 15 mph cannot be mistaken. This "lift droop" measured is plotted in Figure 99 as a function of crossflow to through flow velocity ratio. It is at this point necessary to evaluate the data against one more variable, horsepower. The lift droop plotted in Figure 99 is for a constant fan speed. Reviewing the specific data points involved such as readings 505 and 507, it can be shown that a major portion of this lift loss can be accounted for by a change in fan power absorption as indicated in the following tabulation:

Reading	Approx. Wind Condition (mph)	Thrust Corrected to 100% N_F (lbs.)	% Change	HP @ 100% N_F	% Change
505	5 west	6850	-	4295	-
507	10 west	6575	4	4134	3.7

The power reduction corresponding to a 4% thrust reduction based on the fan laws would be $(0.96)^{3/2}$ or $\approx$ 6%. The power change measured however was only -3.7%. This indicates that, if the fan were allowed to overspeed by $(1.307)^{1/3}$ or $\approx$ 1.2%, the lift would increase by $(1.012)^2$ or $\approx$ 2.5%.

The significance of this is that there are apparently two aspects to the lift droop phenomenon:

a. power absorption effect
b. induced flow effect

Further, from analysis of the available data it appears that the induced effect (i.e., the variation of the stagnation streamline

position on the wing upper surface plus the associated induced flow fields) is a smaller and relatively constant value say 1.5 to 2.5% of fan lift. The remainder of the lift loss can be accounted for in every case by a reduction in fan power absorbed. The mechanism by which the wind causes the fan power absorption to vary in this manner is not defined, however, in some cases this was seen to be as much as 7 to 8% in power change.

Testing of a fan-in-wing configuration in a good low-speed tunnel with appropriate consideration to model to tunnel size relationship and with static pressure surveys conducted on the wing upper surface, along with additional data to analyze flow and pressure changes in the fan with wind velocity is considered essential to further understanding of this problem. It is likely that other variables such as employment of flaps would be significant, in this case probably advantageous (reduction of upper surface area behind fan). Some additional insight to this problem is anticipated during the forthcoming fan-in-wing wind tunnel program.

VI. HARDWARE INSPECTION RESULTS

A complete fan disassembly and parts inspection was accomplished in April following the testing. Detailed inspection results for each component are given below:

FORWARD FRAME AND SCROLL

1. Bearings showed no sign of wear.

2. The frame showed no sign of fatigue. No zyglo inspection was made.

3. The forward honeycomb, abradable air seal was rubbed intermittently over about 250° of the circumference, with the deepest radial rub at the 12 o'clock position (1/8 inch). The maximum axial rub occurred at the 3 o'clock position and penetrated approximately 3/8 inch. These are pictured in Figures 100a and 100b.

4. The scroll center mount (0°) bolts were loose, so the scroll was removed from the frame to tighten this mount. The bolts had been installed with an asbestos seal around the bolt head to prevent leakage; the asbestos was burned away. The mount was reassembled without this packing. Fan 001 has this same part eliminated.

5. The studs in the scroll seals were badly rusted and require replacement with A286 bolts.

6. All finger seals were in place.

7. The trunnion mounts were zygloed and no indications were found.

8. The insulation sections were visually inspected and appear to be satisfactory.

REAR FRAME

1. The insulation blanket had two spanwise rubs from the turbine bucket shrouds (Figure 101). This is the first rubbing experience at this location. Patches were made to fill these cuts from the back side.

2. Two saw cuts in the flange on the active arc side had separated (Figure 102) and several other saw cuts were compressed. These have been relieved. There are slight indications on the scroll where the rear frame interfered. These show up on the tie rod support legs and one of the scroll hot section re-inforcing ribs. The frame and tie rod supports will be relieved in these areas to provide more room for thermal growth.

3. The exit louvers were removed and reinstalled twice during the test program to accommodate the exit measuring section testing and then also removed at teardown. The ends of the aluminum louver near the hot stream show slight buckling and one was bent at the tip (Figure 103), due to a rub on the heat shield installed to cover the diverter valve mounts. No repair is planned. Normal wear on the louver actuation pins was noted. Some shimming will be required at reassembly to remove excess tolerance.

4. The honeycomb air seals had a slight rub at 12 o'clock.

5. No turbine shroud seals were installed during this test, and this did not result in any apparent adverse effects in the hardware, except as this may have contributed to the thermal growth interference with the scroll noted above.

ROTOR

1. Four spanwise cracks were found in the forward torque band at the end of testing. One of these is shown in Figure 104 (same type as observed with Fan 001, buildup No. 4).

2. The disc (SAE 4340 steel) was extremely rusted, showing the effect of being installed in the outside facility during five winter months. This has been cleaned.

3. Two torque-band tabs had slight cracks (via zyglo) similar to Fan 001, buildup No. 4, but not as severe.

4. Platforms were zygloed and were satisfactory.

5. One retainer ring had a zyglo indication on one platform tab. This retainer will be replaced.

6. Blades magnafluxed satisfactorily. No signs of dovetail fretting or wear.

7. One carrier had a zyglo indication about 1/4 inch long (Figure 105) on the side rail on one end. This carrier will have to be replaced.

8. The same carrier had lost part of one bucket tip shroud (Figure 106) and this may account for the insulation blanket rub on the rear frame.

9. The carrier pins have not been measured for bow, but they exhibit normal bow by visual inspection. Currently, these are considered expendable and are replaced at every buildup.

10. The covers showed no visible signs of wear.

DIVERTER VALVE

The valve and doors were zygloed and found to be essentially the same as before test. There were some small zyglo indications around some spot welds, but no change from before test. A few minor skin ripples due to high temperature operation were noted.

FRAME DEFLECTION TEST

Prior to removing the fan from the test facility, a frame deflection test was conducted. The fan was disconnected from the wing at 9 o'clock but retained in the wing mounts at 3, 6 and 12 o'clock. The wing fairing was removed and four dial indicators were located on the top edge of the bellmouth. The fan was pre-loaded at the 9 o'clock position with 25 pounds weight and a zero reading taken. Successive readings for 50 pounds additional weight were taken in increments to 225 pounds. Then, an additional weight of 190 pounds was used. For the 390 pounds applied after the preload, the maximum deflection (at the 9 o'clock position) was 0.185 inches and is shown as a function of load in Figure 107. Data were recorded at three other locations and are included in the figure.

Calculated deflection of the 9 o'clock position of the frames in the axial direction for the same loading is 0.270 inches. The results indicate the frame stiffness to be better than predicted since the actual deflection was 31.5% less than calculated. The circular inlet vane was installed for the deflection test and any added stiffness from this is not included in the calculation. Measured relative movement of the rotor and frames during gyro testing was discussed in a previous section (Pitch Maneuver Loading).

VII. RECOMMENDATIONS

The nature of the work under contract DA 44-TC-584 is such that specific individual recommendations are made in the regular and continuing working relationships between the contractor, TRECOM and NASA-Ames. Such recommendations are usually presented in correspondence and in the bi-monthly technical progress reports and are not restated here. Also, in the body of this report, individual technical recommendations are incorporated in the technical discussions of which they are appropriately an inseparable part.

The intent of this part of the report is to summarize the major program recommendations relating to the continuation of the work. These are:

A. Complete the present contract as planned which includes a wind tunnel test program for the X353-5 in a fan-in-wing configuration to be conducted at the NASA-Ames. This program provides for approximately 75 hours of wind tunnel testing including: determination of fan-in-wing characteristics and problems with various fan inlet and lift configurations; transition studies; longitudinal and lateral stability determination; roll, pitch and yaw control force capabilities, requirements and couplings; conversion point demonstration; and ground effect investigations. For part of the program, a rotor with reoriented blades for a higher power absorption - speed relationship and with a stronger dovetail attachment for combined load margin will be tested.

B. Begin the Flight Research Vehicle Program, as currently proposed, and the initiation of the propulsion system and aircraft programs. This will permit hardware design and procurement to proceed while the results of item (A) and previous testing are used to define the ground and flight tests of the Flight Research Program. In this way, orderly and continuous progress can be made toward the demon-

stration of a lift fan powered airplane in free flight.

C. Both TRECOM and General Electric make available to the NASA-Ames their respectively owned lift fans at the conclusion of the testing described in item (A). This would permit possible additional wind tunnel tests of the NASA fan-in-wing wind tunnel model modified to incorporate features of the selected flight research vehicle aircraft and would provide early determination of the aircraft characteristics.

D. Initiate a model test program to investigate the first order effects of aircraft configuration variations on lift, drag, pitching moment and interactions, and to identify transition requirements.

VIII. REFERENCES

1. Joyce, J., Fabrication, Test and Analysis of a Tip Turbine Lift Fan VTOL Propulsion System, Report of Phase I April 1959 - February 1960, USA TRECOM Contract No. DA 44-177-TC-584, Project No. 9R 38-01-017-04, Technical Report TREC 60-42, General Electric Company, Flight Propulsion Laboratory Dept., August 31, 1960, unclassified.

2. Przedpelski, Z.J., Results of Wind-Tunnel Tests of a Full Scale, Fuselage Mounted, Tip Turbine Driven Lift Fan, Report of Phase II, Volume 1, initial 20 hours of wind-tunnel tests, March - August 1960, USA TRECOM Contract No. DA 44-177-TC-584, Project No. 9R 38-01-020-02, Technical Report TREC 61-15, General Electric Company, Flight Propulsion Laboratory Dept., January 1961, unclassified.

3. Przedpelski, Z.J., Results of Wind-Tunnel Tests of a Full Scale, Fuselage Mounted, Tip Turbine Driven Lift Fan, Report of Phase II, Volume 2, additional 30 hours of wind-tunnel tests, September - December 1960, USA TRECOM Contract No. DA 44-177-TC-584, Project No. 9R 38-01-020-02, Technical Report No. TREC 61-15, General Electric Company, Flight Propulsion Laboratory Dept., April 1961, unclassified.

4. Downer, G.T., Engine Tests of a Full Scale J85-Size Diverter Valve for V/STOL Applications, R61FPD35, General Electric Company, Flight Propulsion Laboratory Dept., January 24, 1961, unclassified.

5. Przedpelski, Z.J., Simonson, M.R., Christner, S.N., X353-5 Scale Model Scroll Aerodynamics Test, R59FPD811, General Electric Company, Flight Propulsion Laboratory Dept., April 25, 1960, unclassified.

6. Przedpelski, Z.J., Results of Wind Tunnel Tests of a Full Scale, Fuselage Mounted, Tip Turbine Driven Lift Fan, Report of Phase II, Volume 3, additional 20 hours of wind tunnel tests in ground effect, January - June 1961, USA TRECOM Contract No. DA 44-177-TC-584, Project No. 9R 38-01-020-02, Technical Report No. TREC 61-15, General Electric Company, Flight Propulsion Laboratory Dept., October 1961, unclassified.

7. X353-5 VTOL Engine Study Data, DF59FPD547, General Electric Company, Flight Propulsion Laboratory Dept., July 1959, unclassified.

TABLE A-1

FAN PERFORMANCE CALCULATION STANDARDS

RESULT	HOW OBTAINED	FORMULA
System Vertical Lift	Direct Measurement - 3 Load Cells	N/A
System Horizontal Thrust	Direct Measurement - 2 Load Cells	N/A
Fan Rotor Pressure Ratio	Ratio of Rotor Exit to Rotor Inlet Average Total Pressure	$P_{t\,10.6} / P_{t\,10.3}$
Fan Stage Pressure Ratio	Ratio of Stator Exit to Rotor Inlet Average Total Pressure	$P_{t\,11.0} / P_{T\,10.3}$
Fan Rotor Temperature Ratio	Ratio of Rotor Exit to Rotor Inlet Average Total Temperature	$\frac{T_{t\,10.3} + \Delta T_{t\,10.6\text{-}10.3}}{T_{t\,10.3}}$
Fan Rotor Efficiency	Ideal Isentropic Temperature Rise Divided by Actual Temperature Rise	$\frac{T_{t\,10.3}\left[\left(\frac{P_{t\,10.6}}{P_{t\,10.3}}\right)^{\frac{\gamma-1}{\gamma}} - 1\right]}{\Delta T_{t\,10.6\text{-}10.3}}$
Fan Stage Efficiency	Ideal Isentropic Temperature Rise Divided by Actual Temperature Rise	$\frac{T_{t\,10.3}\left[\left(\frac{P_{t\,11.0}}{P_{t\,10.3}}\right)^{\frac{\gamma-1}{\gamma}} - 1\right]}{\Delta T_{t\,10.6\text{-}10.3}}$
Inlet Flow Coefficient	Evaluation of Boundary Layer Thickness from Boundary Layer Pressure Measurements	$C_{F\,10.2} = (P_{t\,B10.2}, P_{t\,10.3})$
Fan Weight Flow	Standard Compressible Flow Calculation	$C_{F10.2} A_{10.2} \sqrt{\frac{g}{R}} \frac{P_{t\,10.3}}{\sqrt{T_{t\,10.3}}} \left(\frac{P_{s\,10.2}}{P_{t\,10.3}}\right)^{\frac{1}{\gamma}} \sqrt{\frac{2\gamma}{\gamma-1}\left[1-\left(\frac{P_{s\,10.2}}{P_{t\,10.3}}\right)^{\frac{\gamma-1}{\gamma}}\right]}$
% Corrected Weight Flow	% of Design flow (534 lbs./sec.) corrected to Standard Conditions	$\frac{W_{10.2}\sqrt{\theta_{10.3}}}{\delta_{10.3}(5.34)}$
% Corrected Fan Speed	% of Design Speed (2640 rpm) corrected to Standard Conditions	$\frac{RPM}{\sqrt{\theta_{10.3}}(26.4)}$
Air Properties (Fan and Turbine)	Standard Equations Based on K&K Gas Tables	$C_p, \gamma, R, h = f(T, W, f)$
Fan H.P.	Power Absorbed by Fan	$\frac{778}{550}(\Delta T_{t\,10.6\text{-}10.3}) C_{p10.3} W_{10.2}$
Fan Rotor Thrust (Calculated)	Momentum Thrust Calculated at Rotor Exit	$\frac{W_{10.2}}{g}\sqrt{2gJC_p T_{t\,10.6}\left[1-\left(\frac{1}{\frac{P_{t\,10.6}}{P_{amb}}}\right)^{\frac{\gamma-1}{\gamma}}\right]}$
Fan Stage Thrust (Calculated)	Momentum Thrust Calculated at Stator Exit	$\frac{W_{10.2}}{g}\sqrt{2gJC_p T_{t\,10.6}\left[1-\left(\frac{1}{\frac{P_{t\,11.0}}{P_{amb}}}\right)^{\frac{\gamma-1}{\gamma}}\right]}$
Turbine Residual Thrust (Calculated)	Momentum Thrust Calculated at Turbine Stator Exit	$\frac{W_{5.6}}{g}\sqrt{2gJC_p T_{t\,5.6}\left[1-\left(\frac{1}{\frac{P_{t\,5.6}}{P_{amb}}}\right)^{\frac{\gamma-1}{\gamma}}\right]}$

Air Properties (Fan and Turbine)	Standard Equations Based on K&K Gas Tables	C_p
Fan H. P.	Power Absorbed by Fan	$\frac{778}{550}(\Delta T_{t10.6-10.3})C_{p10.3}W_{10.2}$
Fan Rotor Thrust (Calculated)	Momentum Thrust Calculated at Rotor Exit	$\frac{W_{10.2}}{g}\sqrt{2gJC_p T_{t10.6}\left[1-\left(\frac{1}{\frac{P_{t10.6}}{P_{amb}}}\right)^{\frac{\gamma-1}{\gamma}}\right]}$
Fan Stage Thrust (Calculated)	Momentum Thrust Calculated at Stator Exit	$\frac{W_{10.2}}{g}\sqrt{2gJC_p T_{t10.6}\left[1-\left(\frac{1}{\frac{P_{t11.0}}{P_{amb}}}\right)^{\frac{\gamma-1}{\gamma}}\right]}$
Turbine Residual Thrust (Calculated)	Momentum Thrust Calculated at Turbine Stator Exit	$\frac{W_{5.6}}{g}\sqrt{2gJC_p T_{t5.6}\left[1-\left(\frac{1}{\frac{P_{t5.6}}{P_{amb}}}\right)^{\frac{\gamma-1}{\gamma}}\right]}$
Total Calculated Thrust	Sum of Fan Stage and Turbine Residual Thrust	$F_{11.0}+F_{5.6}$
Turbine Leakage	From Heat Balance	$28\left[\frac{W_{10.2}(.115)(T_{t10.6}-T_{t10.6})}{W_{5.4}\left(\frac{C_{p5.4}}{C_{p10.3}}\right)(T_{t5.4}-T_{t5.6})}\right]$
Turbine Leakage	From Static Pressure Difference Between Fan and Turbine Stream and Clearance Area	$A_{cl}\sqrt{\rho_{6.45}\Delta P_{s5.45-10.3}}$
Product Efficiency	Ideal Fan Work Divided by Ideal Turbine Work	$\frac{W_{10.2}C_{p10.3}T_{t10.3}\left[\left(\frac{P_{t11}}{P_{t10.3}}\right)^{\frac{\gamma-1}{\gamma}}-1\right]}{W_{5.1}\left[h_{5.4}-h_{5.6\,ideal}\right]}$
Total Available H. P.	Total Available Turbine H. P. Assuming Isentropic Expansion to Ambient Pressure	$\frac{778}{550}W_{5.4}C_{p5.4}T_{t5.4}\left[1-\left(\frac{P_{amb}}{P_{t5.4}}\right)^{\frac{\gamma-1}{\gamma}}\right]$
% Reaction	Measure of Relative Velocity Ahead and Behind the Rotor from Static Pressure Data	$100\left(\frac{h_{s5.45\,ideal}-h_{s5.5\,ideal}}{h_{t5.4}-h_{s5.5\,ideal}}\right)$
Turbine H. P.	Actual Rate of Energy Extraction	$\frac{778}{550}W_{5.5}(h_{t5.4}-h_{t5.6})$
Turbine Energy Function	Energy Extraction from Turbine Divided by Total Inlet Energy	$\frac{h_{t5.4}-h_{t5.6}}{h_{t5.4}}$
Turbine Efficiency	Actual Energy Extraction Divided by Isentropic Energy Extraction	$\frac{h_{t5.4}-h_{t5.6}}{h_{t5.4}-h_{t5.6\,ideal}}$
Turbine Efficiency	Energy Absorbed by Fan Divided by Isentropic Energy Extraction	$\frac{W_{10.2}C_{p10.3}\Delta T_{t10.6-10.3}}{h_{t5.4}-h_{t5.6\,ideal}}$
Turbine Inlet Flow Function	Turbine Inlet Conditions of Temperature weight Flow and Pressure	$\frac{W_{5.4}\sqrt{T_{t5.3}}}{P_{t5.4}}$
Turbine Inlet Pressure	Calculated from Model Scroll and Elbow Test Results	$\frac{P_{t5.4}}{P_{t5.1}}=f\left(M_{n5.1}\right)$ Experimental Curve
All Mach Numbers	Calculated from Flow Function	$\frac{\frac{W\sqrt{TR}}{PA}}{\frac{W\sqrt{TR}}{PA}\text{ (Critical)}}=\frac{1.728\,M_n}{(1+.2M_n^2)^3}$
Turbine Weight Flow	Measured with an ASME Nozzle upstream of the facility burner plus fuel added in the burner.	$W_{5.1a\,94.4}\frac{P_{t1.0}}{\sqrt{T_{t1.0}}}\left(\frac{P_{s1.0}}{P_{t1.0}}\right)^{.7143}\bullet\left(1-\frac{P_{s1.0}}{P_{t1.0}}\right)^{\frac{1}{2}}+f$

TABLE A-2 DEFINITIONS AND SYMBOLS

A_F	Fan exit area = 17.8 sq. ft.
a_o	Sonic velocity, ft/sec.
AR	Wing aspect ratio, $\frac{b^2}{S_w}$
b	Wing span, ft.
c	Local wing chord, ft.
$\bar{c}$	Mean wing chord, $\frac{S_w}{b}$, ft.
c.g.	Center of gravity
c_{mac}	Mean aerodynamic chord $\int_{-b/2}^{b/2} \frac{c^2\,dy}{S_w}$
c_p	Specific heat at constant pressure, BTU/lb/°F
CIT	Compressor inlet temperature
C_Z	Fan average (or through flow) velocity, ft/sec.
db	Decibels relative to 0.0002 dynes/cm² or 10^{-13} watts
D_R	Ram drag, lbs.
EGT	Exhaust gas temperature
F	Total fan thrust, lbs.
F_x	Horizontal component of fan thrust, F [sin (α - β_V)], lbs.
F_y	Vertical component of fan thrust, F [cos (β_V - α)], lbs.
g	Acceleration due to gravity = 32.2 ft/sec.²
HP	Horsepower
H_T	Thrust coefficient, $\frac{F}{\rho A_F (V_{tip})^2}$
KC	Kilocycles
N_F	Fan speed, rpm or % of design = 2640 rpm at 100%
N_{J85}	Engine speed, rpm or % of design = 16,500 rpm at 100%
P	Pressure, lbs/sq. in.
PWL	Sound power level in decibels relative to 10^{-13} watts
SPL	Sound pressure level in decibels relative to 0.0002 dynes/cm²
S_w	Wing gross area
T	Temperature, °R or °F
V_p	Tunnel or airplane velocity, knots or m.p.h.
V_{tip}	Fan blade tip speed = 720 ft/sec. at 2640 rpm
V_p/V_{tip}	Velocity ratio parameter (nondimensional)
W	Weight flow, lbs/sec.
y	Spanwise location from aircraft centerline, ft.
α	Angle of attack, degrees or rotor angular acceleration, radians/sec.²
β	Indicated exit louver angle, degrees
β_1	Indicated exit louver angle for every other louver beginning with the first forward louver, degrees
β_2	Indicated exit louver angle for every other louver beginning with the second forward louver, degrees
β_s	Exit louver stagger angle = β_2 - β_1, degrees
β_V	Effective exit louver turning angle, degrees
γ	Specific heat ratio, c_p/c_v
δ	Pressure correction parameter, $P_{ambient}/14.696$
η_R	Fraction of velocity head recovered by fan inlet (includes static loss)
η_{Rotor}	Rotor efficiency = $\frac{\gamma_{10.6}}{\gamma_T}$
η_{Stage}	Stage efficiency = $\frac{\gamma_{11.0}}{\gamma_T}$
θ	Temperature correction parameter, $T_{ambient}/518.7$
ρ	Mass density, slugs/cu. ft.
ϕ	Flow coefficient = $\frac{C_{Z10.3}}{V_{tip}}$
Ψ	Pressure coefficient, $\frac{2}{\gamma-1} \frac{\left[\left(\frac{P_{t2}}{P_{t1}}\right)^{\frac{\gamma-1}{\gamma}} - 1\right]}{(V_{tip}/a_o)^2}$
ω	Rotor angular velocity, radians/sec.
$\bar{\omega}$	Loss coefficient in percent of velocity head at reference station
Ω	Gyroscopic precession rate, radians/sec.

SUBSCRIPTS

c	Corrected
F	Denotes fan
F	Denotes airplane
s	Denotes static
t	Denotes total
w	Denotes wing or wetted area
10.1, 5.3 etc.	Denotes measurement plane identification (See Figure 19.)

TABLE A-3 TEST RESULTS (50 HOUR FAN-IN-WING TEST - EVENDALE)

Run No.	Reading No.	Fan Speed (N_p) - RPM	Corrected Fan Speed ($N_p/\sqrt{\theta_{10.3}}$) - %	Fan Weight Flow (W_p) - lbs/sec	Corrected Fan Weight Flow ($W_p\sqrt{\theta_{10.3}}/\delta$) - %	Fan Inlet Temp. ($T_{10.3}$) - °R	Rotor Discharge Pressure Coefficient ($P_{10.6}$)	Stage Discharge Pressure Coefficient ($P_{11.6}$)	Diverter Valve Inlet Pressure ($P_{t\ 5.15}$) - psia	Fan Turbine Inlet Flow ($W_{5.4}$) - lbs/sec	Fan Turbine Inlet Temp. ($T_{t\ 5.4}$) - °R EGT	Fan Turbine Pressure Ratio ($P_{t\ 5.4}/P_{amb}$)	Corrected Available HP ($HP_{5.4}/\delta\sqrt{\theta_{10.3}}$)	Corrected Thrust (F/δ) - Lbs.	Vertical Thrust (F_y) - Lbs.	Horizontal Thrust (F_x) - Lbs.	Thrust Angle (β_y) - Deg.	Indicated Exit Louver Angle (β_1) - Deg.	Indicated Exit Louver Angle (β_2) - Deg.	J85 Corrected Speed ($N_{J85}/\sqrt{\theta_{2.0}}$) - %	Pressure Correction Parameter (δ)	Temperature Correction Parameter ($\sqrt{\theta_{10.3}}$)	Wind Velocity - MPH	Wind Direction (N-0°, E-90°, S-180°, W-270°)
1	1	0	0	0	0	NA	NA	NA	18.61	NA	NA	NA	NA	NC	NA	627	NA	NA	NA	72.1	1.002	NA	NM	NM
	2	0	0	0	0				20.94							1000				82.2				
	3	0	0	0	0				26.36							1772				92.4				
2	4	0	0	0	0	NA	NA	NA	17.49	NA	NA	NA	NA	NC	NA	400	NA	NA	NA	69.4	0.995	NA	NM	NM
	5								23.28							1160				90.6				
	6								30.01							2055				100.3				
	7	1111	41.8	NC	NC	526	NM	NM	17.25	NC	1380	NC	NC	1065	1085	34	1.8	0	0	67.6	1.003	1.007		
	8	1113	41.9			528			17.23		1402			1057	1070	37	2.0			67.7	1.008	1.008		
	9	2270	85.6			522			25.45	36.58	1448	1.599	2202	4190	4190	57	0.8			92.9	1.007	1.003		
3	10	0	0	0	0	NA	NA	NA	17.66	NA	1307	NA	NA	NC	NA	385	NA	NA	NA	69.9	0.992	NA	NM	NM
	11	2235	86.2	NC	NC	501	0.325	NM	25.68	37.60	1400	1.609	2291	4292	4288	70	0.9	0	0	93.6		0.982		
	12	2450	94.4			503	0.306		27.98	39.29	1547	1.750	3099	5102	5088	140	1.6			95.1		0.984		
	13	1147	44.1			506	NM		17.43	NC	1346	NC	NC	1167	1158	20	1.0			68.1		0.987		
	14	NM	NM			NM			29.63	42.23	1507	1.853		5595	5443	1085	11.3	10	10	NM		NM		
	15	2606	99.4			511			29.59	41.60	1547	1.855	3569	5547	5455	1060	11.9			96.6		0.993		
4	16	1158	NC	NC	NC	NC	NC	NC	NC	NC	1321	NC	NC	1518	1496	115	4.4	0	0	72.1	0.988	NM	NM	NM
	17	0	0	0	0	NA	NA	NA		NA	NA	NA	NA	NC	NA	685	NA	NA	NA	80.3		NA		
	18															805				88.2				
	19															1200				89.3				
	20															1580				95.3				
	21															1870				98.3				
	22															2125				101.4				
5	23	0	0	0	0	NA	NA	NA	NC	NA	NA	NA	NA	NC	NA	517	NA	NA	NA	70.4	0.991	NA	NM	NM
	24															873				81.5				
	25															1643				91.8				
	26															1993				95.8				
	27															2063				NC				
	28	1200	46.3	NC	NC	500	NC	NC		NC	1300	NC	NC	1205	1187	75	3.6	0	0	68.8	0.987	0.981		
	29	1155	44.4			505					1249			1164	1110	295	14.9	10	10	68.6		0.986		
	30	1658	63.2			512	0.339		20.26		1436			2315	2235	478	12.1			82.7		0.993		
	31	2200	84.4			507	0.327		25.10	35.50	1493	1.593	2258	4202	4037	950	13.2			91.6		0.988		
	32	1640	62.6			511	NC		20.07	NC	1393	NC	NC	2396	2312	500	12.2			82.2		0.992		
	33	1595	60.8			512	0.342		19.91		1410			2107	1913	838	23.7	20	20	81.4	0.991	0.993		
	34	1560	58.7			526	0.348		19.45		1464			1894	1535	1080	35.1	30	30	79.0		1.006		
	35	1580	59.1			532	0.353		19.56		1460			1855	1385	1209	41.0	35	35	79.4		1.012		

TABLE A-3 TEST RESULTS (50 HOUR FAN-IN-WING TEST - EVENDALE) Continued

Run No.	Reading No.	Fan Speed (N_p) - RPM	Corrected Fan Speed ($N_p/\theta_{10.3}$) - %	Fan Weight Flow (W_a) - lbs/sec	Corrected Fan Weight Flow ($W_a\sqrt{\theta_{10.3}}/\delta$) - %	Fan Inlet Temp ($T_{10.3}$) - °R	Rotor Discharge Pressure Coefficient ($T_{10.6}$)	Stage Discharge Pressure Coefficient ($T_{11.0}$)	Diverter Valve Inlet Pressure ($P_{t\ 5.1}$) - psia	Fan Turbine Inlet Flow ($W_{5.4}$) - lbs/sec	Fan Turbine Inlet Temp. ($T_{t\ 5.4}$) - °R EGT	Fan Turbine Pressure Ratio ($P_{t\ 5.4}/P_{amb}$)	Corrected Available HP ($HP_{5.4}/\delta\sqrt{\theta_{10.3}}$)	Corrected Thrust (F/δ) - Lbs.	Vertical Thrust (F_y) - Lbs.	Horizontal Thrust (F_x) - Lbs.	Thrust Angle (ξ_v) - Deg.	Indicated Exit Louver Angle (β_1) - Deg.	Indicated Exit Louver Angle (ζ_2) - Deg.	J85 Corrected Speed ($N_{J85}/\theta_{2.0}$) - %	Pressure Correction Parameter (δ)	Temperature Correction Parameter ($\sqrt{\theta_{10.3}}$)	Wind Velocity - MPH	Wind Direction (N-0°, E-90°, S-180°, W-270°)
5	36	1620	60.8	NC	NC	529	0.353	NC	19.71	NC	1435	NC	NC	1841	1254	1326	45.8	40	40	79.9	0.991	1.010	NM	NM
	37	1690	64.0			520	0.364		20.24		1413			1856	1162	1425	50.4	44	44	81.6		1.000		
	38A	1672	63.9			512	NC		20.66		1363			2406	2374	60	1.5	0	0	83.3	0.987	0.993		
6	38B	1153	NC	NC	NC	NM	NC	NC	NC	NC	NC	NC	NC	1454	1433	22	0.9	0	0	69.0	0.985	NC	NM	NM
	39	1152												1435	1413	32	1.3			69.0				
	40	1150												1224	1205	45	2.1			68.7				
	41	1137												1288	1083	662	31.4	30	30	67.7	0.985			
7	42	1133	43.9	NC	NC	496	NC	NC	NC	NC	NC	NC	NC	1150	1118	237	12.0	10	10	67.9	0.994	0.978	NM	NM
	43	1657	64.3			494			20.63		1346			2373	2300	525	12.9			84.1		0.976		
	44	1625	63.0			495			20.24		1348			2304	2290	45	1.1	0	0	83.4		0.977		
8	45	1180	45.4	NC	NC	503	NC	NC	17.54	NC	NM	NC	NC	1222	1211	6	0	0	0	69.5	0.991	0.984	NM	NM
	46	1650	63.2			509			20.46		1363			2346	2320	150	3.7			83.1		0.990		
	47	1670	63.8			510			20.59		1367			2425	2320	625	15.1	10	10	93.3		0.991		
	48	2240	85.4			512			25.74	36.01	1534	1.624	2420	4497	4305	1153	15.0			92.6		0.993		
	49	2240	85.4			511			25.64	NC	NM	1.619	NC	4415	4362	344	4.5	0	0	91.8		0.993		
	50	2440	93.7			505			28.09	38.53	1625	1.771	3286	5396	5320	545	5.8			95.0		0.986		
	51	2255	86.0			513			25.71	36.16	1524	1.624	2409	4506	4453	333	4.3			92.0		0.993		
	52	2410	91.9			514			27.41	37.94	1592	1.727	2975	5215	5014	1255	14.0	10	10	94.6		0.996		
	53	1615	61.8			509			20.14	NC	1399	NC	NC	2227	2193	-245	-6.4	-15	-5	81.9		0.990		
	54	1623	62.2			509			20.23		1408			2083	2053	-211	-5.9	-20	0	81.9				
	55	1610	61.6			509			19.93		1421			1869	1848	-120	-3.3	-21	+2	81.4				
	56	1625	62.1			510			20.15		1395			2206	2180	155	3.5	-5	+5	81.9		0.991		
	57	1620	62.1			507			20.11		1403			2212	2184	183	4.0	-10	+10	82.0		0.988		
	58	1625	62.2			509			20.19		1401			1992	1968	148	3.7	-12	+12	82.2		0.990		
	59	1650	63.1			510			20.29		1394			NC	NM	NM	NC	5	15	82.9		0.991		
	60	1640	62.7			510			20.39		1391			2222	2146	495	13.0	0	20	83.1		0.991		
	61	1637	62.3			514			20.32		1396			1984	1912	458	13.5	-2	+22	82.7		0.995		
	62	1670	63.8			510			20.58		1372			2354	2086	1043	26.6	15	25	83.3		0.991		
	63	1660	63.5			509			20.47		1376			2160	1946	891	24.6	10	30	83.2		0.990		
	64	1695	64.7			512			20.68		1365			2099	1927	783	22.1	7	32	83.4		0.993		
	65	1692	64.9			507			20.61		1376			2245	1633	1510	42.8	30	40	83.2		0.988		
	66	1710	65.6			507			20.60		1391			1929	1450	1247	40.6	25	45	82.8		0.988		
	67	1705	65.4			509			20.53		1396			1747	1343	1093	39.2	22	47	82.7		0.990		
	68	1630	62.4			509			20.44		1395			2286	2184	603	15.4	5	15	82.9		0.990		
	69	1635	62.2			514			20.31		1383			2312	2054	1015	26.4	20	20	82.9		0.995		

TABLE A-3 TEST RESULTS (50 HOUR FAN-IN-WING TEST - EVENDALE) Continued

Run No.	Reading No.	Fan Speed (N_F) - RPM	Corrected Fan Speed ($N_F/\sqrt{\theta_{10.3}}$) - %	Fan Weight Flow (W_F) - lbs/sec	Corrected Fan Weight Flow ($W_F\sqrt{\theta_{10.3}}/\delta$) - %	Fan Inlet Temp. ($T_{10.3}$) - °R	Rotor Discharge Pressure Coefficient ($P_{18.6}$)	Stage Discharge Pressure Coefficient ($P_{11.0}$)	Diverter Valve Inlet Pressure ($P_{t\ 5.15}$) - psia	Fan Turbine Inlet Flow ($W_{5.4}$) - lbs/sec	Fan Turbine Inlet Temp. ($T_{t\ 5.4}$) - °R EGT	Fan Turbine Pressure Ratio ($P_{t\ 5.4}/P_{amb}$)	Corrected Available HP ($HP_{5.4}/\delta\sqrt{\theta_{10.3}}$)	Corrected Thrust (F/δ) - Lbs.	Vertical Thrust (F_y) - Lbs.	Horizontal Thrust (F_x) - Lbs.	Thrust Angle (β_v) - Deg.	Indicated Exit Louver Angle (β_1) - Deg.	Indicated Exit Louver Angle (β_2) - Deg.	J85 Corrected Speed ($N_{J85}/\sqrt{\theta_{2.0}}$) - %	Pressure Correction Parameter (δ)	Temperature Correction Parameter ($\sqrt{\theta_{10.3}}$)	Wind Velocity - MPH	Wind Direction (N-0°, E-90°, S-180°, W-270°)
8	70	1715	65.6	NC	NC	510	NC	NC	20.82	NC	1377	NC	NC	2308	1677	1555	42.8	35	35	83.8	0.991	0.991	NM	NM
	71	2230	85.1			511			25.26	35.69	1488	1.595	2253	4009	2681	2937	42.6			91.2		0.993		
	72	2220	85.1			508			25.54	36.49	1470	1.612	2337	3922	2558	2931	41.3	30	40	91.6		0.989		
	73	2260	85.1			511			25.50	36.19	1488	1.610	2332	3617	2235	2808	38.8	25	45	91.1		0.993		
	74	2245	85.4			514			25.52	35.80	1524	1.611	2353	4382	4330	336	4.5	0	0	91.6		0.996		
	75	2255	85.7			516			25.60	35.77	1539	1.616	2394	4420	4370	310	4.0			91.8		0.997		
	76	1650	63.3			507			20.48	NC	1406	NC	NC	2417	2387	210	5.0			84.0		0.988		
	77	2250	85.8			513			25.69	35.89	1544	1.622	2417	4508	4457	317	4.1			92.2		0.993		
	78	2470	94.0			515			28.08	38.47	1628	1.770	3364	5510	5443	440	4.6			95.2		0.996		
	79	2240	85.6			510			25.74	36.10	1530	1.626	2427	4567	4510	380	4.8			92.3		0.991		
	80	2460	93.9			511			28.06	38.63	1610	1.769	3351	5434	5372	391	4.2			95.1		0.993		
	81	2260	86.3			513			25.88	36.25	2532	1.633	2459	4625	4578	234	2.9			92.2		0.993		
	82	1655	63.3			510			20.52	NC	1408	NC	NC	2409	2382	170	4.1			81.1		0.991		
9	83	1154	44.2	NC	NC	507	NC	NC	17.45	NC	1364	NC	NC	1197	1180	130	6.3	0	0	69.1	0.992	0.988	NM	NM
	84	1200	46.0			508			17.64		1328			1185	940	705	36.8	30	30	69.7		0.990		
	85	1605	61.3			511			20.35		1382			2344	2315	215	5.3	0	0	82.7		0.992		
	86	2245	85.7			511			26.00	36.18	1550	1.643	2522	4668	4605	380	4.7			92.9	0.990			
	87	2455	93.4			514			28.28	39.03	1604	1.784	3293	5481	5250	1370	14.6	10	10	96.1		0.995		
	88	1130	43.1			512			17.48	NC	1317	NC	NC	1177	1125	305	15.2			70.0		0.993		
	89	1630	62.1			513			20.68		1368			2481	2375	625	14.7			84.7		0.994		
	90	2260	85.4			521			25.87	36.54	1504	1.635	2413	4360	4145	1205	16.2			93.8		1.002		
	91	2470	93.4			522			28.12	39.27	1567	1.774	3170	5411	5190	1330	14.4			96.1				
	92	2600	98.3			522	0.341		29.86	40.84	1634	1.884	3752	6017	5775	1460	14.2			98.0				
	93	2270	86.2			518	NC		26.07	36.87	1504	1.647	2485	4617	4410	1200	15.2			94.2		0.998		
	94	2435	92.2			520			28.07	38.86	1592	1.775	3194	5390	5145	1370	14.9			96.7	0.988	1.000		
	95	2615	99.0			519	0.345		30.31	40.94	1672	1.916	3946	6196	5925	1540	14.6			98.7				
	96	2265	86.1			516	NC		26.32	36.99	1528	1.666	2600	4686	4480	1170	14.7			94.2		0.997		
	97	1655	62.9			516			20.57	NC	1383	NC	NC	2403	2365	215	5.2	0	0	84.3				
	98	1710	65.0			516			21.10		1374			2533	2265	1065	25.2	20	20	85.5				
	99	1715	65.2			515			21.35		1381			2470	1960	1455	36.6	30	30	85.4		0.996		
	100	1737	66.6			507			21.12		1380			2640	1780	1655	42.9	35	35	85.5		0.988		
	101	1710	65.4			510			21.26		1381			2359	1535	1755	48.8	40	40	85.7		0.991		
	102	1800	65.4			505			21.39		1377			2174	1280	1725	53.4	44	45	86.0		0.987		
	103	0	0	NA	NA	NA	NA	NA	17.53	NA	NA	NA	NA	NC	NA	510	NA	NA	NA	69.5		NA		
	104	0	0						30.46							2495				101.5				

TABLE A-3 TEST RESULTS (50 HOUR FAN-IN-WING TEST - EVENDALE) Continued

Run No.	Reading No.	Fan Speed (N_F) - RPM	Corrected Fan Speed ($N_F/\theta_{10.3}$) - %	Fan Weight Flow (W_F) - lbs/sec	Corrected Fan Weight Flow ($W_F\sqrt{\theta_{10.3}}/\delta$) - %	Fan Inlet Temp. ($T_{10.3}$) - °R	Rotor Discharge Pressure Coefficient ($P_{10.6}$)	Stage Discharge Pressure Coefficient ($P_{11.6}$)	Diverter Valve Inlet Pressure ($P_{t\ 5.15}$) - psia	Fan Turbine Inlet Flow ($W_{5.4}$) - lbs/sec	Fan Turbine Inlet Temp. ($T_{t\ 5.4}$) - °R EGT	Fan Turbine Pressure Ratio ($P_{t\ 5.4}/P_{amb}$)	Corrected Available HP ($HP_{5.4}/\delta\sqrt{\theta_{10.3}}$)	Corrected Thrust (F/δ) - Lbs.	Vertical Thrust (F_y) - Lbs.	Horizontal Thrust (F_x) - Lbs.	Thrust Angle (β_v) - Deg.	Indicated Exit Louver Angle (β_1) - Deg.	Indicated Exit Louver Angle (β_2) - Deg.	J85 Corrected Speed ($N_{J85}/\theta_{2.0}$) - %	Pressure Correction Parameter (δ)	Temperature Correction Parameter ($\theta_{10.3}$)	Wind Velocity - MPH	Wind Direction (N-0°, E-90°, S-180°, W-270°)
9	105	1100	42.0	NC	NC	510	NC	NC	17.27	NC	1380	NC	NC	1108	1050	310	16.5	10	10	69.1	0.988	0.991	NM	NM
	106	1675	64.0			511			20.86		1372			2505	2375	690	16.2			84.9	0.987	0.992		
	107	2270	86.4			514			25.91	36.42	1519	1.642	2472	4598	4390	1150	14.7			95.3		0.995		
	108	2450	92.9			518			28.05	38.87	1584	1.770	3176	5324	5090	1305	14.4			96.9		0.999		
	109	2605	98.7			520			30.15	40.99	1651	1.907	3887	6001	5745	1442	14.1					1.000		
	110	2240	85.2			515			25.95	36.33	1530	1.644	2484	4585	4365	1195	15.3			94.7		0.996		
	111	2460	93.0			521			28.23	38.98	1602	1.786	3267	5394	5145	1370	14.9			96.8		1.002		
	112	2603	98.6			520			30.07	41.04	1641	1.903	3865	6059	5780	1535	14.9			98.9		1.000		
	113	2240	85.0			517			25.88	35.72	1579	1.639	2499	4553	4383	340	4.4	-5	+5	94.8		0.998		
	114	2255	85.8			515			25.98	35.92	1574	1.645	2538	4278	4215	265	3.6	-10	+10	94.3		0.996		
	115	2260	85.9			515			25.92	35.80	1577	1.642	2532	3868	3810	240	3.6	-15	+15	93.6				
	116	1654	62.8			517			20.59	NC	1383	NC	NC	2303	2180	645	16.5	10	10	84.7		0.998		
	117	1150	44.0			509			17.33		1295			1149	1070	375	19.3			68.9		0.990		
	118	1660	63.0			518			20.40	27.45	1413	1.310		2405	2280	660	16.2			83.1		0.998		
	119	2265	85.6			521			25.74	35.85	1547	1.631	2448	4539	4325	1170	15.1			91.9		1.002		
	120	1164	44.4			513			17.31	NC	1326	NC	NC	1151	1090	320	16.4			68.0		0.994		
10	121	1106	42.6	NC	NC	501	NC	NC	17.39	NC	1344	NC	NC	1133	1105	250	12.8	10	10		0.986		NM	NM
	122	1632	62.8			503			20.45		1344			1360	1265	500								
	123	1090	41.8			507			17.08		1372			1031	1010	205	11.5							
	124	1658	63.5			508			20.80		1402			2455	2395	540	12.7							
	125	2275	87.0			509			26.02		1526			4461	4365	920	11.9							
	126	2260	86.9			503			26.14	36.71	1532	1.658	2602	4646	4580	100	1.2	0	0	94.3		0.985		
	127	2265	87.0			504			26.20	36.73	1536	1.662	2604	4671	4505	955	12.0	10	10	95.4		0.986		
	128	2253	85.9			513			25.78	35.96	1549	1.636	2471	4566	4500	125	1.6	0	0	94.6		0.994		
	129	1675	63.9			512			20.92	NC	1402	NC	NC	2516	2480	70	1.6			84.7		0.993		
	130	1668	63.8			509			20.65		1382			2411	2320	520	12.7	10	10	85.2		0.990		
	131	2285	87.4			509			26.47	37.39	1516	1.680	2668	4765	4590	980	12.0	10	9.5	95.1		0.990		
	132	2268	86.8			509			26.30	37.26	1509	1.669	2607	4740	4665	195	2.4	0	0	95.2		0.990		
	133	2260	85.5			520			26.25	37.31	1493	1.666	2553	4653	4580	160	2.0	-5	+5	95.1		1.001		
	134	2284	87.2			516			26.35	36.81	1551	1.672	2642	4487	4420	20	0.3	-10	+10	93.8		0.997		
	135	2272	85.6			524			NM	NC	1527	NC	NC	3837	3780	45	0.7	-15	+15	94.4		1.005		
	136	2270	87.4			503			26.21	36.85	1526	1.663	2584	3885	3620	1240	18.9	5	35	94.7		0.984		
	137	2262	86.7			505			26.21	36.96	1517	1.663	2593	4365	4010	1550	21.2	10	30	94.6		0.987		
	138	2265	86.7			509			26.18	36.82	1526	1.662	2590	4509	4125	1645	21.7	15	25	94.7		0.990		
	139	2268	86.7			510			26.36	38.88	1545	1.672	2653	4606	4160	1810	23.5	20	20	94.4		0.991		

TABLE A-3 TEST RESULTS (50 HOUR FAN-IN-WING TEST - EVENDALE) Continued

Run No.	Reading No.	Fan Speed (N_p) - RPM	Corrected Fan Speed ($N_p/\theta_{10.3}$) - %	Fan Weight Flow (W_p) - lbs/sec	Corrected Fan Weight Flow ($W_p\sqrt{\theta_{10.3}}/\delta$) - %	Fan Inlet Temp. ($T_{10.3}$) - °R	Rotor Discharge Pressure Coefficient ($T_{10.6}$)	Stage Discharge Pressure Coefficient ($T_{11.0}$)	Diverter Valve Inlet Pressure ($P_{t\ 5.15}$) - psia	Fan Turbine Inlet Flow ($W_{5.4}$) - lbs/sec	Fan Turbine Inlet Temp. ($T_{t\ 5.4}$) - °R EGT	Fan Turbine Pressure Ratio ($P_{t\ 5.4}/P_{amb}$)	Corrected Available HP ($HP_{5.4}/\delta\sqrt{\theta_{10.3}}$)	Corrected Thrust (F/δ) - Lbs.	Vertical Thrust (F_y) - Lbs.	Horizontal Thrust (F_x) - Lbs.	Thrust Angle (θ_v) - Deg.	Indicated Exit Louver Angle (β_1) - Deg.	Indicated Exit Louver Angle (ξ_2) - Deg.	J85 Corrected Speed ($N_{J85}/\theta_{2.0}$) - %	Pressure Correction Parameter (δ)	Temperature Correction Parameter ($\theta_{10.3}$)	Wind Velocity - MPH	Wind Direction (N-0°, E-90°, S-180°, W-270°)
10	140	2263	86.7	NC	NC	508	NC	NC	26.16	36.70	1533	1.661	2597	4438	3815	2135	29.3	25	25	95.0	0.985	0.989	NM	NM
	141	2300	88.2			507			26.48	37.25	1528	1.680	2682	4486	3605	2555	35.3	30	30	94.9		0.988		
	142	2250	86.1			509			26.00	36.58	1524	1.651	2537	4171	3105	2690	41.0	35	35	94.4		0.990		
	143	2242	86.1			505			26.46	NC	NM	NC	NC	4661	4495	935	11.8	10	10	NM		0.987		
	144	2215	84.6			511			25.93					4579	4465	640	8.2	6	6			0.992		
	145	2310	88.3			510			27.06					5051	4950	500	5.8	3	3			0.991		
	146	2320	88.9			506			26.97					5030	4950	175	2.0	0	0			0.988		
	147	2325	89.2			505			27.16					5089	5015	-110	-1.3	-3	-3			0.987		
	148	2320	88.9			505			27.13					5072	4985	-335	-3.9	-6	-6			0.987		
	149	2310	87.5			519			26.79					4817	4710	-570	-6.9	-9	-9			1.000		
	150	1669	64.1			508			20.84		1404			2478	2380	540	12.8	10	10	83.9		0.987		
	151	1630	62.0			515			20.26		1374			1939	1300	1400	47.1	40	40	83.8		0.996		
	152	1645	62.7			513			20.23		1385			1729	1065	1330	51.3	44	45	83.0		0.994		
	153	1095	42.0			507			17.19		1328			1063	1025	215	11.9	10	10	69.1		0.988		
	154	1125	42.8			515			17.21		1303			1116	1075	230	12.1			69.1		0.996		
	155	2275	86.3			518			26.23	36.82	1531	1.662	2577	4688	4520	945	11.8			94.7		0.999		
	156	2455	92.7			523			28.30	39.51	1565	1.791	3204	5453	5265	1120	12.0			97.2	0.987	1.003		
	157	2447	91.8			528			27.80	38.75	1575	1.760	3073	5289	5220	25	0.3	0	0	96.5		1.009		
	158	2448	92.5			522			27.78	38.47	1582	1.758	3077	5242	5140	-590	-6.6	-10	-10	96.2		1.003		
	159	2432	91.7			523			27.56	38.09	1590	1.745	3016	5111	5040	-230	-2.6	-10	0	95.8		1.004		
	160	2417	90.8			528			27.33	37.66	1599	1.730	2943	5077	5010	-115	-1.3	-5	-5	96.0		1.008		
	161	2458	92.3			529			28.01	38.61	1608	1.773	3176	5333	5255	300	3.3	0	0	96.4		1.009		
	162	2450	92.5			523			27.99	38.85	1574	1.771	3128	5432	5305	775	8.3	5	5	96.6		1.003		
	163	2440	92.3			521			28.24	39.33	1574	1.787	3200	5391	5175	1240	13.5	10	10	97.4		1.001		
	164	2470	93.8			516			28.57	39.80	1563	1.807	3302	5470	5135	1665	17.9	15	15	97.5		0.997		
	165	2462	93.8			513			28.59	39.89	1558	1.809	3315	5449	4925	2160	23.7	20	20	97.6		0.994		
	166	2455	93.4			514			28.34	39.73	1543	1.793	3200	5133	4130	2935	35.4	30	30	97.3		0.995		
	167	2462	94.1			510			28.02	39.16	1552	1.773	3153	4509	3035	3255	47.0	40	40	96.7		0.991		
	168	2460	93.7			513			27.93	39.29	1533	1.767	3091	4453	3115	3100	44.9	35	45	96.7		0.994		
	169	2467	94.1			512			27.93	39.33	1532	1.769	3107	4284	2980	3000	45.2	38	47	95.2		0.993		
	170	2457	94.0			509			27.94	39.34	1530	1.768	3099	4113	3580	1915	28.8	15	45	96.9		0.990		
	171	2445	93.7			507			28.38	39.85	1538	1.786	3260	4694	3935	2445	31.8	20	40	97.1		0.988		
	172	2450	93.6			513			28.28	39.81	1530	1.789	3199	5076	4185	2755	33.4	25	35	97.2		0.994		
	173	2456	94.0			508			28.40	39.81	1544	1.797	3256	5326	4890	1930	21.5	15	25	97.4		0.989		
	174	2450	93.6			511			28.38	39.80	1542	1.796	3243	5103	4730	1730	20.1	10	30	97.3		0.992		

TABLE A-3 TEST RESULTS (50 HOUR FAN-IN-WING TEST - EVENDALE) Continued

Run No.	Reading No.	Fan Speed (N_p) - RPM	Corrected Fan Speed ($N_p/\theta_{10.3}$) - %	Fan Weight Flow (W_p) - lbs/sec	Corrected Fan Weight Flow ($W_p\sqrt{\theta}/\delta_{10.3}$) - %	Fan Inlet Temp. ($T_{10.3}$) - °R	Exter Discharge Pressure Coefficient ($C_{10.6}$)	Nozz Discharge Pressure Coefficient ($C_{11.0}$)	Diverter Valve Inlet Pressure ($P_{t\ 5.15}$) - psia	Fan Turbine Inlet Flow ($W_{5.4}$) - lbs/sec	Fan Turbine Inlet Temp. ($T_{t\ 5.4}$) - °R EGT	Fan Turbine Pressure Ratio ($P_{t\ 5.4}/P_{amb}$)	Corrected Available HP ($HP_{5.4}/\delta\sqrt{\theta}_{10.3}$)	Corrected Thrust (F/δ) - Lbs.	Vertical Thrust (F_y) - Lbs.	Horizontal Thrust (F_x) - Lbs.	Thrust Angle (β_v) - Deg.	Indicated Exit Louver Angle (β_1) - Deg.	Indicated Exit Louver Angle (β_2) - Deg.	J85 Corrected Speed ($N_{J85}/\theta_{2.0}$) - %	Pressure Correction Parameter (δ)	Temperature Correction Parameter ($\sqrt{\theta}_{10.3}$)	Wind Velocity - MPH	Wind Direction (N-0°, E-90°, S-180°, W-270°)
10	175	2450	92.9	NC	NC	518	NC	NC	27.94	39.37	1538	1.769	3085	4469	4215	1300	17.1	5	35	96.4	0.987	0.999	NM	NM
	176	2448	92.9			517			28.14	39.40	1559	1.781	3178	4728	4620	655	8.1	-5	+25	96.9		0.998		
	177	2443	93.4			510			28.35	39.71	1557	1.795	3278	5249	5100	915	10.2	0	20	97.2		0.991		
	178	2460	93.6			515			28.69	39.92	1578	1.816	3368	5545	5370	1055	11.1	5	15	97.4		0.996		
	179	2480	93.4			525			28.15	38.96	1595	1.782	3189	4731	4670	5	0.1	-15	+15	96.5		1.006		
	180	2420	90.8			428			27.78	38.48	1593	1.758	3070	5057	4990	110	1.4	-10	+10	96.0		1.009		
	181	2450	91.9			530			27.99	38.76	1594	1.772	3117	5297	5225	175	1.9	-5	+5	97.4		1.010		
	182	2448	91.8			530			27.88	38.71	1586	1.764	3094	5260	5180	350	3.9	0	0	96.0		1.010		
	183	2595	97.1			532			29.73	40.21	1670	1.881	3742	5734	5840	430	4.2			98.3		1.012		
	184	2590	97.4			527			29.66	40.11	1668	1.877	3732	4929	5850	170	1.7	-5	+5	NC		1.007		
	185	2603	98.0			526			29.62	39.96	1677	1.874	3728	5697	5620	175	1.8	-10	+10			1.006		
	186	2610	98.4			524			29.79	NC	NM	1.885	NC	5279	5210	55	0.6	-15	+15			1.005		
	187	2455	92.6			524			28.16	39.13	1580	1.782	3181	5382	5170	1220	13.3	10	10	96.8		1.004		
	188	2600	99.1			513			30.09	41.88	1575	1.904	3809	6053	5835	1280	12.4			NC		0.994		
	189	1137	43.3			515			17.29	NC	1301	NC	NC	1090	1040	275	14.8			81.0		0.996		
11	190	1100	42.1	NC	NC	509	NC	NC	17.37	NC	1312	NC	NC	1158	1155	55	NA	NA	NA	68.3	0.99	0.990	NM	NM
	191	1625	61.4			522			20.82	32.94	1365	1.438	1491	2545	2535	105				84.1		1.003		
	192	1610	60.8			523			20.40	NC	1358	NC	NC	2476	2465	100				83.8				
	193	1640	61.0			537			20.44		1344			2446	2435	45				84.1		1.018		
	194	1660	63.0			517			20.83		1322			2596	2585	50				84.4		0.998		
	195	1670	63.4			516			20.96		1308			2676	2665	10				84.4		0.997		
	196	1640	62.0			519			20.86		1325			2652	2640	70				84.7		1.001		
	197	1610	60.6			526			20.27		1357			2345	2335	75				83.4		1.006		
	198	1680	63.3			523			20.98	30.62	1226	1.330	943	2562	2550	90				84.8		1.004		
	199	1705	64.1			528			20.96	30.36	1245	1.329	982	2516	2505	70				84.7		1.008		
	200	1735	65.2			527			20.91	30.27	1237	1.326	962	2442	2430	80				84.6		1.007		
	201	1730	65.0			528			20.88	30.08	1245	1.325	958	2411	2400	75				84.4		1.009		
	202	2300	86.3			528			26.34	38.96	1384	1.651	2396	4771	75	110				94.6				
	203	2230	84.1			524			26.12	38.74	1375	1.638	2358	4810	4790	90				93.8		1.005		
	204	2255	84.7			528			26.34	38.37	1372	1.622	2275	4484	4465	60				93.5		1.009		
	205	2260	84.9			528			26.18	38.20	1363	1.619	2219	4484	4465	50				93.4				
	206	2240	84.1			529			26.22	38.79	1385	1.644	2374	4770	4750	85				94.0				
12	207	1115	42.2	NC	NC	521	NC	NC	NC	NC	1353	NC	NC	918	901	-2	NA	NA	NA	68.7	0.982	1.002	NM	NM
	208	1660	62.9	314	59.9	518			20.66	28.67	1341	1.325	1006	2594	2547	-6				85.1		1.000		
	209	2251	86.1	425	80.1	509			26.24	37.13	1509	1.665	2569	4912	4824	-20				95.1		0.990		

TABLE A-3 TEST RESULTS (50 HOUR FAN-IN-WING TEST - EVENDALE) Continued

Run No.	Reading No.	Fan Speed (N_p) - RPM	Corrected Fan Speed ($N_p/\theta_{10}^{.5}$) - %	Fan Weight Flow (W_p) - lbs/sec	Corrected Fan Weight Flow ($W_p\sqrt{\theta_{10}}/\delta_{10}$) - %	Fan Inlet Temp. (T_{10}) - °R	Rotor Discharge Pressure Coefficient ($P_{10.6}$)	Stage Discharge Pressure Coefficient ($P_{11.0}$)	Diverter Valve Inlet Pressure ($P_{t\ 5.15}$) - psia	Fan Turbine Inlet Flow ($W_{5.4}$) - lbs/sec	Fan Turbine Inlet Temp. ($T_{t\ 5.4}$) - °R EGT	Fan Turbine Pressure Ratio ($P_{t\ 5.4}/P_{amb}$)	Corrected Available HP ($HP_{5.4}\sqrt{\theta}/\delta_{10.3}$)	Corrected Thrust (F/E) - Lbs.	Vertical Thrust (F_y) - Lbs.	Horizontal Thrust (F_x) - Lbs.	Thrust Angle (θ_v) - Deg.	Indicated Exit Louver Angle (θ_1) - Deg.	Indicated Exit Louver Angle (θ_2) - Deg.	J85 Corrected Speed ($N_{J85}/\theta_{2.0}^{.5}$) - %	Pressure Correction Parameter (δ)	Temperature Correction Parameter ($\theta_{10.3}$)	Wind Velocity - MPH	Wind Direction (N-0°, E-90°, S-180°, W-270°)
12	210	2407	92.1	454	85.8	508	NC	NC	28.26	39.28	1579	1.790	3246	5658	5555	-102	NA	NA	NA	97.5	0.982	0.990	NM	NM
	211	2573	98.6	479	90.3	507			30.25	41.24	1647	1.916	3948	6488	6370	136				99.3		0.989		
	212	2209	84.5	422	79.6	509			26.01	36.95	1497	1.651	2491	4810	4723	-34				94.9		0.990		
	213	2421	92.6	454	85.8	508			28.33	39.36	1580	1.794	3271	5733	5629	-94				97.4		0.990		
	214	2548	98.0	NC	NC	503			30.37	41.26	1659	1.924	4024	6477	6357	194				99.5		0.985		
	215	1643	62.8	318	60.5	510			20.79	28.78	1360	1.332	1024	2587	2540	33				85.2		0.999		
	216	1105	41.7	NC	NC	523			NC	NC	1304	NC	NC	1119	1099	21				68.8		1.004		
	217	1104	41.7			523					1327			1154	1132	52				68.9		1.003		
	218	1651	62.8			516			20.74	28.58	1368	1.330	1028	2639	2591	52				85.2		0.996		
	219	2222	84.6			514			24.50	34.56	1501	1.576	2159	2944	4855	17				95.2		0.995		
	220	2427	92.4			514			28.66	39.57	1605	1.815	3422	5888	5781	86				97.6		0.995		
	221	2556	NC			NM			29.95	NC	NM	NC	NC	6510	6393	31				NM		0.996		
	222	1664	63.3			515			20.72	28.40	1383	1.328	1029	2605	2557	57				84.6		0.996		
	223	1108	41.7			525			17.10	NC	1320	NC	NC	1132	1112	-8				68.7		1.005		
13	224	OMITTED																						
	225	1093	41.8	NC	NC	513	NC	NC	17.15	NC	1330	NC	NC	1085	1114	31	NA	NA	NA	68.5	0.992	0.994	NM	NM
	226	1120	42.7			518			17.13		1365			1090	1119	11				67.5		0.999		
	227	1668	63.3			523			20.71		1402			2444	2472	49				84.1		1.003		
	228	2275	85.9			530			26.42	36.65	1567	1.661	2593	4786	4814	6				94.7		1.010		
	229	2480	93.2			530			28.50	38.76	1648	1.790	3283	5510	5539	79				96.4		1.010		
	230	1100	NC			NM			NM	NC	NM	NC	NC	1085	1114	41				67.8		NM		
	231	1682	63.6			524			20.98		1383			2507	2536	51				84.9		1.004		
	232	2275	85.9			531			26.25	36.34	1576	1.652	2494	4686	4706	86				94.2		1.011		
	233	2505	94.1			532			28.44	38.61	1654	1.786	3264	5468	5496	51				95.7		1.012		
	234	1115	42.2			NM			NC	NC	NM	NC	NC	1070	1099	61				68.2		NM		
	235	1650	62.1			521			20.65		1386			2403	2432	39				84.4		1.002		
	236	2300	86.6			529			26.53	36.97	1558	1.670	2626	5711	4739	134				94.5		1.010		
	237	2452	92.2			531			28.35	38.62	1644	1.782	3245	5445	5474	94				96.6		1.011		
	238	2255	84.8			529			26.15	36.36	1560	1.646	2512	4543	4572	91				93.5		1.010		
	239	2470	92.5			535			28.30	38.44	1654	1.779	3230	5405	5434	96				96.1		1.015		
	240	2280	85.6			530			26.00	35.89	1579	1.637	2493	4535	4564	98				93.4		1.010		
	241	2250	84.9			524			26.18	36.20	1578	1.648	2551	4615	4644	126				93.8		1.004		
	242	1645	62.2			522			21.66	NC	1377	NC	NC	2408	2437	91				84.6		1.003		
	243	1100	41.8			515			17.24		1316			2037	2066	31				68.7		0.996		
14	244	1100	41.8	NC	NC	515	NC	NC	17.02	NC	1283	NC	NC	NA	NA	NA	NA	NA	NA	67.2	0.976	0.996	NM	NM

TABLE A-3 TEST RESULTS (50 HOUR FAN-IN-WING TEST - EVENDALE) Continued

Run No.	Reading No.	Fan Speed (N_p) - RPM	Corrected Fan Speed ($N_p/\sqrt{\theta_{10.3}}$) - %	Fan Weight Flow (W_p) - lbs/sec	Corrected Fan Weight Flow ($W_p\sqrt{\theta_{10.3}}/\delta$) - %	Fan Inlet Temp. ($T_{10.3}$) - °R	Rotor Discharge Pressure Coefficient ($P_{10.8}$)	Stage Discharge Pressure Coefficient ($P_{11.8}$)	Diverter Valve Inlet Pressure ($P_{t\ 5.15}$) - psia	Fan Turbine Inlet Flow ($W_{5.4}$) - lbs/sec	Fan Turbine Inlet Temp. ($T_{t\ 5.4}$) - °R EGT	Fan Turbine Pressure Ratio ($P_{t\ 5.4}/P_{amb}$)	Corrected Available HP ($HP_{5.4}/\delta\sqrt{\theta_{10.3}}$)	Corrected Thrust (F/δ) - Lbs.	Vertical Thrust (F_y) - Lbs.	Horizontal Thrust (F_x) - Lbs.	Thrust Angle (θ_v) - Deg.	Indicated Exit Louver Angle (θ_1) - Deg.	Indicated Exit Louver Angle (θ_2) - Deg.	J85 Corrected Speed ($N_{J85}/\sqrt{\theta_{2.0}}$) - %	Pressure Correction Parameter (δ)	Temperature Correction Parameter ($\sqrt{\theta_{10.3}}$)	Wind Velocity - MPH	Wind Direction (N-0°, E-90°, S-180°, W-270°)
14	245	1660	63.0	NC	NC	516	NC	NC	20.46	NC	1378	NC	NC	NA	NA	NA	NA	NA	NA	85.7	0.976	0.997	NM	NM
	246	2220	86.5			513			26.02	36.65	1520	1.666	2590							95.4		0.994		
	247	1115	42.3			516			17.07	NC	1310	NC	NC							70.9		0.997		
	248	1055	39.5			531			17.55		1367									67.1		1.012		
	249	1670	63.4			516			20.78		1372									85.0		0.997		
	250	1590	60.1			521			20.04		1417									83.7		1.002		
	251	1600	60.3			522			20.04		1417									83.7		1.003		
	252	1660	62.9			519			20.2		1425									83.9		1.000		
	253	1630	61.7			520			19.99		1417									83.3		1.001		
	254	1600	60.2			526			19.68		1431									83.4		1.007		
	255	1510	56.9			525			19.25		1444									82.1		1.006		
	256	1540	58.0			524			19.55		1414									84.2		1.005		
	257	2285	86.5			520			26.08	36.18	1572	1.663	2622							94.6		1.001		
	258	2275	86.1			520			25.92	36.02	1563	1.654	2560							93.6		1.001		
	259	2225	84.1			522			25.46	35.47	1551	1.626	2410							93.1		1.002		
	260	2273	86.1			520			25.36	35.08	1567	1.618	2406							92.8		1.001		
	261	2265	85.0			528			25.21	NC	NM	1.610	NC							NM		1.009		
	262	2220	82.4			540			25.11	34.73	1564	1.603	2285							92.5		1.020		
	263	2220	82.4			540			24.99	NC	NM	1.596	NC							NM		1.020		
	264	2245	84.9			522			25.50	35.44	1558	1.628	2443							92.4		1.002		
	265	2225	83.8			526			25.53	NC	NM	1.629	NC							NM		1.006		
	266	2230	84.2			522			25.56	35.81	1536	1.632	2441							92.9		1.003		
	267	2245	84.6			525			25.44	35.52	1544	1.624	2405							92.7		1.006		
	268	2265	85.7			520			25.29	35.44	1528	1.615	2370							92.2		1.001		
	269	2230	84.0			525			25.09	34.95	1542	1.603	2294							92.9		1.006		
	270	2240	84.4			524			25.37	35.27	1552	1.619	2396							92.6		1.005		
	271	2245	84.9			521			25.66	35.86	1543	1.637	2481							93.2		1.002		
	272	1655	62.5			523			20.44	NC	1418	NC	NC							83.4		1.003		
	273	1645	62.0			523			20.33		1441									84.0		1.004		
	274	1670	63.0			523			20.30		1440									83.9		1.004		
	275	1660	62.3			530			20.07		1459									82.2		1.010		
	276	1615	60.6			530			20.26		1440									83.0		1.010		
	277	1660	62.4			528			20.11		1469									83.3		1.008		
	278	1665	62.6			526			20.38		1420									86.0		1.007		
	279	1635	61.7			523			20.31		1413									85.0		1.004		

TABLE A-3 TEST RESULTS (50 HOUR FAN-IN-WING TEST - EVENDALE) Continued

Run No.	Reading No.	Fan Speed (N_p) - RPM	Corrected Fan Speed ($N_p/\theta_{10.3}$) - %	Fan Weight Flow (W_p) - lbs/sec	Corrected Fan Weight Flow ($W_p\sqrt{\theta_{10.3}}/\delta$) - %	Fan Inlet Temp. ($T_{10.3}$) - °R	Rotor Discharge Pressure Coefficient ($C_{10.6}$)	Stage Discharge Pressure Coefficient ($C_{11.0}$)	Diverter Valve Inlet Pressure ($P_{t\ 5.15}$) - psia	Fan Turbine Inlet Flow ($W_{5.4}$) - lbs/sec	Fan Turbine Inlet Temp. ($T_{t\ 5.4}$) - °R EGT	Fan Turbine Pressure Ratio ($P_{t\ 5.4}/P_{amb}$)	Corrected Available HP ($HP_{5.4}/\delta\sqrt{\theta}_{10.3}$)	Corrected Thrust (F/δ) - Lbs.	Vertical Thrust (F_y) - Lbs.	Horizontal Thrust (F_x) - Lbs.	Thrust Angle (β_y) - Deg.	Indicated Exit Louver Angle (β_1) - Deg.	Indicated Exit Louver Angle (β_2) - Deg.	J85 Corrected Speed ($N_{J85}/\theta_{2.0}$) - %	Pressure Correction Parameter (δ)	Temperature Correction Parameter ($\sqrt{\theta}_{10.3}$)	Wind Velocity - MPH	Wind Direction (N-0°, E-90°, S-180°, W-270°)
14	280	1085	40.7	NC	NC	528	NC	NC	16.82	NC	1436	NC	NC	NA	NA	NA	NA	NA	NA	66.7	0.976	1.009	NM	NM
15	281	1111	41.8	NC	NC	528	NC	NC	17.34	NC	1285	NC	NC	1289	1275	20	0.90	NA	NA	68.6	0.989	1.008	NM	NM
	282	1660	62.1			533			20.52		1372			2574	2545	45	1.01			83.5		1.013		
	283	1658	61.9			535			20.55		1380			2585	2555	60	1.35			83.6		1.015		
	284	2257	84.1			536			25.79	36.82	1478	1.632	2365	4707	4655	50	0.62			92.3		1.016		
	285	2260	84.6			531			25.68	36.50	1490	1.625	2357	4683	4630	70	0.87			92.9		1.012		
	286	2245	84.1			530			25.52	36.34	1481	1.615	2303	4556	4505	40	0.51			92.3		1.011		
	287	1645	61.3			537			20.30	NC	1370	NC	NC	2472	2445	20	0.47			82.9		1.017		
	288	1160	43.3			535			17.43	NC	1241	NC	NC	1284	1270	15	0.68			68.5		1.015		
16	289	1100	NC	NC	NC	NC	NC	NC	NC	NC	NC	NC	NC	NC	NA	NA	NC	0	0	NC	NC	NC	NM	NM
17	290	1105	42.5	NC	NC	503	NC	NC	NC	NC	NC	NC	NC	NM	NM	NM	NM			69.7	0.989	0.984	NM	NM
	291	1102	42.4			503														69.2		0.984		
	292	1110	42.9			500														69.4		0.981		
	293	1649	63.6			501														85.0		0.982		
	294	2466	94.0			513														97.5		0.994		
	295	1117	43.1			500														69.4		0.981		
	296	2240	85.9			507														94.7		0.988		
18	297	1128	42.8	NC	NC	516	NC	NC	NM	NC	NC	NC	NC	NC	NM	NM	NC	0	0	69.8	0.994	0.997	NM	NM
	298	1140	43.2			519														70.2		1.000		
	299	1655	62.6			520														85.0		1.001		
	300	1130	42.8			520														69.3		1.001		
	301	2470	93.2			523														97.4		1.004		
	302	1110	42.00			521														68.3		1.002		
19	303	1135	43.5	NC	NC	506.9	NC	NC	16.86	NC	NM	NC	NC	1233	1185	27	1.31	0	0	68.8	0.961	0.988	NM	NM
	304	2240	86.1			504			25.18	35.48	1519	1.639	2478	4751	4565	57	0.72			93.6		0.985		
	305	2440	93.6			506			26.64	38.11	1606	1.797	3318	5854	5625	67	0.68			95.9		0.987		
	306	2560	98.0			509			29.05	39.78	1627	1.888	3767	6406	6155	97	0.90			97.9		0.990		
	307	2525	96.6			509.3			28.69	39.21	1633	1.864	3653	6229	5985	92	0.88			97.9		0.990		
	308	1675	64.3			506.6			19.93	NC	1379	NC	NC	2540	2440	77	1.81			84.4		0.987		
	309	1096	41.3			525			16.74		1319			1150	1105	32	1.66			NC		1.005		
20	310	1125	42.5	NC	NC	521	NC	NC	17.13	NC	1370	NC	NC	1218	1185	-17	-0.8	0	0	67.3	0.973	1.002	8	320
	311	1650	61.9			529			20.22		1377			2513	2445	-14	-0.4			84.0		1.009	6	330
	312	2280	85.3			532			25.36	38.92	1513	1.629	2346	4774	4645	30	0.4			94.4		1.012	7	345
	313	2480	92.7			533			28.08	42.09	1613	1.802	3275	5859	5700	78	0.8			96.4		1.014	7	300
	314	2530	95.1			528	0.375		29.32	40.12	1631	1.883	3738	6331	6160	-45	-0.4			98.5		1.008	8	330

TABLE A-3 TEST RESULTS (50 HOUR FAN-IN-WING TEST - EVENDALE) Continued

Run No.	Reading No.	Fan Speed (N_p) - RPM	Corrected Fan Speed ($N_p/\sqrt{\theta_{10.3}}$) - %	Fan Weight Flow (W_p) - lbs/sec	Corrected Fan Weight Flow ($W_p\sqrt{\theta_{10.3}}/\delta$) - %	Fan Inlet Temp. ($T_{10.3}$) - °R	Water Discharge Pressure Coefficient ($C_{P_{10.6}}$)	Steam Discharge Pressure Coefficient ($C_{P_{11.8}}$)	Diverter Valve Inlet Pressure ($P_{t\ 5.15}$) - psia	Fan Turbine Inlet Flow ($W_{5.4}$) - lbs/sec	Fan Turbine Inlet Temp. ($T_{t\ 5.4}$) - °R EGT	Fan Turbine Pressure Ratio ($P_{t\ 5.4}/P_{amb}$)	Corrected Available HP ($HP_{5.4}/\delta\sqrt{\theta_{10.3}}$)	Corrected Thrust (F/δ) - Lbs.	Vertical Thrust (F_y) - Lbs.	Horizontal Thrust (F_x) - Lbs.	Thrust Angle (β_v) - Deg.	Indicated Exit Louver Angle (β_1) - Deg.	Indicated Exit Louver Angle (β_2) - Deg.	J85 Corrected Speed ($N_{J85}/\sqrt{\theta_{2.0}}$) - %	Pressure Correction Parameter (δ)	Temperature Correction Parameter ($\sqrt{\theta_{10.3}}$)	Wind Velocity - MPH	Wind Direction (N-0°, E-90°, S-180°, W-270°)
20	315	2530	95.3	NC	NC	524	NC	NC	29.33	40.04	1639	1.883	3749	6216	5930	1058	10.1	10	10	98.5	0.973	1.005	8	310
	316	1140	43.3			517			NC	NC	1307	NC	NC	1156	1110	183	9.4			68.6		0.998	8	320
	317	1115	42.3			517					1299			1135	1090	178	9.3			69.0		0.998	8	320
	318	2265	85.7			520			26.26	37.43	1506	1.686	2657	5165	5025	112	1.3	0	0	95.5		1.001	2	280
	319	2455	92.5			524			28.76	39.58	1614	1.846	3538	6177	6010	53	0.5			97.8		1.005	2	280
	320	2600	98.0			524	0.379		30.27	40.94	1670	1.942	4048	6773	6590	13	0.1			98.8		1.005	2	280
	321	2460	92.6			526	NC		28.63	3942	1612	1.838	3519	6099	5935	-25	-0.2			97.7		1.006	2	280
	322	2455	93.2			518			28.57	39.71	1582	1.834	3463	6088	5920	-217	-2.1	-3	-3	97.7		0.998	2	280
	323	2490	94.5			517			28.61	39.32	1618	1.836	3512	6054	5865	-552	-5.4	-6	-6	97.9		0.998	2	280
	324	2410	91.5			517			27.96	38.53	1610	1.795	3305	5826	5640	-572	-5.8	-6	-6	97.2		0.998	2	280
	325	2420	91.0			426			27.99	38.58	1609	1.796	3264	5778	5560	-837	-8.6	-10	-10	97.2		1.007	2	280
	326	2410	91.6			516			28.03	38.59	1612	1.799	3311	5850	5690	-150	-1.5	-3	-3	97.2		0.997	2	280
	327	2355	88.2			531			27.94	38.54	1606	1.793	3240	5820	5660	190	1.9	0	0	97.0		1.011	2	280
	328	2440	91.8			526			28.48	39.12	1620	1.829	3442	5985	5805	444	4.4	3	3	97.6		1.007	1	300
	329	2430	91.3			528			28.24	38.69	1628	1.813	3344	5944	5725	798	8.0	6	6	97.4		1.008	1	300
	330	2420	91.4			522			28.30	38.94	1614	1.817	3389	5870	5575	1223	12.4	10	10	97.5		1.003	1	300
	331	2450	92.0			528			28.06	38.57	1618	1.801	3298	5707	5298	1643	17.3	15	15	97.0		1.009	1	300
	332	2430	91.5			525			28.06	38.72	1606	1.801	3300	5624	5049	2073	22.4	20	20	97.1		1.006	2	250
	333	2420	90.8			529			27.52	37.78	1622	1.766	3167	5202	4195	2793	30.9	30	30	95.7		1.010	2	250
	334	2412	90.8			526			27.33	37.47	1626	1.754	3095	4891	3647	3040	39.8	35	35	95.9		1.006	1	300
	335	2440	92.6			518			27.69	38.14	1611	1.777	3205	4627	3155	3193	45.2	40	40	96.8		0.998	1	300
	336	2490	94.6			516			28.40	39.01	1620	1.823	3444	5991	5830	58	0.6	0	0	97.6		0.997	1	300
	337	2560	96.3			527	0.386		30.15	41.02	1651	1.935	3987	6686	6505	123	1.1			99.0		1.007	1	300
	338	2580	96.9			528	NC		30.16	41.03	1651	1.936	3980	6757	6575	80	0.7			99.4		1.009	2	300
	339	2263	85.1			527			26.14	36.67	1536	1.680	2657	5078	4940	103	1.2			94.7		1.007	2	300
	340	2265	84.5			534			25.69	3603	1532	1.651	2495	4909	4740	-593	-7.2	-10	-10	94.3		1.015	2	300
	341	2267	85.3			526			NM	NC	1538	NC	NC	5096	4955	203	2.4	0	0	94.4		1.006	2	300
	342	2263	85.3			525			26.39	37.10	1535	1.695	2716	5079	4825	1033	12.1	10	10	95.4		1.005	2	300
	343	2260	85.1			525			26.16	36.68	1538	1.680	2653	4963	4610	1453	17.5	15	15	95.3		1.006	2	260
	344	2265	85.5			523			26.19	36.69	1543	1.682	2666	4877	4365	1823	22.7	20	20	95.1		1.004	2	260
	345	2267	85.3			527			26.00	36.29	1550	1.670	2603	4582	3685	2478	34.0	30	30	94.4	0.974	1.007	2	260
	346	2220	83.5			527			25.15	34.76	1570	1.616	2371	3990	2990	2511	40.0	35	35	93.1		1.007	2	50
	347	2277	86.0			522			25.68	36.02	1531	1.649	2503	3980	2685	2758	45.1	40	40	94.6		1.003	2	300
	348	2280	86.6			517			26.51	37.27	1535	1.701	2767	5200	5065	80	0.9	0	0	95.7		0.997	2	300
	349	2450	92.2			527			28.78	39.77	1600	1.846	3500	6099	5940	103	1.0			98.0		1.007	2	310

TABLE A-3 TEST RESULTS (50 HOUR FAN-IN-WING TEST - EVENDALE) Continued

Run No.	Reading No.	Fan Speed (N_p) - RPM	Corrected Fan Speed ($N_p/\theta_{10.3}$) - %	Fan Weight Flow (W_p) - lbs/sec	Corrected Fan Weight Flow ($W_p/\theta_{10.3}/\delta$) - %	Fan Inlet Temp. ($T_{10.3}$) - °R	Rotor Discharge Pressure Coefficient ($C_{10.6}$)	Stage Discharge Pressure Coefficient ($C_{11.6}$)	Diverter Valve Inlet Pressure ($P_{t\ 5.15}$) - psia	Fan Turbine Inlet Flow ($W_{5.4}$) - lbs/sec	Fan Turbine Inlet Temp. ($T_{t\ 5.4}$) - °R EGT	Fan Turbine Pressure Ratio ($P_{t\ 5.4}/P_{amb}$)	Corrected Available HP ($HP_{5.4}/\delta/\theta_{10.3}$)	Corrected Thrust (F/t) - Lbs.	Vertical Thrust (F_y) - Lbs.	Horizontal Thrust (F_x) - Lbs.	Thrust Angle (β_v) - Deg.	Indicated Exit Louver Angle (β_1) - Deg.	Indicated Exit Louver Angle (β_2) - Deg.	J85 Corrected Speed ($N_{J85}/\theta_{2.0}$) - %	Pressure Correction Parameter (δ)	Temperature Correction Parameter ($\theta_{10.3}$)	Wind Velocity - MPH	Wind Direction (N-0°, E-90°, S-180°, W-270°)
20	350	2570	96.5	NC	NC	528	0.381	NC	30.05	40.83	1656	1.928	3930	6649	6475	163	1.4	0	0	99.1	0.974	1.009	3	345
	351	1630	61.3			527	NC		NC	NC	1353	NC	NC	2568	2500	58	1.3			84.3		1.008	2	330
	352	1615	60.5			531					1355			3465	3360	-312	-5.3	-10	-10	84.2		1.011	1	180
	353	1643	62.2			518					1345			2649	2580	48	1.1	0	0	85.1		1.000	1	255
	354	1643	62.4			516					1333			2606	2485	518	11.8	10	10	85.0		0.997	1	255
	355	1630	61.9			516					1348			2571	2400	713	16.6	15	15	84.6		0.997	2	250
	356	1632	61.9			518					1353			2540	2285	947	23.1	20	20	84.8		0.999	2	250
	357	1620	61.4			519					1365			2322	1870	1273	34.3	30	30	84.2		1.000	2	250
	358	1650	62.2			524					1389			2338	1765	1438	39.2	35	35	83.9		1.005	2	250
	359	1660	62.8			520					NM			2097	1420	1468	45.2	40	40	83.0		1.001	2	315
	360	1650	62.4			521					1382			2163	1440	1538	46.2			84.6		1.001	2	280
	361	1630	61.4			526					1330			2650	2580	68	1.5	0	0	85.0		1.006	2	280
	362	1105	41.9			518					1278			1206	1175	8	0.4			69.2		0.998	2	280
	363	1650	62.3			522					1321			2706	2635	63	0.1			85.4		1.003	1	290
	364	2410	90.9			523			28.37	39.49	1573	1.819	3353	5973	5818	-27	-0.3	-5	+5	97.8		1.004	1	290
	365	2410	90.9			524			28.25	39.39	1571	1.812	3292		5500	-52	-0.5	-10	+10	97.7		1.004	2	300
	366	2415	90.8			527			28.22	39.42	1566	1.810	3262		4925	-97	-1.2	-15	+15	97.5		1.008	1	300
	367	2440	92.0			525			28.07	39.20	1567	1.800	3246		5475	1013	10.5	5	15	97.4		1.005	1	300
	368	2470	93.3			522			28.36	39.49	1576	1.819	3358		5450	798	8.3	0	20	97.8		1.003	1	300
	369	2420	91.5			522			28.13	39.34	1562	1.805	3276		4970	558	6.4	-5	+25	97.1		1.002	1	360
	370	2416	91.4			521			27.94	39.18	1553	1.792	3216		4590	1438	17.4	5	35	97.1		1.001	1.0	360
	371	2428	91.8			522			28.21	39.45	1563	1.809	3286		5060	1803	19.6	10	30	97.7		1.002	0.5	270
	372	2430	92.1			518			28.19	39.40	1565	1.808	3293		5145	1973	21.0	15	25	97.7		0.999	0.5	270
	373	2367	89.2			524			27.41	38.17	1576	1.758	3043		4205	2688	32.6	25	35	96.7		1.005	0.5	270
	374	2413	91.7			516			27.76	38.79	1565	1.782	3157		4185	2398	29.7	20	40	97.1		0.997	0.5	330
	375	2431	91.0			532			27.89	38.83	1576	1.789	3338		5395	-897	-9.5	-15	-5	97.2		1.012	0.5	330
	376	2420	91.2			525			38.09	39.56	1568	1.802	3296		5175	-917	-10.1	-20	0	97.6		1.005	0.5	340
	377	1112	42.2			516			NC	NC	1282	NC	NC		1180	33	1.6	0	0	69.6		0.997	1.0	45
21	378	1140	43.7	NC	NC	508	NC	NC	17.13	NC	NM	NC	NC	1205	1175	-32	-1.6	0	0	69.9	0.975	0.989	10	280
	379	1655	63.4			508			20.65	29.17	1329	1.338	1046	2708	2640	-22	-0.5			85.5		0.989	17	270
	380	2267	86.7			509			26.50	37.85	1487	1.698	2761	5126	4997	-80	-0.9			95.5		0.990	12	270
	381	2468	94.5			508			28.83	39.91	1594	1.846	3574	6066	5915	40	0.4			98.0		0.989	14	270
	382	2580	98.8			508	0.370		30.48	41.46	1652	1.952	4150	6810	6640	65	0.6			100.1		0.989	15	270
	383	2582	98.9			507	0.369		30.19	40.98	1659	1.934	4059	6610	6445	18	0.2			100.1		0.989	5	270
	384A	2600	99.5			509	0.369		30.52	41.42	1660	1.955	4161	6672	6505	60	0.5			100.5		0.990	5	270

TABLE A-3 TEST RESULTS (50 HOUR FAN-IN-WING TEST - EVENDALE) Continued

Run No.	Reading No.	Fan Speed (N_F) - RPM	Corrected Fan Speed ($N_F/\theta_{10.3}$) - %	Fan Weight Flow (W_a) - lbs/sec	Corrected Fan Weight Flow ($W_a\sqrt{\theta_{10.3}}/\delta$) - %	Fan Inlet Temp. ($T_{10.3}$) - °R	Rotor Discharge Pressure Coefficient ($C_{10.0}$)	Stage Discharge Pressure Coefficient ($C_{11.0}$)	Diverter Valve Inlet Pressure ($P_{t\ 5.15}$) - psia	Fan Turbine Inlet Flow ($W_{5.4}$) - lbs/sec	Fan Turbine Inlet Temp. ($T_{t\ 5.4}$) - °R EGT	Fan Turbine Pressure Ratio ($P_{t\ 5.4}/P_{amb}$)	Corrected Available HP ($HP_{5.4}/\delta\sqrt{\theta}_{10.3}$)	Corrected Thrust (F/δ) - Lbs.	Vertical Thrust (F_y) - Lbs.	Horizontal Thrust (F_x) - Lbs.	Thrust Angle (β_y) - Deg.	Indicated Exit Louver Angle (β_1) - Deg.	Indicated Exit Louver Angle (β_2) - Deg.	J85 Corrected Speed ($N_{J85}/\theta_{2.0}$) - %	Pressure Correction Parameter (δ)	Temperature Correction Parameter ($\sqrt{\theta}_{10.3}$)	Wind Velocity - MPH	Wind Direction (N-0°, E-90°, S-180°, W-270°)
21	384B	2600	99.5	NC	NC	509	NC	NC	30.48	41.36	1660	1.952	4161	6618	6453	-38	-0.3	0	0	100.5	0.975	0.990	5	270
	385	2450	93.5			508			28.78	40.07	1576	1.843	3513	6069	5907	-363	-3.5	-3	-3	98.0		0.989	12	270
	386	2466	94.0			513			28.65	39.88	1577	1.835	3472	5945	5778	-463	-4.6	-6	-6	97.5		0.994	12	270
	387	2438	93.0			512			28.56	39.87	1568	1.829	3435	6059	5830	-955	-9.3	-10	-10	97.5		0.993	13	280
	388	2440	93.4			509			28.32	39.58	1568	1.814	3357	5862	5715	-99	-1.0	0	0	97.9		0.990	10	270
	389	2451	94.0			507			28.78	40.19	1567	1.843	3524	6017	5838	258	2.5	3	3	97.7		0.988	15	270
	390	2470	94.6			506			28.82	40.25	1568	1.846	3533	6040	5820	612	6.0	6	6	97.9		0.989	13	270
	391	2475	94.9			507			28.84	40.26	1568	1.847	3534	6102	5845	773	7.5	10	10	98.1		0.988	15	270
	392A	2620	100.0			508	0.372		30.60	41.43	1667	1.960	4212	6762	6591	-174	-1.5	0	0	100.7		0.989	10	260
	392B	2620	100.0			508	NC		30.68	41.54	1667	1.965	4212	6716	6547	-108	-0.9			100.7		0.989	10	260
22	393	1100	42.2	NC	NC	507	NC	NC	NC	NC	1297	NC	NC	808	788	-75	-5.5	0	0	69.1	0.980	0.988	NM	NM
	394	1652	63.4			506			20.75	29.03	1355	1.338	1078	2684	2630	-40	-1.4			85.3		0.987	14	270
	395	2235	86.6			508			26.52	37.55	1513	1.691	2722	5061	4960	40	0.5			95.5		0.989	11	270
	396	2477	94.9			508	NC		29.07	40.40	1579	1.853	3538	6092	5970	20	0.2			98.0		0.989	9	280
	397	2610	100.0			508	0.374		30.83	41.60	1659	1.965	4227	6884	6745	85	0.7			100.1		0.989	10	270
	398A	2580	98.6			510	0.379		30.64	41.47	1658	1.953	4148	6642	6355	1170	10.4	10	10	99.6		0.991	10	270
	398B	2580	98.6			510	NC		NM	NC	1658	NC	NC	6616	6375	1185	10.5			99.6		0.991	10	270
	399A	2590	98.9			511	0.373		30.52	41.47	1656	1.946	4155	6745	6610	-35	-0.3	0	0	99.6		0.992	15	280
	399B	2590	98.9			511	NC		NM	NC	1656	NC	NC	6659	6525	-115	-1.0			99.6		0.992	15	280
	400	2455	94.1			507			29.07	40.37	1592	1.853	3578	6134	6010	-100	-1.0			98.1		0.988	15	270
	401	2250	86.2			508			26.46	37.49	1516	1.687	2677	5067	5965	-100	-1.1			95.2		0.989	14	270
	402	1670	64.0			507			20.70	29.02	1343	1.335	1029	2654	2600	-100	-2.2			85.1		0.988	14	290
	403	1120	42.9			507			NC	NC	1285	NC	NC	838	813	-115	-8.0			69.1		0.988	NM	NM
	404	1150	44.0			508					1290			2524	778	-85	-6.2			69.2		0.989		
	405	1090	41.5			513					1289			683	668	-25	-2.2			68.5		0.994		
	406	2230	85.0			513			26.08	36.27	1513	1.663	2580	4893	4795	-60	-0.7			94.7		0.994	8	260
	407	1128	NC			NM			NC	NC	1322	NC	NC	877	858	-35	-2.3			69.6		NC	8	260
	408	1650							20.48	27.26	1456	1.319	1029	2431	2390	-20	-0.5			84.5	0.983		7	260
	409	1642							21.37	29.16	1446	1.371	1253	2544	2500	-63	-1.4			85.1			7	260
	410	2272							26.27	37.18	1503	1.670	2634	4787	4705	-92	-1.1			94.8			9	270
	411	2241							26.19	37.15	1496	1.666	2590	4726	4645	-110	-1.4			94.6			9	270
	412	2235							25.83	36.41	1504	1.644	2505	4522	4445	-57	-0.7			94.8			9	270
	413	2250							26.21	37.02	1509	1.667	2617	4715	4635	-30	-0.4			94.5			7	270
	414	2242							26.05	37.01	1492	1.657	2552	4601	4040	860	10.5	10	10	94.6			7	310
	415	2240	85.2			515			26.18	37.26	1486	1.665	2561	4727	4647	47	0.6	0	0	94.9		0.996	7	300

TABLE A-3 TEST RESULTS (50 HOUR FAN-IN-WING TEST - EVENDALE) Continued

Run No.	Reading No.	Fan Speed (N_p) - RPM	Corrected Fan Speed ($N_p/\theta_{10.3}$) - %	Fan Weight Flow (W_p) - lbs/sec	Corrected Fan Weight Flow ($W_p\sqrt{\theta_{10.3}}/\delta$) - %	Fan Inlet Temp. ($T_{10.3}$) - °R	Rotor Discharge Pressure Coefficient ($Y_{10.6}$)	Stage Discharge Pressure Coefficient ($Y_{11.0}$)	Diverter Valve Inlet Pressure ($P_{t\ 5.15}$) - psia	Fan Turbine Inlet Flow ($W_{5.4}$) - lbs/sec	Fan Turbine Inlet Temp. ($T_{t\ 5.4}$) - °R EGT	Fan Turbine Pressure Ratio ($P_{t\ 5.4}/P_{amb}$)	Corrected Available HP ($HP_{5.4}/\delta\sqrt{\theta}_{10.3}$)	Corrected Thrust (F/t) - Lbs.	Vertical Thrust (F_y) - Lbs.	Horizontal Thrust (F_x) - Lbs.	Thrust Angle (β_v) - Deg.	Indicated Exit Louver Angle (β_1) - Deg.	Indicated Exit Louver Angle (β_2) - Deg.	J85 Corrected Speed ($N_{J85}/\sqrt{\theta_{2.0}}$) - %	Pressure Correction Parameter (δ)	Temperature Correction Parameter ($\sqrt{\theta_{10.3}}$)	Wind Velocity - MPH	Wind Direction (N-0°, E-90°, S-180°, W-270°)
22	416	1650	63.3	NC	NC	507	NC	NC	20.82	29.67	1307	1.339	1063	2553	2510	-10	-0.2	0	0	85.1	0.983	0.988	4	285
	417	1650	63.3			507			20.79	29.87	1287	1.337	1049	2564	2520	3	0			85.2		0.988	4	285
	418	2252	86.0			510			26.47	38.10	1464	1.683	2657	4799	4717	45	0.5			95.3		0.991	3	285
	419	2269	86.7			510			26.37	37.73	1470	1.677	2624	4794	4712	80	1.0			95.0		0.991	2	285
	420	2460	93.8			512			28.81	40.34	1559	1.830	3452	5707	5610	40	0.4			97.7		0.993	2	300
	421	2471	94.6			508			28.76	40.38	1550	1.828	3436	5717	5620	51	0.5			97.7		0.989	2	300
	422A	2605	99.4			511			30.58	42.17	1607	1.943	4052	6376	6267	117	1.1			99.5		0.993	3	300
	422B	2591	98.8			511	0.342		30.20	41.65	1604	1.919	3947	6242	6135	101	1.0			99.5		0.993	3	300
	423	2600	98.5			519	0.345		30.27	41.66	1613	1.923	3932	6257	6150	92	0.9			99.3		1.000	2	300
	424A	2572	98.4			509	NC		30.16	41.49	1615	1.917	3949	6089	5875	1140	11.0	10	10	99.0		0.990	3	290
	424B	2570	98.3			509			29.89	41.13	1614	1.899	3858	6104	5890	1145	11.0			99.0		0.990	3	290
	425	2441	93.5			508			28.57	40.10	1551	1.816	3364	5490	5300	1015	10.8			97.3		0.989	3	290
	426	2249	86.3			506			26.24	37.27	1492	1.669	2625	4637	4480	845	10.7			94.8		0.987	4	290
	427	2459	94.4			506			28.65	40.02	1566	1.820	3415	5512	5410	290	3.1	3	3	97.5		0.987	4	290
	428	2480	94.1			517			28.84	40.11	1580	1.833	3470	5732	5630	-245	-2.5	-3	-3	97.6		0.998	3	280
	429A	2592	99.2			509			NM	NC	1628	NC	NC	6253	6145	160	1.5	0	0	99.2		0.990	3	280
	429B	2590	99.1			509					1628			6227	6120	115	1.1			99.2		0.990	3	280
	430A	2585	98.5			512	0.342				1626			6279	6170	140	1.3			99.3		0.994	3	280
	430B	2590	98.7			512	NC				1626			6229	6120	175	1.6			99.3		0.994	3	280
	431	2450	93.9			506					1558			5581	5485	80	0.1			97.2		0.988	2	270
	432	2442	93.6			507					1562			5525	5430	75	0.1			97.4		0.988	2	270
	433	2448	94.1			505					1481			4762	4680	90	1.1			95.1		0.986	2	270
	434	2220	84.7			511					1490			4681	4600	90	1.1			94.9		0.993	6	280
	435	1660	63.6			506					1328			2518	2475	-20	-0.5			85.0		0.988	6	280
	436	1651	63.4			506					1326			2518	2475	0	0			84.9		0.987	8	270
	437	1150	44.1			507					1280			878	863	10	0.7			70.0		0.988	8	270
23	NO READINGS TAKEN																							
24	438	1092	41.8	NC	NC	509	NC	NC	16.89	NC	1297	NC	NC	1045	1017	-10	-0.6	0	0	68.9	0.973	0.990	NM	NM
	439	1675	63.7			514			20.50	28.82	1364	1.329	998	2760	2685	-20	-0.4			85.2		0.995	11	315
	440	2250	84.7			526			25.82	36.48	1509	1.659	2509	5155	5015	90	1.0			95.5		1.006	7	305
	441	2443	92.0			526			27.80	38.56	1589	1.784	3187	5778	5620	145	1.5			97.2		1.006	10	315
	442	2570	97.0			523	0.380		29.76	40.64	1639	1.909	3858	6558	6380	105	1.0			99.1		1.004	10	315
	443	2592	98.4			517	NC		29.96	NC	NM	1.922	NC	6629	6450	65	0.6			99.3		0.998	10	330
	444	2585	98.1			517	0.384		30.02	41.03	1635	1.926	4014	6751	6569	63	0.6			99.3		0.998	10	340
	445	2595	98.4			518	0.383		30.03	40.98	1641	1.927	4017	6665	6485	23	0.2			99.1		0.999	9	325

TABLE A-3 TEST RESULTS (50 HOUR FAN-IN-WING TEST - EVENDALE) Continued

Run No.	Reading No.	Fan Speed (N_f) - RPM	Corrected Fan Speed ($N_f/\theta_{10.3}$) - %	Fan Weight Flow (W_f) - lbs/sec	Corrected Fan Weight Flow ($W_f\sqrt{\theta_{10.3}}/\delta$) - %	Fan Inlet Temp. ($T_{10.3}$) - °R	Inter Discharge Pressure Coefficient ($\bar{P}$ 10.8)	Stage Discharge Pressure Coefficient ($\bar{P}$ 11.8)	Diverter Valve Inlet Pressure (P_t 5.15) - psia	Fan Turbine Inlet Flow ($W_{5.4}$) - lbs/sec	Fan Turbine Inlet Temp. (T_t 5.4) - °R EGT	Fan Turbine Pressure Ratio (P_t 5.4/P_{amb})	Corrected Available HP ($HP_{5.4}/\delta\sqrt{\theta_{10.3}}$)	Corrected Thrust (F/δ) - Lbs.	Vertical Thrust (F_y) - Lbs.	Horizontal Thrust (F_x) - Lbs.	Thrust Angle (β_v) - Deg.	Indicated Exit Louver Angle (β_1) - Deg.	Indicated Exit Louver Angle (β_2) - Deg.	J85 Corrected Speed ($N_{J85}/\sqrt{\theta_{2.0}}$) - %	Pressure Correction Parameter (δ)	Temperature Correction Parameter ($\sqrt{\theta_{10.3}}$)	Wind Velocity - MPH	Wind Direction (N-0°, E-90°, S-180°, W-270°)
24	446	2471	93.6	NC	NC	518	NC	NC	28.74	39.82	1591	1.843	3498	6209	6040	111	1.1	0	0	97.9	0.973	1.000	7	345
	447	2255	85.8			514			26.38	37.34	1523	1.692	2742	5177	5037	15	0.2			95.4		0.995	8	300
	448	1670	63.0			523			20.38	28.35	1371	1.322	987	2550	2480	70	1.6			85.0		1.004	10	285
	449	1100	41.3			529			16.70	NC	1329	NC	NC	1090	1060	45	2.4			68.1		1.009	10	300
	450	1667	63.2			518			20.34	28.02	1398	1.320	1001	2582	2512	-45	-1.0			83.8		0.999	8	300
	451	2280	86.4			519			25.80	36.25	1526	1.657	2552	5103	4965	40	0.5			93.2		1.000	10	300
	452	2480	93.4			526			27.65	38.11	1609	1.774	3171	5903	5743	93	0.9			95.1		1.006	10	315
	453	2565	97.0			521	0.385		29.37	40.01	1657	1.885	3764	6605	6427	43	0.4			97.1		1.002	8	325
	454	2252	85.4			518	NC		25.98	37.17	1474	1.669	2536	4999	4863	113	1.3			97.1		0.999	7	300
	455	2477	93.2			527			29.16	NC	1634	NC	NC	5971	5810	-37	-0.4			97.2		1.007	2	280
	456	2343	89.0			517			29.24		1642			5429	5282	-3	0			97.2		0.997	7	260
	457	2290	87.1			515			29.19	36.0	1630			5244	5102	35	0.4			97.3		0.996	8	255
	458	2295	87.5			513			29.61	NC	1644			5346	5202	43	0.5			97.3		0.994	2	270
	459	2268	85.8			520			29.23	35.5	1631			5150	5010	87	0.2			97.2		1.001	3	310
	460	2420	91.4			522			28.48	NC	1576			6012	5850	44	0.4			100.9		1.003	6	235
	461	2530	95.5			523			29.72		1628			6525	6348	95	0.1			100.6		1.004	3	235
	462	2360	90.0			512			30.18		1535			NC	NM	NM	NC			101.2		0.993	3	230
	463A	2590	97.3			528			30.12	40.75	1670	1.932	4003	6807	6622	135	1.2			98.5		1.008	3	320
	463B	2570	96.6			528			30.12	NC	1670	NC	NC	6755	6569	128	1.1			98.5		1.008	3	320
	464A	2581	86.8			529			29.86	40.43	1667	1.916	3908	6697	6515	125	1.1			98.8		1.010	3	308
	464B	2579	96.7			529			29.86	NC	1667	NC	NC	6631	6507	153	1.3			98.8		1.010	3	308
	465A	2602	97.5			531			30.69	41.44	1676	1.969	4179	6776	6590	180	1.6			98.7		1.011	1	320
	465B	2590	97.0			531			30.69	NC	1676	NC	NC	6964	6772	103	0.9			98.7		1.011	1	320
	466A	2600	97.5			530			30.50	41.29	1668	1.957	4113	6606	6285	1347	12.1	10	10	98.7		1.010	0	210
	466B	2590	97.1			530			30.50	NC	1668	NC	NC	6794	6472	1326	11.6			98.7		1.010	0	210
	467A	2580	97.6			520			30.69	41.49	1672	1.969	4200	6915	6728	80	0.7	0	0	99.2		1.001	0	210
	467B	2585	97.8			520			30.69	NC	1672	NC	NC	NC	NM	NM	NC			99.2		1.001	0	210
	468	2610	99.5			511			30.69	41.48	1673	1.969	4251	6987	6795	-195	-1.6	-2	-2	99.3		0.993	.5	210
	469	2610	99.7			510			30.71	41.53	1671	1.970	4225	6984	6785	-387	-3.3	-4	-4	99.3		0.992	.5	210
	470	2606	99.5			510			30.72	41.57	1669	1.971	4253	6975	6760	-598	-5.1	-6	-6	99.3		0.992	.5	210
	471	2609	99.6			510			30.72	41.68	1660	1.971	4242	6956	6720	-809	-6.9	-8	-8	99.3		0.992	1.5	210
	472	2603	99.3			510			30.71	41.54	1670	1.970	4221	6943	6680	-1007	-8.9	-10	-10	99.3		0.993	1.5	230
	473	2605	99.5			510			30.68	41.57	1664	1.968	4213	6950	6753	355	3.2	2	2	99.3		0.992	3	205
	474	2602	99.2			512			30.75	41.66	1665	1.973	4259	6939	6725	600	5.1	4	4	99.3		0.993	3	230
	475	2605	99.4			511			30.70	41.58	1666	1.970	4214	6914	6675	840	7.2	6	6	99.3		0.993	4	220

TABLE A-3 TEST RESULTS (50 HOUR FAN-IN-WING TEST - EVENDALE) Continued

Run No.	Reading No.	Fan Speed (N_F) - RPM	Corrected Fan Speed ($N_F/\sqrt{\theta}_{10.3}$) - %	Fan Weight Flow (W_F) - lbs/sec	Corrected Fan Weight Flow ($W_F\sqrt{\theta}_{10.3}/\delta$) - %	Fan Inlet Temp. ($T_{t_{10.3}}$) - °R	Inter Discharge Pressure Coefficient ($P_{10.6}$)	Stage Discharge Pressure Coefficient ($P_{11.6}$)	Diverter Valve Inlet Pressure ($P_{t\ 5.15}$) - psia	Fan Turbine Inlet Flow ($W_{5.4}$) - lbs/sec	Fan Turbine Inlet Temp. ($T_{t\ 5.4}$) - °R EGT	Fan Turbine Pressure Ratio ($P_{t\ 5.4}/P_{amb}$)	Corrected Available HP ($HP_{5.4}/\delta\sqrt{\theta}_{10.3}$)	Corrected Thrust (F/t) - Lbs.	Vertical Thrust (F_y) - Lbs.	Horizontal Thrust (F_x) - Lbs.	Thrust Angle (β_v) - Deg.	Indicated Exit Louver Angle (β_1) - Deg.	Indicated Exit Louver Angle (ζ_2) - Deg.	JO5 Corrected Speed ($N_{J05}/\sqrt{\theta}_{2.0}$) - %	Pressure Correction Parameter (δ)	Temperature Correction Parameter ($\sqrt{\theta}_{10.3}$)	Wind Velocity - MPH	Wind Direction (N-0°, E-90°, S-180°, W-270°)
24	476	2607	99.5	NC	NC	511	NC	NC	30.72	41.64	1663	1.971	4244	6895	6620	1090	9.3	8	8	99.3	0.973	0.993	3	225
	477	2460	93.9			511			28.85	39.93	1596	1.852	3480	6224	6055	105	1.0	0	0	97.5		0.992	3	235
	478	1666	63.6			511			20.76	29.35	1380	1.342	1107	2709	2641	32	0.7			85.1	0.975	0.993	3.5	250
	479	1044	39.8			511			NC	NC	1302	NC	NC	NC	NC	13	0.6			69.8		0.992	1	230
	480	0	0			509				NA	1339	NA	NA		NA	501	NA			69.7		0.990	1	210
	481					509			20.18		1376					1039				83.6		0.990	0	200
	482					508			25.07		1447					1697				93.8		0.989	1	225
	483					508			27.27		1510					2040				97.1		0.989	2	220
	484					508			29.38		1582					2350				100.0		0.989	1	220
	485					508			29.85		1615					2417				101.1		0.989	1	220
	486					507			29.88		1613					2422				101.2		0.988	0	220
	487					506			29.43		1588					2357				100.0		0.988	0	180
	488					507			27.32		1514					2045				97.0		0.988	0	180
	489					507			25.22		1446					1722				93.8		0.988	0	180
	490					507			20.26		1369					1063				83.8		0.988	0	170
	491					508			27.87		1528					2145				97.8		0.990	0	150
	492	405	15.5			508			29.89	7.2	1626	NC	NC	1831	375	1745	77.9			98.0		0.989	1	210
	493	1338	51.3			507			28.60	21.3	1593			2026	1858	670	19.8			96.7		0.988	0	190
	494	1344	51.5			507			25.62	22.2	1458			1892	1767	532	16.8			96.6		0.988	2	190
	495	1595	61.1			506			29.82	24.5	1636			2598	2475	542	12.4			96.8		0.988	2	190
	496	1595	61.1			507			27.11	25.8	1536			2645	2550	385	8.6			96.7		0.988	2	180
	497	1578	60.4			507			25.57	26.0	1443			2629	2520	465	10.5			96.7		0.989	0	240
	498	1810	69.4			506			26.45	29.5	1497			3283	3188	283	5.1			96.7		0.988	1	210
25	499	1140	44.0	NC	NC	500	NC	NC	NC	NC	1266	NC	NC	1453	1410	-110	-4.5	NA	NA	70.4	0.973	0.981	NM	NM
	500	1647	65.5			500			20.81		1292			2785	2707	-135	-2.9			85.8		0.981	15	255
	501	2270	87.5	458	86.6	502	0.373	0.302	26.81	38.62	1464	1.721	2855	5228	5085	-132	-1.5			96.1		0.983	12	260
	502	2278	88.0	NC	NC	500	NC	NC	26.87	38.84	1456	1.725	2858	5467	5315	-234	-2.5			95.9		0.981	5	255
	503	2478	95.7			499			29.15	40.88	1554	1.870	3667	6290	6115	-240	-2.3			98.2		0.981	12	260
	504	2468	95.3			500			29.08	40.79	1553	1.866	3634	6325	6151	-196	-1.8			98.3		0.981	8	260
	505	2598	100.3	522	98.6	500	0.384	0.295	30.88	42.09	1644	1.981	4331	7077	6884	-151	-1.3			100.7		0.981	5	250
	506	2606	100.8	531	100.1	498	0.377	0.308	30.93	42.19	1642	1.985	4358	7102	6907	-196	-1.6			100.9		0.979	13	260
	507	2602	100.5	523	98.7	499	0.376	0.301	30.50	41.61	1642	1.957	4196	6828	6640	-235	-2.0			100.6		0.981	10	260
	508	2612	101.0	527	99.3	498	0.381	0.304	30.94	42.28	1636	1.985	4350	7026	6833	-203	-1.7			100.8		0.979	6	260
	509	2472	95.5	NC	NC	500	NC	NC	29.19	40.92	1555	1.873	3678	6350	6175	-208	-1.9			97.9		0.981	10	260
	510	2478	95.5			502			29.25	40.96	1559	1.877	3700	6408	6233	-166	-1.5			97.8		0.983	9	270

TABLE A-3 TEST RESULTS (50 HOUR FAN-IN-WING TEST - EVENDALE) Continued

Run No.	Reading No.	Fan Speed (N_p) - RPM	Corrected Fan Speed ($N_p/\theta_{10.3}$) - %	Fan Weight Flow (W_p) - lbs/sec	Corrected Fan Weight Flow ($W_p\sqrt{\theta_{10.3}}/\delta$) - %	Fan Inlet Temp. ($T_{10.3}$) - °R	Outer Discharge Pressure Coefficient ($C_{P_{20.0}}$)	Diagn Discharge Pressure Coefficient ($C_{P_{11.0}}$)	Diverter Valve Inlet Pressure ($P_{t\ 5.15}$) - psia	Fan Turbine Inlet Flow ($W_{5.4}$) - lbs/sec	Fan Turbine Inlet Temp. ($T_{t\ 5.4}$) - °R EGT	Fan Turbine Pressure Ratio ($P_{t\ 5.4}/P_{amb}$)	Corrected Available HP ($HP_{5.4}\sqrt{\delta}/\theta_{10.3}$)	Corrected Thrust (F/t) - Lbs.	Vertical Thrust (F_y) - Lbs.	Horizontal Thrust (F_x) - Lbs.	Thrust Angle (θ_v) - Deg.	Indicated Exit Louver Angle (θ_1) - Deg.	Indicated Exit Louver Angle (θ_2) - Deg.	J65 Corrected Speed ($N_{J85}/\theta_{2.0}$) - %	Pressure Correction Parameter (δ)	Temperature Correction Parameter ($\sqrt{\theta_{10.3}}$)	Wind Velocity - MPH	Wind Direction (N-0°, E-90°, S-180°, W-270°)
25	511	2617	101.1	527	99.4	498	0.372	0.303	30.89	42.13	1643	1.982	4336	7042	6850	-168	-1.4	NA	NA	100.5	0.973	0.980	9	270
	512	2602	100.6	526	99.2	499	0.375	0.304	30.91	42.20	1640	1.984	4342	7118	6923	-189	-1.6			100.8		0.980	8	270
	513	2600	100.5	527	99.4	499	0.382	0.307	30.92	42.17	1643	1.984	4346	7088	6895	-145	-1.2			100.7		0.980	8	265
	514	2282	88.1	NC	NC	499	NC	NC	26.80	38.71	1456	1.720	2842	5380	5233	-158	-1.7			95.8		0.981	8	265
	515	2278	88.0			498			26.69	38.57	1453	1.714	2819	5276	5132	-136	-1.5			95.8		0.980	8	265
	516	1658	64.1			499			20.76	NC	1282	NC	NC	2750	2675	-88	-1.9			85.3		0.980	9	245
	517	1160	44.8			499			NC		1250			1460	1419	-78	-3.1			70.5		0.980	NM	NM
	518	1112	43.0			500					1291			933	907	-45	-2.8			69.9		0.981	NM	NM
	519	2582	99.7	528	99.3	500	0.379	0.315	30.79	42.21	1626	1.971	4250	7431	7252	-118	-0.9			100.5	0.976	0.981	3	260
	520	2579	99.6	521	98.1	499	0.378	0.308	30.71	42.05	1630	1.965	4225	7261	7086	-121	-1.0			100.3		0.981	2	255
	521	2581	99.7	NC	NC	499	NC	NC	30.80	42.20	1628	1.971	4249	7422	7243	-114	-0.9			100.6		0.981	3	270
	522	2577	98.7			508			30.54	41.66	1642	1.954	4139	7277	7102	-22	-0.2			100.3		0.989	1	310
	523	2592	100.0			499			30.77	41.95	1644	1.969	4245	7410	7232	-28	-0.2			100.5		0.981	1	255
26	524	1149	NC	NC	NC	NM	NC	NC	NC	NC	1364	NC	NC	NC	NM	NM	NC	0	0	69.6	0.989	NC	NM	NM
	525	2253	NC						26.15	36.66	1535	1.654								94.5			5	40
	526	1128	42.3			530			NC	NC	1345	NC		1187	1173	50	2.4			68.5		1.011	NM	NM
	527	1690	63.0			537			20.79	28.73	1380	1.331		2622	2590	75	1.7			84.4	0.988	1.018	6	350
	528	2259	84.7	416	79.6	530	0.375		26.61	37.49	1524	1.684	2645	5177	5115	55	0.6			95.1		1.010	4	315
	529	2282	85.2	NC	NC	533	NC		26.61	37.74	1504	1.684	2620	5144	5070	-345	-3.9	-5	-5	95.3		1.014	5	45
	530	2275	84.9			535			26.27	36.72	1548	1.663	2564	4976	4880	-600	-7.0	-10	-10	94.5		1.015	5	25
	531	2270	84.5	405	78.0	537	0.388		26.27	46.68	1551	1.663	2557	4909	4745	-1005	-12.0	-15	-15	94.7		1.017	4	355
	532	2243	93/3	4-7	78.5	540	0.388		25.84	36.07	1544	1.636	2411	4757	4695	215	2.6	0	0	94.1		1.020	3	360
	533	2252	83.6	NC	NC	540	NC		26.35	37.05	1529	1.668	2544	4847	4680	1015	12.9	10	10	94.7		1.020	5	30
	534	2245	83.3			541			25.86	36.28	1529	1.637	2395	4712	4430	1430	17.3	15	15	94.8		1.021	5	10
	535	2245	82.9	390	75.9	546	0.404		26.13	36.61	1537	1.654	2473	4661	4215	1855	23.8	20	20	94.7		1.026	7	5
	536	2281	84.2	NC	NC	546	NC		26.06	36.51	1538	1.650	2446	4644	4040	2175	28.3	25	25	94.1		1.026	6	20
	537	2310	85.9	368	71.0	539	0.383		26.29	36.56	1563	1.664	2572	4638	3780	2590	34.4	30	30	94.4		1.019	6	15
	538	2288	85.5	351	67.5	534	0.382		26.12	36.62	1535	1.653	2503	4292	3265	2705	39.6	35	35	94.1		1.014	4	355
	539	1672	62.3	NC	NC	537	NC		20.91	29.00	1377	1.338	NC	2689	2655	105	2.3	0	0	85.0		1.017	5	10
	540	1125	42.0			534			NC	NC	1323	NC		1221	1205	45	2.1			68.4		1.014	NM	NM
	541	1090	40.9			529					1345			1161	1143	95	4.8			68.7		1.010		
	542	2466	91.9	447	86.0	535	0.379		28.41	38.83	1636	1.796	3291	5915	5840	215	2.1			96.7		1.016	4	50
	543	2470	91.9	NC	NC	538	NC		28.59	39.07	1636	1.807	3317	5962	5885	-275	-2.7	-5	-5	97.0		1.018	5	115
	544	2481	93.7			522	0.391		29.30	40.13	1629	1.852	3576	6198	6097	-575	-5.4	-10	-10	97.8		1.003	4	100
	545	2450	92.5	454	86.3	522	0.391		28.86	39.51	1630	1.824	3445	5922	5750	-1083	-10.7	-15	-15	97.4		1.003	4	60

TABLE A-3 TEST RESULTS (50 HOUR FAN-IN-WING TEST - EVENDALE) Continued

Run No.	Reading No.	Fan Speed (N_p) - RPM	Corrected Fan Speed ($N_p/\theta_{10.3}$) - %	Fan Weight Flow (W_p) - lbs/sec	Corrected Fan Weight Flow ($W_p\sqrt{\theta_{10.3}}/\delta$) - %	Fan Inlet Temp. ($T_{10.3}$) - °R	Inter Discharge Pressure Coefficient ($P_{13.0}$)	Stage Discharge Pressure Coefficient ($P_{11.0}$)	Diverter Valve Inlet Pressure ($P_{t\ 5.15}$) - psia	Fan Turbine Inlet Flow ($W_{5.4}$) - lbs/sec	Fan Turbine Inlet Temp. ($T_{t\ 5.4}$) - °R EGT	Fan Turbine Pressure Ratio ($P_{t\ 5.4}/P_{amb}$)	Corrected Available HP ($HP_{5.4}/\delta\theta_{10.3}$)	Corrected Thrust (F/δ) - Lbs.	Vertical Thrust (F_y) - Lbs.	Horizontal Thrust (F_x) - Lbs.	Thrust Angle (θ_V) - Deg.	Indicated Exit Louver Angle (β_1) - Deg.	Indicated Exit Louver Angle (β_2) - Deg.	J85 Corrected Speed ($N_{J85}/\theta_{2.0}$) - %	Pressure Correction Parameter (δ)	Temperature Correction Parameter ($\theta_{10.3}$)	Wind Velocity - MPH	Wind Direction (N-0°, E-90°, S-180°, W-270°)
26	546	2466	92.8	462	88.1	526	0.394	NC	29.07	39.72	1637	1.837	3505	6126	6040	395	3.7	0	0	97.3	0.988	1.006	3	110
	547	2440	90.7	NC	NC	538	NC		28.42	38.67	1651	1.796	3300	5850	5645	1240	12.3	10	10	96.4		1.019	2	160
	548	2486	93.1	439	84.1	530	0.387		29.05	39.36	1664	1.836	3527	6007	5430	2395	23.8	20	20	96.3		1.011	7	105
	549	2473	92.1	NC	NC	537	NC		28.31	38.42	1659	1.789	3269	5563	4845	2595	28.4	25	25	96.1		1.017	8	105
	550	2470	92.3	402	77.1	532	0.390		27.32	37.11	6649	1.728	2950	5496	4465	3090	34.7	30	30	97.6		1.013	2	270
	551	2474	92.3	373	71.8	535	0.381		28.34	38.57	1650	1.791	3271	5076	3840	3225	40.0	35	35	96.5		1.015	5	50
	552	2530	93.9	460	88.9	540	0.384		29.40	39.79	1668	1.858	3589	6322	6240	270	2.5	0	0	97.8		1.020	6	60
	553	1150	43.3	NC	NC	526	NC		17.49	19.70	1350	1.146	NC	1194	935	720	37.6	30	30	69.0		1.006	7	105
	554A	2572	97.0	486	92.4	523	0.391		30.66	41.47	1670	1.938	4049	6734	6635	495	4.3	0	0	98.7		1.004	6	90
	554B	2550	96.2	NC	NC	523	NC	NC	NM	NC	NM	NC	NC	6732	6633	495	4.3	0	0	98.7	0.988	1.004	6	90

NA - NOT APPLICABLE
NC - NOT CALCULATED
NM - NOT MEASURED

TABLE A-4

SUMMARY OF TEST TRANSIENTS

β (Deg.)	Time Period of Acceleration or Deceleration, 1 min.	10 sec.	5 sec.	1 sec.	Number of Accelerations	Number of Decelerations
0	X				2	2
0		X			1	1
0			X		1	1
0				X	1	1
10		X			1	1
10			X		2	2
10				X	1	1
20		X			2	2
20			X		1	1
20				X	1	1
30		X			1	1
30			X		1	1
30				X	1	1
35		X			1	1
35			X		1	1
35				X	1	1
				TOTAL	19	19

Run	Fan Speed (rpm)	Diverter Valve Switch From	To	Time Period of Diverter Valve Switch (sec.)	Engine Speed (rpm)	Engine Overspeed (rpm)
21	2500	D*	ST*	3.15	16,040	16,600
	2450	D	ST	3.10	16,000	16,520
	2250	D	ST	2.60	15,560	16,080
	2250	D	ST	3.20	15,600	16,080
	1925	D	ST	4.00	14,600	15,120
	1875	D	ST	6.00	13,880	14,360
	1125	D	ST	4.40	-	-
	1910	ST	D	3.80	14,680	15,160
	1650	ST	D	5.16	13,900	14,400
	1050	ST	D	4.42	11,400	12,000
	2430	ST	D	3.40	16,040	16,560
	2270	ST	D	3.50	15,600	16,120
	2250	ST	D	13.00	15,640	16,120
22	2270	ST	D	1.38	15,640	16,120
	2270	D	ST	1.68	15,640	16,120
	2270	ST	D	3.63	15,600	16,080
	2260	D	ST	1.80	15,560	16,080
	1910	ST	D	1.18	14,680	15,160
	1910	D	ST	2.08	14,680	15,160
	1910	ST	D	1.96	14,680	15,120
	1910	D	ST	1.96	14,600	15,120
	1700	ST	D	1.10	14,080	14,520
	1675	D	ST	1.84	14,080	14,520
	1700	ST	D	1.80	14,080	14,520
	1850	D	ST	2.00	14,000	14,400
	1140	ST	D	1.28	11,400	11,700
	1110	D	ST	1.98	11,320	11,760
24	1650	D	ST	1.20	14,160	14,600
	2300	D	ST	1.32	16,270	16,840
	2300	D	ST	1.32	16,260	16,800
	2300	ST	D	1.12	15,920	16,440
	2250	D	ST	1.24	15,880	16,440
	2250	D	ST	1.24	15,880	16,440
	1150	D	ST	1.50	11,640	12,000
	1120	ST	D	1.00	11,360	11,680
	2450	ST	D	1.84	16,280	16,840
	2450	ST	D	1.32	16,240	16,840
	2475	ST	D	2.04	15,920	16,440
	1680	ST	D	0.86	14,200	14,640

* Diverted flow is designated D
Straight through flow is designated ST

TABLE A-5

NARROW BAND ANALYSIS OF FAN EXIT SOUND PRESSURE LEVEL TRAVERSE (FAN SPEED 2565 RPM)

	SPL in db re 0.0002 dynes/cm^2 for Tip ← Traverse Positions → Hub																		
Fan Blade Passing Frequency	0	1	2	3	4	5	6	7	8	9	10	11	12	13	14	15	16	17	18
1st Harmonic 1540 cps	131	131	133	132	130	128	128	128	128	131	131	131	132	133	133	133	131	130	128
2nd Harmonic 3080 cps	127	128	128	127	128	127	129	131	132	133	133	133	133	132	131	131	128	127	127

a. 3% of band width, signal to noise ratio 6-9 db

b.

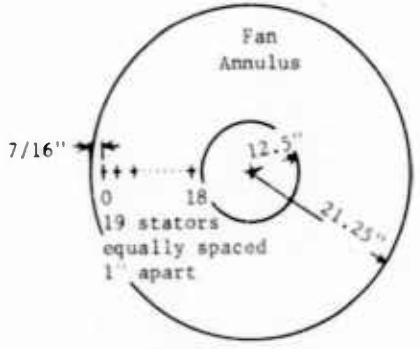

APPENDIX B

SAMPLE J85 WEIGHT FLOW CALCULATION

Reading 108:

Four static pressures were measured in the straight section of the J85 bellmouth approximately eight inches ahead of the front frame:

$$\frac{P_{amb.} - P_{s\ 2.0\ ave.}}{\delta} = \frac{49.31}{0.983} = 50.16 \text{ inches } H_2O$$

Using Figure B-1, bellmouth flow curve:

$$\frac{W_{2.0}\sqrt{\theta}_{2.0}}{\delta} = 42.10 \text{ lbs/sec.}$$

Obtain compressor bleed from Figure B-2 for $N_{J85}/\sqrt{\theta}_{2.0} = 96.9\%$:

$$W_{bleed}/W_{2.0} = 0.023$$

Weight flow after compressor bleed:

$$\frac{W_{2.5}\sqrt{\theta}_{2.0}}{\delta} = \frac{W_{2.0}\sqrt{\theta}_{2.0}}{\delta} (1.000 - 0.023) = 41.13 \text{ lbs/sec.}$$

Substracting eighth stage leakage which is a constant value of 0.8%[a] to obtain compressor discharge weight flow gives:

$$\frac{W_{3.0}\sqrt{\theta}_{2.0}}{\delta} = \frac{W_{2.5}\sqrt{\theta}_{2.0}}{\delta} (1.000 - 0.008) = 40.80 \text{ lbs/sec.}$$

---

[a] Source: SAED, GE, Lynn, Mass.

Obtain weight flow at J85 turbine discharge by adding fuel flow:

Fuel flow for Reading No. 108 = 2100 lbs/hour

$$W_{5.15} = \frac{W_{3.0}\sqrt{\theta}_{2.0}}{\delta} \quad \frac{\delta}{\sqrt{\theta}_{2.0}} \text{ lbs/sec.} + \frac{2100}{3600} \text{ lbs/sec.}$$

$$= 40.80 \quad \frac{0.983}{1.000} + 0.58$$

$$= 40.11 + 0.58 = 40.69 \text{ lbs/sec.}$$

DERIVATION OF DIVERTER VALVE AND SCROLL LOSS CURVES AND ANALYSIS OF DIVERTER VALVE BLEED AND LIFT FAN HORSEPOWER

Fan system loss curves were derived to simplify the calculation for horsepower at the fan turbine nozzle inlet, station 5.4. Three sets of curves were made to cover a range of diverter valve bleed up to 8%. The curves are for 0%, 4%, and 8% bleed.

To calculate horsepower an iterative process is required. The first calculation assumes 0%, 4%, or 8% bleed. The weight flow at station 5.4 is calculated and the amount of bleed is obtained. This value of bleed is then used for the second calculation; no more than two calculations were required.

Table B-1 summarizes the calculations used to derive the curves. The following is the method used:

A range of station 5.15 Mach numbers was selected. Corresponding diverter valve and diffusers losses, $P_{t5.3}/P_{t5.15}$, were taken from the full scale diverter valve test[a] curves (see Figure B-3). The flow function at station 5.15 is obtained from the one-dimensional compressible flow equation:

$$\frac{W_{5.15}\sqrt{T_{t5.15}R}}{P_{t5.15}A_{5.15}} = M \frac{\sqrt{\gamma g}}{\left(1 + \frac{\gamma - 1}{2} M^2\right)^{\frac{\gamma + 1}{2(\gamma - 1)}}}$$

The flow functions at the scroll inlet, station 5.3, and the fan turbine nozzle inlet, station 5.4, were obtained by applying the area change, pressure change and weight flow change between these stations and the station 5.15 flow function assuming no temperature change:

[a] Reference 4

$$\frac{W_{5.3}\sqrt{T_{t5.3}R}}{P_{t5.3}A_{5.3}} = \frac{A_{5.15}}{A_{5.3}} \quad \frac{W_{5.3}}{W_{5.15}} \quad \frac{W_{5.15}\sqrt{T_{t5.15}R}}{(P_{t5.3}/P_{t5.15})\ P_{t5.15}A_{5.15}}$$

$$\frac{W_{5.4}\sqrt{T_{t5.4}}}{P_{t5.4}} = \left(\frac{W_{5.4}}{W_{5.15}}\right) \quad \frac{A_{5.15}}{(P_{t5.4}/P_{t5.15})\sqrt{R}} \quad \frac{W_{5.15}\sqrt{T_{t5.15}R}}{P_{t5.15}A_{5.15}}$$

The scroll inlet Mach number, $M_{5.3}$, is obtained from the relationship of flow function versus Mach number for one-dimensional compressible flow. The scroll inlet total to static pressure ratio, $P_{t5.3}/P_{s5.3}$, is obtained from the isentropic compressible flow equation:

$$P_t/P_s = \left(1 + \frac{\gamma - 1}{2} M^2\right)^{\frac{\gamma}{\gamma - 1}}$$

The scroll pressure loss coefficient corresponding to this inlet Mach number, Table III in reference 5 is:

$$\frac{P_{t5.3} - P_{t5.4}}{P_{t5.3} - P_{s5.3}} = 0.722$$

Therefore the scroll total pressure loss as a function of scroll inlet total pressure is:

$$\frac{P_{t5.3} - P_{t5.4}}{P_{t5.3} - P_{s5.3}} \left(1 - \frac{P_{s5.3}}{P_{t5.3}}\right) = \frac{P_{t5.3} - P_{t5.4}}{P_{t5.3}} = 1 - \frac{P_{t5.4}}{P_{t5.3}}.$$

The ratio of total pressure at the fan turbine nozzle inlet to diverter valve inlet total pressure is therefore:

$$\left(\frac{P_{t5.4}}{P_{t5.3}}\right)\left(\frac{P_{t5.3}}{P_{t5.15}}\right) = \frac{P_{t5.4}}{P_{t5.15}}$$

The ducting losses obtained from those calculations are presented in Figure B-4 as a function of turbine discharge Mach number, $M_{5.15}$.

A plot of $P_{t5.4}/P_{t5.15}$ versus $\frac{W_{5.4}\sqrt{T_{t5.4}}}{P_{t5.4}}$ was made for the various diverter valve bleeds (see Figure B-5).

The curve of $P_{t5.4}/P_{t5.15}$ versus $P_{t5.15}/P_{amb}$ (Figure B-6) was obtained by using the full scale scroll test flow function curve, Figure B-7, which was derived from the initial lift fan testing (reference 1) and Figure B-5. At the point of choked flow through the scroll the flow function is 60.25. This represents the point of maximum system loss from the diverter valve inlet to the scroll nozzle inlet so each of the curves was made level beyond this point.

An example of the use of these curves is given for Reading 108:

Assume 4% bleed:

$P_{t5.15}/P_{amb}$ = 1.934 (measured)

$P_{t5.4}/P_{t5.15}$ = 0.9150 (from Figure B-6)

$P_{t5.4}$ = $(P_{t5.4}/P_{t5.15})$ $(P_{t5.15})$ = (0.9150) (28.045 psia) = 25.661 psia

$T_{t5.15}$ = 1584°R (measured data)

Apply correction factor from Figure 24 :

$T_{t5.15}$ = 1584 - 30 = 1554°R

$\sqrt{T_{t5.15}}$ = 39.42

$\frac{W_{5.4}\sqrt{T_{t5.4}}}{P_{t5.4}}$ = 60.25 (from Figure B-5)

$$W_{5.4} = \frac{\left(\frac{W_{5.4}\sqrt{T_{5.4}}}{P_{t5.4}}\right) P_{t5.4}}{\sqrt{T_{t5.4}}} = 39.22 \text{ lbs/sec.}$$

$W_{5.15}$ = 40.69 lbs/sec. (See previous section in this appendix, J85 weight flow calculation.)

Therefore, calculated bleed is:

$$\left(\frac{W_{5.15} - W_{5.4}}{W_{5.15}}\right) 100 = \frac{1.47}{40.69} (100) = 3.61\%$$

For closer agreement between assumed and calculated bleed assume a second bleed value equal to 3.50% and interpolate Figures B-5 and B-6 and repeat the calculation process:

$$P_{t5.4}/P_{t5.15} = 0.9155$$

$$P_{t5.4} = (0.9155)\ (28.045) = 25.675 \text{ psia}$$

$$\frac{W_{5.4}\sqrt{T_{t5.4}}}{P_{t5.4}} = 60.25$$

$$W_{5.4} = \frac{(60.25)\ (25.675)}{39.42} = 39.24 \text{ lbs/sec.}$$

Calculated bleed = $\frac{1.45}{40.69}$ (100) = 3.56%

Further iteration is not required; the horsepower at station 5.4, assuming isentropic expansion to ambient pressure, is then obtained from Figure B-8 which is a plot of ideal gas horsepower function versus total to ambient pressure ratio.

($\gamma = 1.33$, $c_p = 0.273$)

$$P_{t5.4}/P_{amb} = (P_{t5.15}/P_{amb})\ (P_{t5.4}/P_{t5.15}) = (1.934)\ (0.9155)$$

$$= 1.770$$

and

$$(HP/T_t W)_{5.4} = 0.0512 \text{ (from Figure B-8)}$$

$$HP_{5.4}/\delta\sqrt{\theta}_{10.3} = \frac{(0.0512)\ (T_{t5.4})\ (W_{5.4})}{\delta\sqrt{\theta}_{10.3}} =$$

$$\frac{(0.0512\ (1554)\ (39.24)}{(0.987)\ (0.999)} = 3166$$

Diverter valve leakage for the case with the valve doors fully closed can be determined in the same manner as bleed percentage is obtained in the above calculation procedure. For example, the leakage at 95% J85-7 speed from Figure 15b is 1.0% of $W_{5.15}$. Data obtained in Reference 4 incicates that the diverter leakage at this condition should be between 0.79% and 0.97%. The close agreement with this prior testing of the leakage obtained by the calculation procedure used in this report lends confidence to the accuracy of fan turbine inlet weight flow determination.

FAN WEIGHT FLOW

The flow calibration curve shown in Figure B-9 was obtained from the test of the fuselage installation (Run 12) with the inlet duct and exit measuring section installed. Flow was calculated[a] from the inlet duct measurements using an estimated area coefficient of 0.97. An exit measuring section area coefficient of 0.952 results when this flow is compared against the theoretical flow based on average total pressure, average static pressure and total temperature in the exit measuring section.

Run 25 (with exit measuring section installed, but without the inlet duct) was used to obtain Figure B-10 which is a curve of fan weight flow versus fan bulletnose ambient to static pressure difference for the fan-in-wing configuration.

The bulletnose static pressure was estimated from a flux plot of the fan-in-wing configuration (based on an IBM program as a function of weight flow). The weight flow calculated from the exit measuring section instrumentation was a consistent 10% lower at a given bulletnose static pressure depression than predicted by this flux plot. This indicates a lower level of velocity around the bulletnose than predicted.

[a] Refer to Performance Calculation Standards, Table A-1.

TABLE B-1

TURBINE DUCTING PRESSURE LOSS CURVE CALCULATIONS

	0% Diverter Valve Bleed					4% Diverter Valve Bleed						8% Diverter Valve Bleed					
M5.15	0.40	0.44	0.48	0.52	0.56	0.40	0.44	0.46	0.48	0.52	0.56	0.40	0.44	0.46	0.48	0.52	0.56
$P_{t5.3}/P_{t5.15}$	0.9662	0.9617	0.9569	0.9517	0.9458	0.9662	0.9617	0.9593	0.9569	0.9517	0.9458	0.9662	0.9617	0.9543	0.9569	0.9517	0.9458
$\left(\frac{W\sqrt{T_t}}{P_t A}\right)_{5.15}$	2.402	2.597	2.773	2.940	3.084	2.402	2.597	2.683	2.773	2.940	3.084	2.402	2.597	2.683	2.773	2.940	3.084
$\left(\frac{W\sqrt{T_t}}{P_t A}\right)_{5.3}$	1.791	1.946	2.088	2.226	2.349	1.717	1.866	1.932	2.002	2.134	2.253	1.646	1.788	1.852	1.919	2.045	2.159
M5.3	0.284	0.313	0.339	0.366	0.389	0.271	0.298	0.309	0.321	0.348	0.369	0.259	0.284	0.295	0.308	0.330	0.351
$P_{t5.3}/P_{s5.3}$	1.054	1.067	1.078	1.095	1.105	1.049	1.060	1.065	1.070	1.083	1.094	1.046	1.055	1.059	1.064	1.074	1.085
$1 - P_{s5.3}/P_{t5.3}$	0.0512	0.0628	0.0724	0.0868	0.0950	0.0467	0.0566	0.0610	0.0654	0.0766	0.0859	0.0440	0.0521	0.0557	0.0602	0.0689	0.0783
$1 - P_{t5.4}/P_{t5.3}$	0.0370	0.0453	0.0523	0.0627	0.0686	0.0337	0.0409	0.0440	0.0472	0.0553	0.0620	0.0318	0.0376	0.0402	0.0435	0.0497	0.0565
$P_{t5.4}/P_{t5.15}$	0.9305	0.9181	0.9069	0.8809	0.9336	0.9224	0.9171	0.9117	0.8991	0.8872	0.9355	0.9355	0.9255	0.9287	0.9153	0.9044	0.8924
$\frac{W_{5.4}\sqrt{T_{t5.4}}}{P_{t5.4}}$	54.44	59.66	64.49	69.52	73.82	52.11	57.02	59.25	61.60	66.22	70.40	49.83	54.46	56.56	58.80	63.09	67.07
$P_{5.4}/P_{amb}$	1.316	1.630	---	---	---	1.262	1.400	1.569	---	---	---	1.221	1.318	1.382	1.520	---	---
$P_{5.15}/P_{amb}$	1.414	1.775	---	---	---	1.352	1.518	1.711	---	---	---	1.305	1.427	1.501	1.661	---	---

Source: SAED, GE, Lynn, Mass.

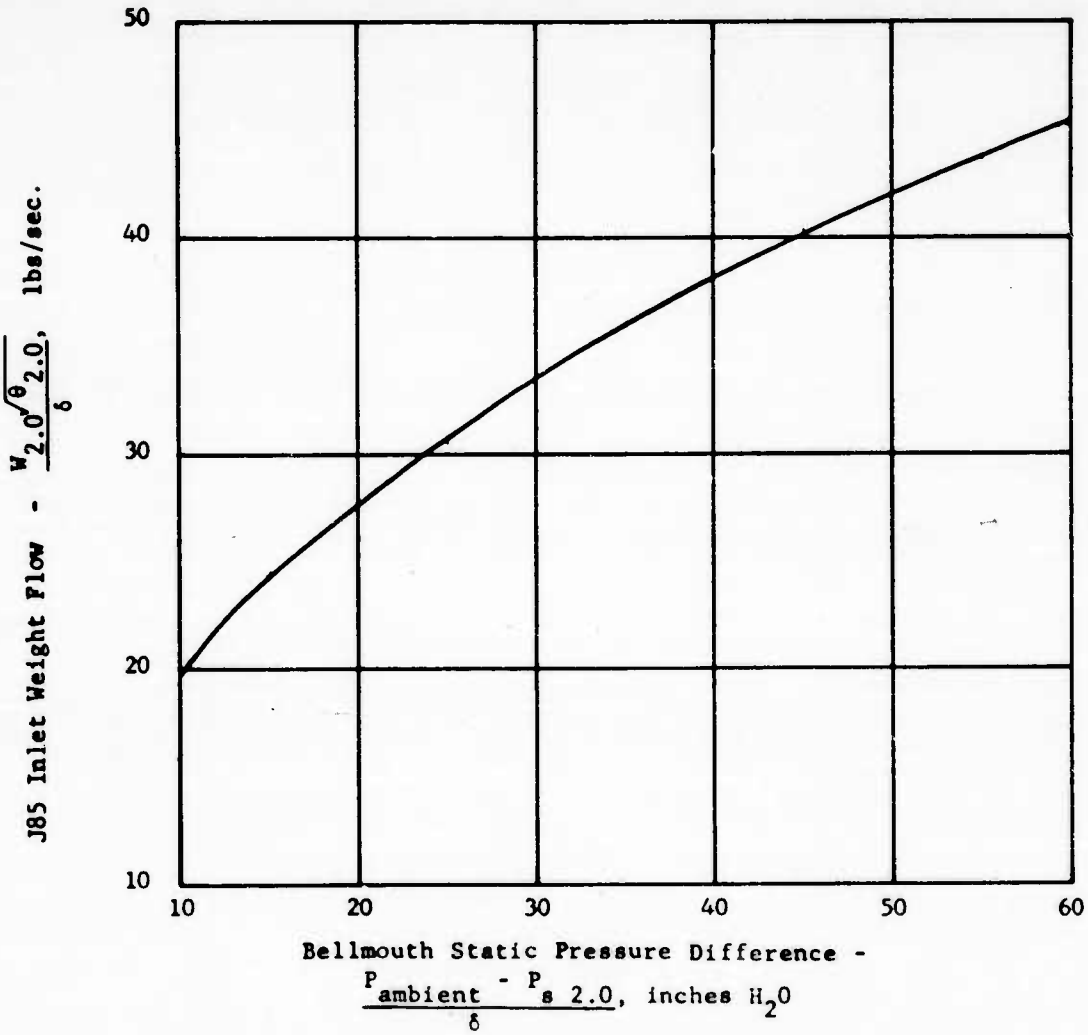

FIGURE B-1 - J85 INLET WEIGHT FLOW VERSUS BELLMOUTH STATIC PRESSURE DIFFERENCE

Source: SAED, GE, Lynn, Mass.

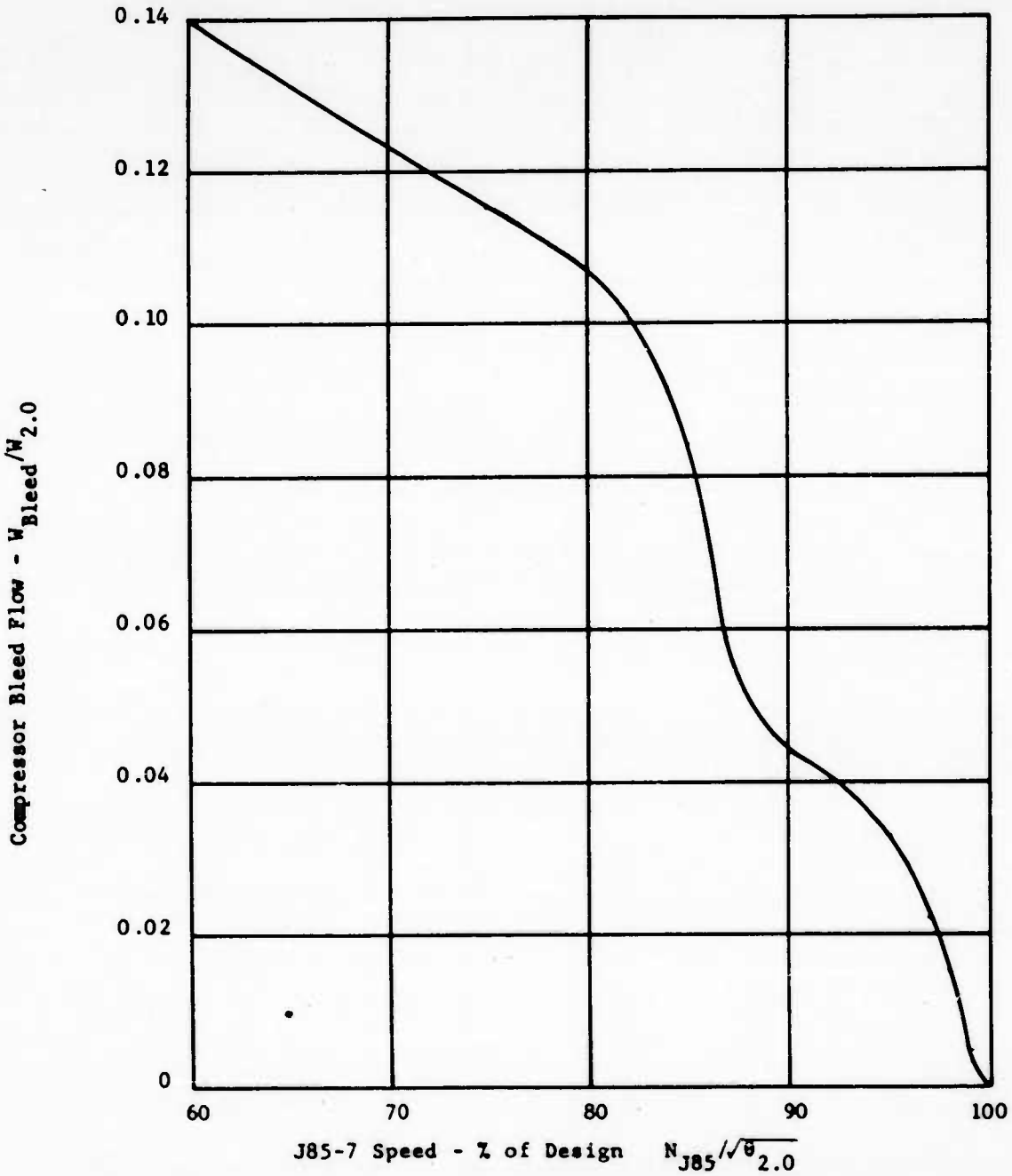

FIGURE B-2 - J85 COMPRESSOR BLEED VERSUS J85 SPEED

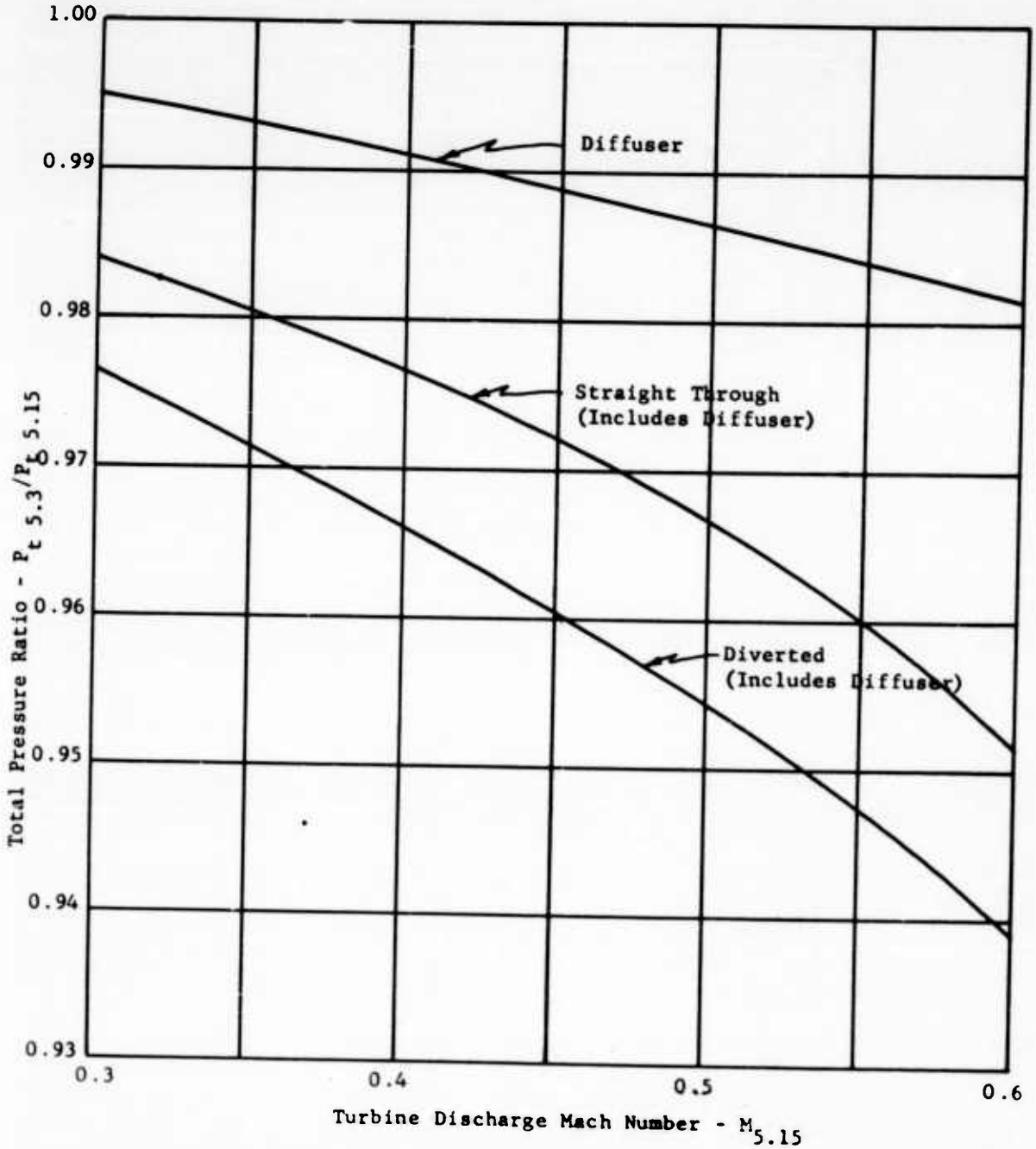

FIGURE B-3 - FULL SCALE DIVERTER VALVE LOSSES AS A FUNCTION OF TURBINE DISCHARGE MACH NUMBER

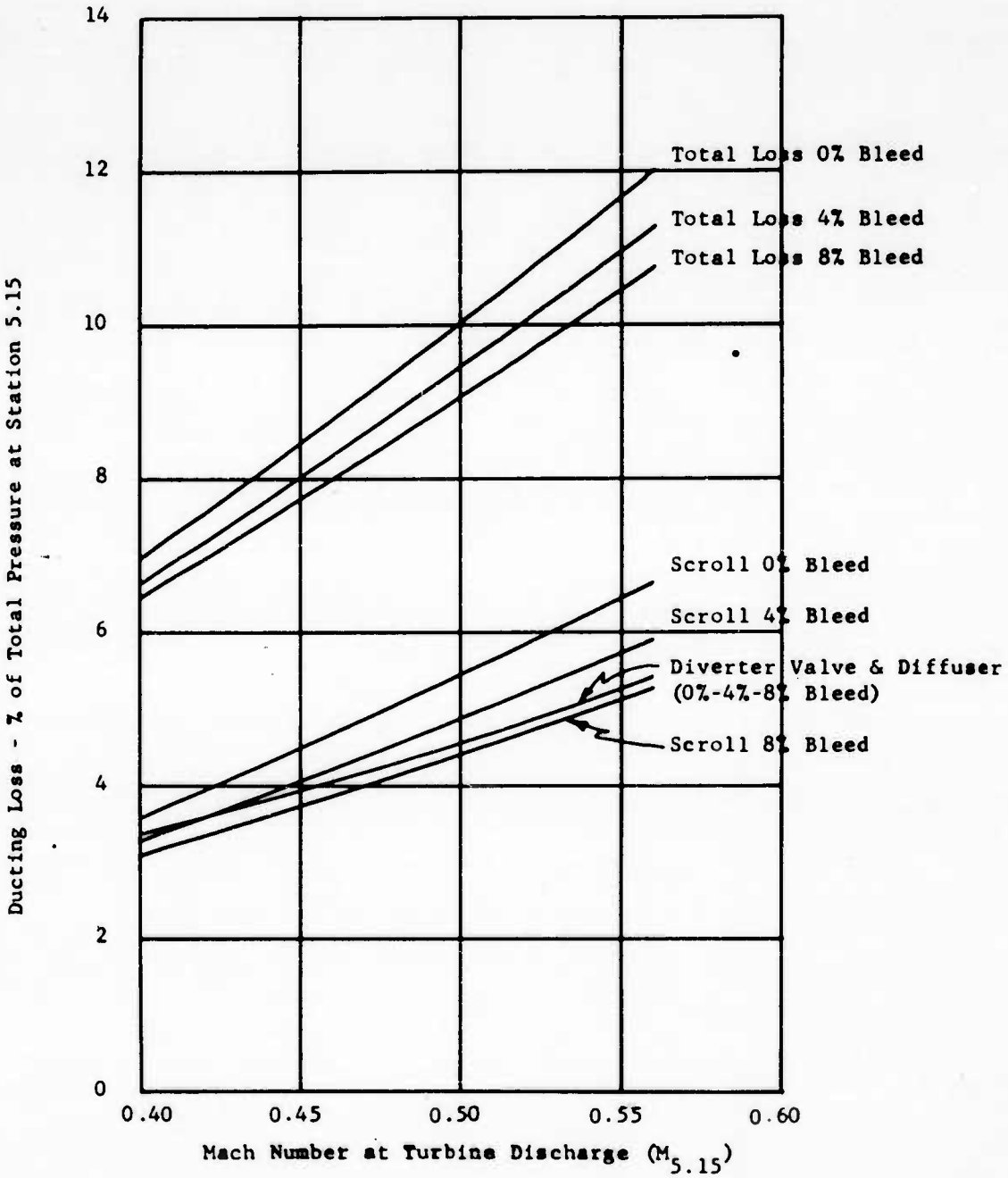

FIGURE B-4 - DUCTING LOSSES VERSUS TURBINE DISCHARGE MACH NUMBER

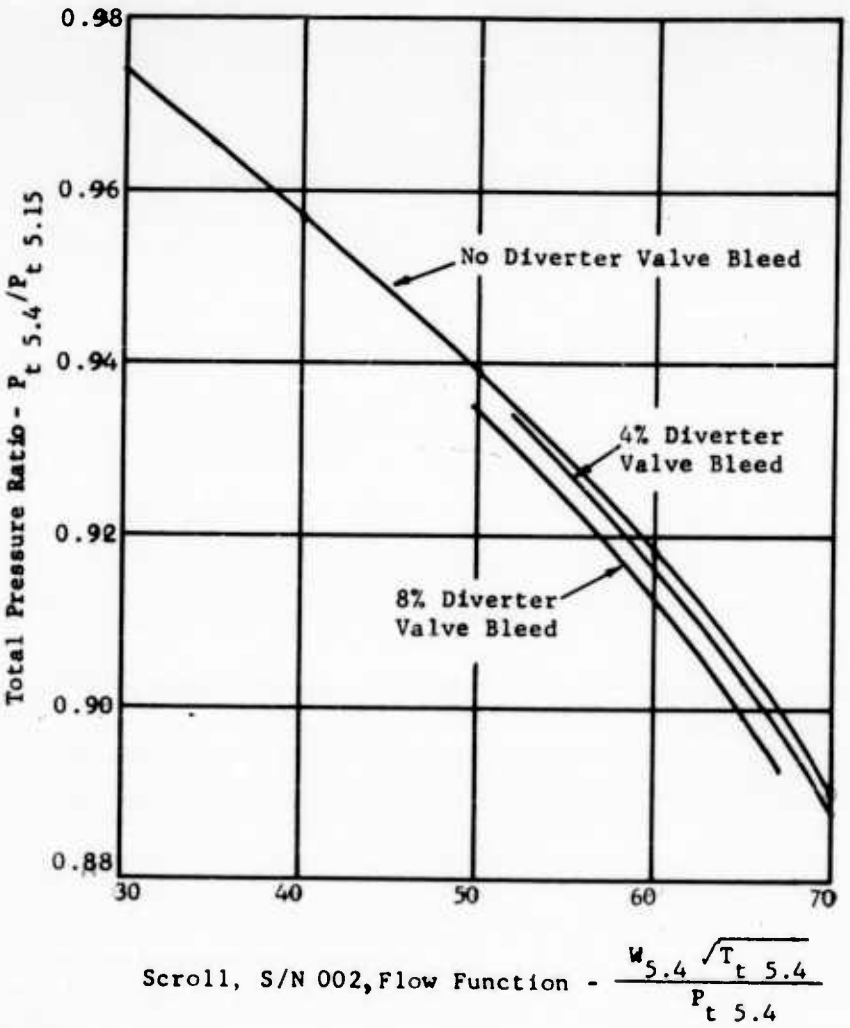

FIGURE B-5 - TURBINE DUCTING TOTAL PRESSURE RATIO (DIFFUSER + DIVERTER VALVE + SCROLL, S/N 002) VERSUS SCROLL, S/N 002, FLOW FUNCTION

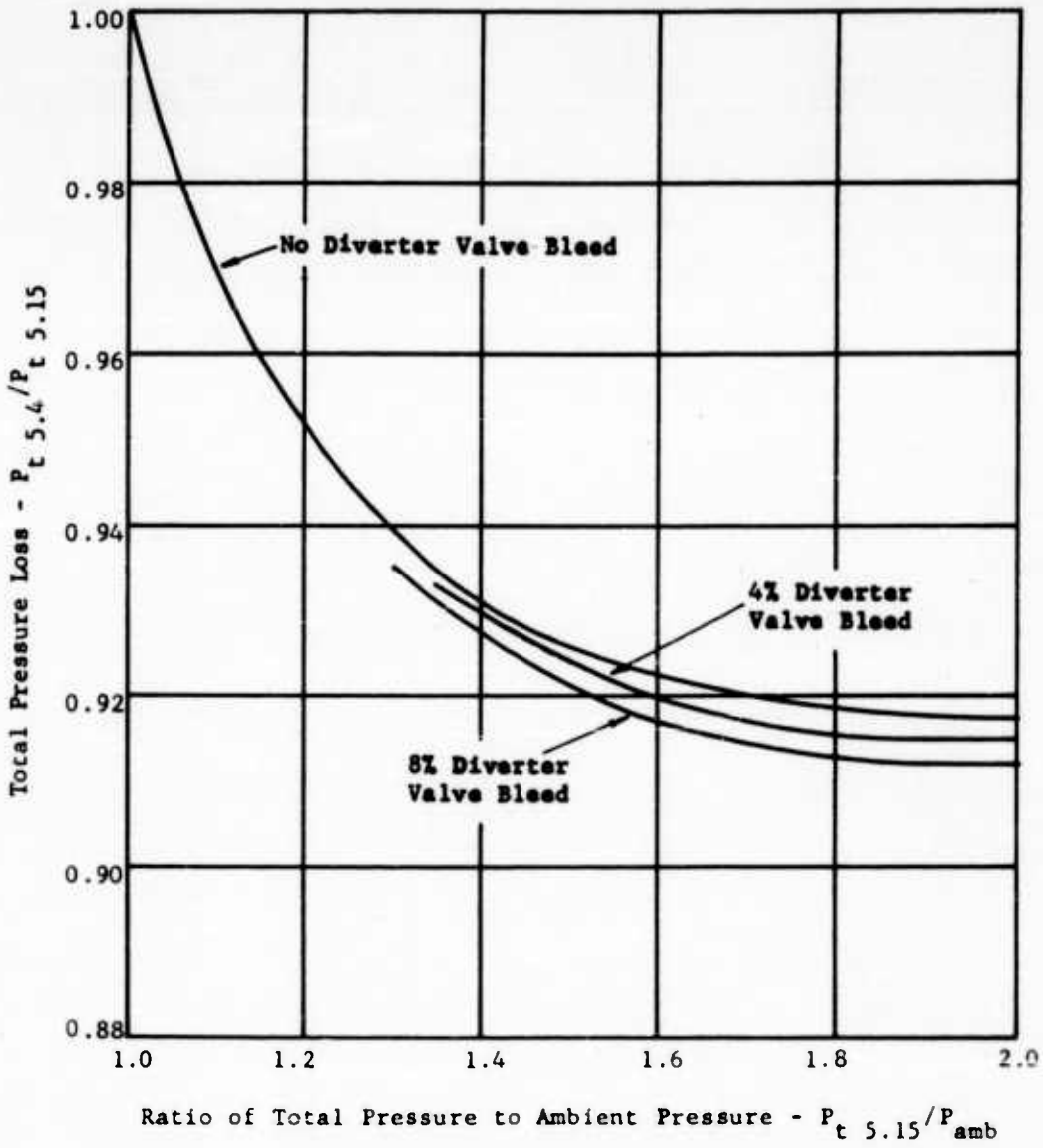

FIGURE B-6 - TURBINE DUCTING PRESSURE LOSS (DIFFUSER + DIVERTER VALVE + SCROLL, S/N 002)

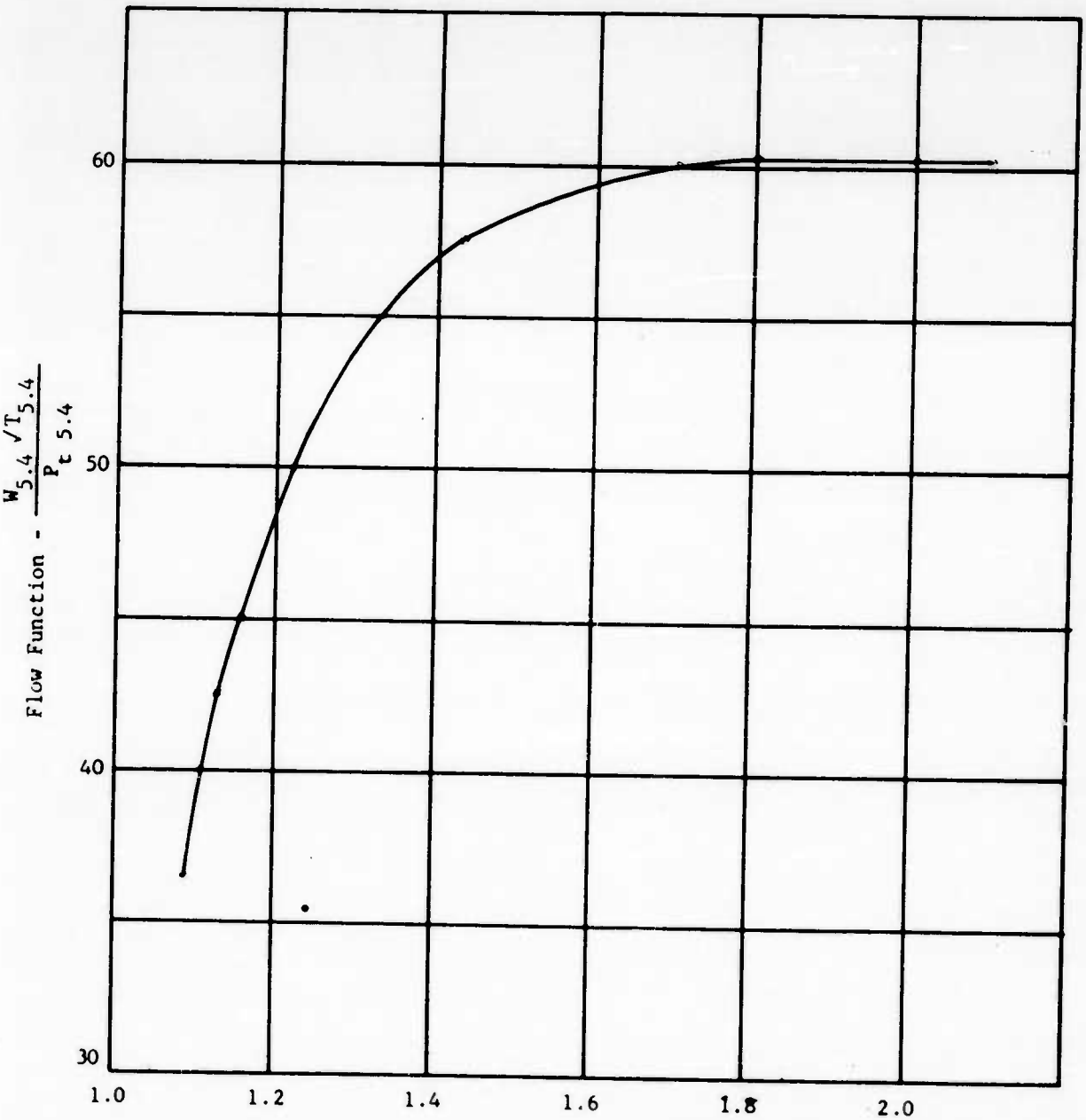

FIGURE B-7 - X353-5 FULL SCALE SCROLL, S/N 002, FLOW FUNCTION

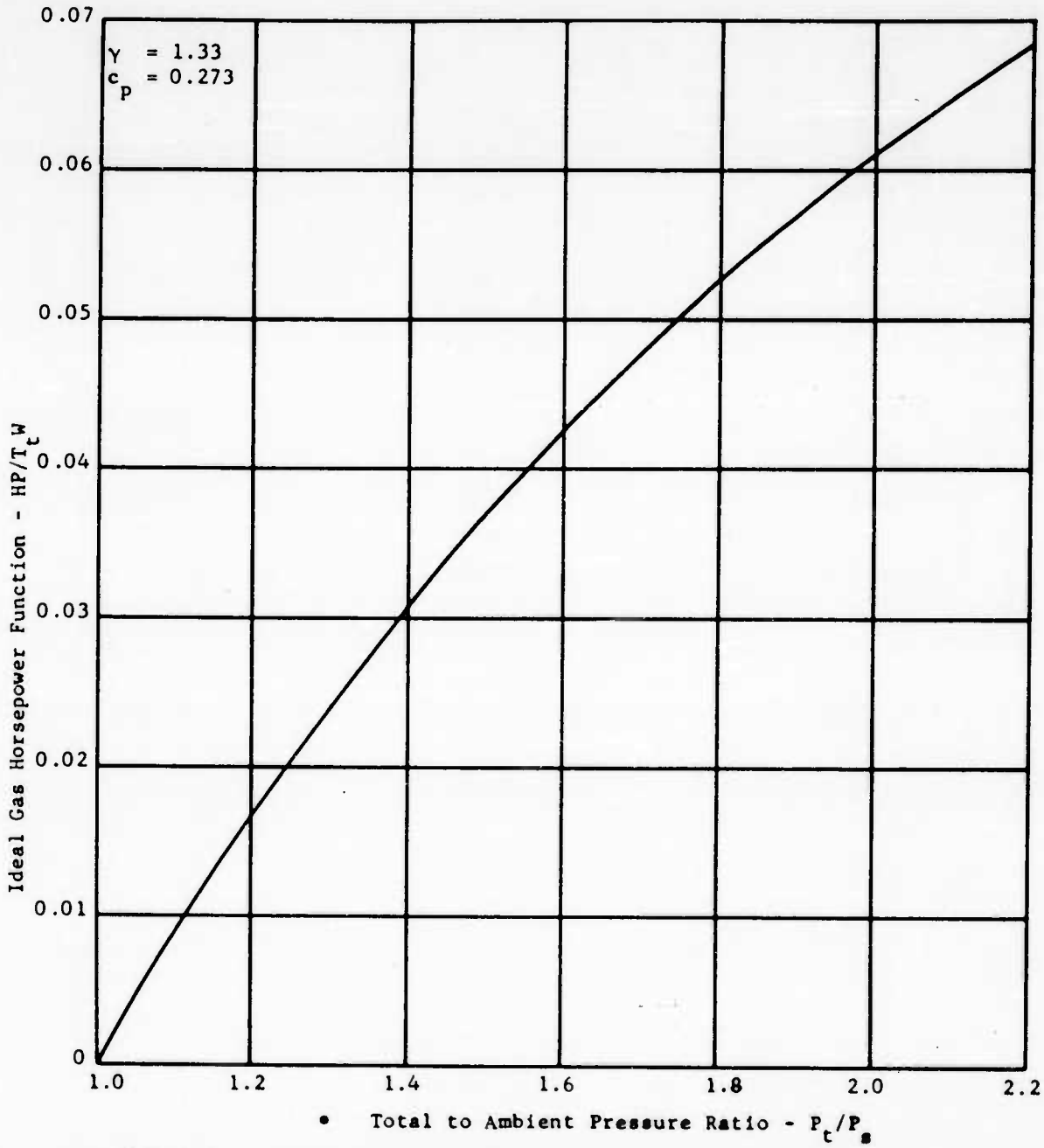

FIGURE B-8 - IDEAL GAS HORSEPOWER FUNCTION VERSUS TOTAL TO AMBIENT PRESSURE RATIO

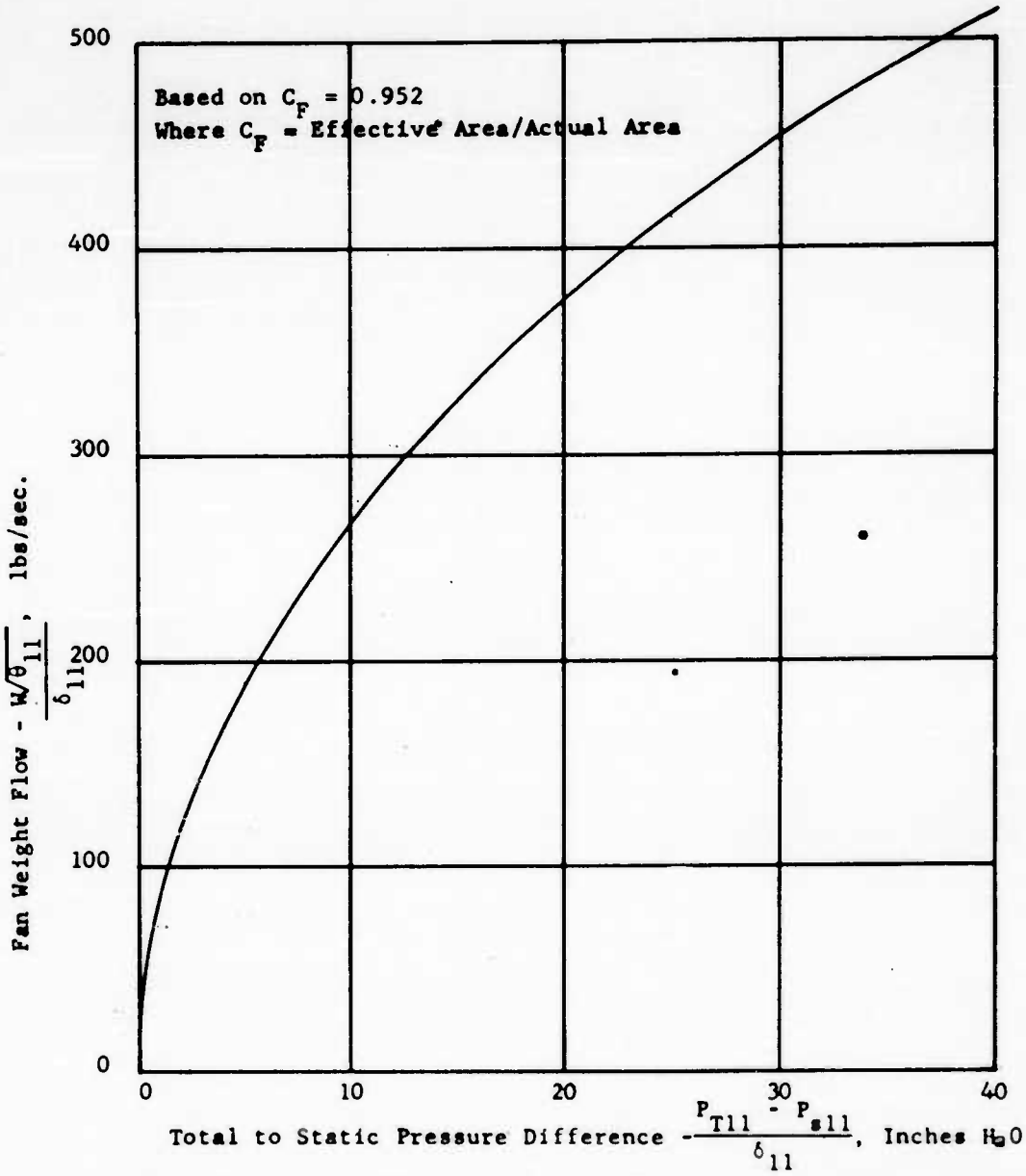

FIGURE B-9 - FAN-IN-WING INLET WEIGHT FLOW CALIBRATION CURVE (EXIT MEASURING DUCT)

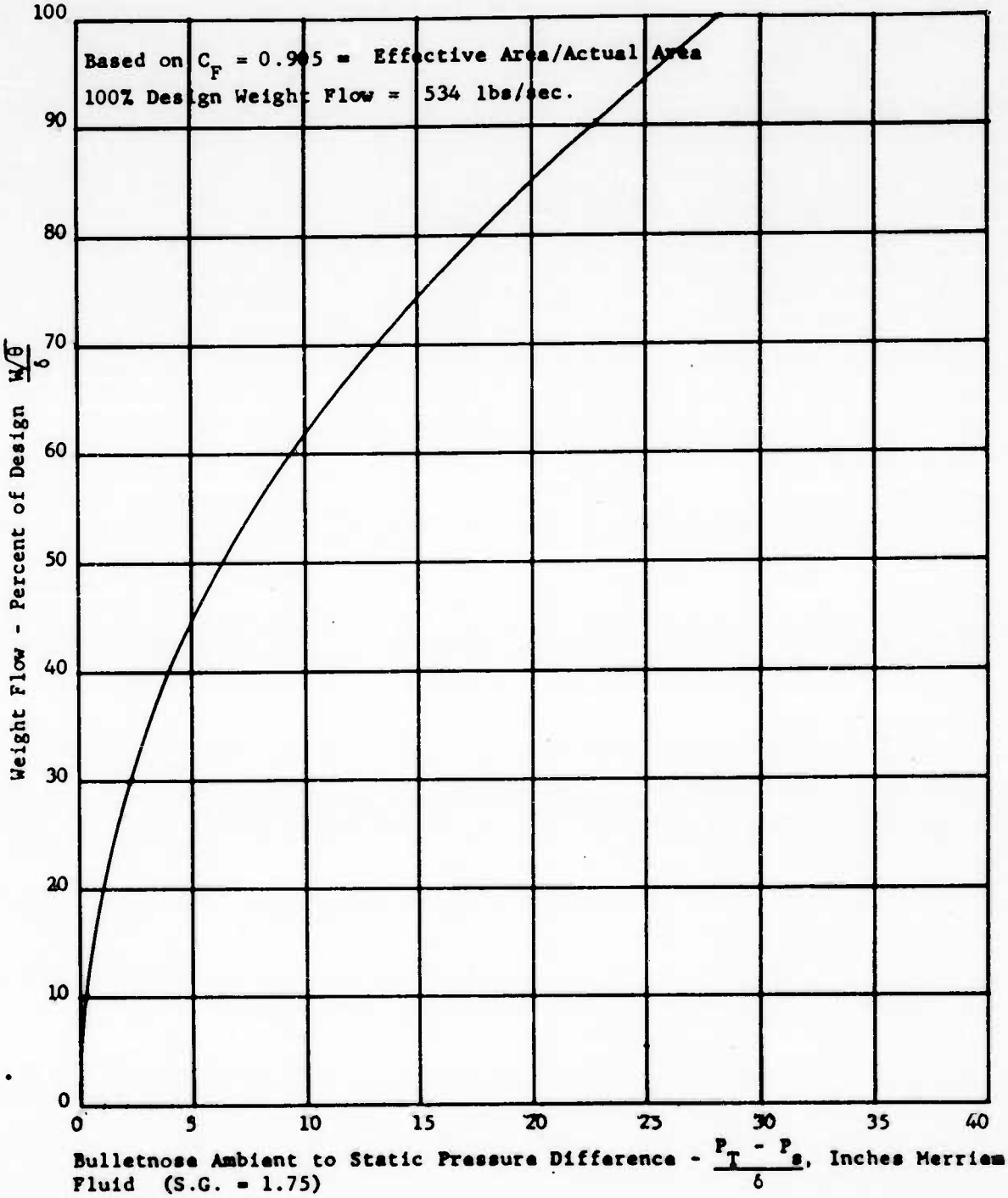

FIGURE B-10 - FAN-IN-WING INLET WEIGHT FLOW VERSUS BULLETNOSE AMBIENT TO STATIC PRESSURE DIFFERENCE

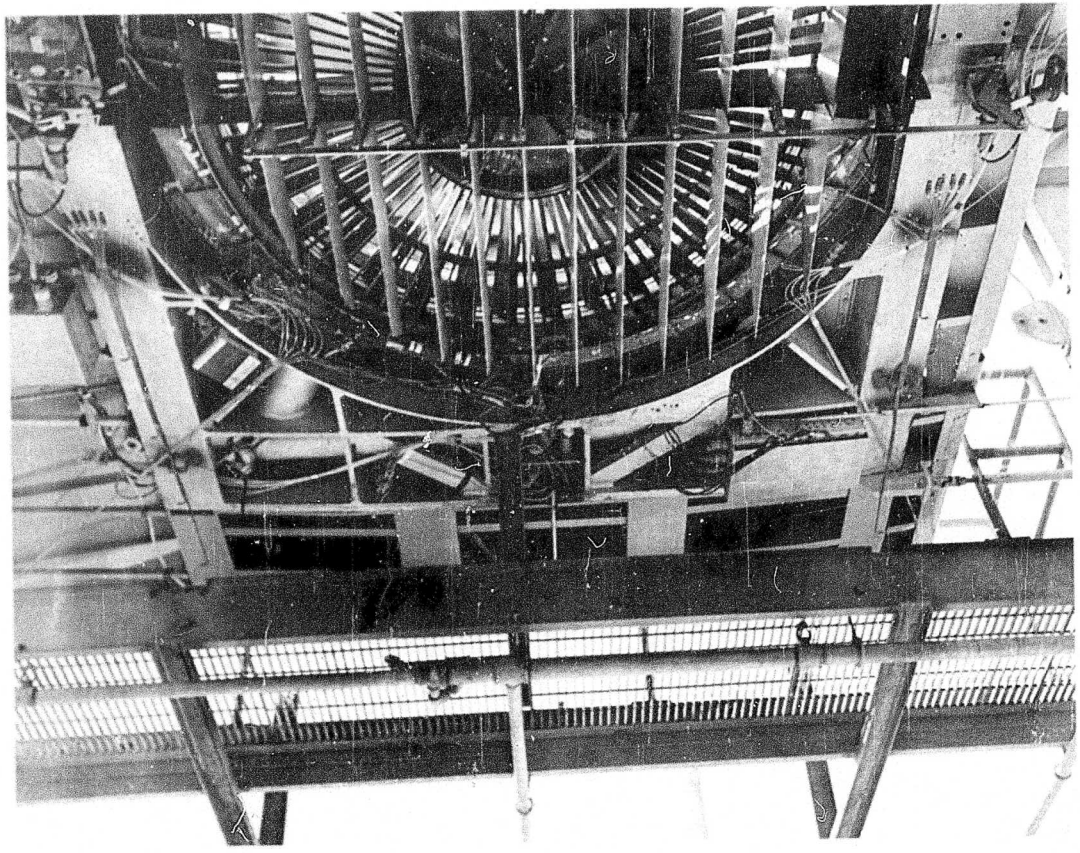

FIGURE 1 VIEW OF FAN INSTALLED IN WING SHOWING EXIT LOUVER ACTUATION DETAILS

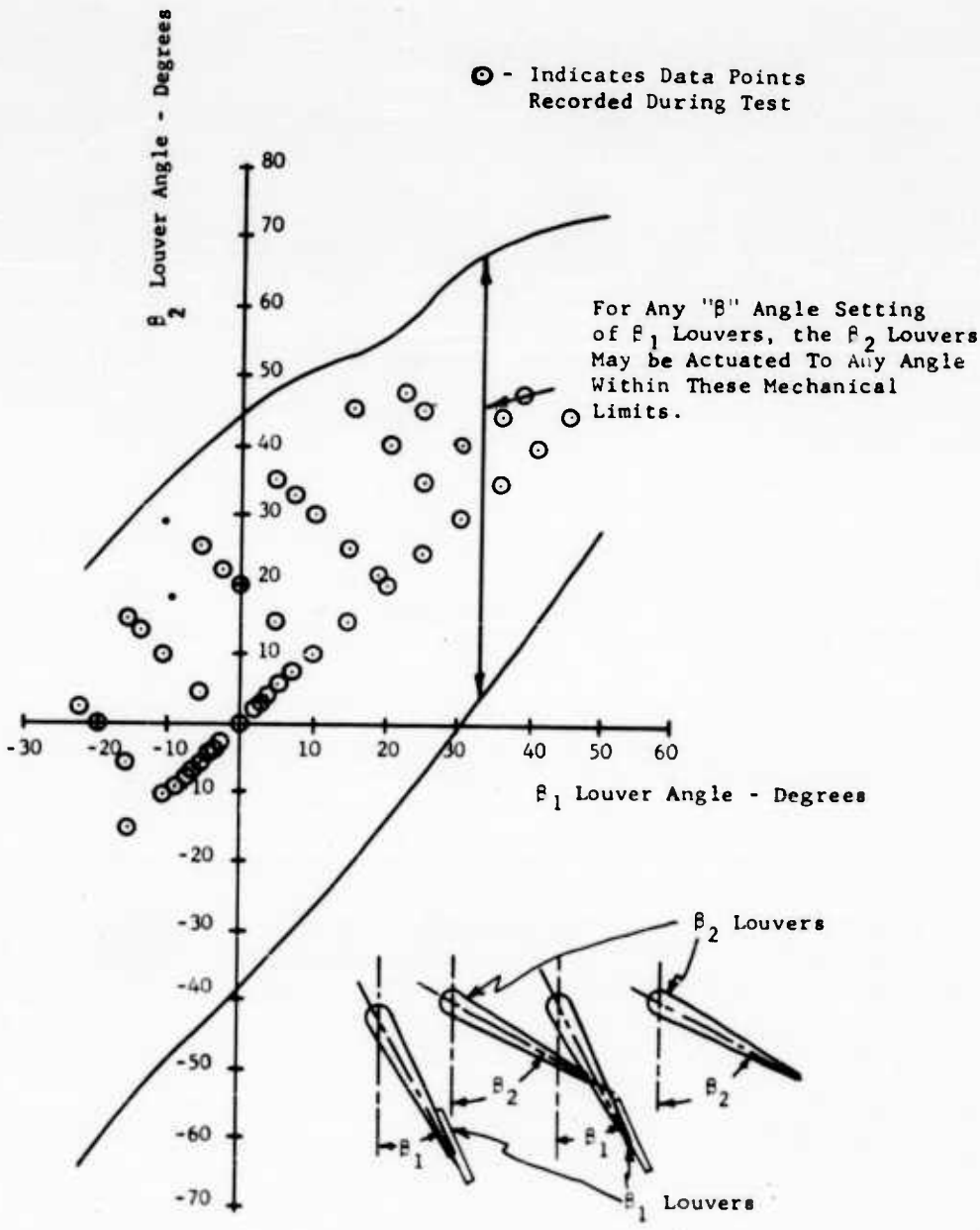

FIGURE 2 - DIFFERENTIAL EXIT LOUVER ACTUATION - MECHANICAL ACTUATION ANGLE LIMITS

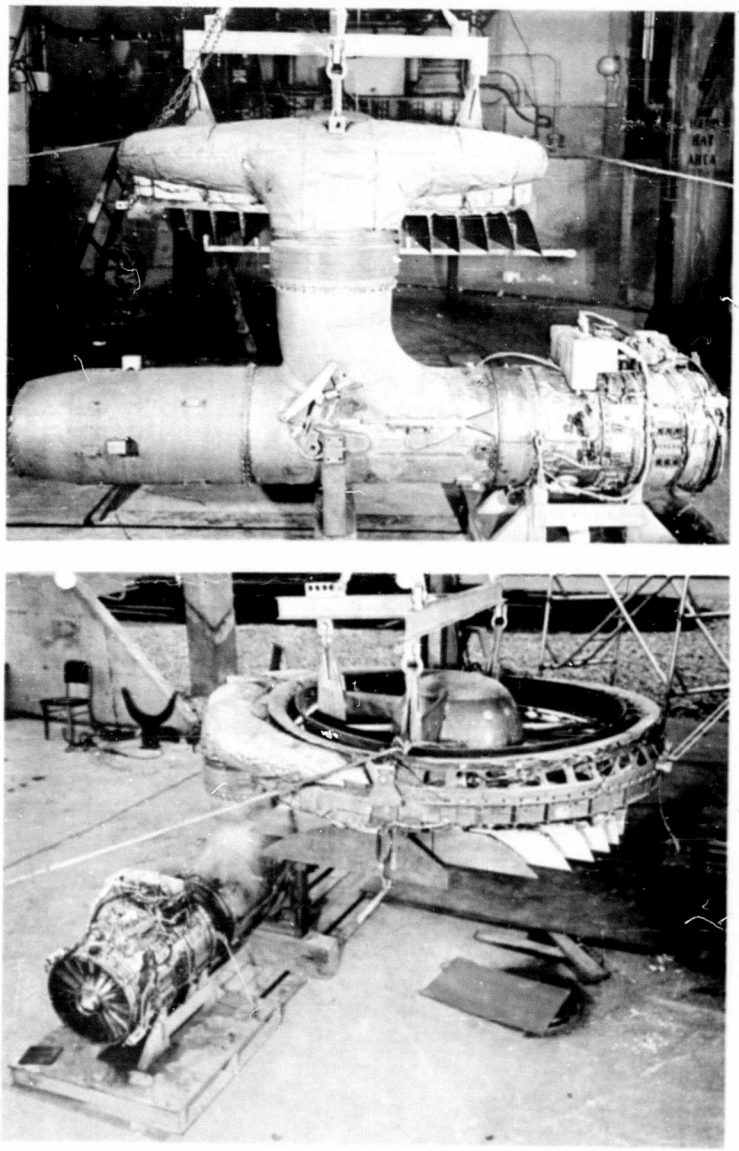

FIGURE 3 VIEWS OF COMPLETE TEST VEHICLE, AFTER TEST

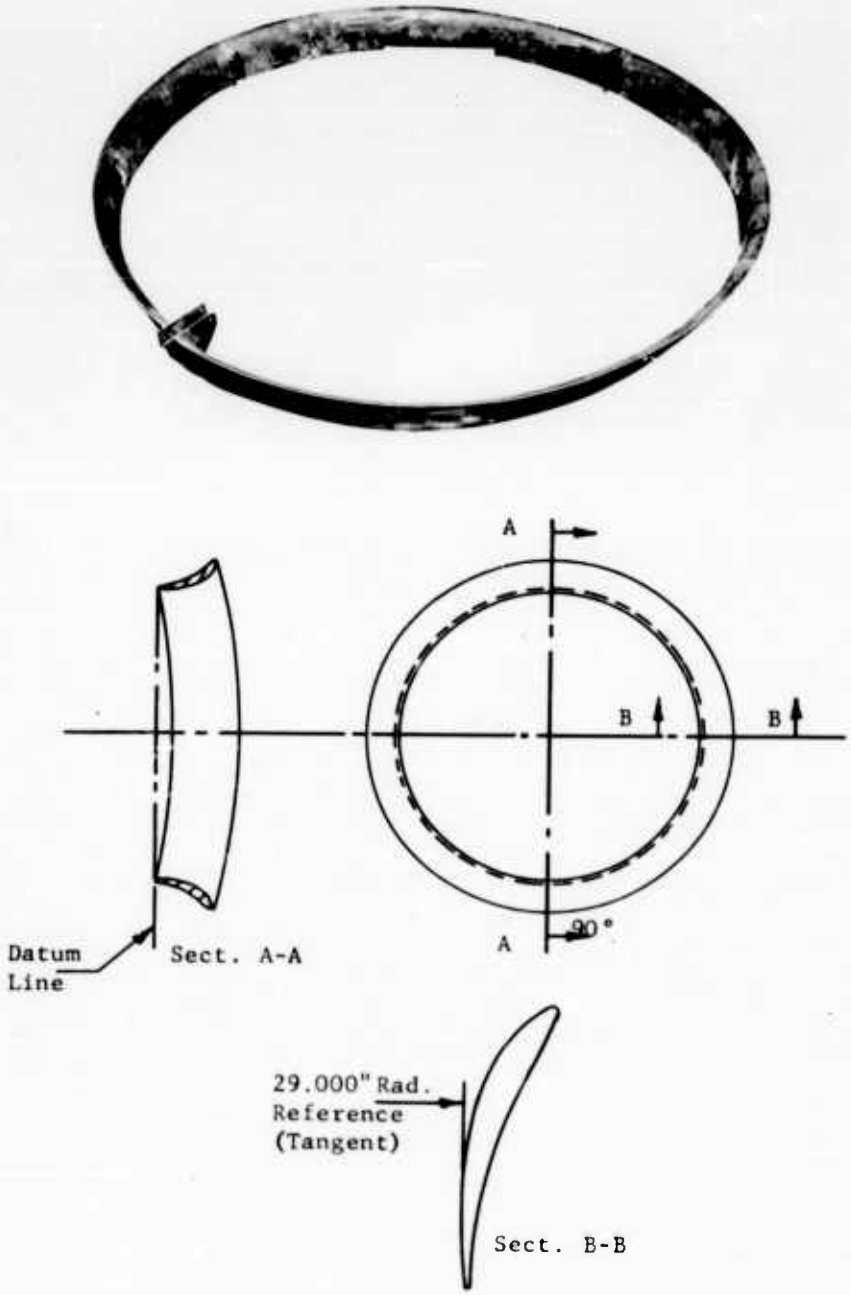

FIGURE 4 360° INLET VANE - OUTLINE

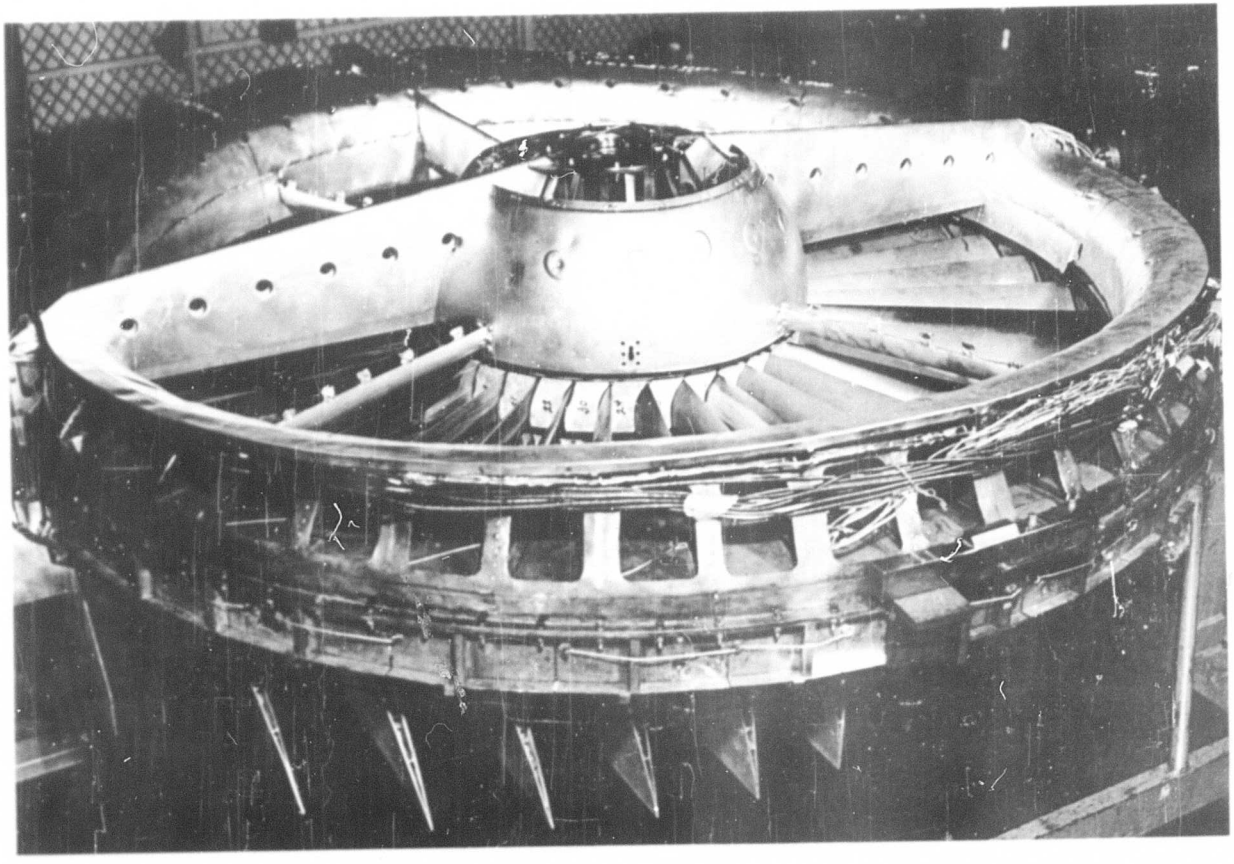

FIGURE 5 FAN ASSEMBLY SHOWING INLET BAFFLE WELDED TO FORWARD FRAME

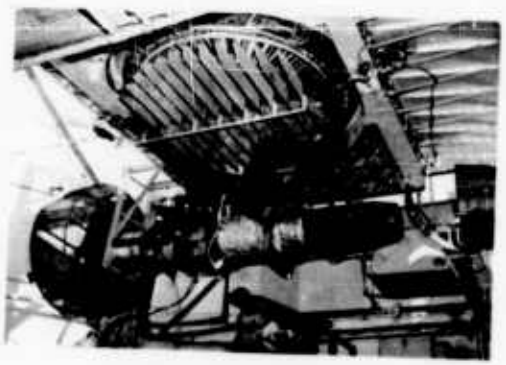

FIGURE 6 FAN INSTALLATION IN THE TEST FACILITY

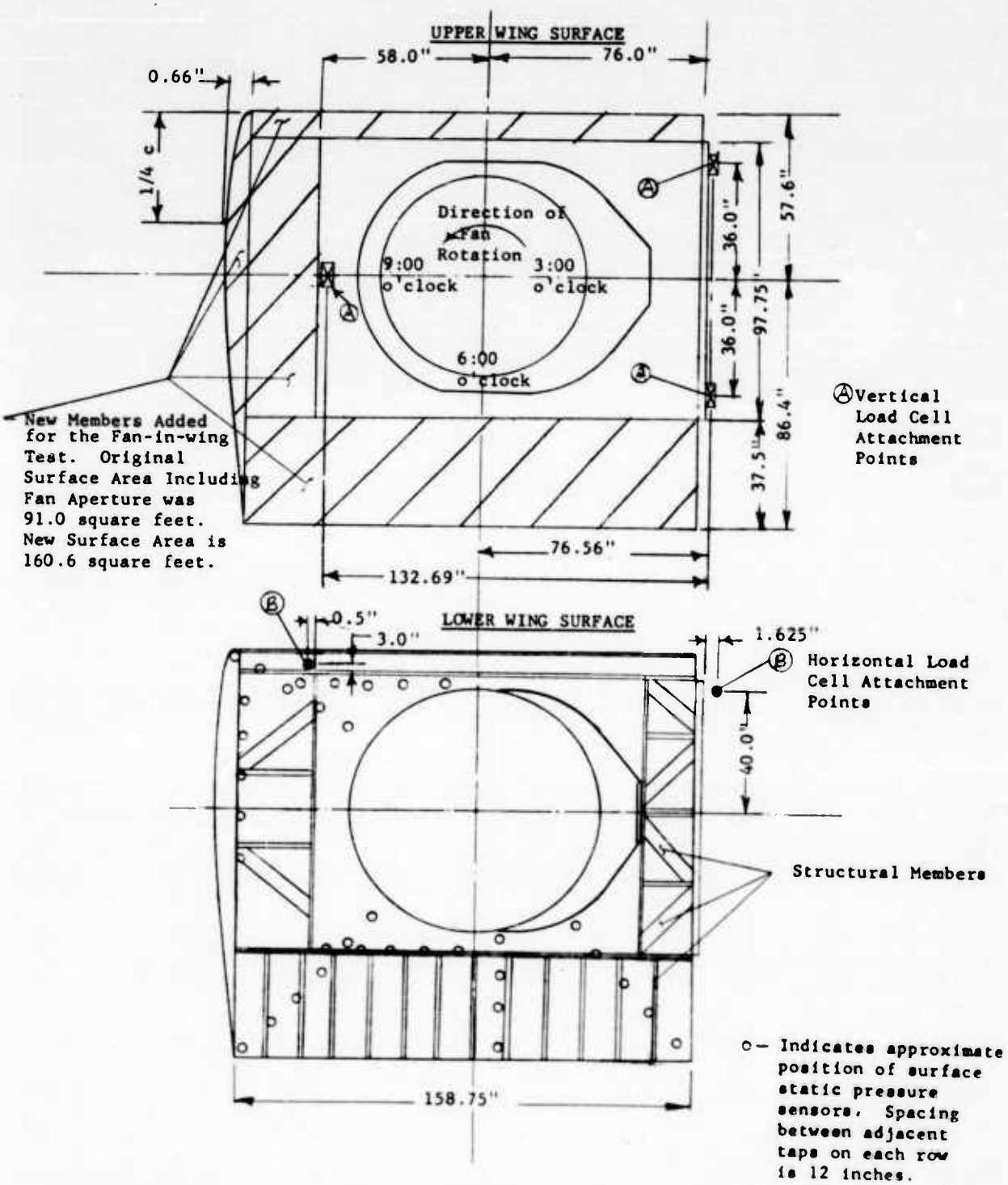

FIGURE 7 - WING DIMENSIONAL DETAILS

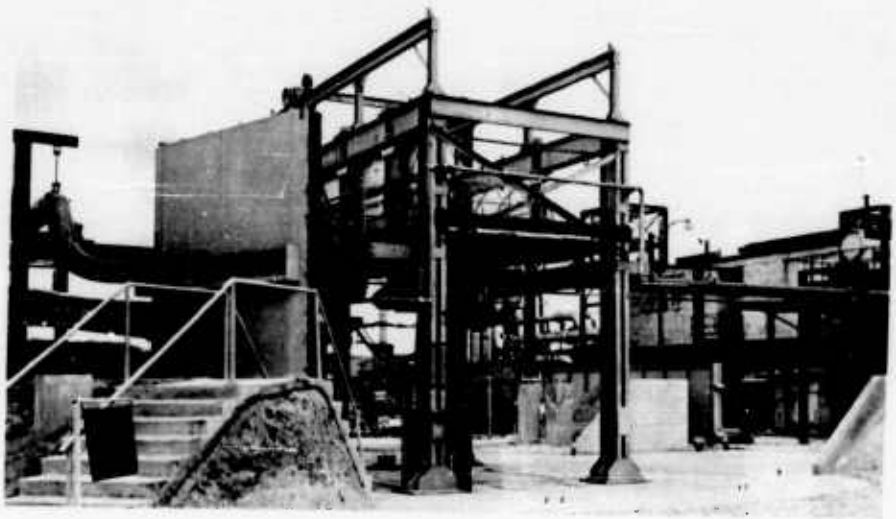

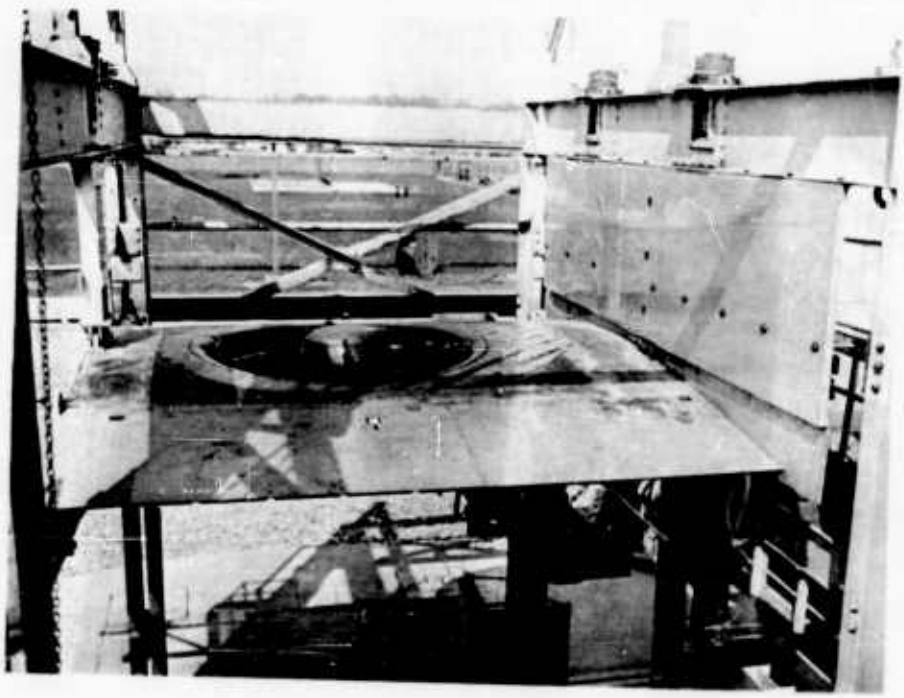

FIGURE 8 VIEWS OF FAN INSTALLATION AFTER REMOVING FACILITY WALLS

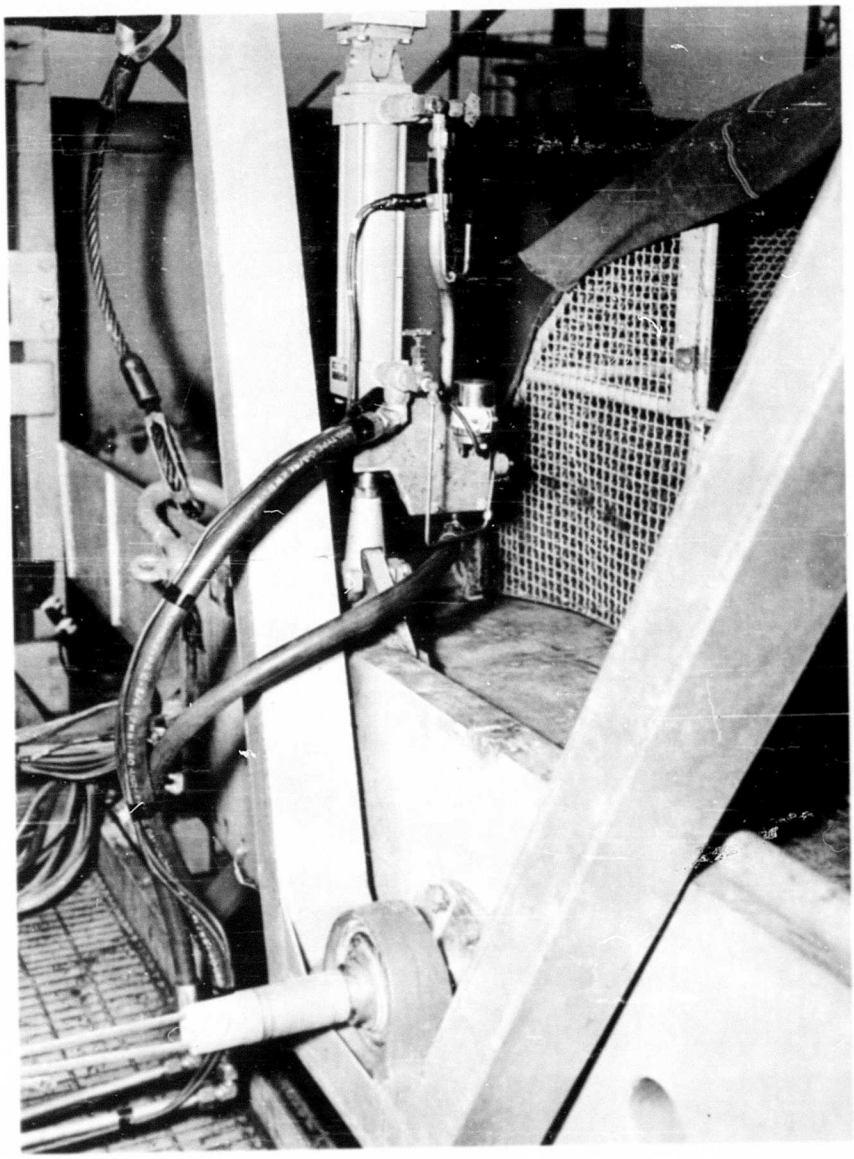

FIGURE 9 ACTUATOR AND TRUNNION SUPPORT FOR PITCHING MANEUVERS

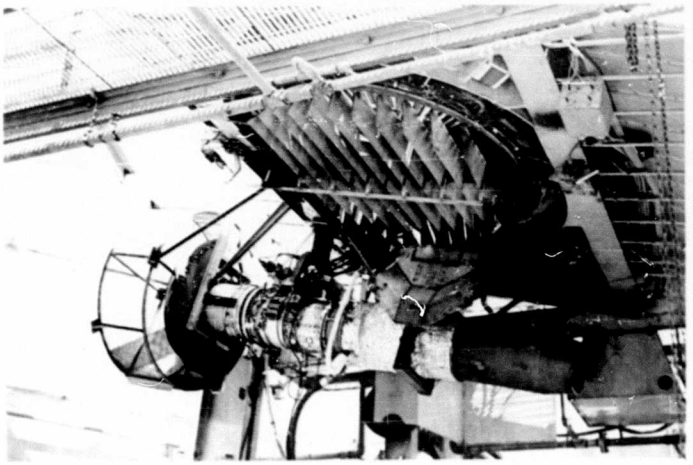

FIGURE 10a WING AT +15° ANGLE OF ATTACK (BEFORE PITCH MANEUVER)

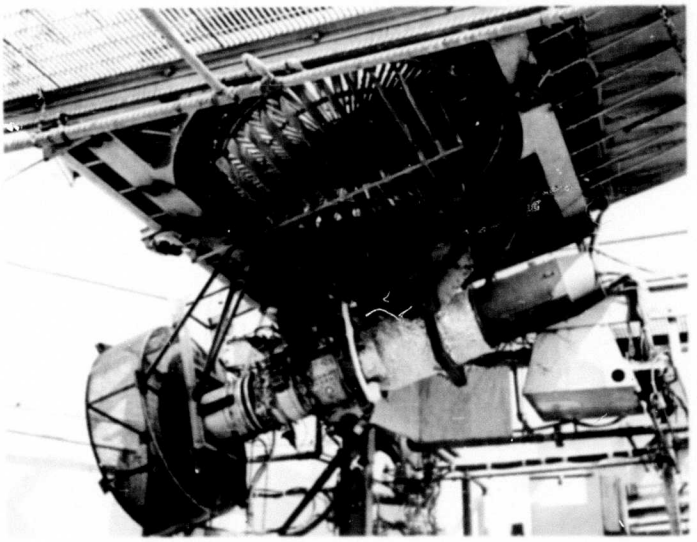

FIGURE 10b WING AT -15° ANGLE OF ATTACK (AFTER PITCH MANEUVER)

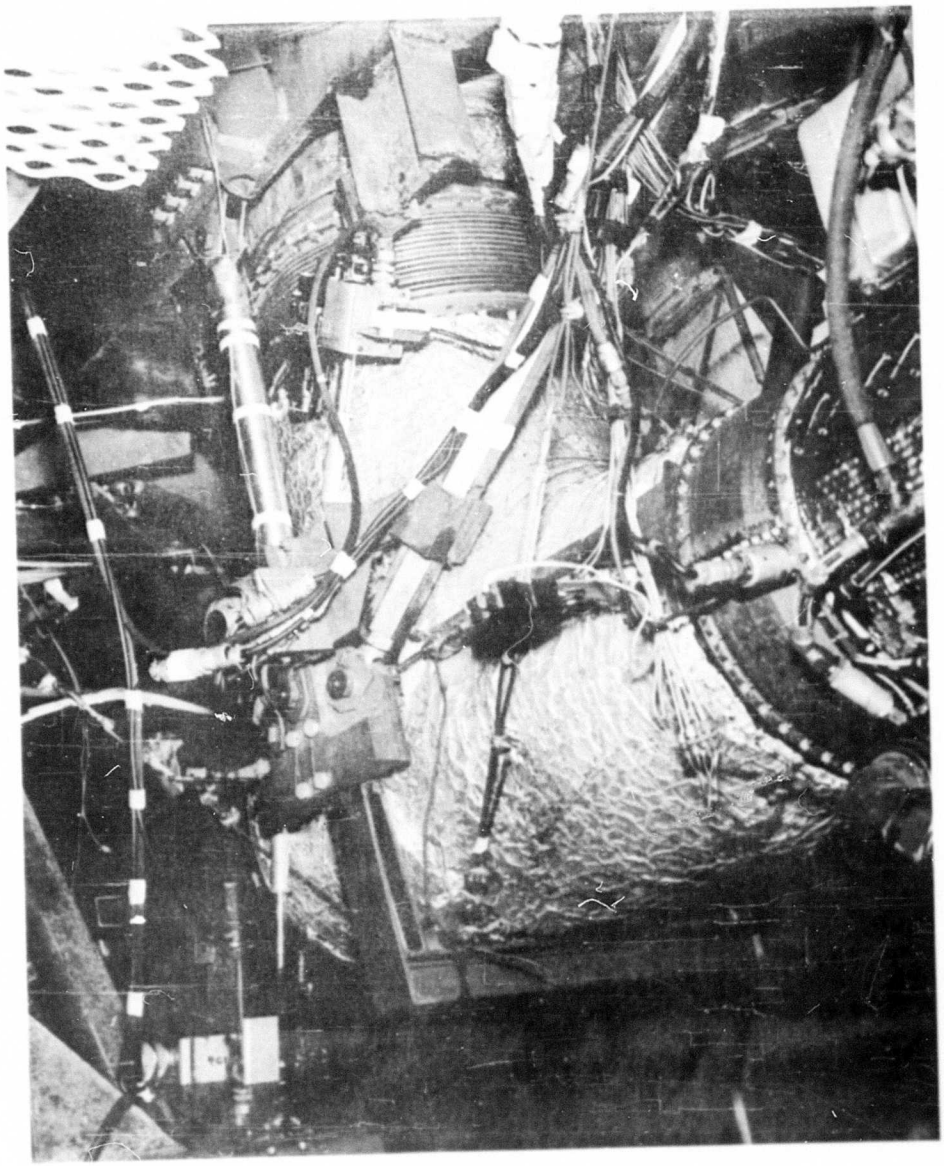

FIGURE 11 DIVERTER VALVE ACTUATION SET UP FOR SPLIT FLOW TESTING

PLANE NO.	J-85
0.0	Ambient
1.0	Inlet
2.0	Compressor Inlet
3.0	Compressor Discharge
4.0	Turbine Inlet
5.1	Turbine Discharge
	FAN (TURBINE)
5.15	Diverter Valve Inlet
5.3	Scroll Inlet
5.4	Turbine Nozzle Inlet
5.45	Turbine Nozzle Discharge
5.5	Turbine Rotor Discharge
5.6	Turbine Stator Discharge
5.8	Exit Louver Discharge

PLANE NO.	FAN
10.0	Fan Louver Inlet
10.3	Fan Rotor Inlet
10.6	Fan Rotor Discharge
11.0	Fan Stator Discharge
13.0	Exit Louver Discharge

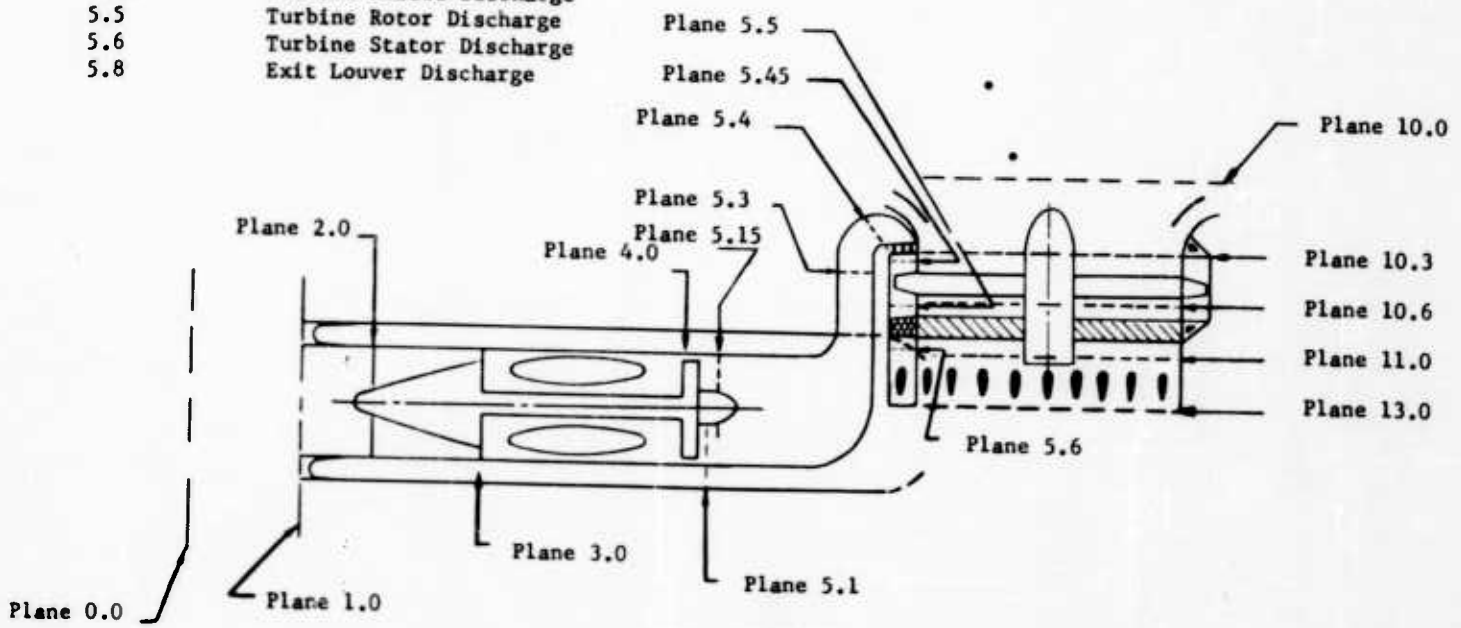

FIGURE 12 - SCHEMATIC OF INSTRUMENTATION PLANES

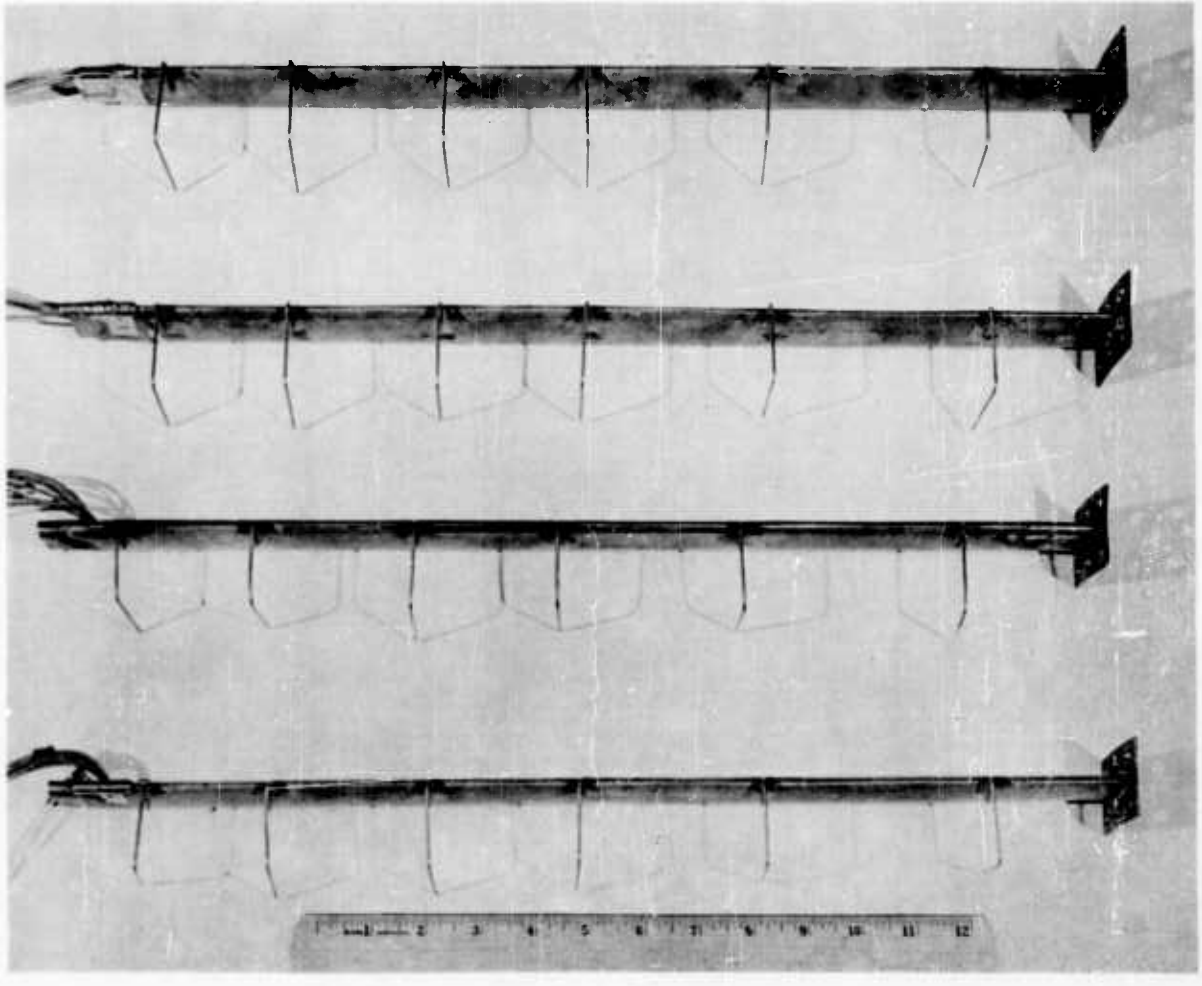

FIGURE 13 INLET TOTAL PRESSURE RAKES MODIFIED FOR RADIAL STATIC PRESSURE MEASUREMENT

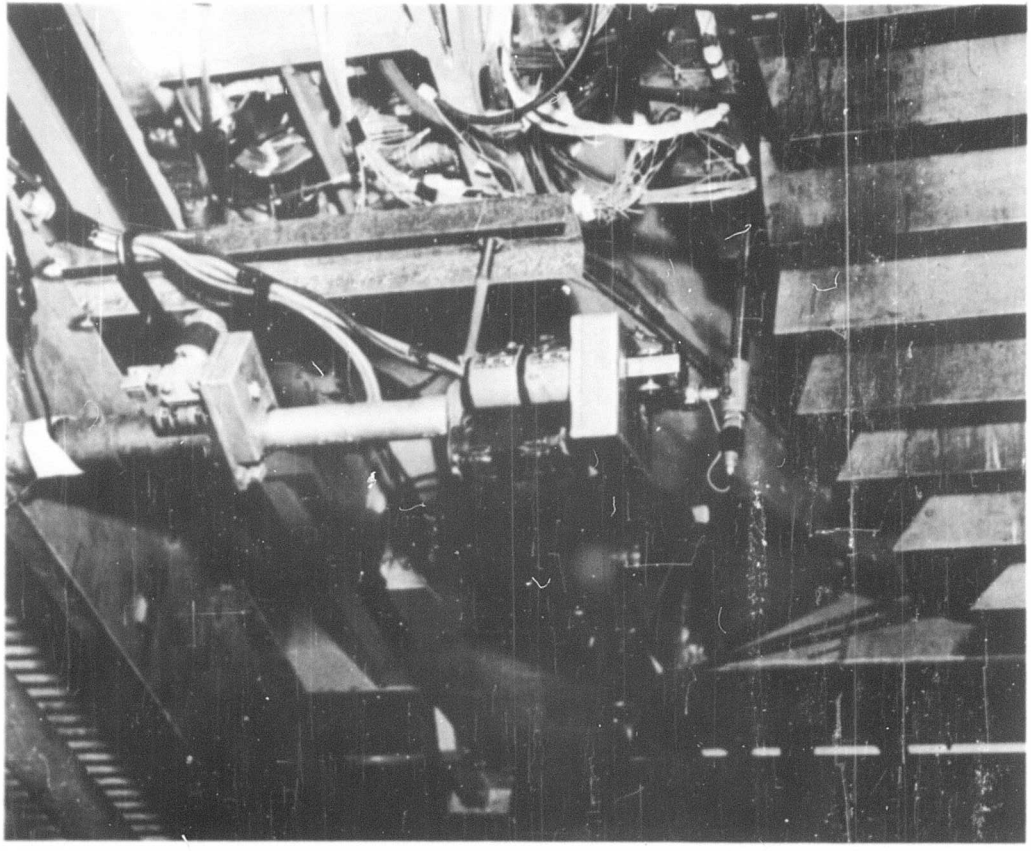

FIGURE 14 FAN DISCHARGE SOUND TRAVERSE PROBE AND ACTUATOR

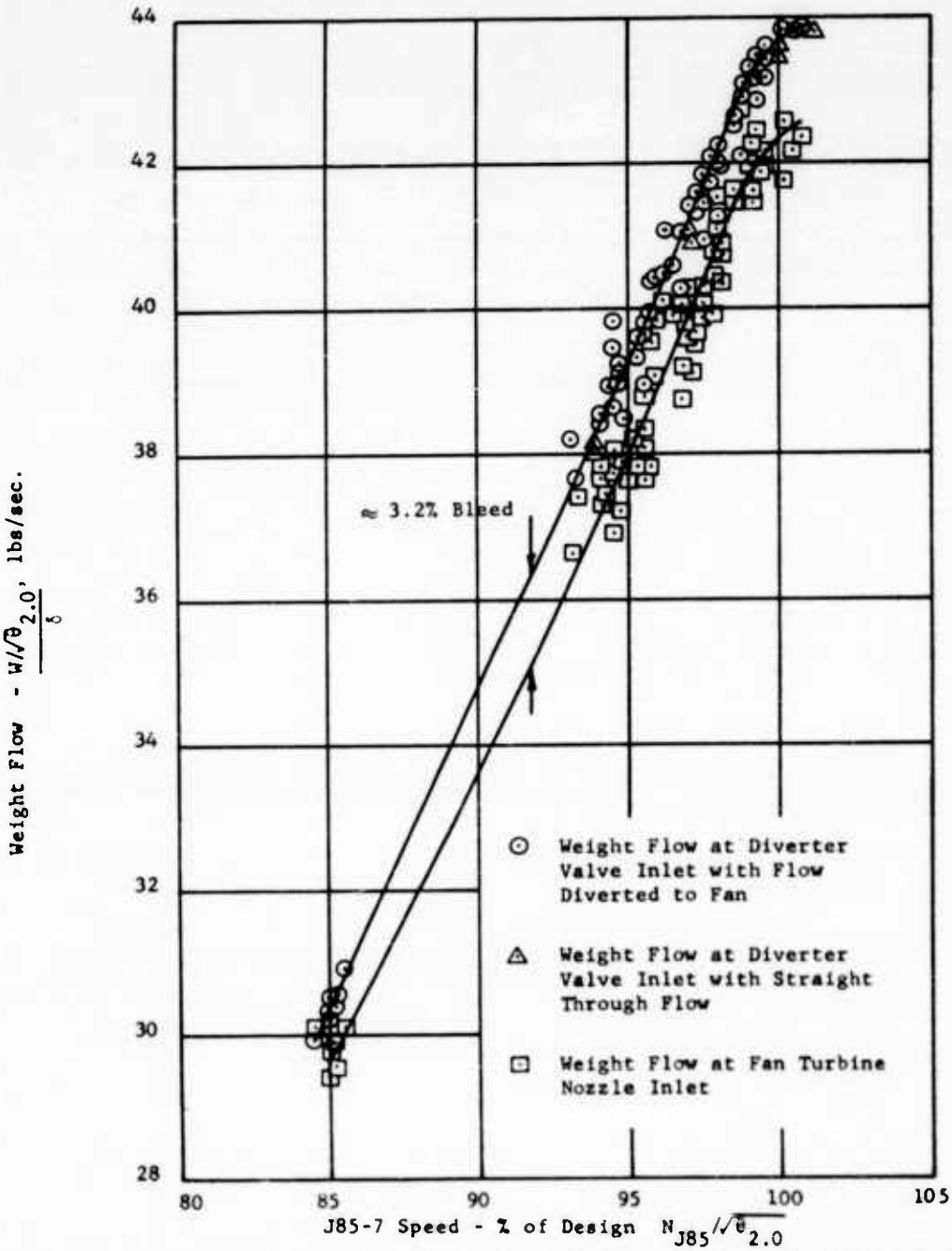

FIGURE 15a - DIVERTER VALVE INLET WEIGHT FLOW AND FAN TURBINE INLET WEIGHT FLOW VERSUS J85-7 SPEED (DIVERTER VALVE SET FOR 3.2% BLEED)

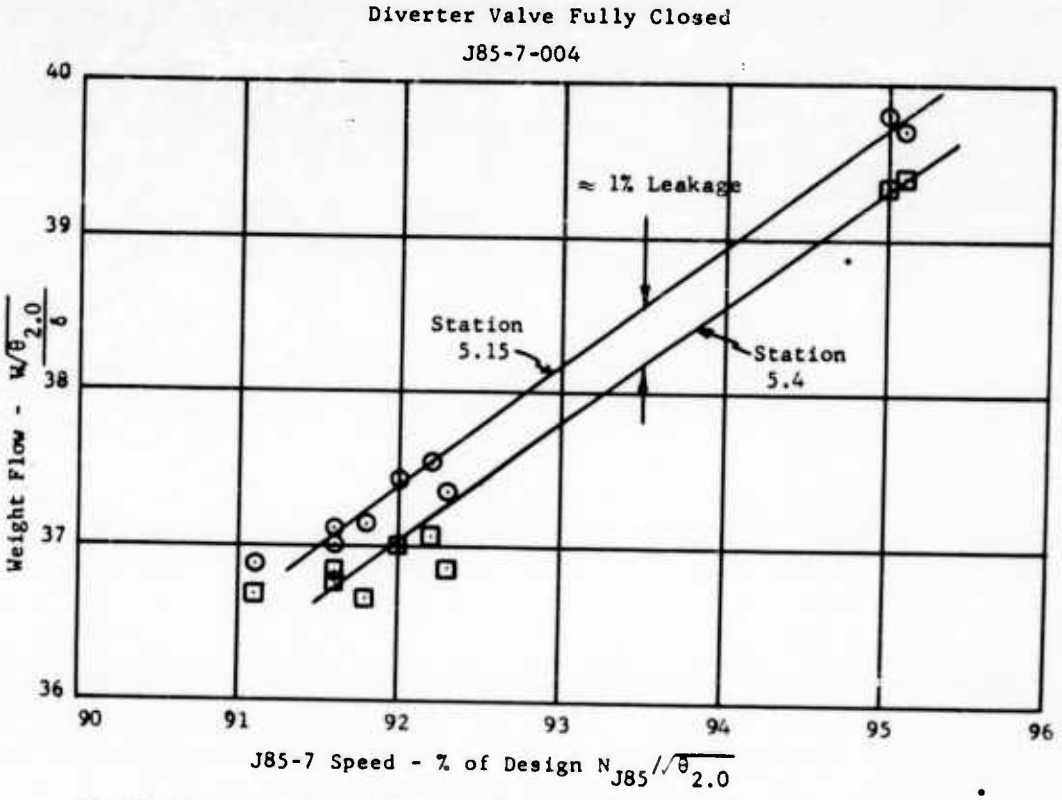

FIGURE 15b - WEIGHT FLOW AT DIVERTER VALVE INLET (STATION 5.15) AND FAN TURBINE NOZZLE INLET (STATION 5.4) VERSUS J85-7 SPEED

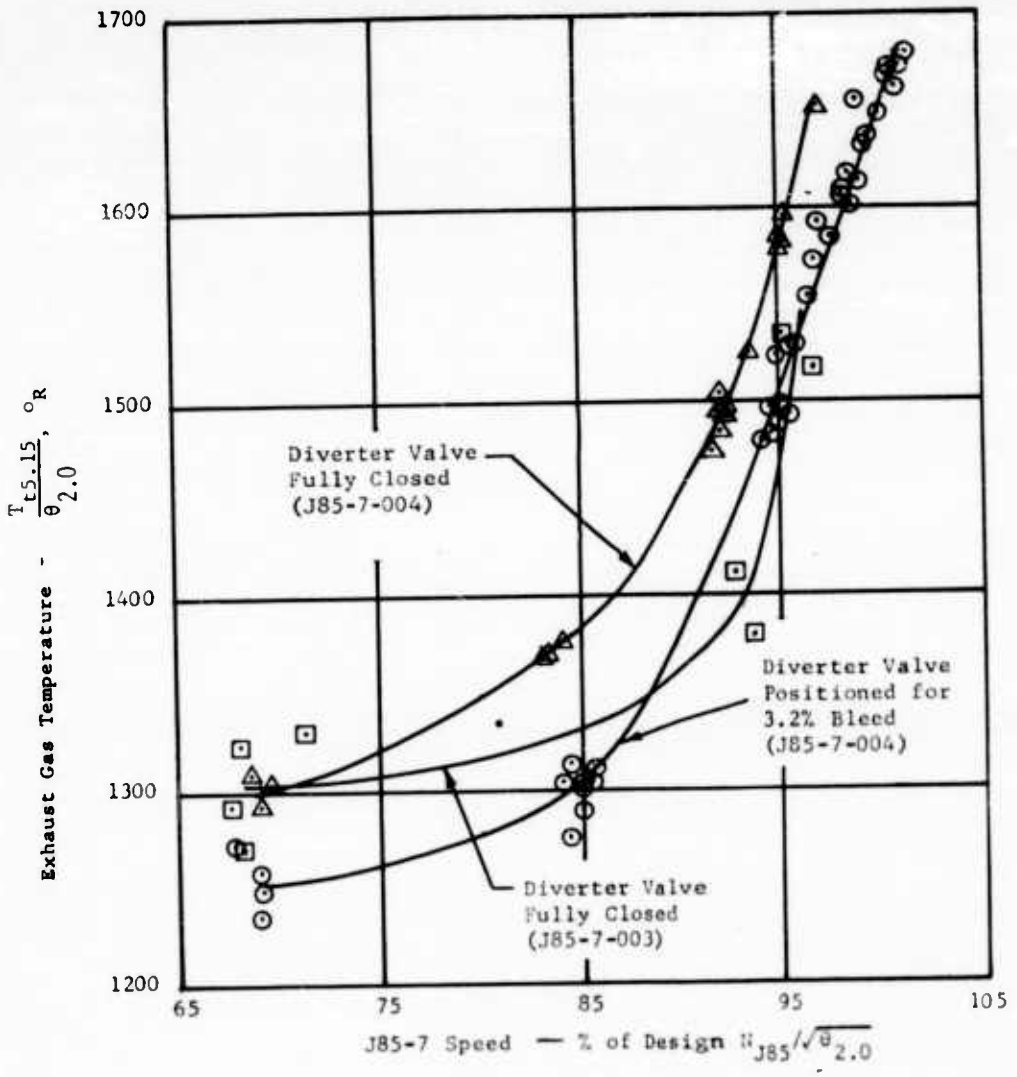

FIGURE 16a - EXHAUST GAS TEMPERATURE VERSUS J85-7 SPEED (DIVERTED FLOW)

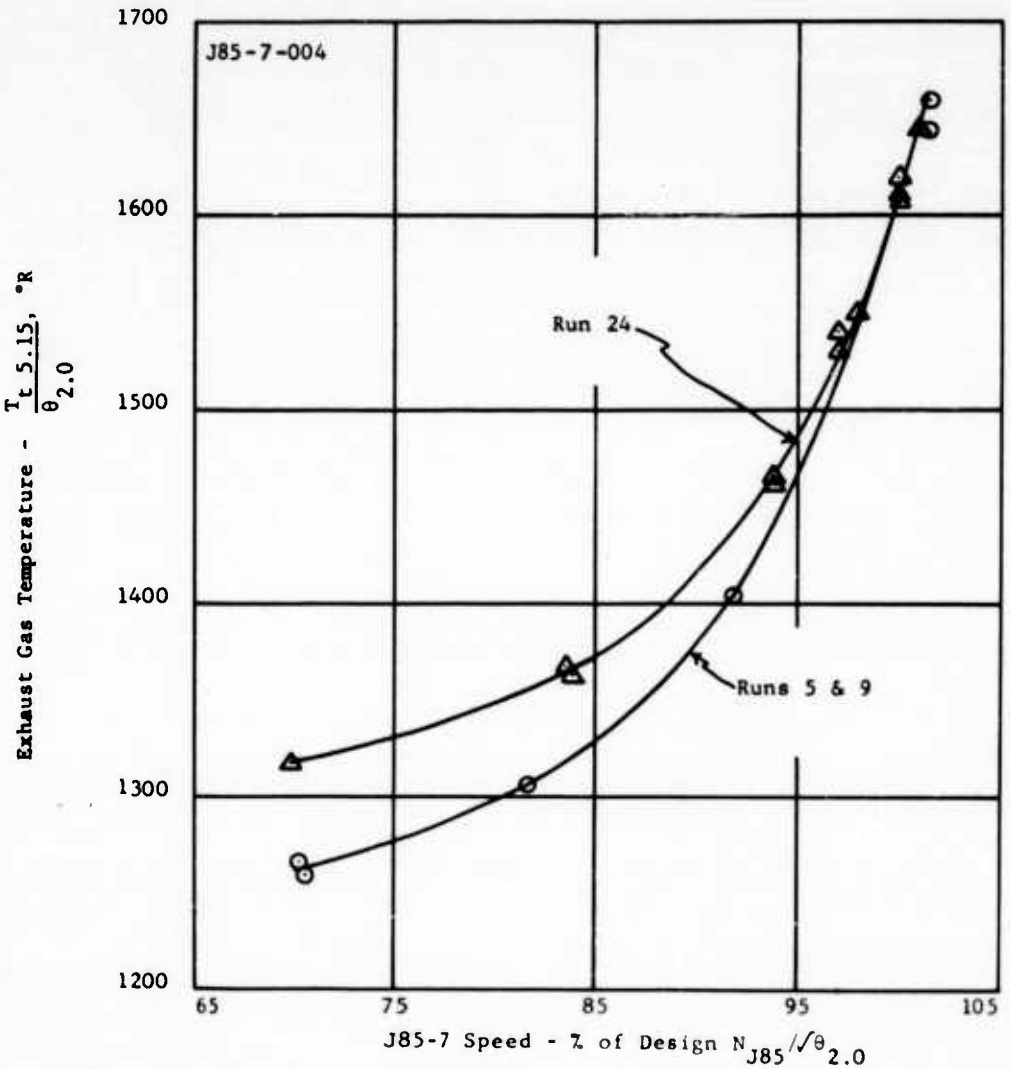

FIGURE 16b - EXHAUST GAS TEMPERATURE VERSUS J85-7 SPEED (STRAIGHT THROUGH FLOW)

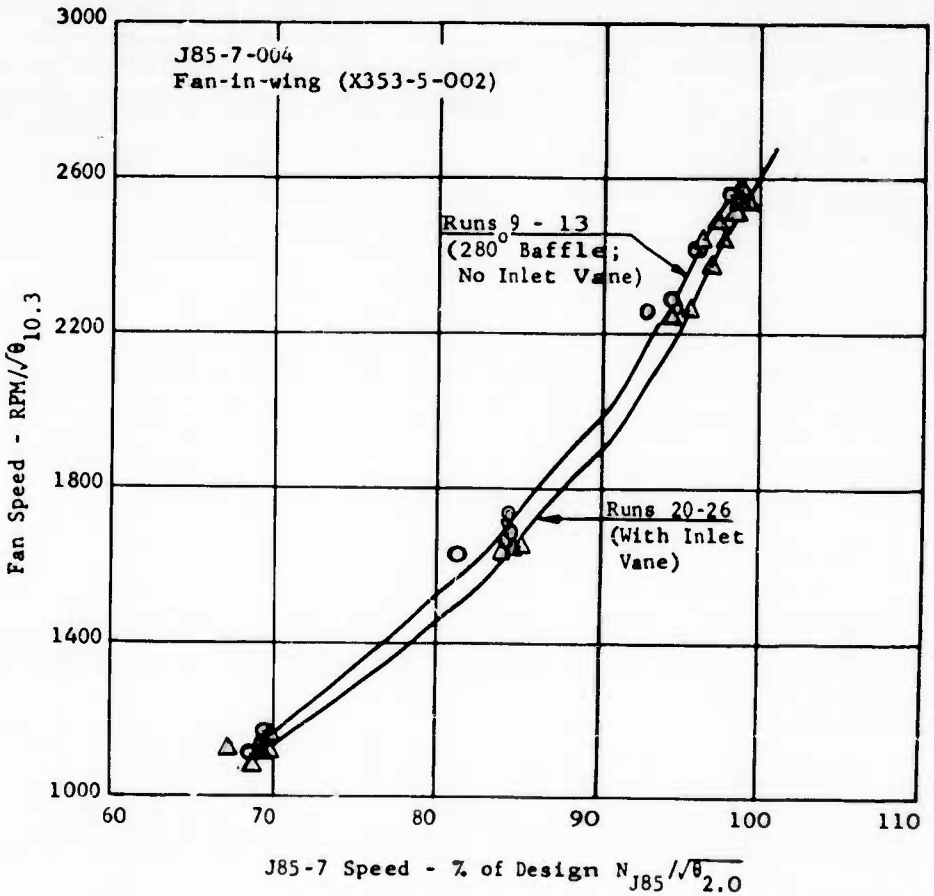

FIGURE 17 - FAN SPEED VERSUS J85-7 SPEED (DIVERTER VALVE POSITIONED FOR APPROXIMATELY 3.2% BLEED)

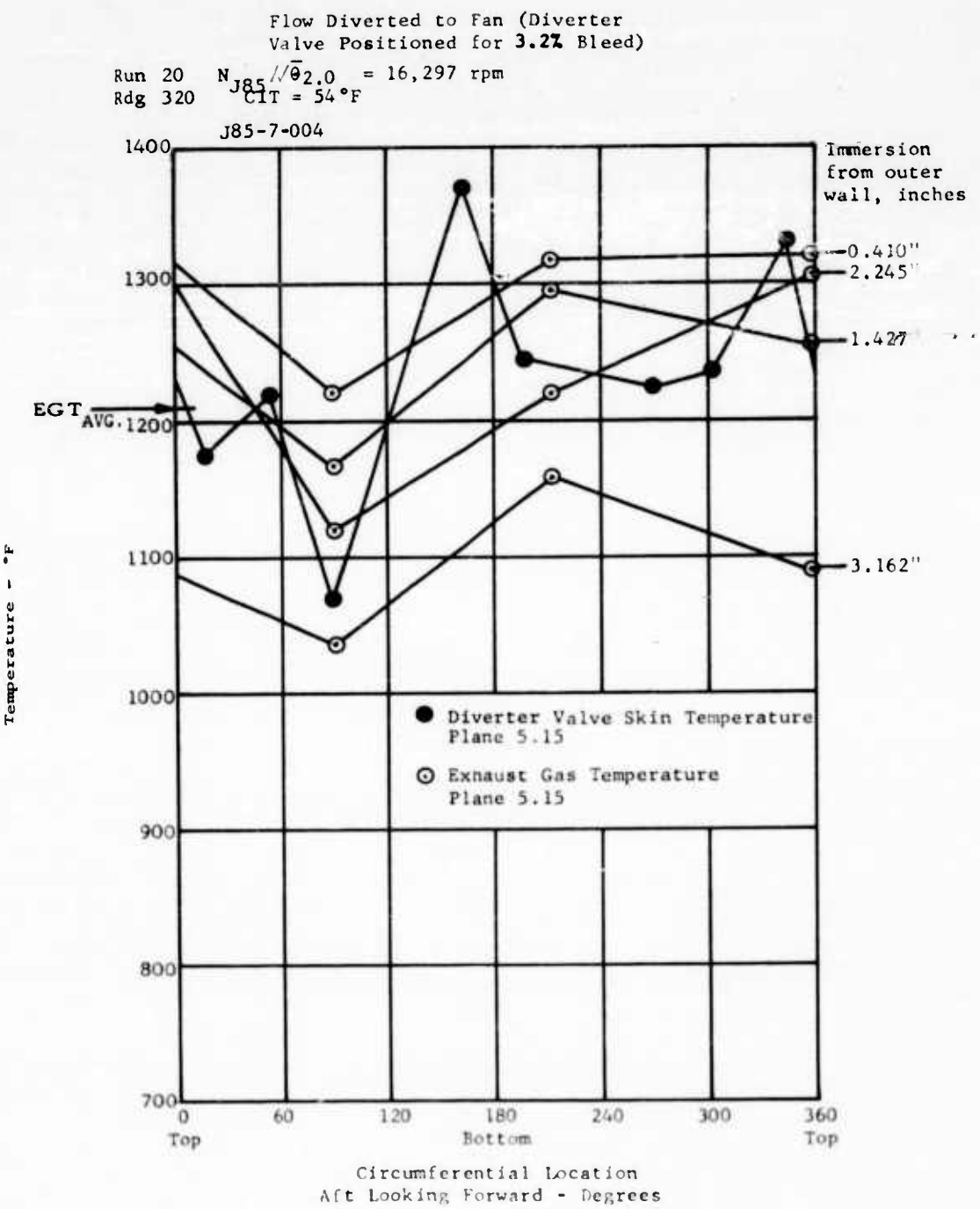

FIGURE 18 - J85-7 CIRCUMFERENTIAL EGT PROFILE AND DIVERTER VALVE SKIN TEMPERATURE

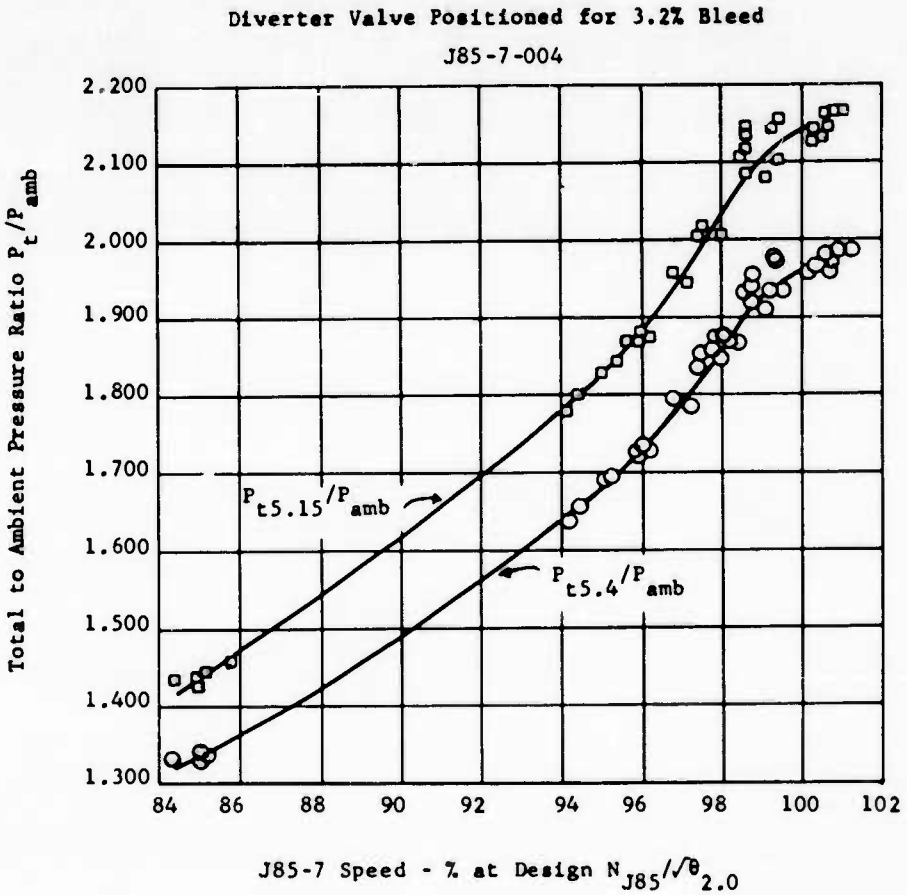

FIGURE 19 - TOTAL TO AMBIENT PRESSURE RATIO AT DIVERTER VALVE INLET (STATION 5.15) AND FAN TURBINE NOZZLE INLET (STATION 5.4) VERSUS J85-7 SPEED

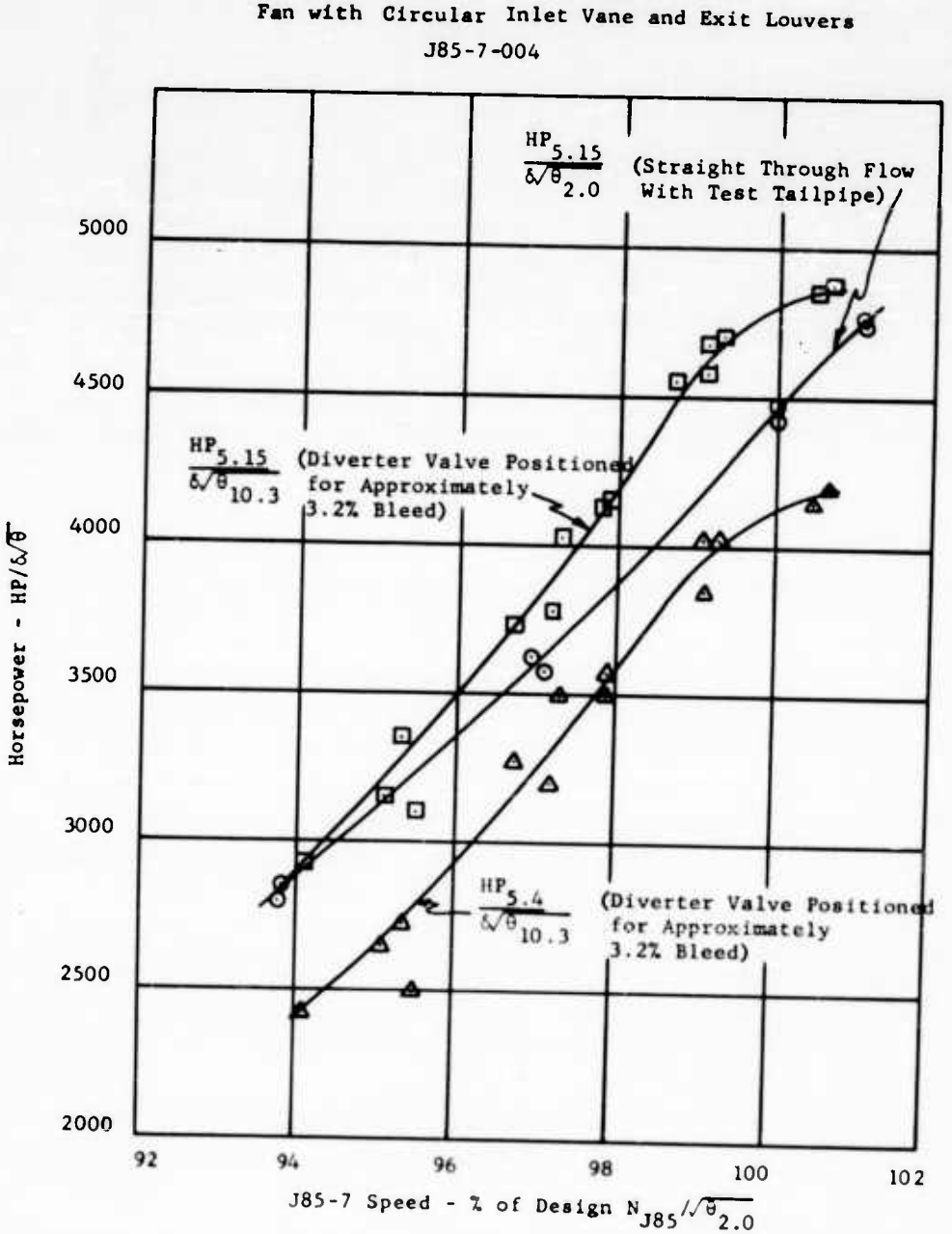

FIGURE 20a - HORSEPOWER AT DIVERTER VALVE INLET (STATION 5.15) AND FAN TURBINE NOZZLE INLET (STATION 5.4) VERSUS J85-7 SPEED.

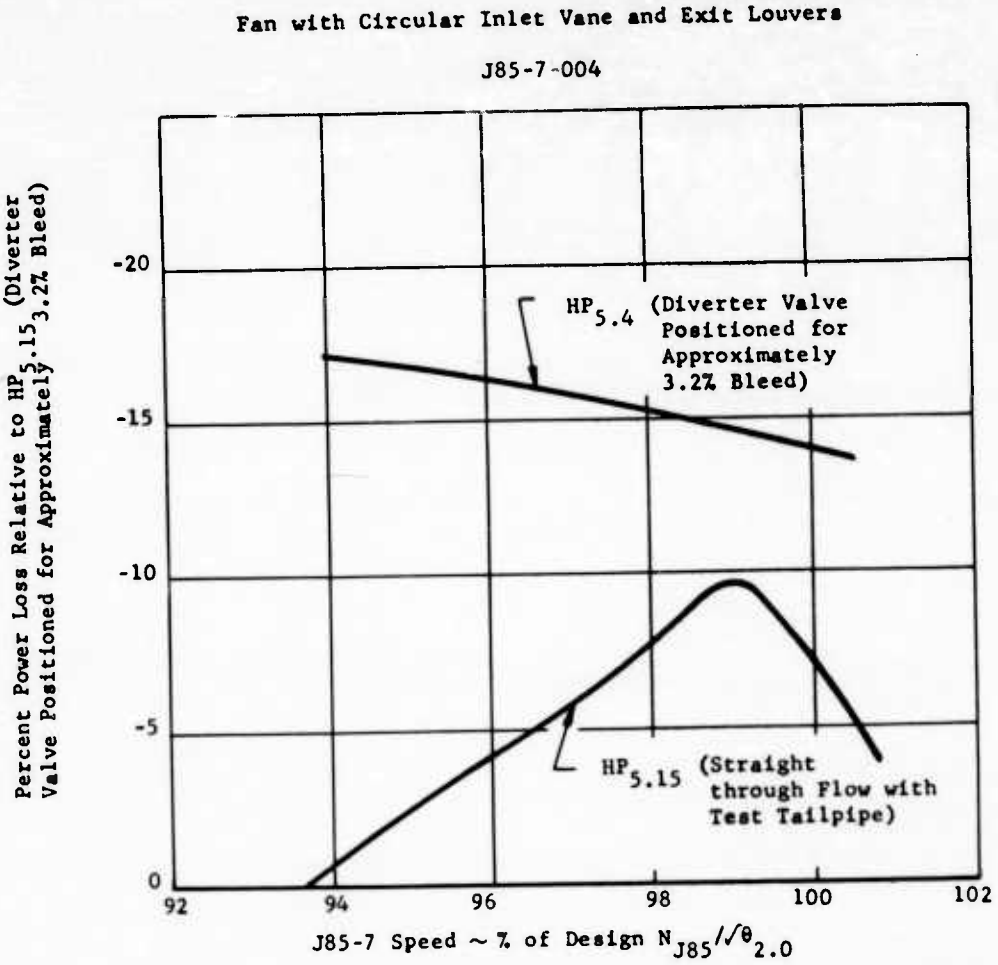

FIGURE 20b - POWER LOSS RELATIVE TO DIVERTER VALVE INLET (STATION 5.15) VERSUS J85-7 SPEED

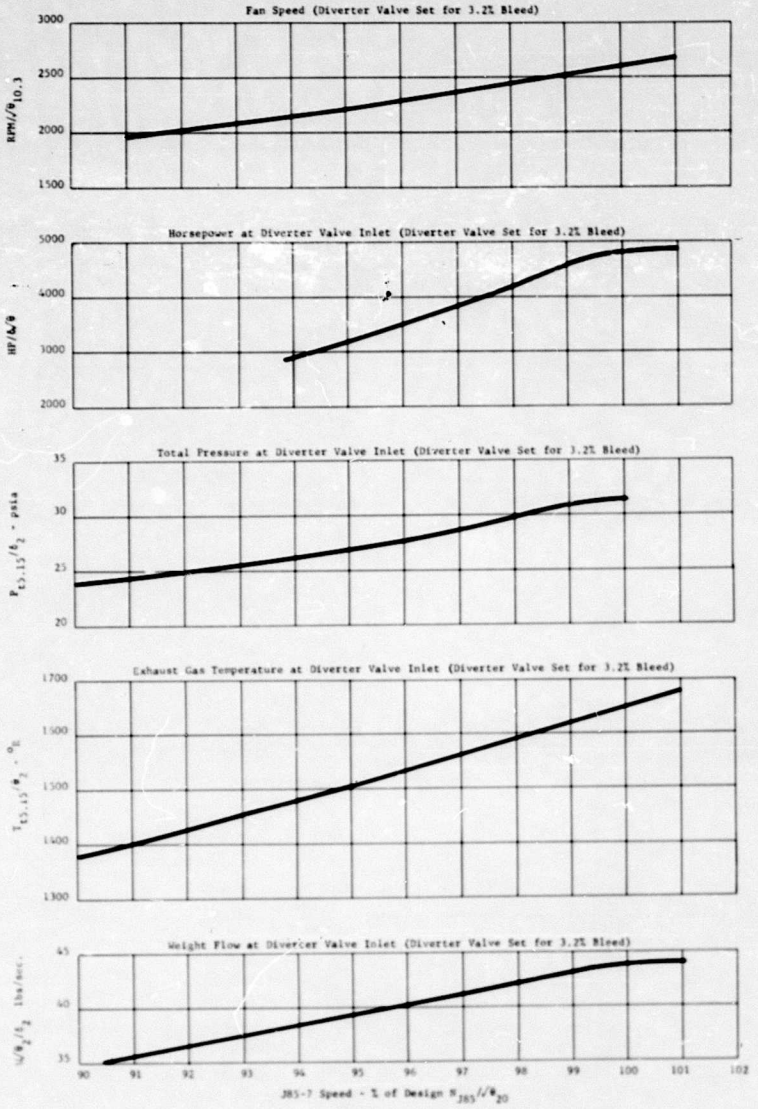

FIGURE 21 **FAN SPEED AND DIVERTER VALVE INLET (STATION 5.15) FLOW CHARACTERISTICS VERSUS J85-7 SPEED**

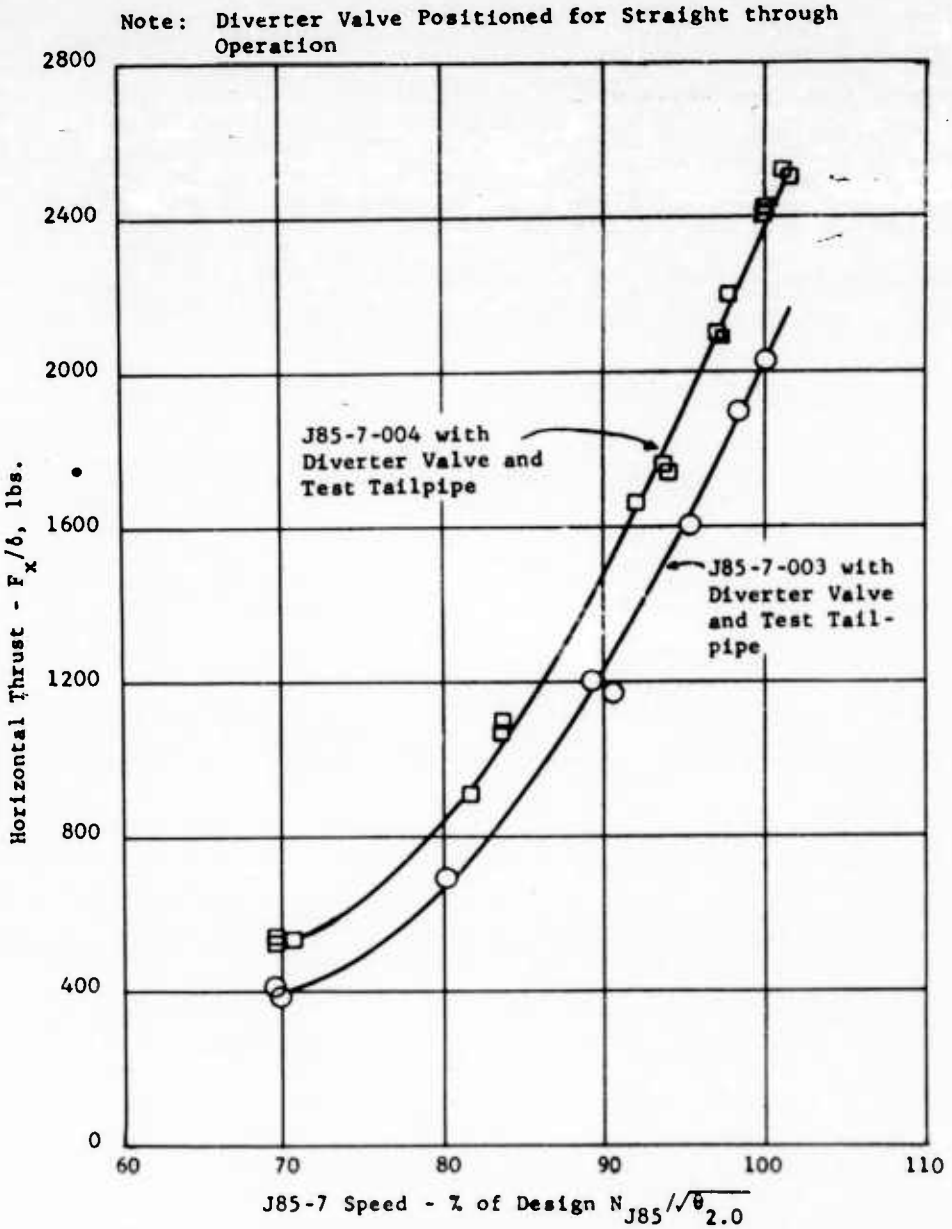

FIGURE 22 - J85-7 THRUST VERSUS SPEED

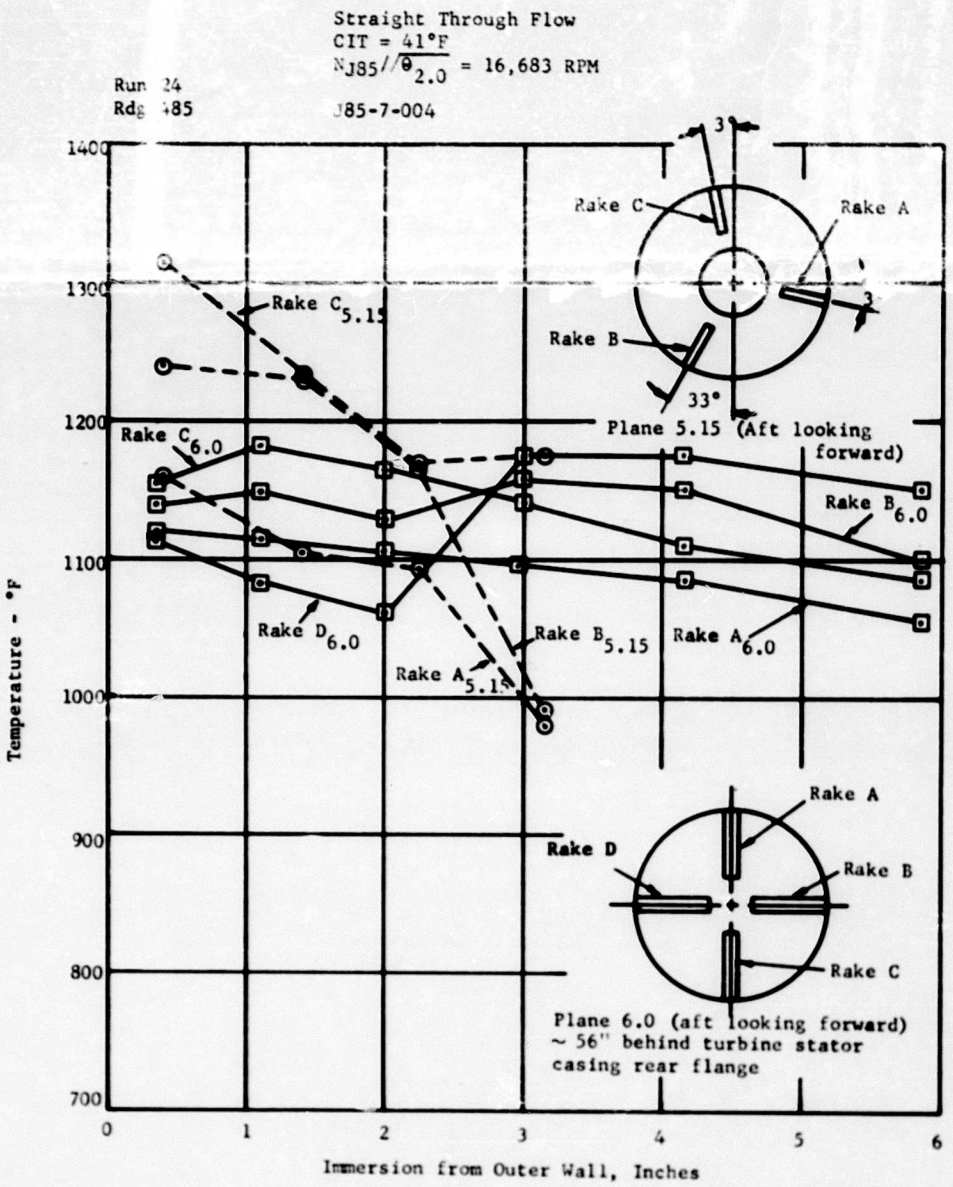

FIGURE 23 - J85-7 EGT PROFILE

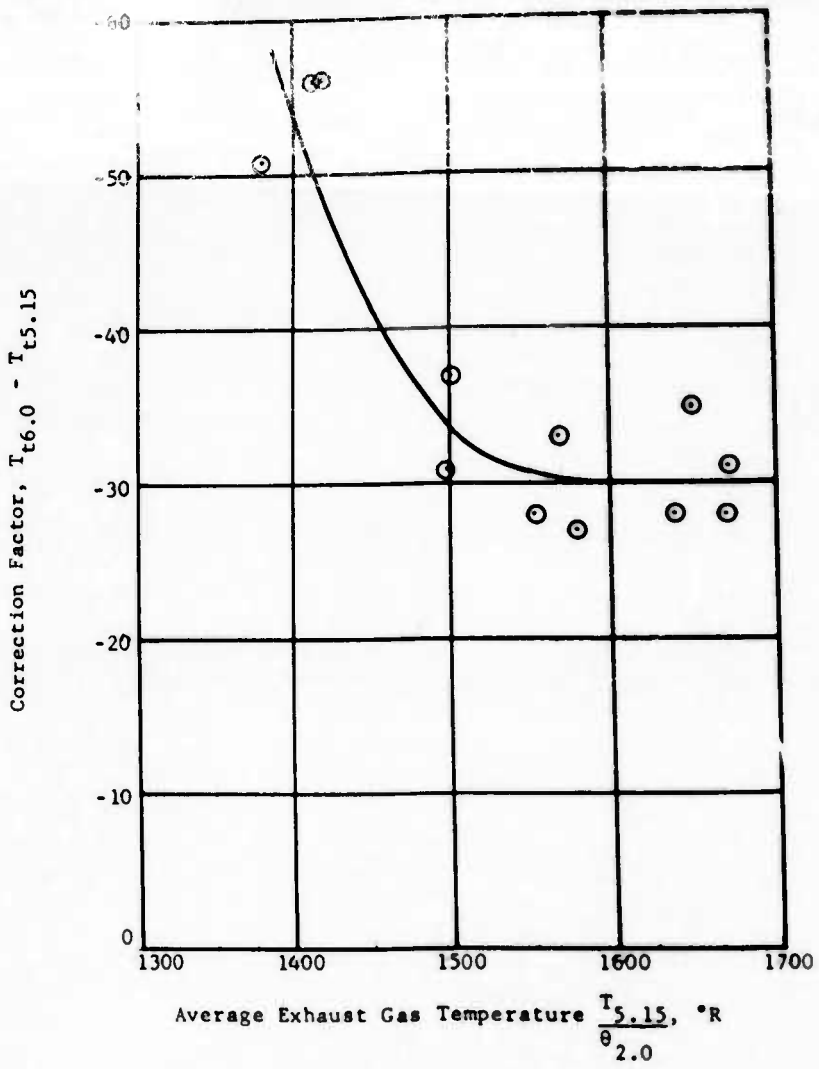

FIGURE 24 - PLANE 5.15 EGT CALIBRATION CURVE

Fan-in-wing with Circular Inlet Vane and Exit Louvers

① Diverter Valve set for Approximately 3.2% Bleed
② " " " " " " "
③ " " Fully Closed
④ " " " "

$\delta = 0^{\circ}$
V_p = 0-5 mph

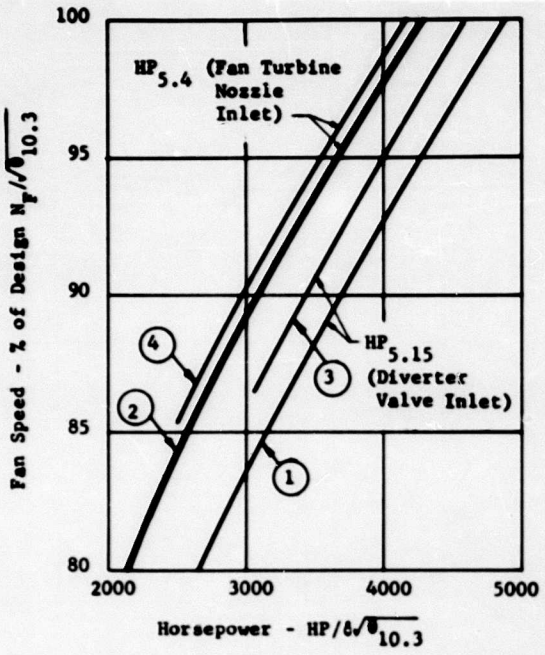

FIGURE 25 - FAN SPEED VERSUS AVAILABLE HORSEPOWER

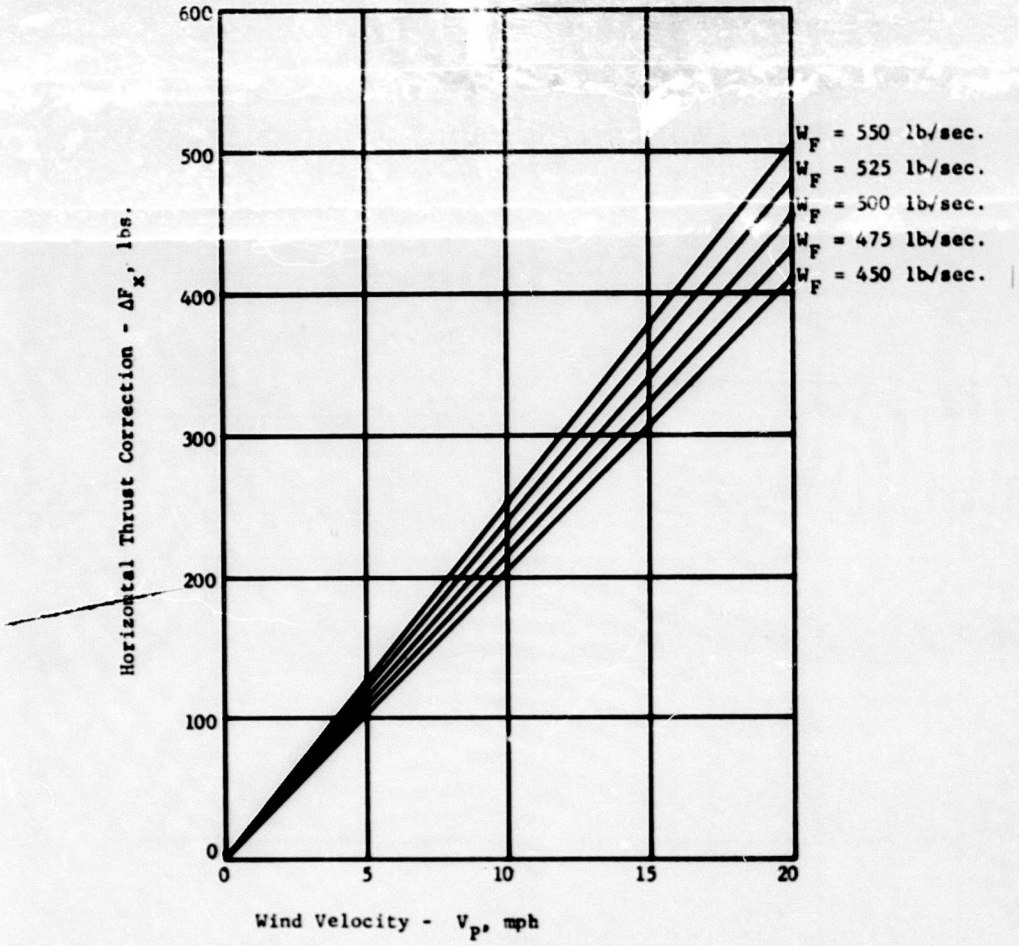

FIGURE 26 - THRUST CORRECTION FOR RAM DRAG DUE TO WIND

Fan-in-wing (X353-5-002)

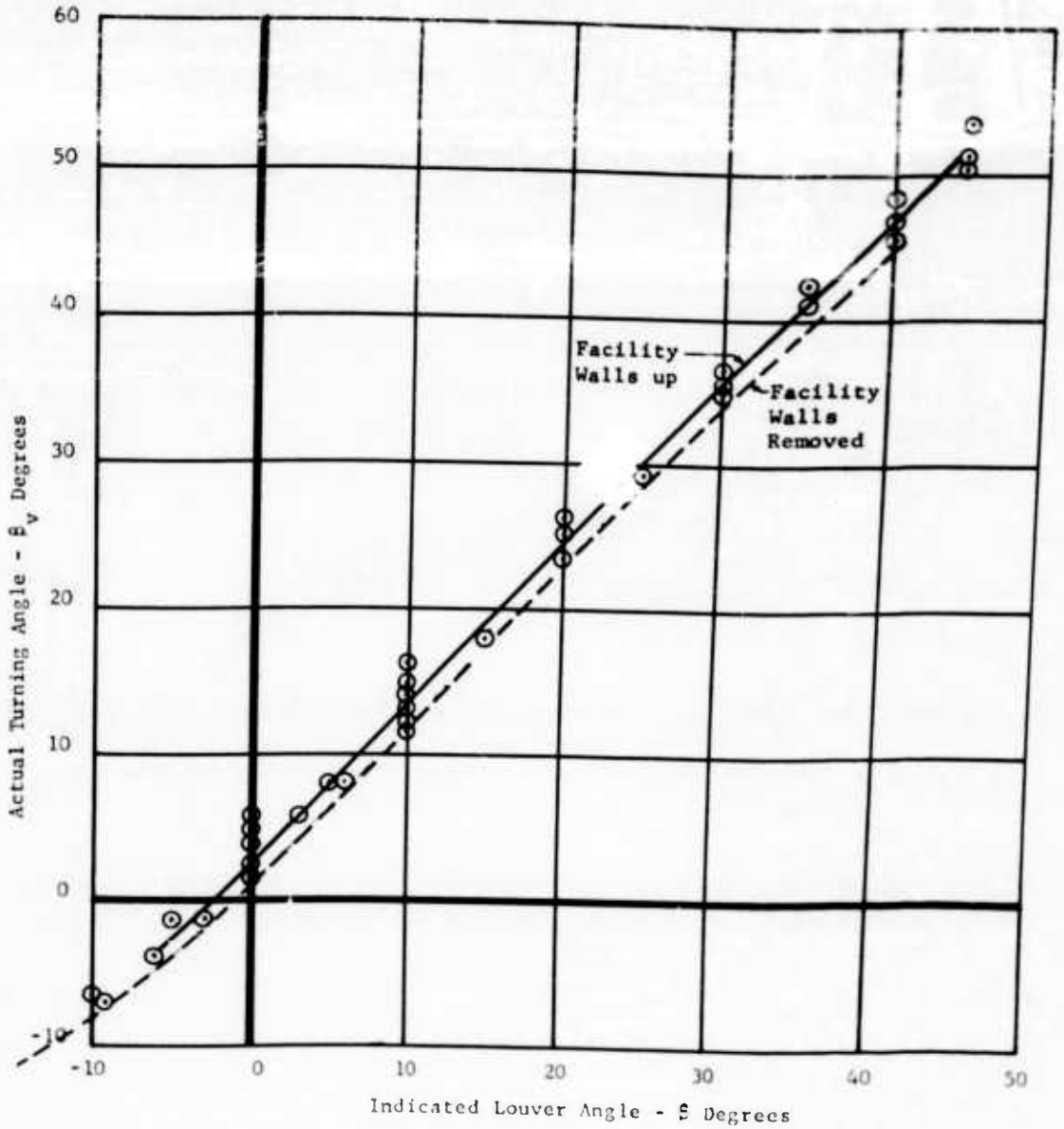

FIGURE 27 - ACTUAL TURNING ANGLE VERSUS INDICATED LOUVER ANGLE

◇ = Fan-in-wing (X353-5-002), 180° Baffle, Circular Inlet Vane, No Facility Walls.

⊙ = Fan-in-fuselage (X353-5-001), Deep Inlet Duct, No Inlet Vane.

⊡ = Fan-in-wing (X353-5-002), 280° Baffle, No Inlet Vane, Facility Walls Up.

◇ = Fan-in-wing (X353-5-002), No Baffle, No Inlet Vane, Facility Walls Up.

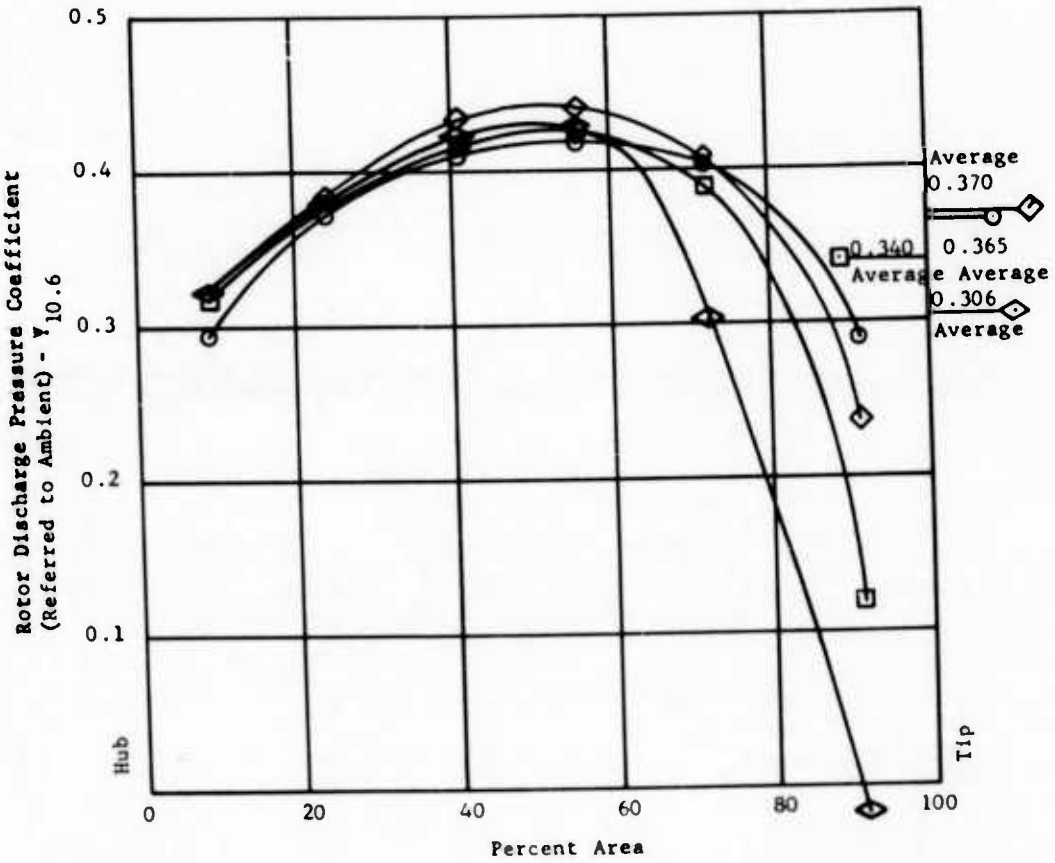

FIGURE 28a - SUMMARY OF FAN PRESSURE COEFFICIENTS

△ = Fan-in-wing (X353-5-003), No Baffle, Circular Inlet Vane, No Facility Walls.

⊙ = Fan-in-fuselage (X353-5-001), Deep Inlet Duct, No Inlet Vane.

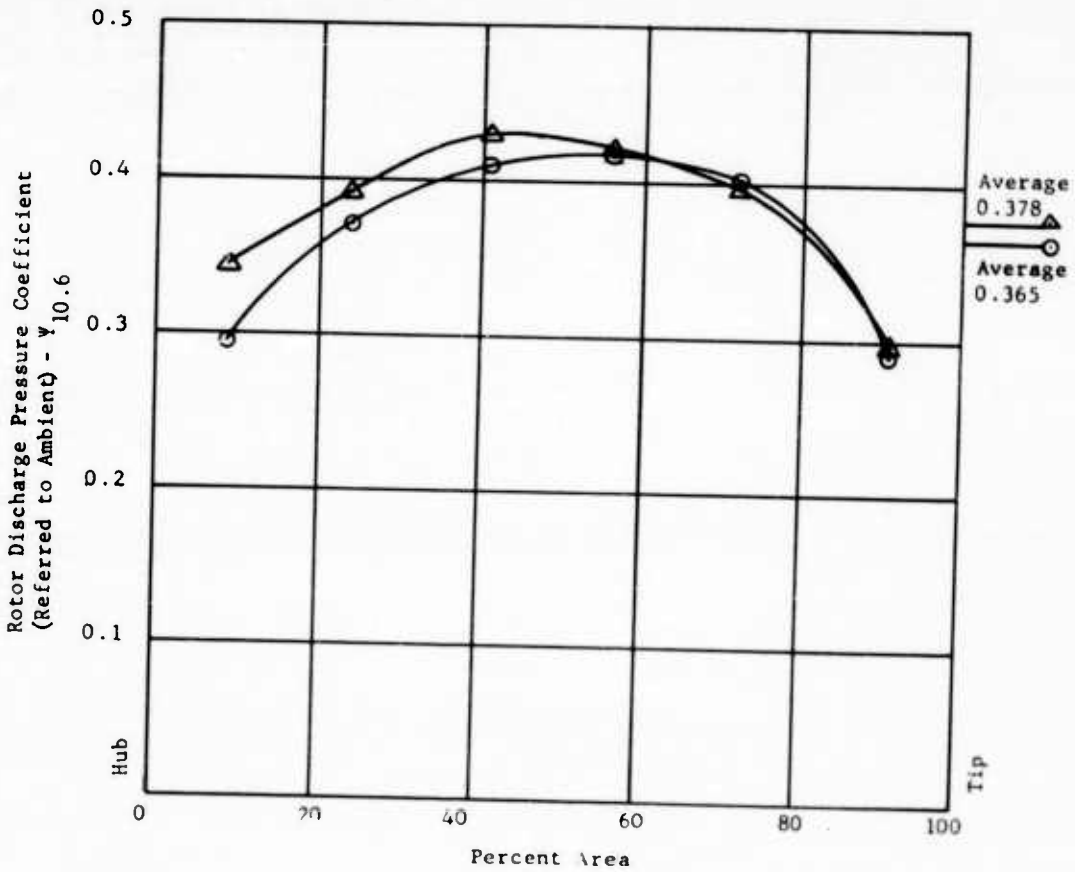

FIGURE 28b - SUMMARY OF FAN PRESSURE COEFFICIENTS

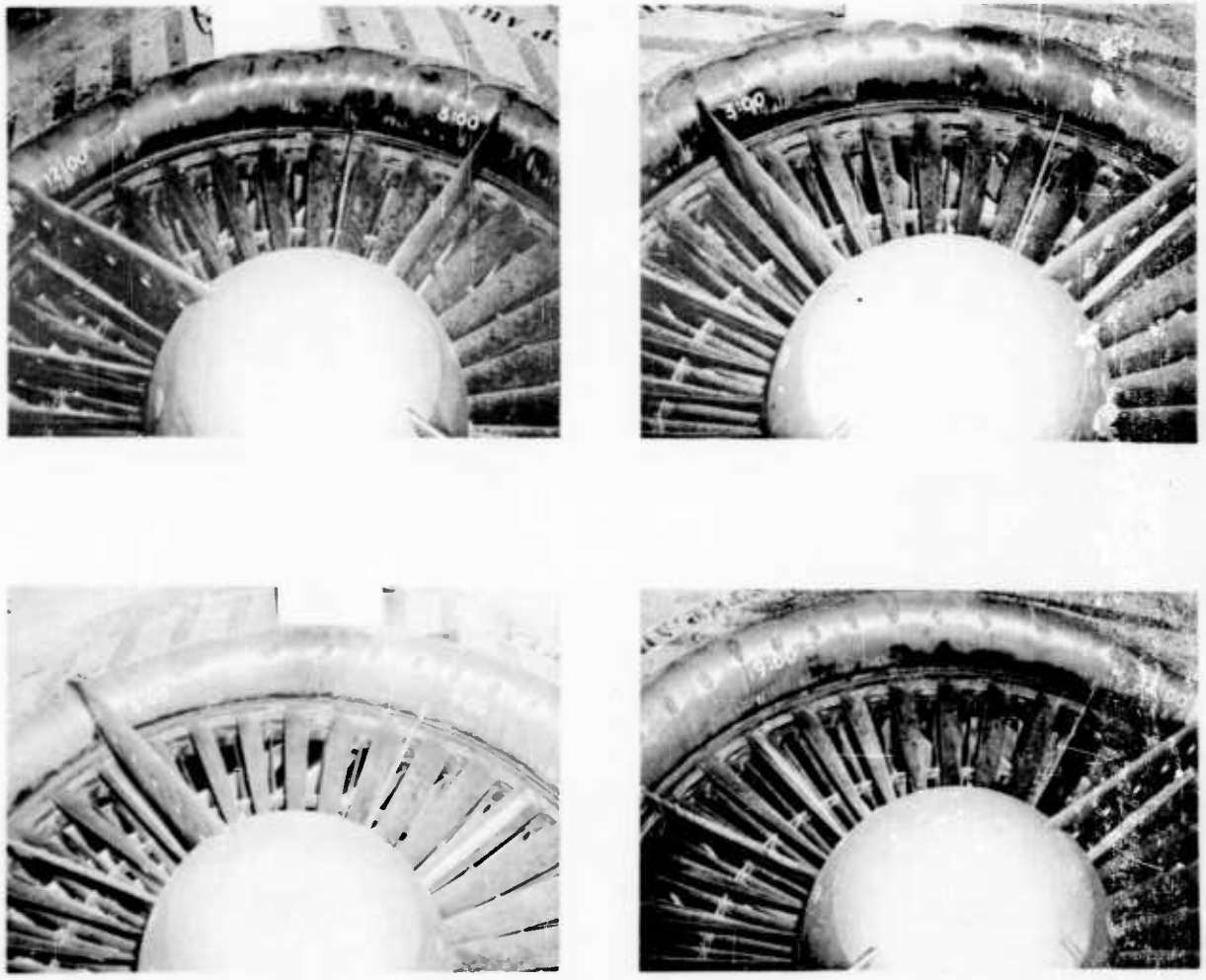

FIGURE 29 BELLMOUTH LAMPBLACK TEST RESULTS (NO BAFFLE)

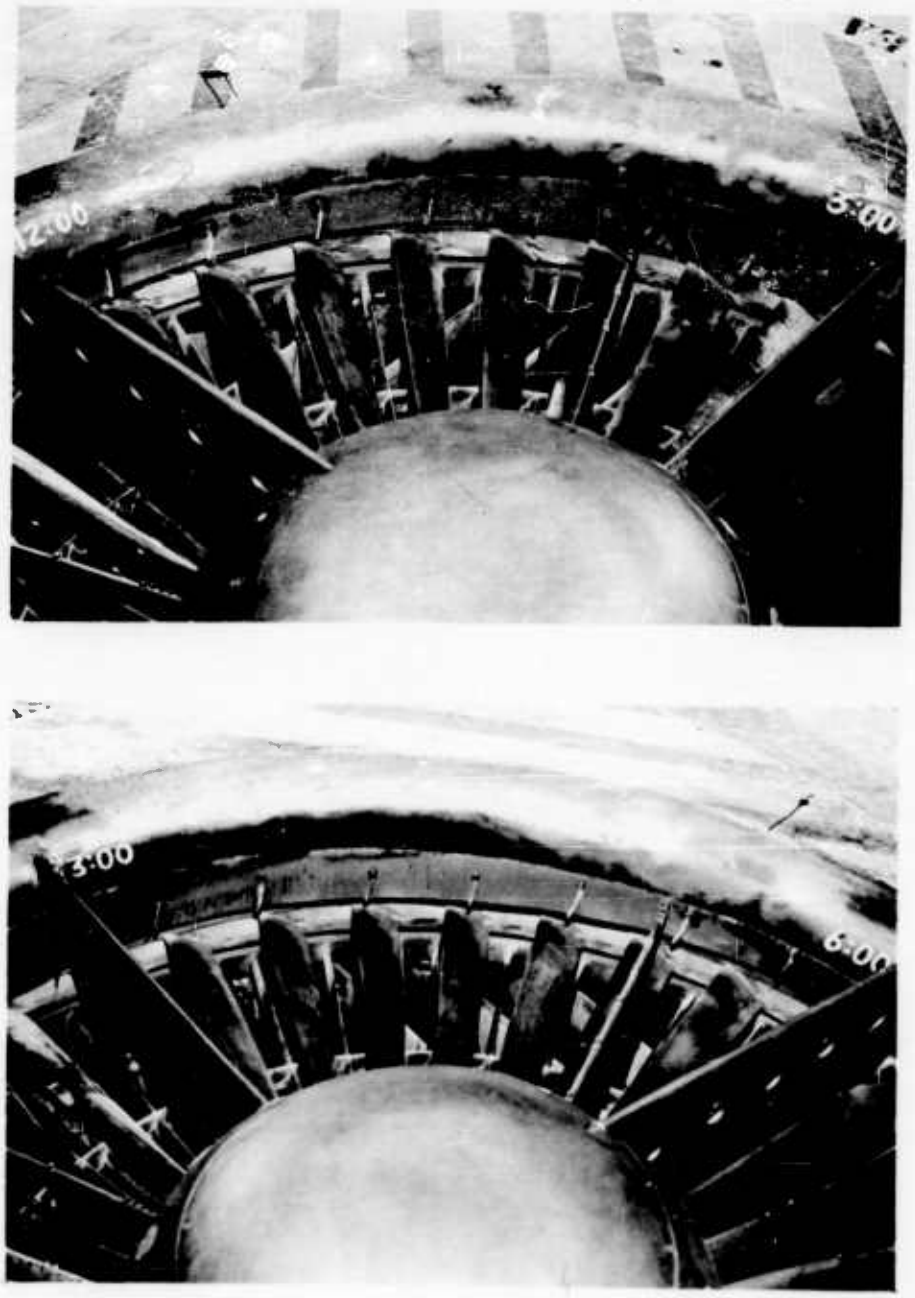

FIGURE 30 BELLMOUTH LAMPBLACK TEST RESULTS (360° BAFFLE INSTALLED)

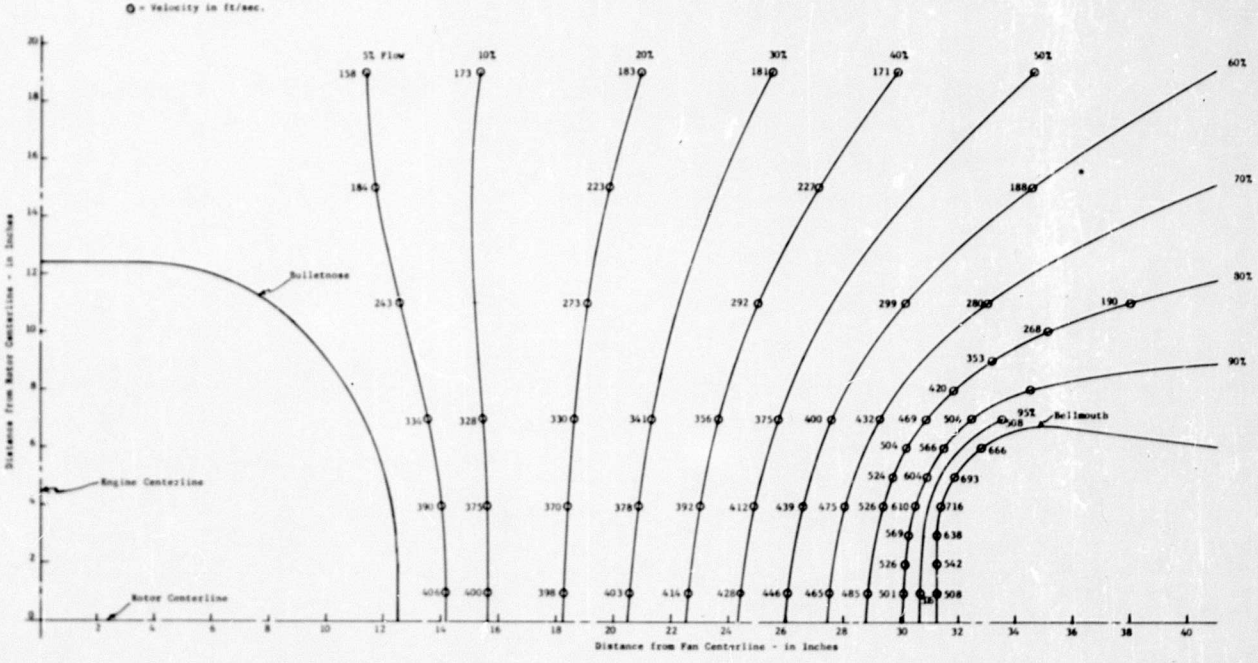

FIGURE 31 FAN-IN-WING INLET FLOW DIAGRAM

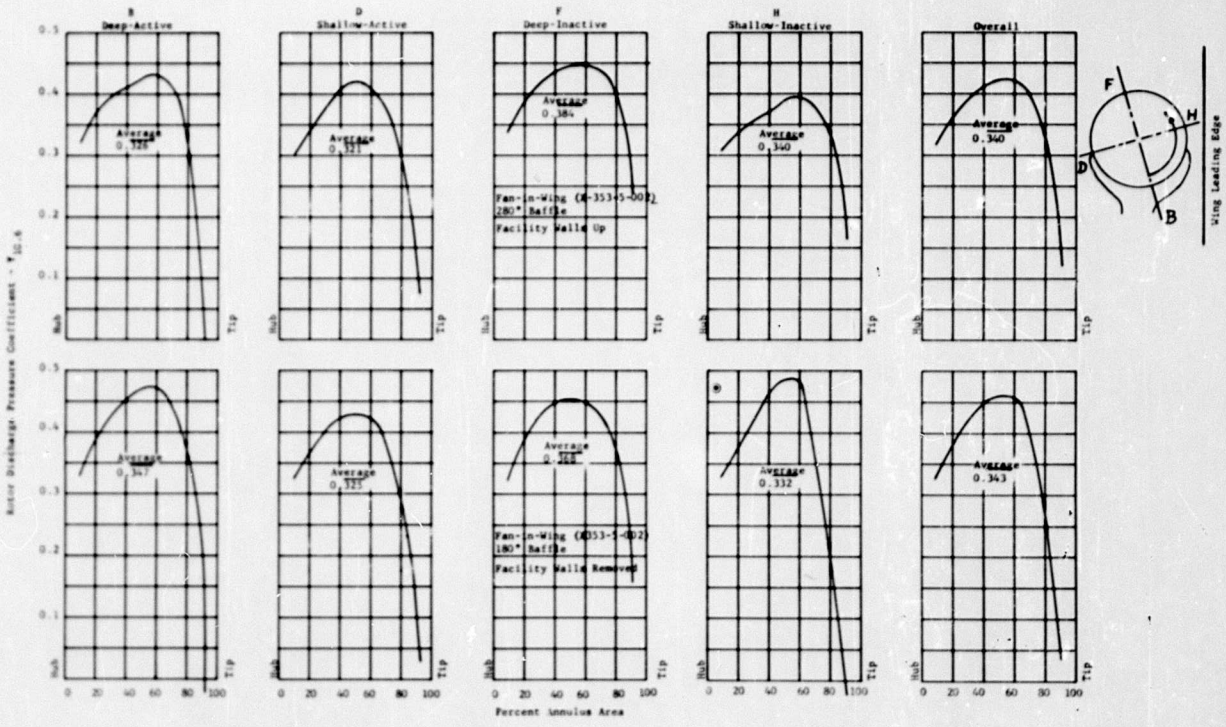

FIGURE 32 INTERNAL PERFORMANCE (FACILITY AND BAFFLE EFFECTS)

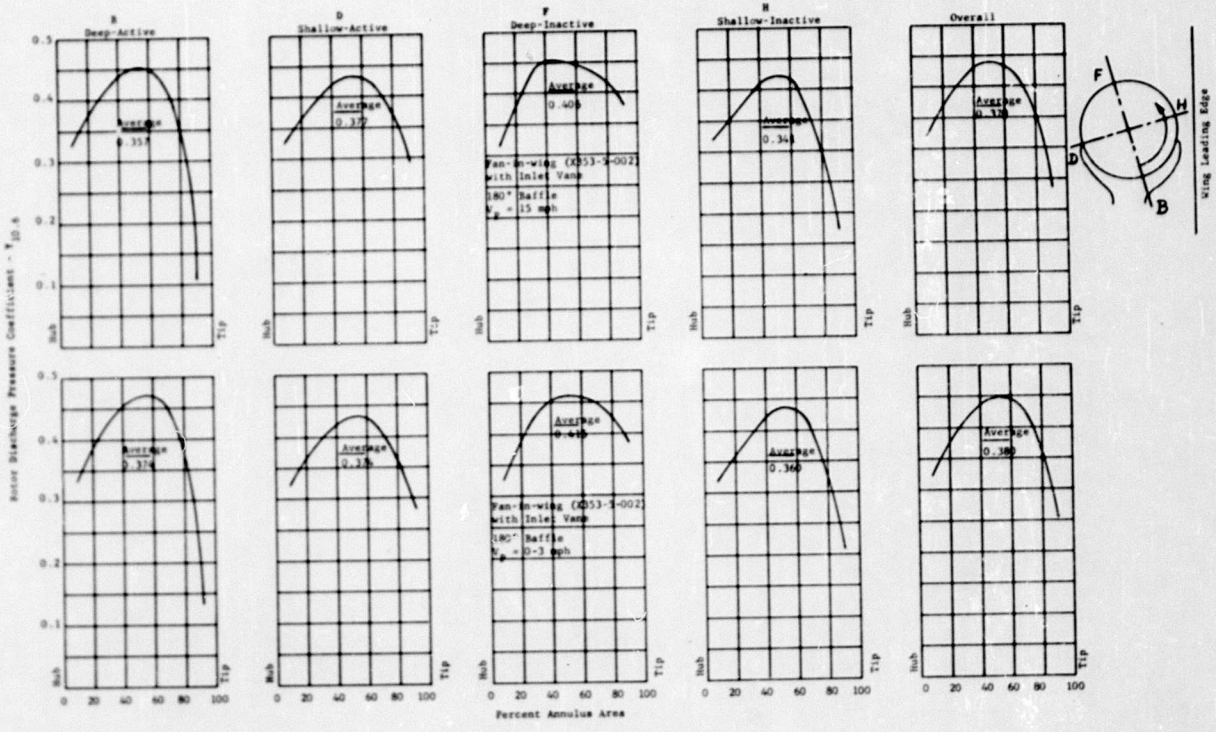

FIGURE 33 **EFFECT OF WIND ON FAN-IN-WING INTERNAL PERFORMANCE (INLET VANE AND 180° BAFFLE)**

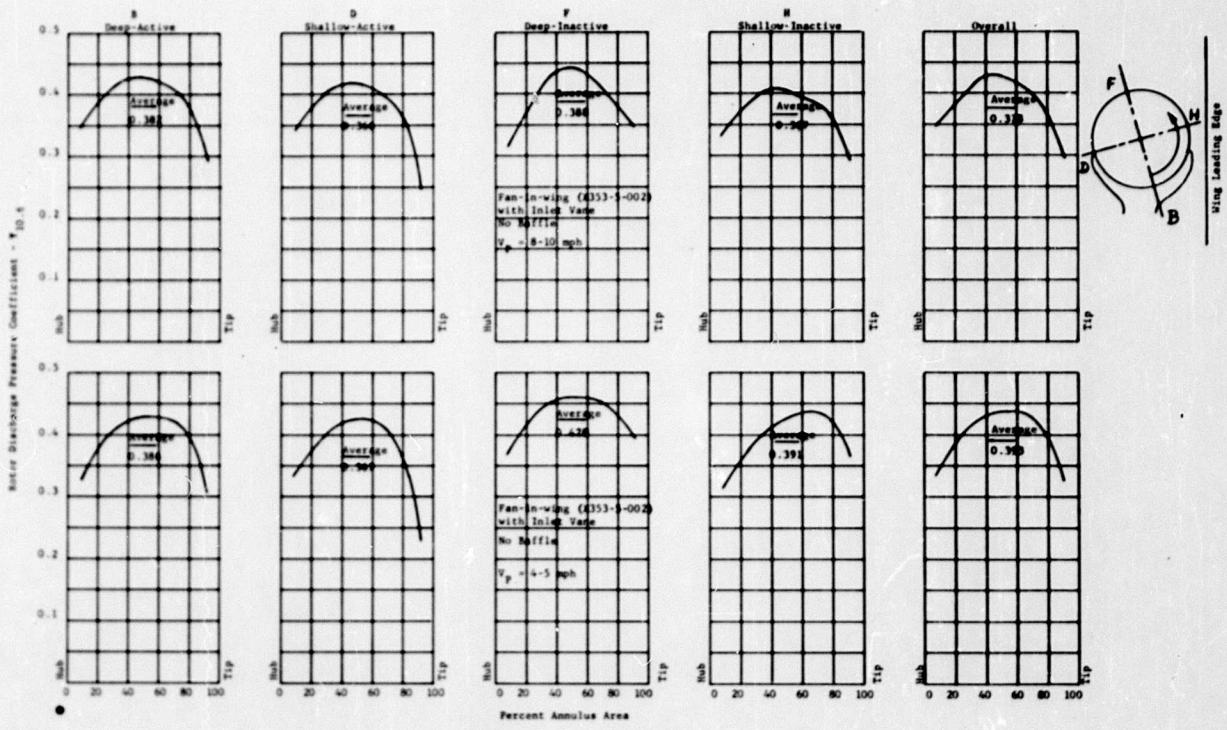

FIGURE 34 EFFECT OF WIND ON FAN INTERNAL PERFORMANCE (INLET VANE ONLY)

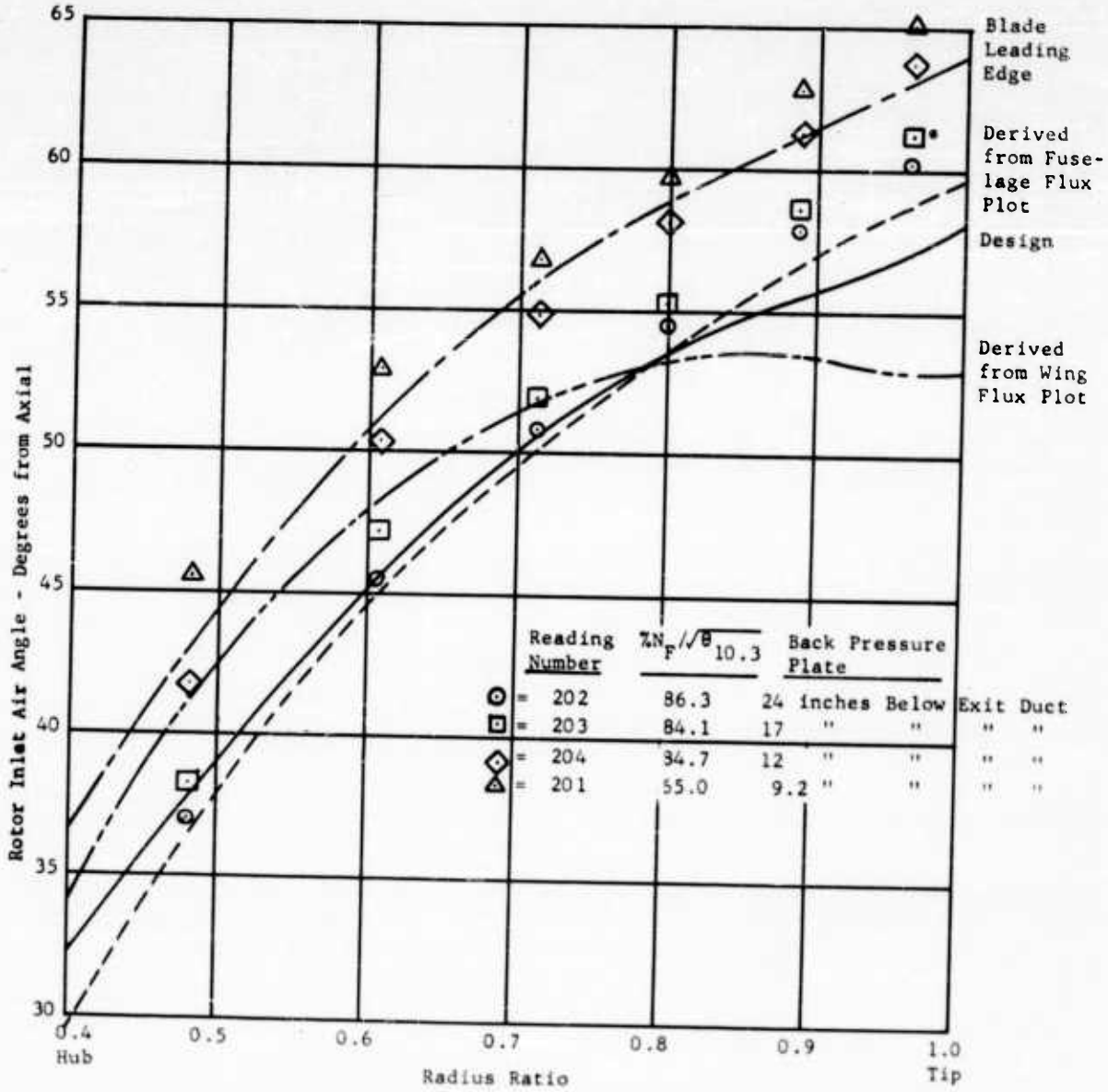

FIGURE 35 - FAN-IN-FUSELAGE (X353-5-002) ROTOR INLET AIR ANGLES VERSUS RADIUS RATIO AT VARIOUS THROTTLE POSITIONS.

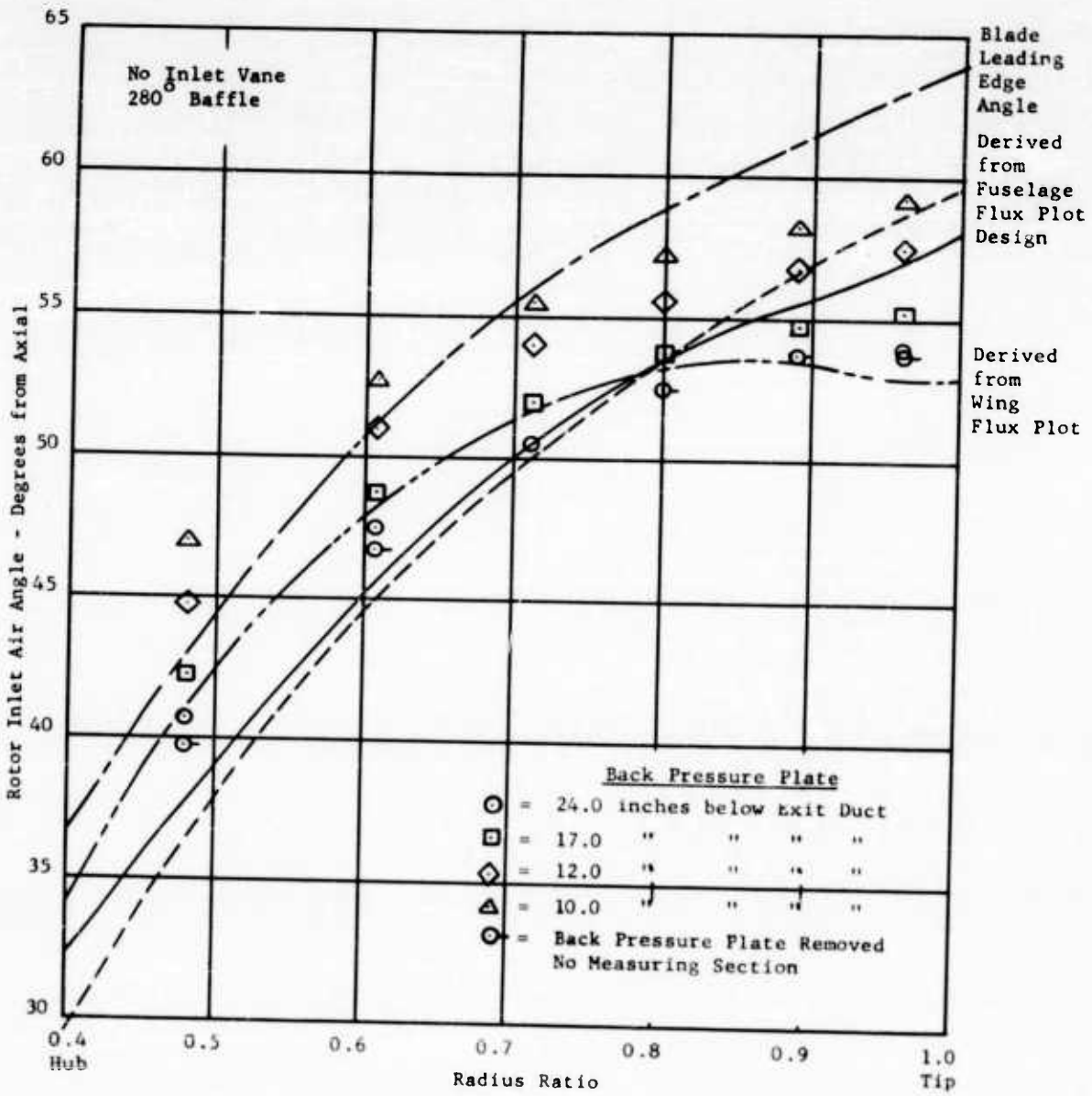

FIGURE 36 - FAN-IN-WING ROTOR INLET AIR ANGLES VERSUS RADIUS RATIO AT VARIOUS THROTTLE POSITIONS

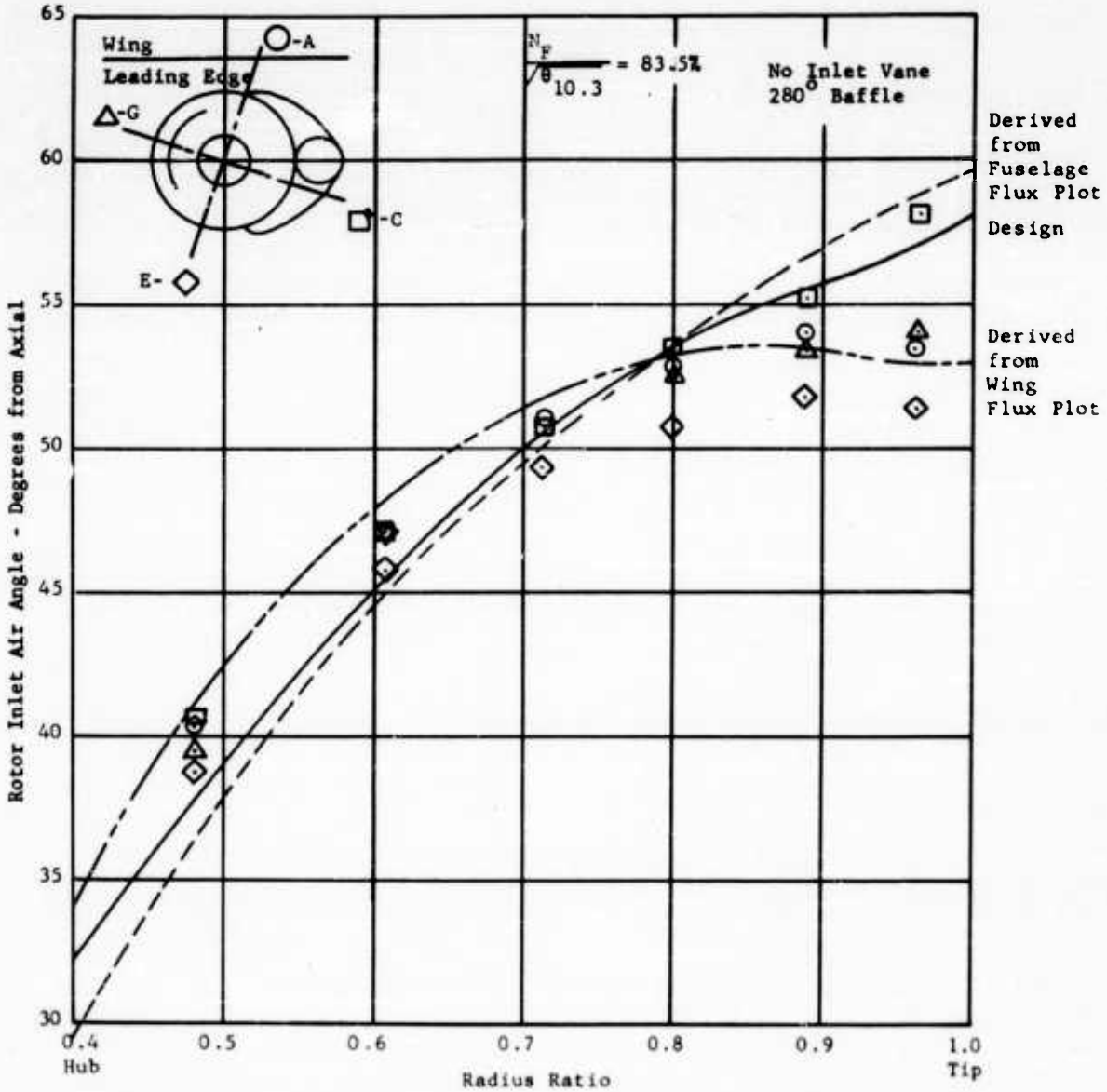

FIGURE 37 - FAN-IN-WING (X353-5-002) ROTOR INLET AIR ANGLES VERSUS RADIUS RATIO AS A FUNCTION OF CIRCUMFERENTIAL LOCATION.

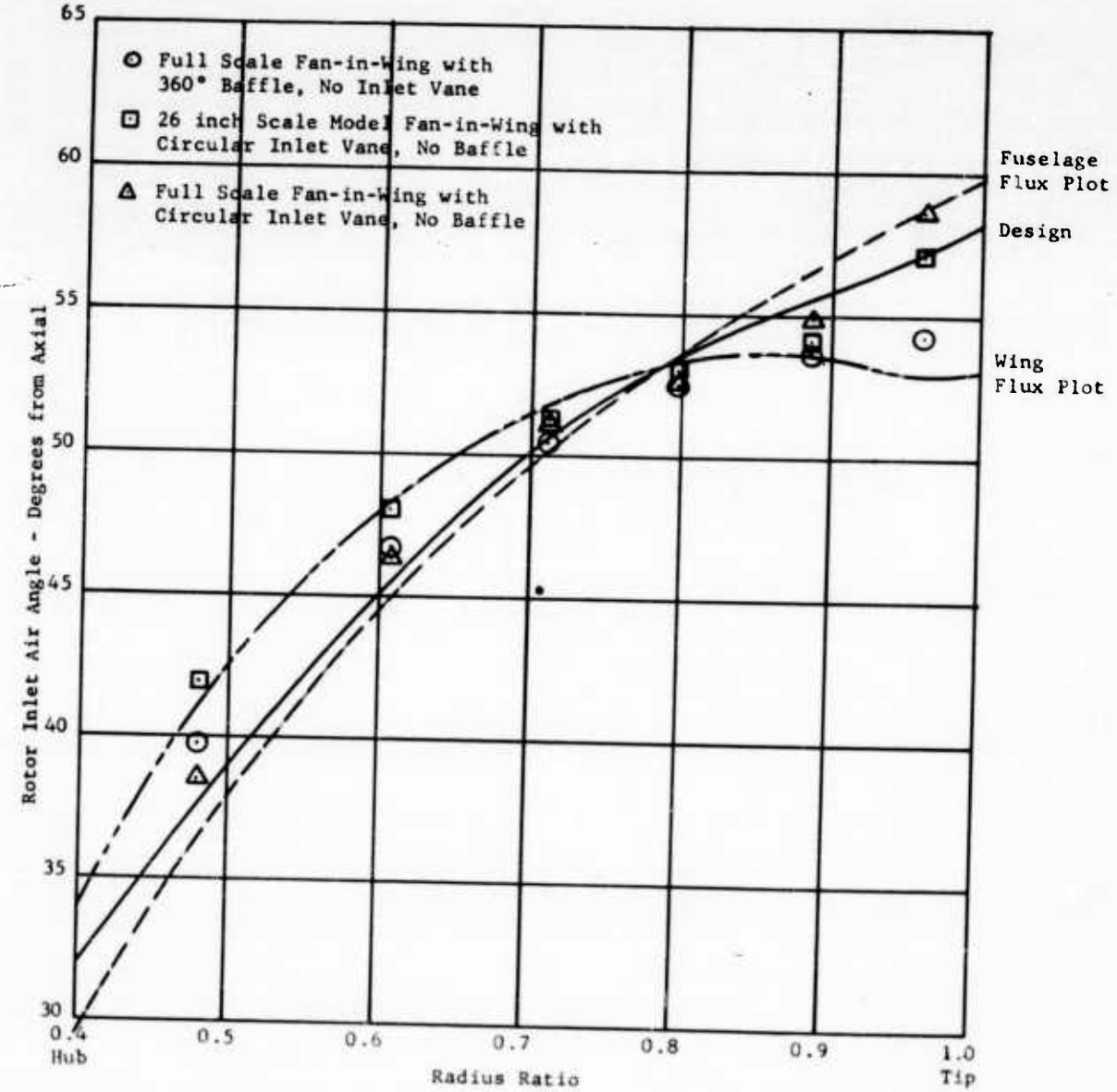

FIGURE 38 - COMPARISON OF SCALE MODEL AND FULL SCALE ROTOR INLET AIR ANGLES (FAN-IN-WING)

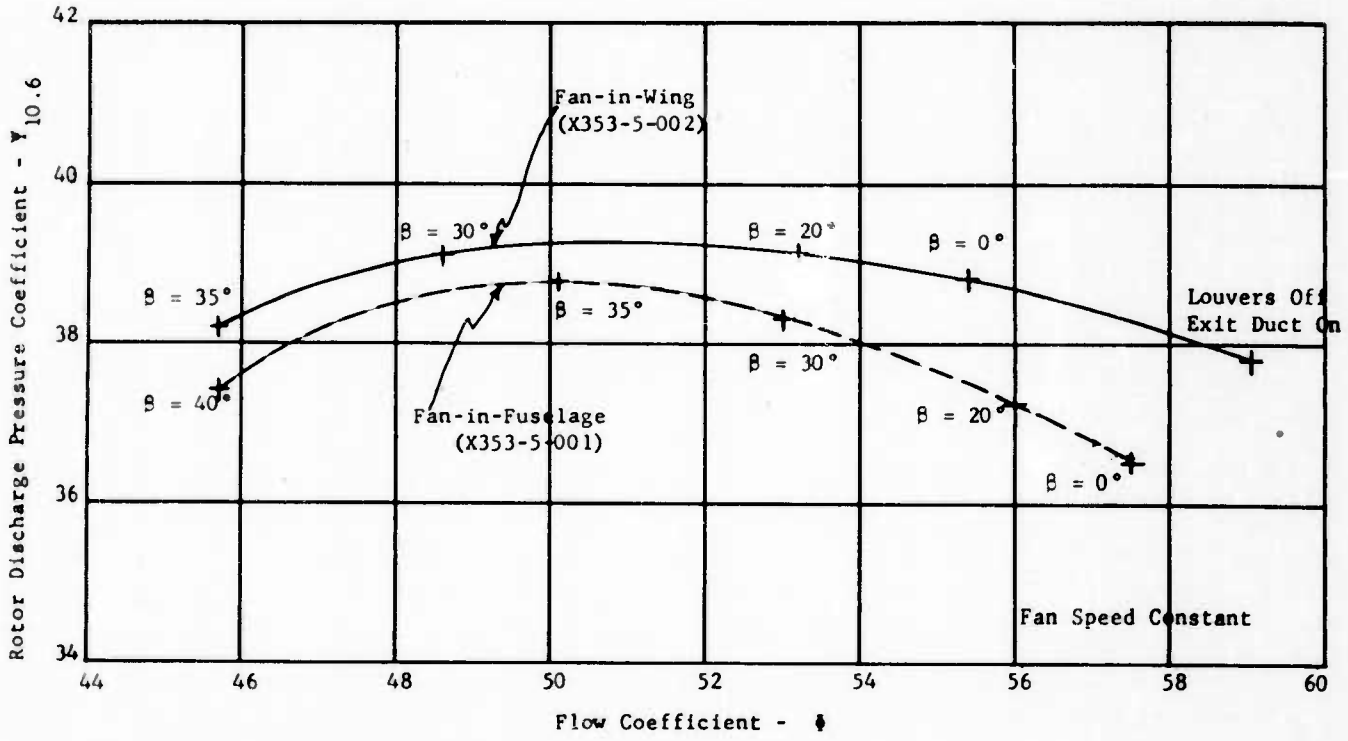

FIGURE 39 - FAN-IN-WING THROTTLE CHARACTERISTIC

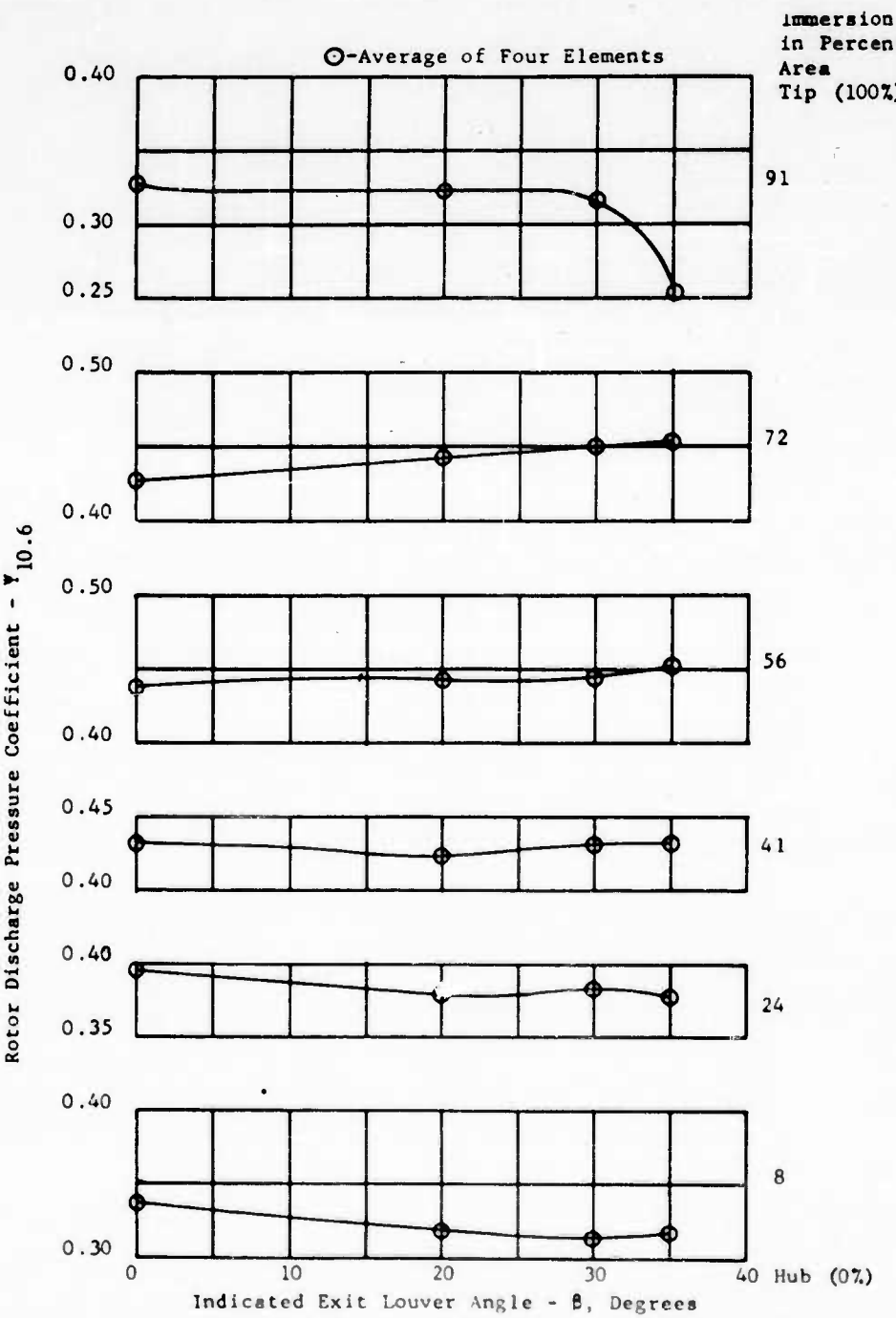

FIGURE 40 - FAN-IN-WING (X353-5-002) ROTOR DISCHARGE PRESSURE COEFFICIENT VERSUS LOUVER ANGLE AT VARIOUS IMMERSIONS.

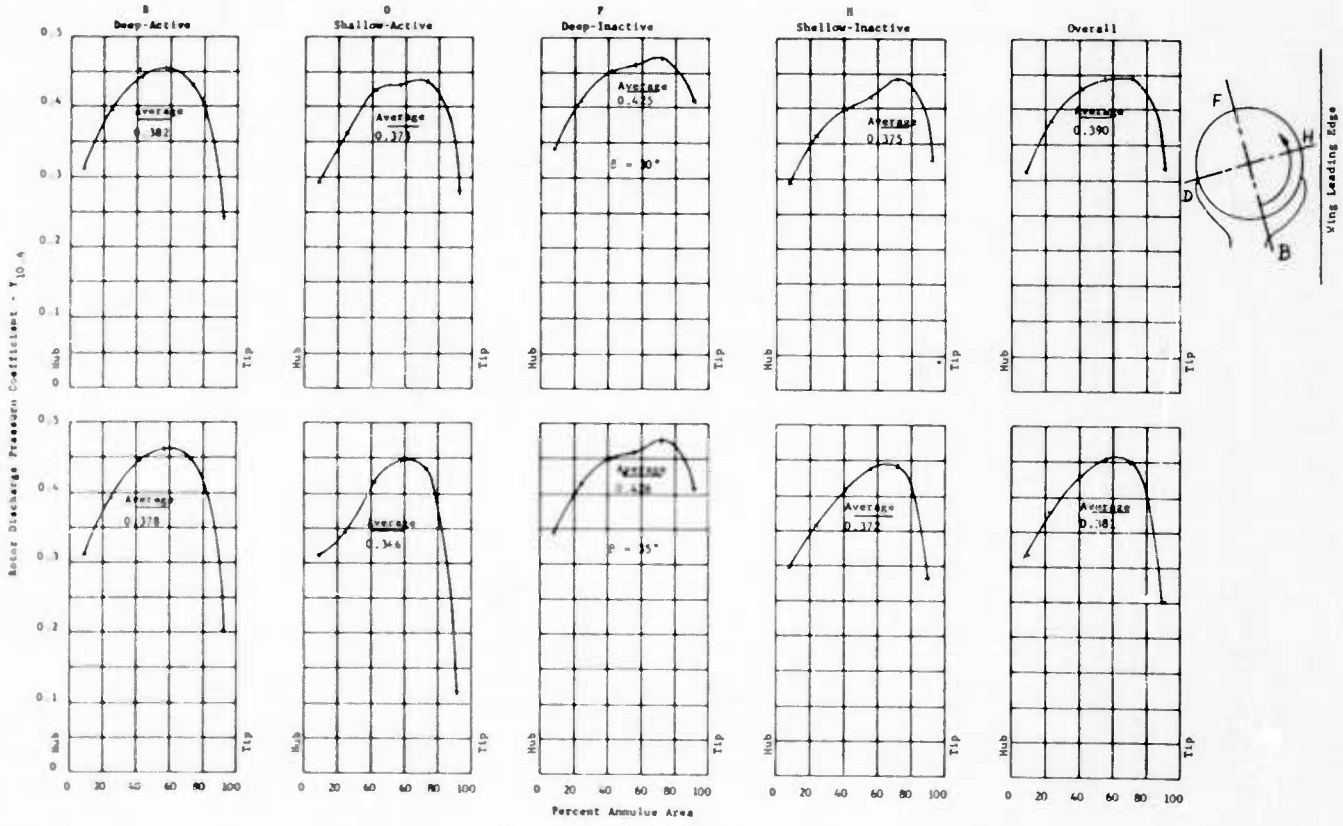

FIGURE 41 FAN-IN-WING ROTOR DISCHARGE PRESSURE COEFFICIENTS AT $\beta = 30^{\circ}$ and $\beta = 35^{\circ}$

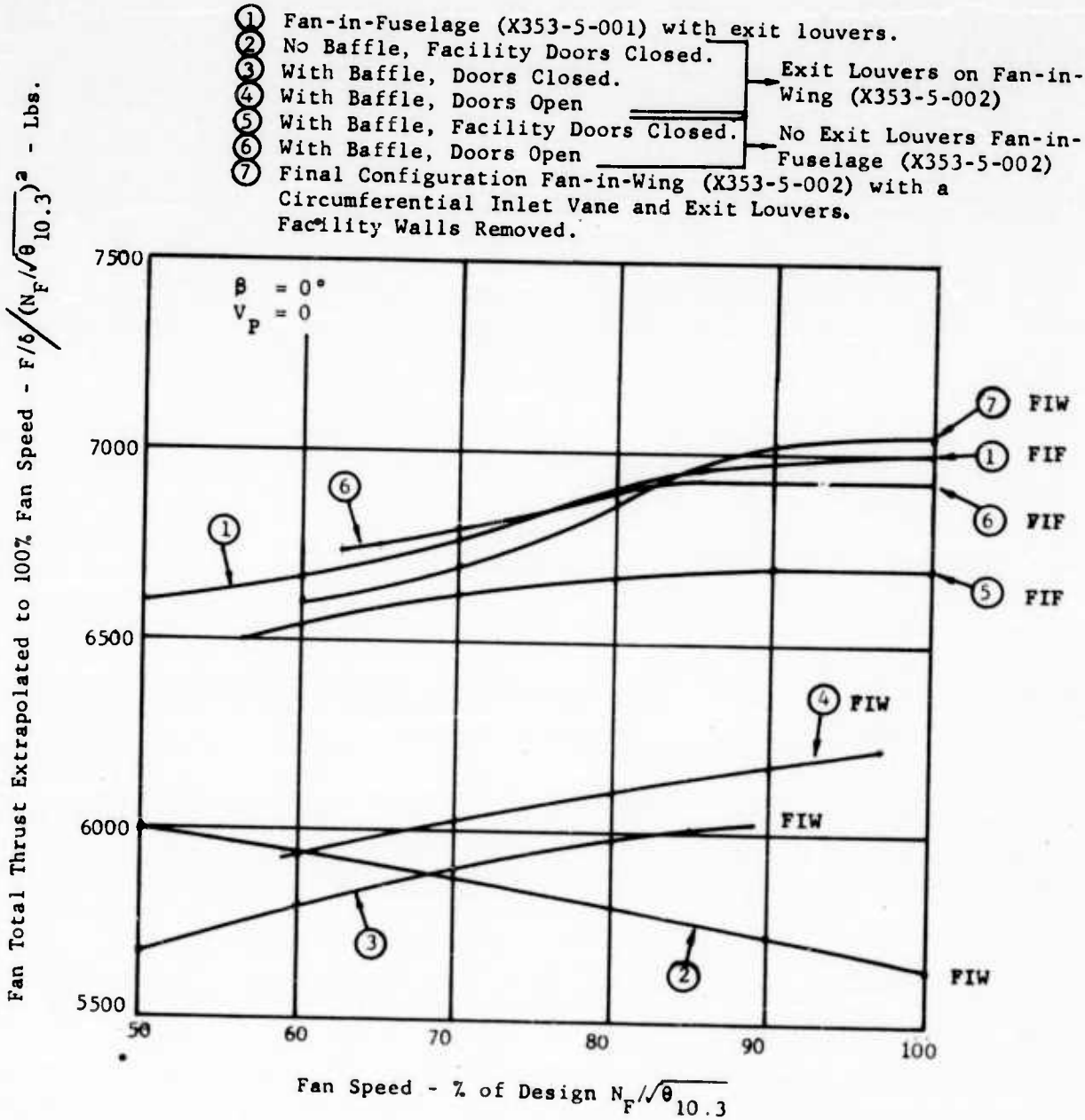

FIGURE 42 - FAN TOTAL THRUST EXTRAPOLATED TO 100% SPEED VERSUS FAN SPEED

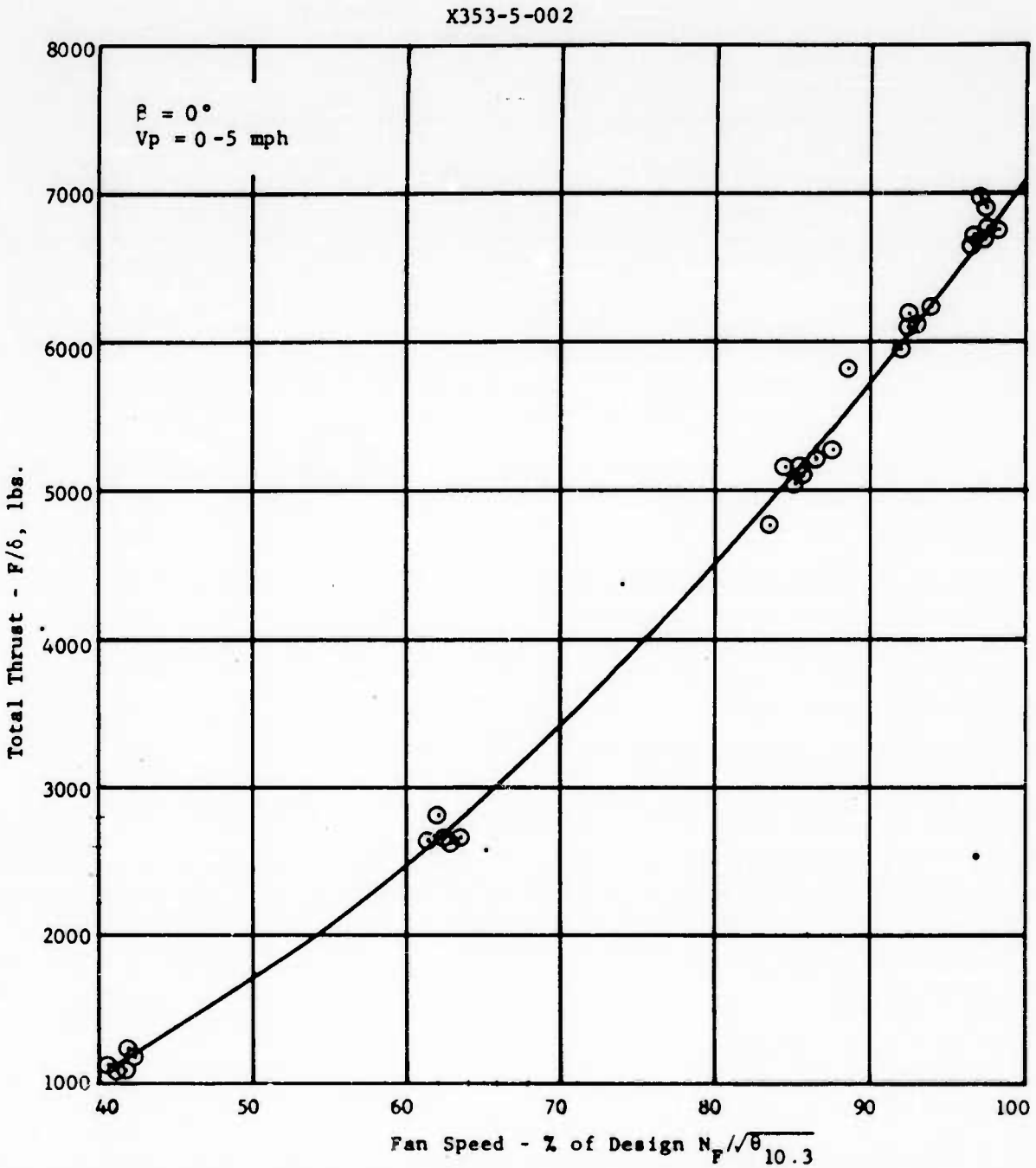

FIGURE 43 - TOTAL FAN THRUST VS. FAN SPEED (FAN-IN-WING WITH CIRCULAR INLET VANE AND EXIT LOUVERS)

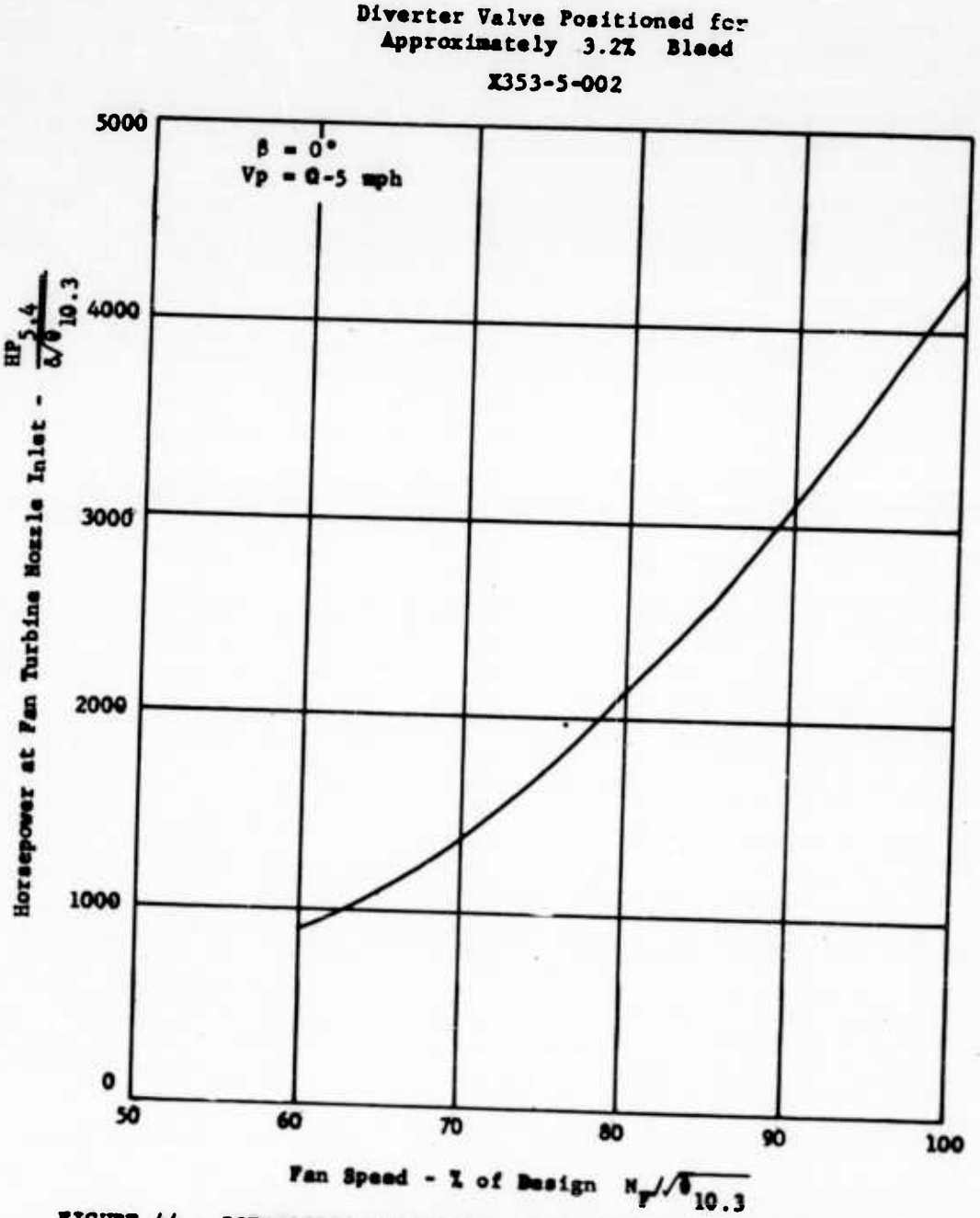

FIGURE 44 - ISENTROPIC HORSEPOWER AVAILABLE AT FAN TURBINE NOZZLE INLET VS FAN SPEED (FAN-IN-WING WITH CIRCULAR INLET VANE AND EXIT LOUVERS)

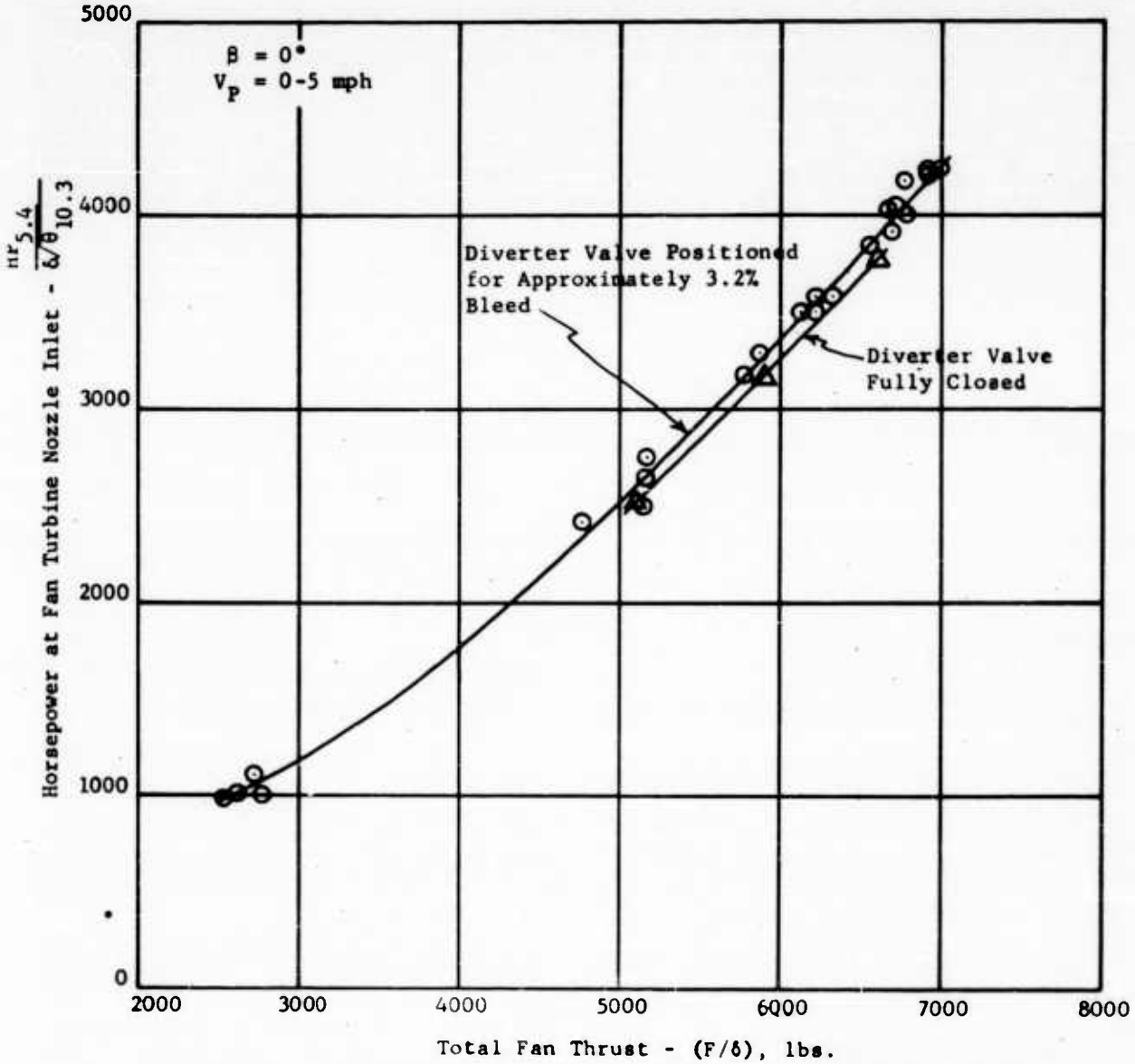

FIGURE 45 - TOTAL FAN THRUST VS. ISENTROPIC HORSEPOWER AVAILABLE AT FAN TURBINE NOZZLE INLET (FAN-IN-WING WITH CIRCULAR INLET VANE AND EXIT LOUVERS).

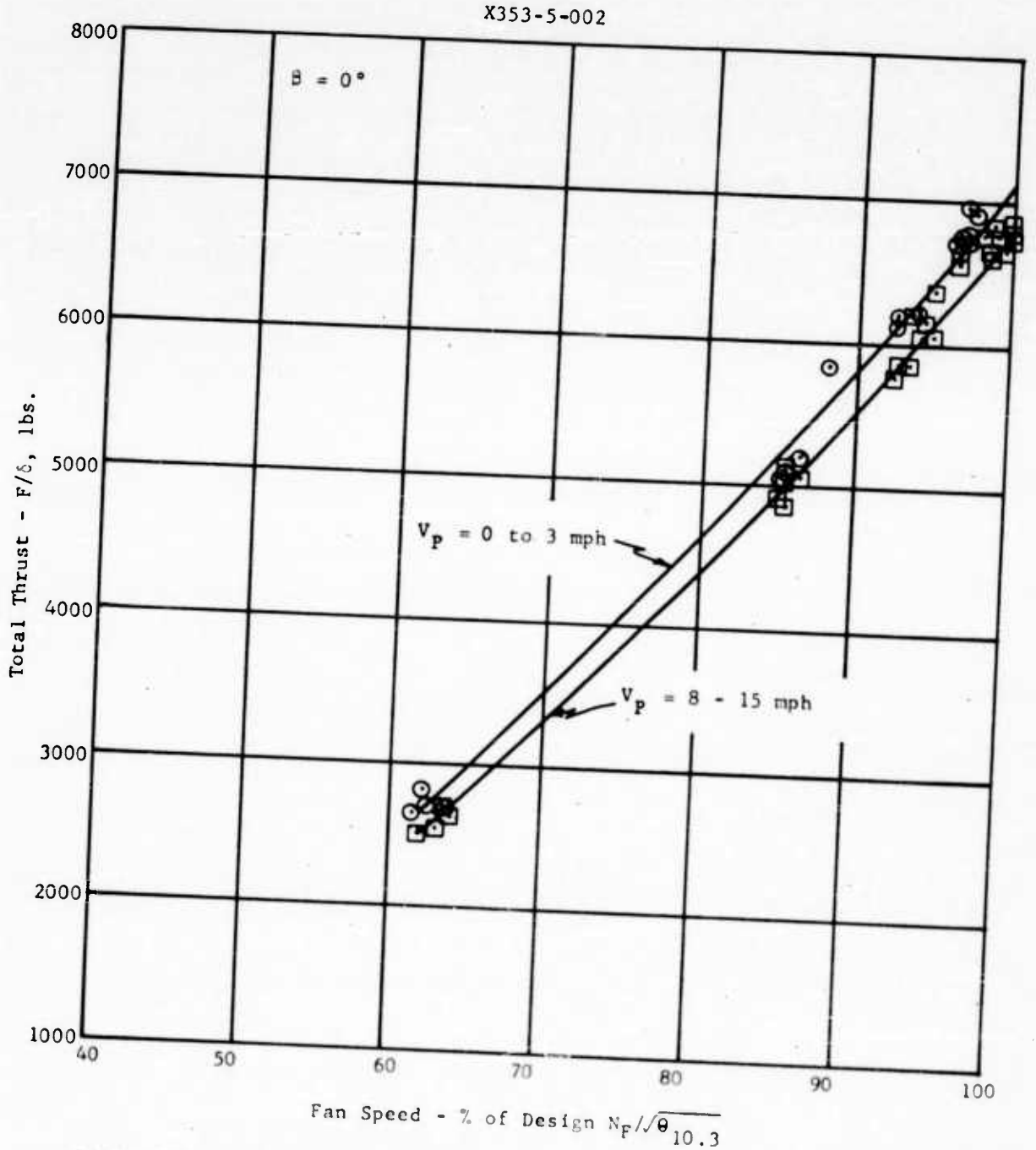

FIGURE 46 - TOTAL FAN THRUST VERSUS FAN SPEED (FAN-IN-WING WITH CIRCULAR INLET VANE AND EXIT LOUVERS)

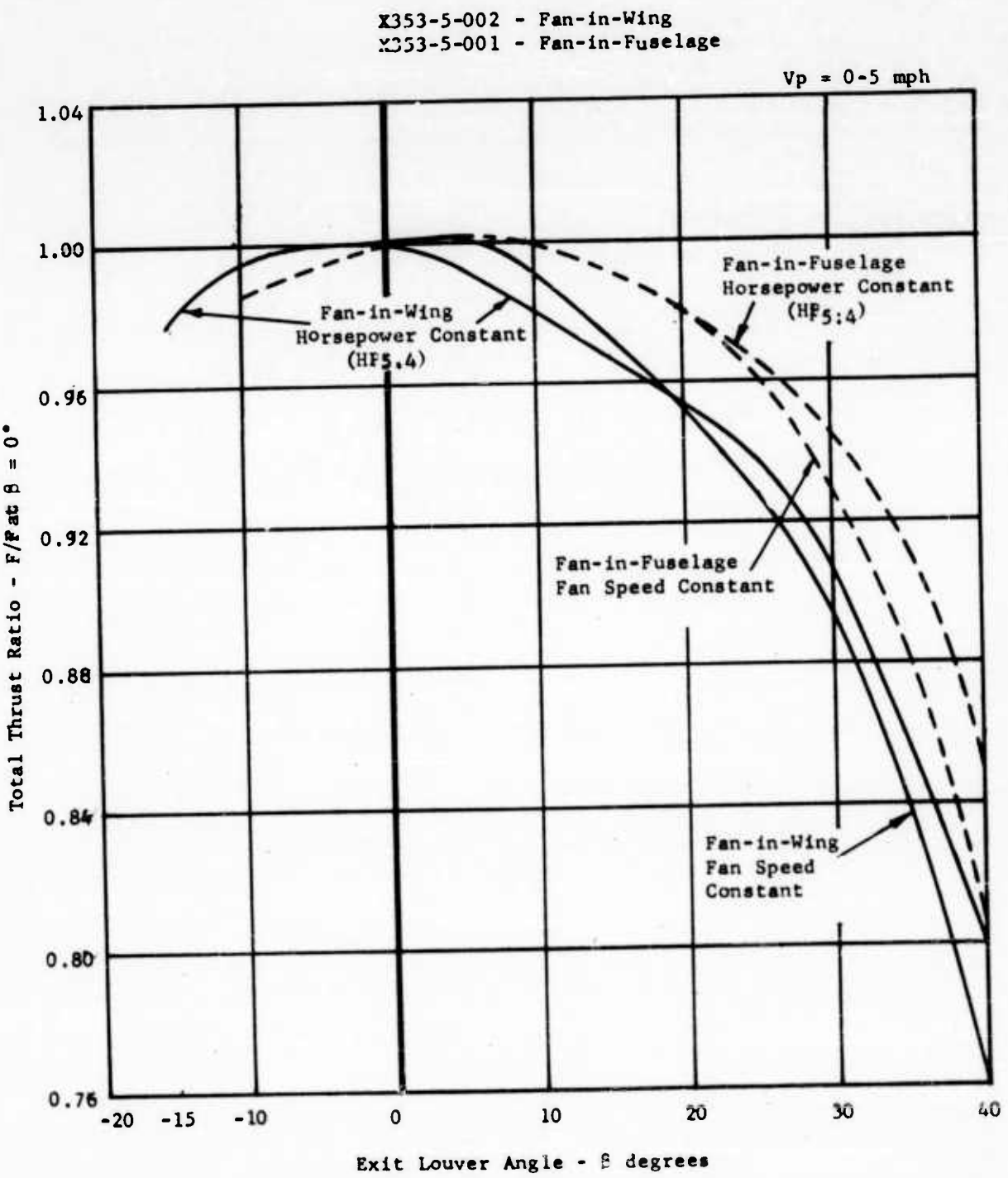

FIGURE 47 - TOTAL THRUST RATIO VERSUS INDICATED LOUVER ANGLE

X353-5-002 - Fan-in-Wing

X353-5-001 - Fan-in-Fuselage

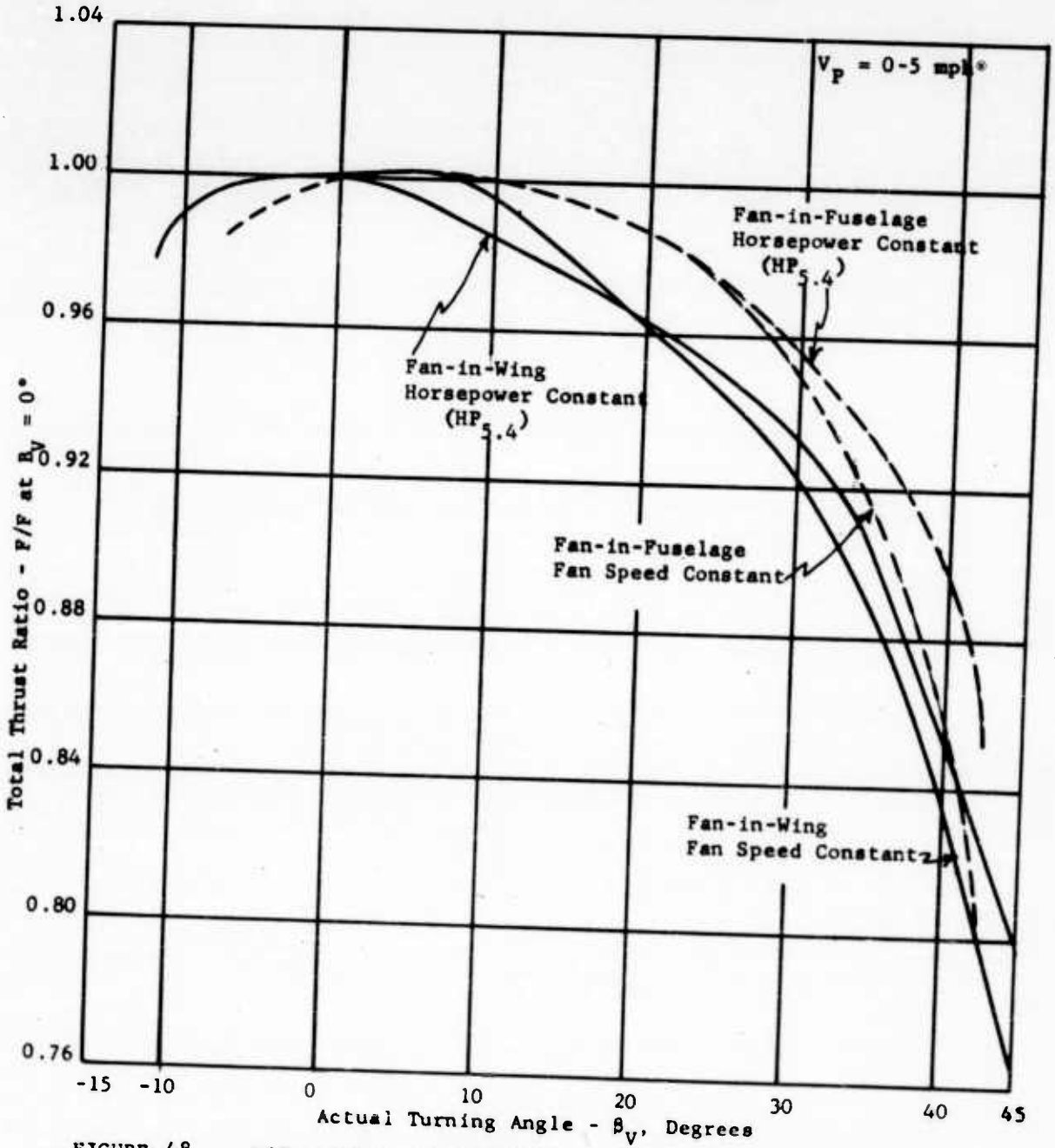

FIGURE 48 - TOTAL THRUST RATIO VERSUS ACTUAL TURNING ANGLE.

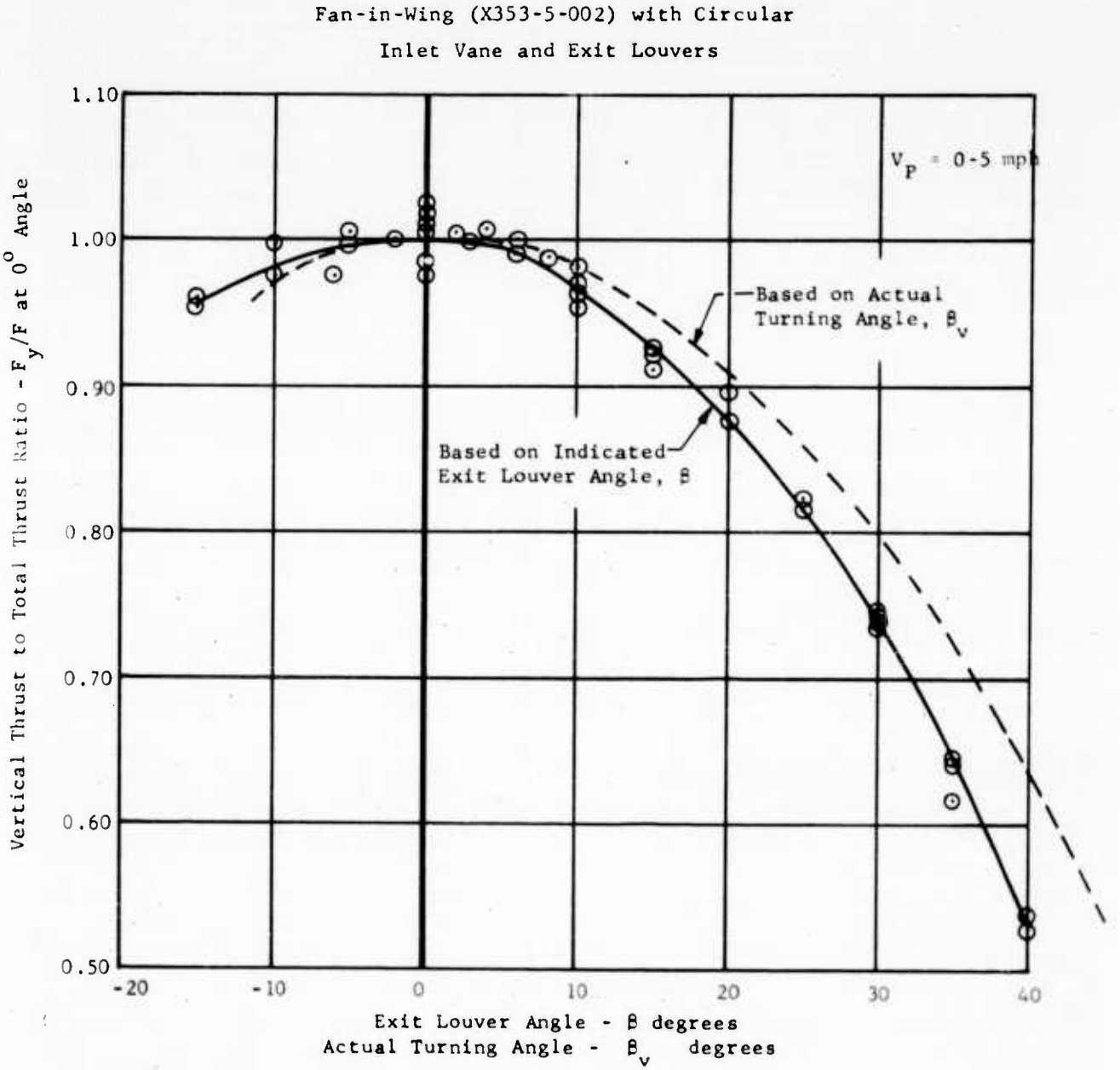

FIGURE 49 - VERTICAL THRUST TO TOTAL THRUST RATIO VS LOUVER ANGLE (CONSTANT FAN SPEED)

Fan-in-Wing (X353-5-002) with Circular Inlet Vane and Exit Louvers.

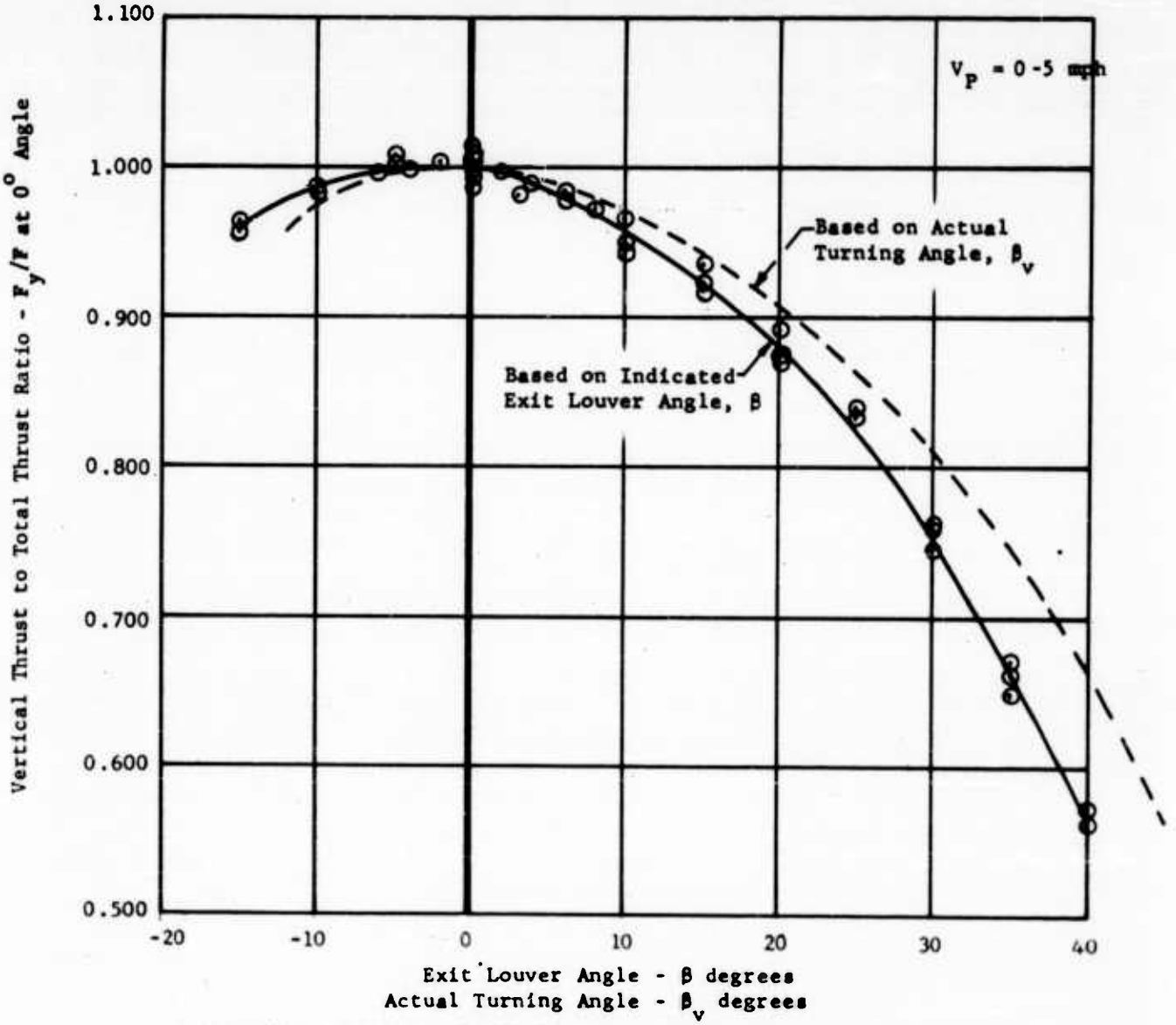

FIGURE 50 - VERTICAL THRUST TO TOTAL THRUST RATIO VS LOUVER ANGLE (CONSTANT FAN HORSEPOWER)

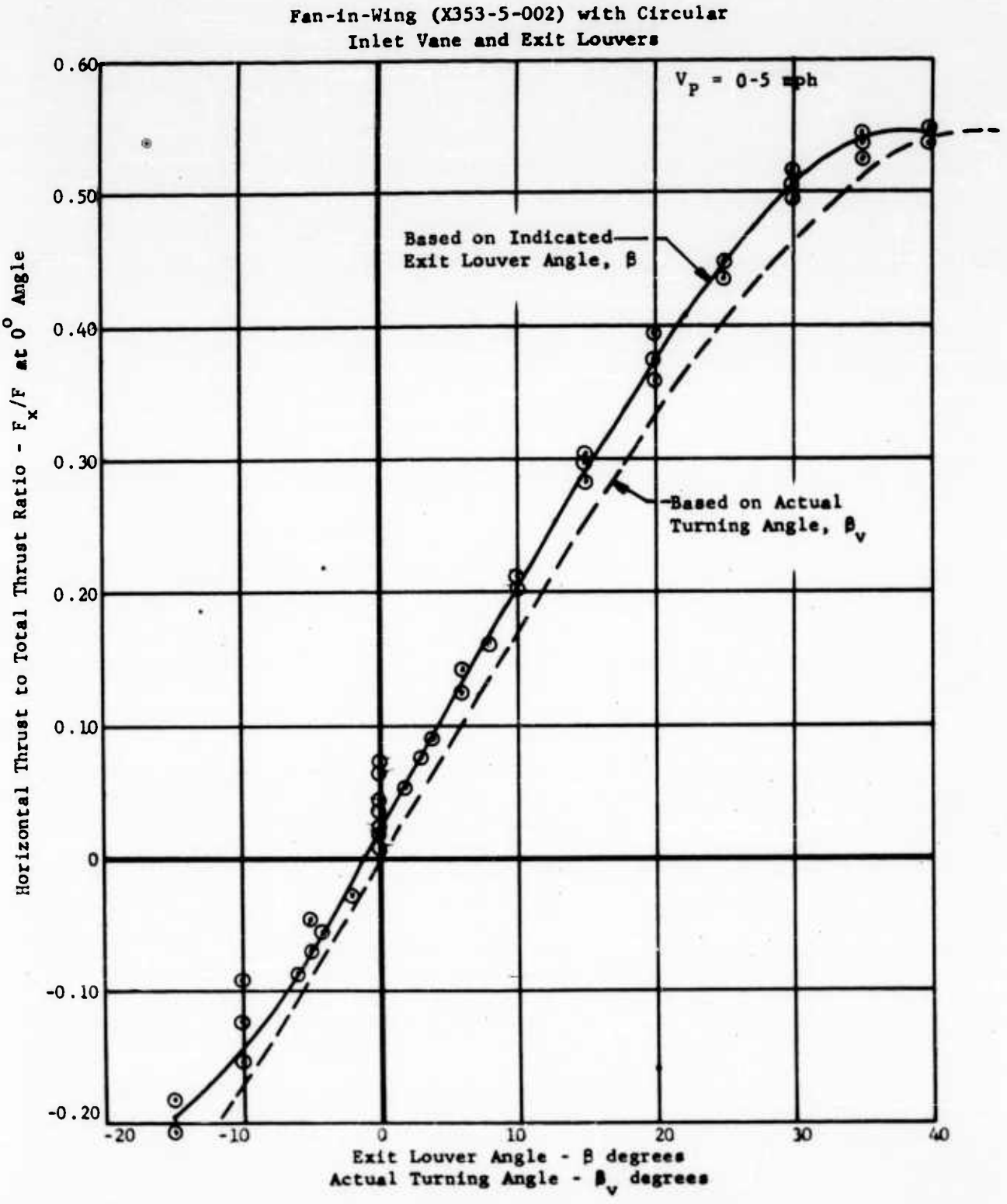

FIGURE 51 - HORIZONTAL THRUST TO TOTAL THRUST RATIO VERSUS LOUVER ANGLE (CONSTANT FAN SPEED)

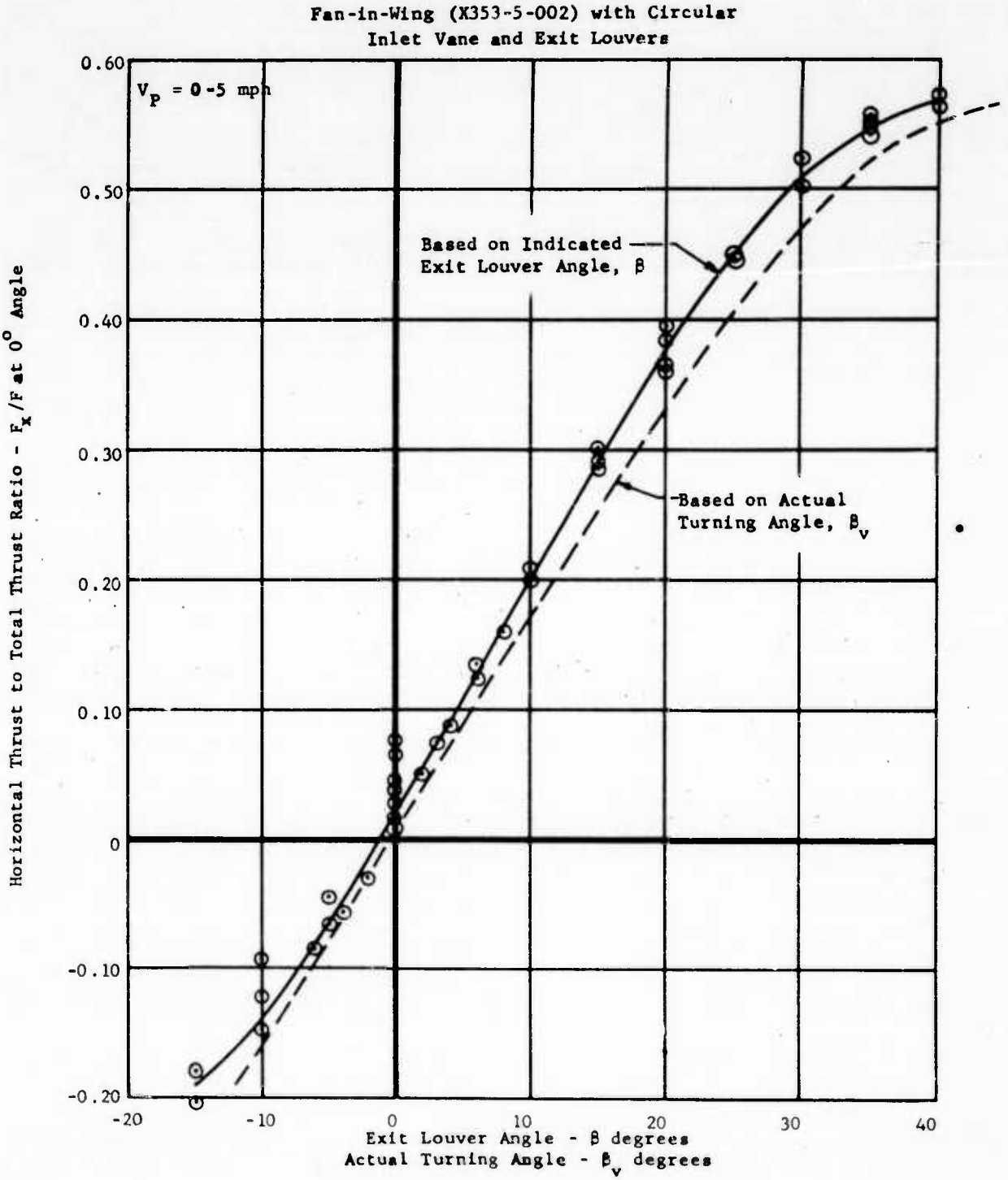

FIGURE 52- HORIZONTAL THRUST TO TOTAL THRUST RATIO VERSUS LOUVER ANGLE (CONSTANT FAN HORSEPOWER)

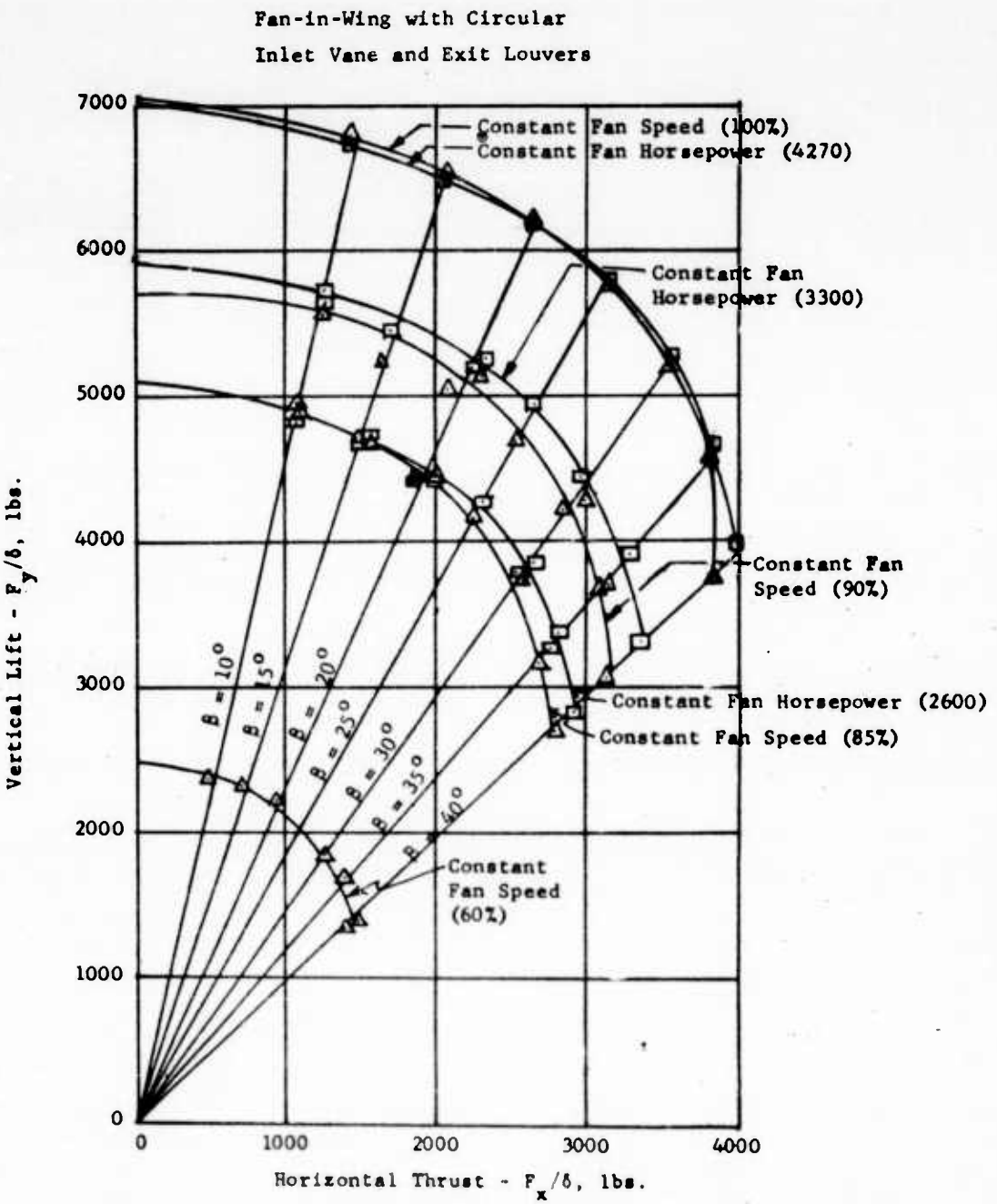

FIGURE 53 - VERTICAL LIFT VERSUS HORIZONTAL THRUST AT CONSTANT FAN HORSEPOWER AND SPEED (FAN-IN-WING)

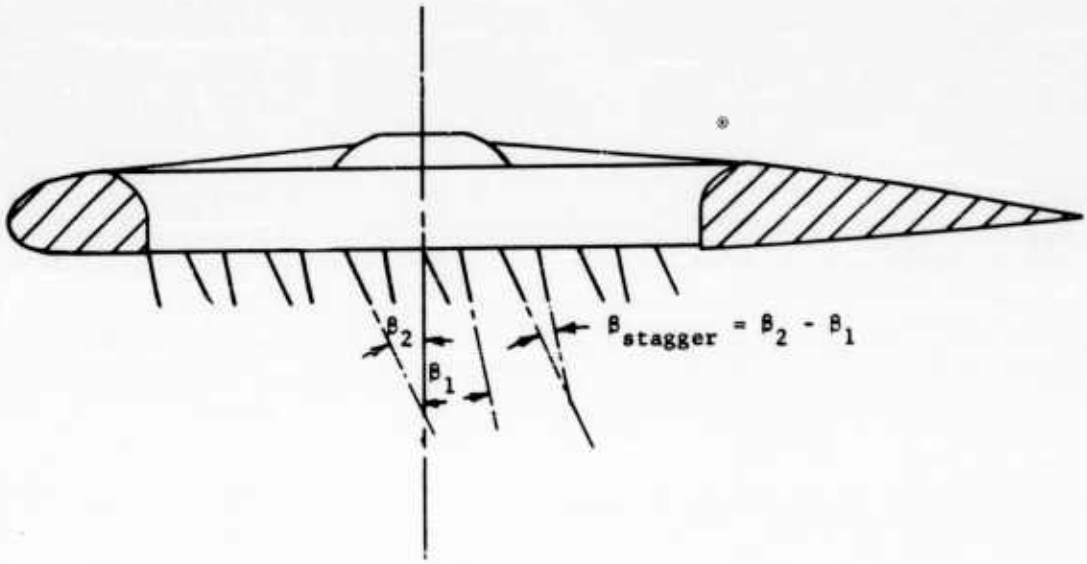

Use of Exit Louver System for Aircraft Control Power (Fans-in-Wing):

1. Roll Trim and Control ..... Differential Staggering
2. Yaw Trim and Control ..... Differential Vectoring
3. Hovering Altitude Control ..... Symmetrical Staggering
4. Transition Propulsion Control ..... Symmetrical Vectoring

FIGURE 54 - SCHEMATIC - DUAL ACTUATED STAGGERED LOUVERS

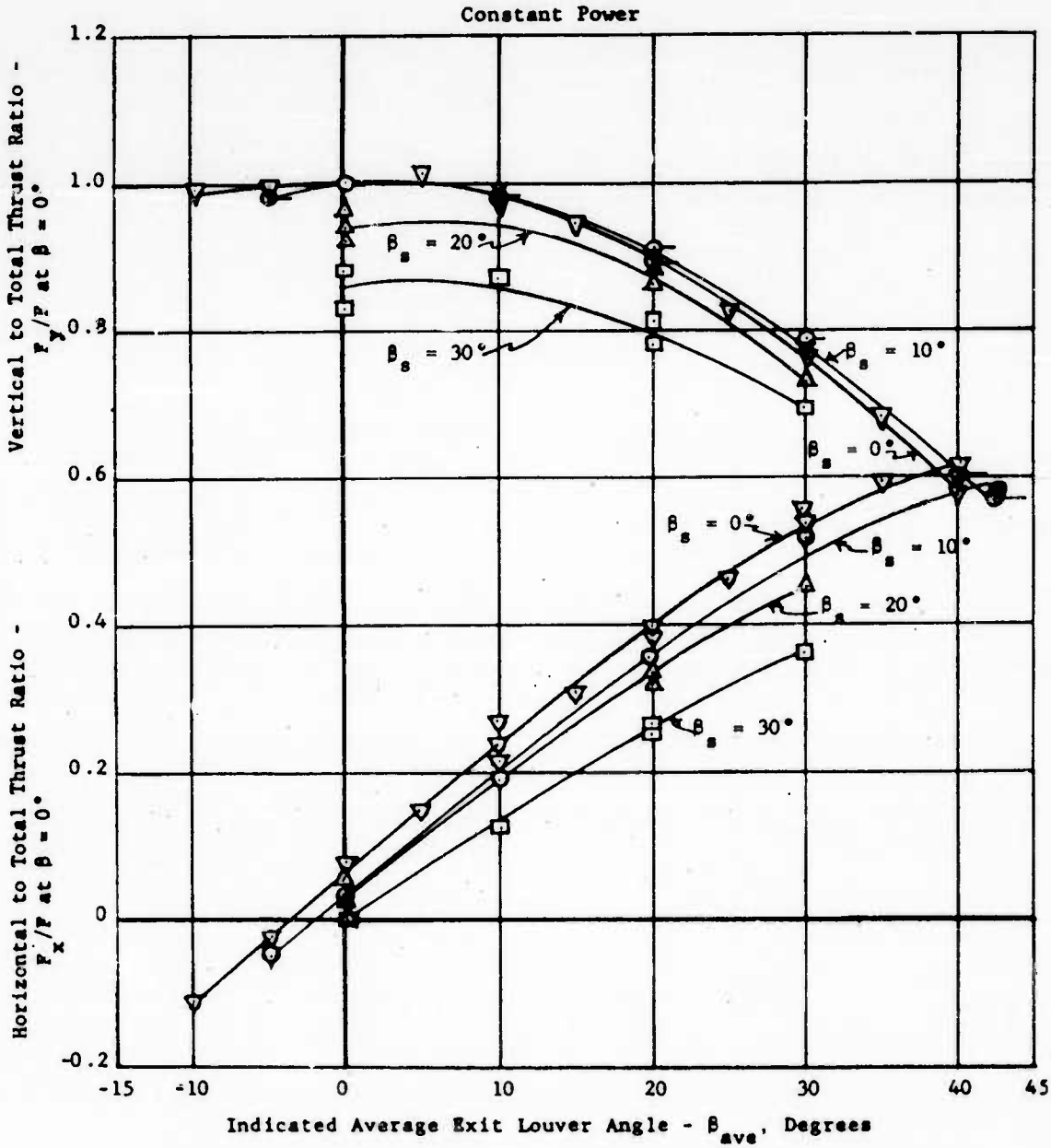

FIGURE 55 - VERTICAL AND HORIZONTAL TO TOTAL THRUST RATIO VERSUS INDICATED AVERAGE EXIT LOUVER ANGLE AS A FUNCTION OF STAGGER ANGLE (FAN-IN-WING WITH BAFFLE AND NO INLET VANE)

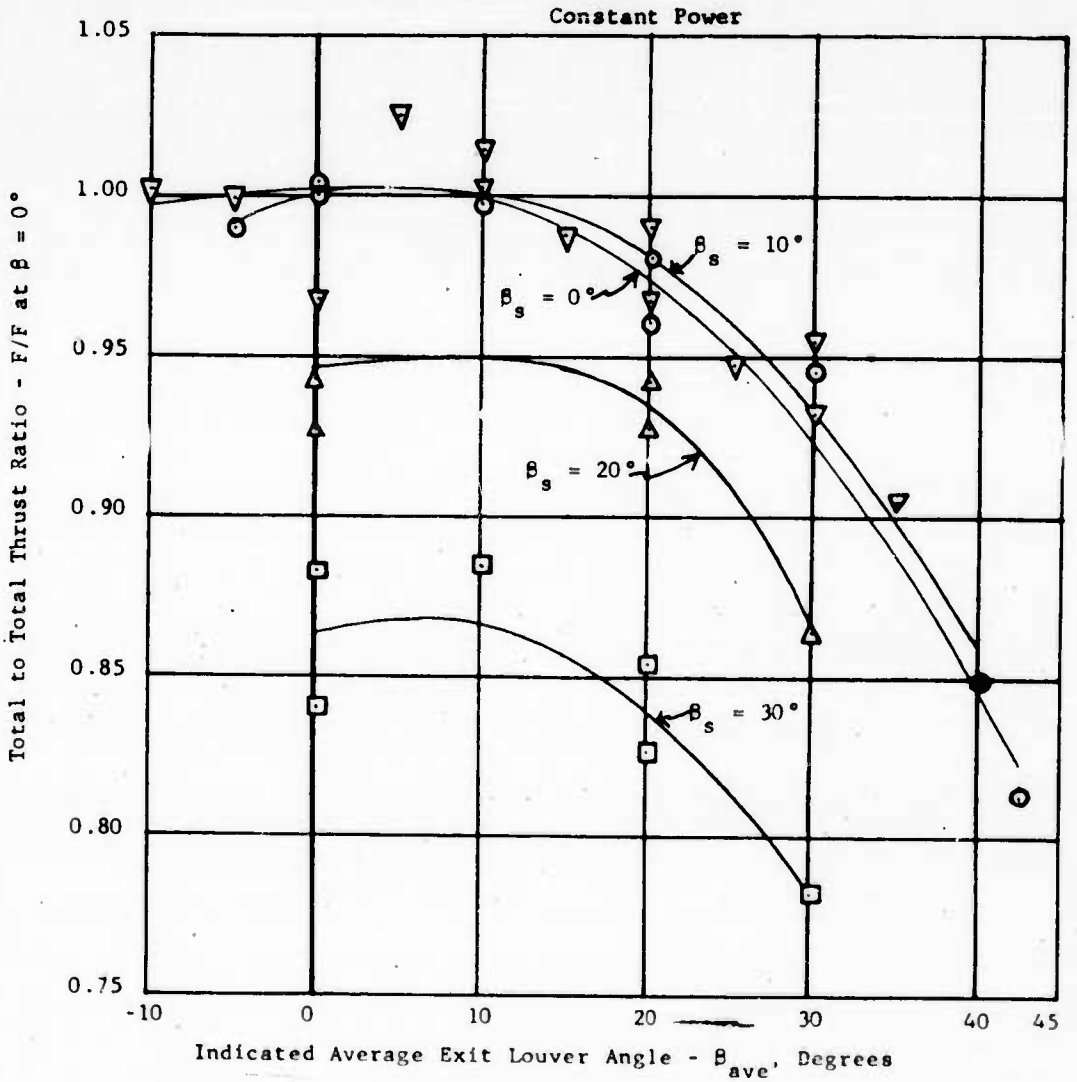

FIGURE 56 - TOTAL TO TOTAL THRUST RATIO VERSUS INDICATED AVERAGE EXIT LOUVER ANGLE AS A FUNCTION OF STAGGER ANGLE (FAN-IN-WING WITH BAFFLE AND NO INLET VANE)

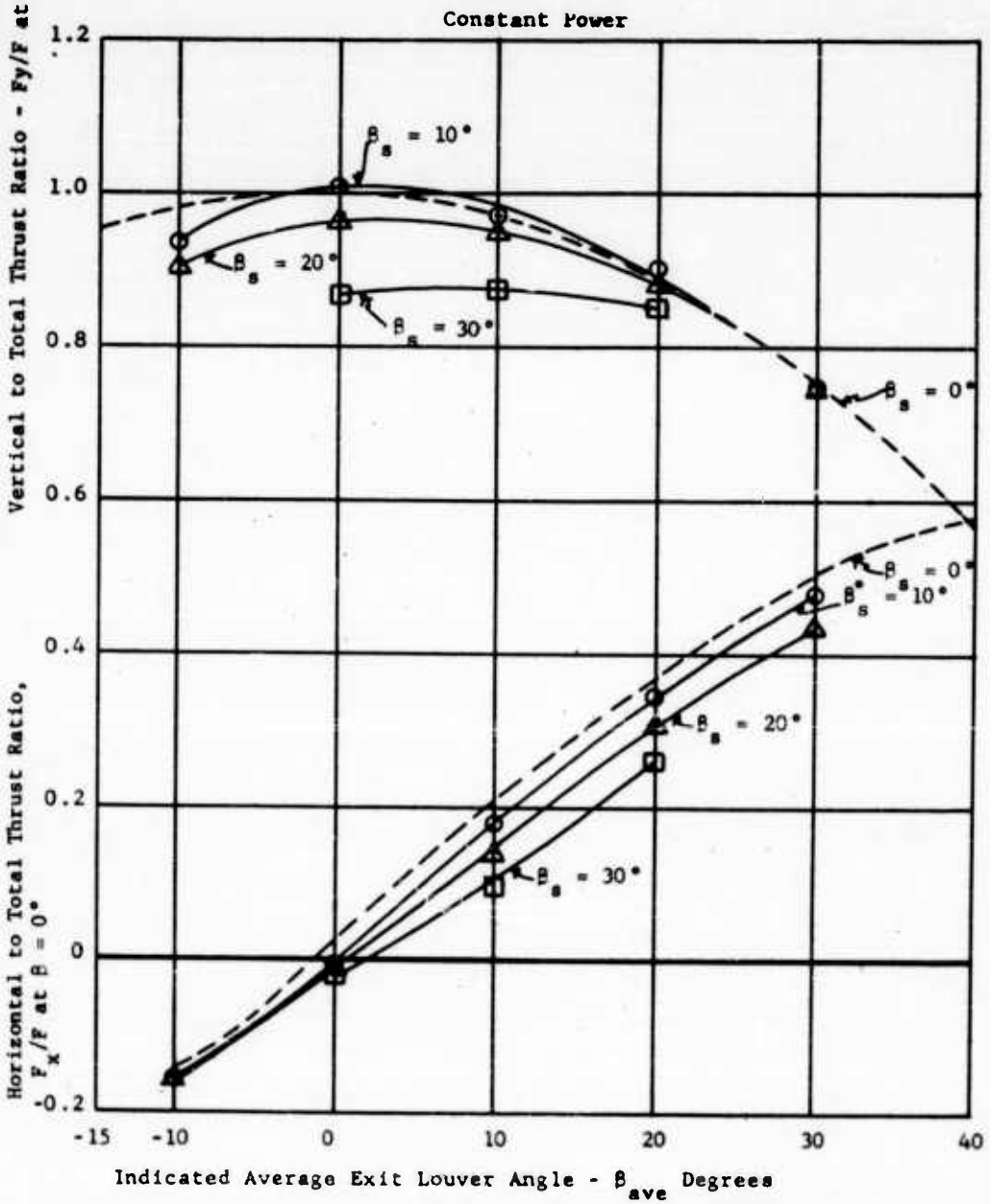

FIGURE 57 - VERTICAL AND HORIZONTAL TO TOTAL THRUST RATIO VERSUS INDICATED AVERAGE EXIT LOUVER ANGLE AS A FUNCTION OF STAGGER ANGLE (FAN-IN-WING WITH INLET VANE AND NO BAFFLE)

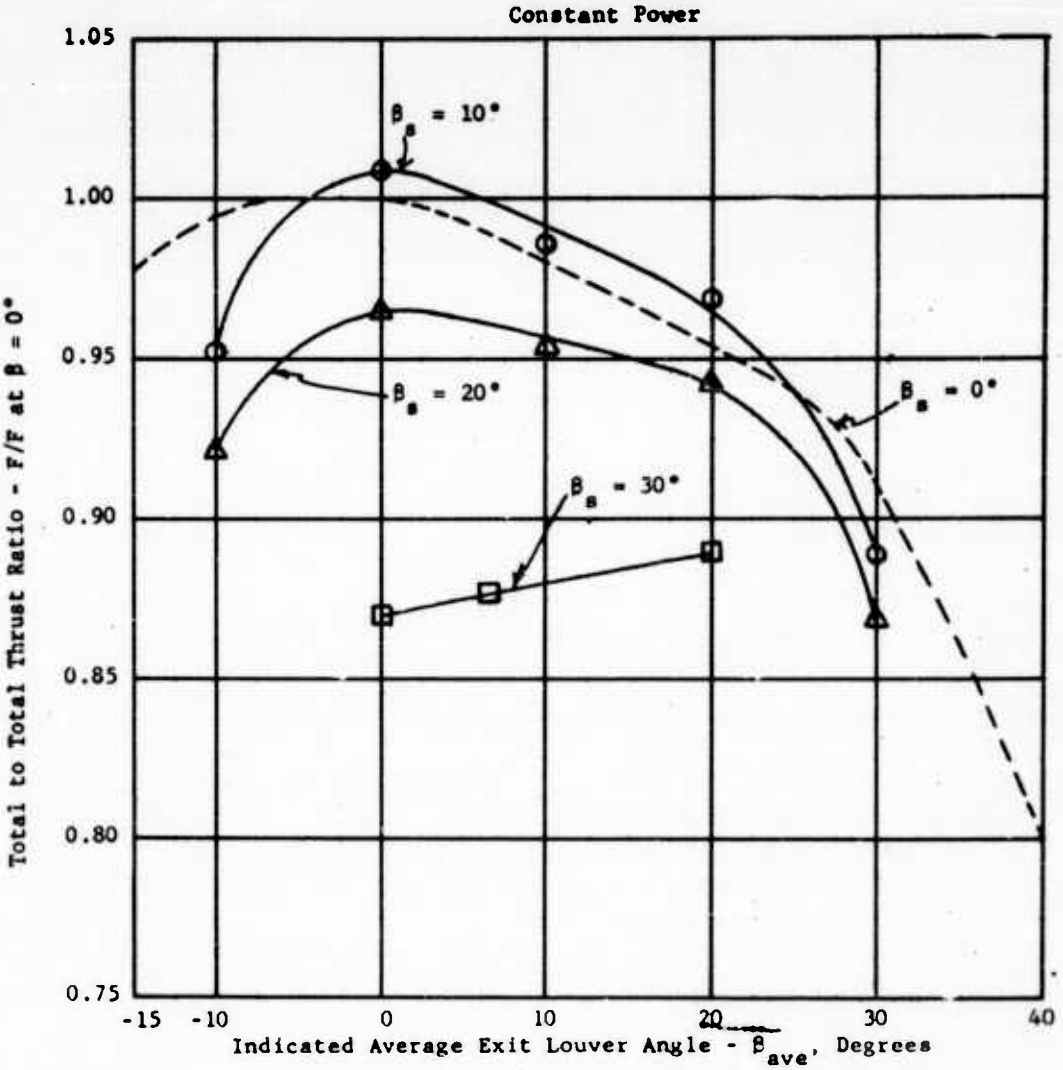

FIGURE 58 - TOTAL TO TOTAL THRUST RATIO VERSUS INDICATED AVERAGE EXIT LOUVER ANGLE AS A FUNCTION OF STAGGER ANGLE (FAN-IN-WING WITH INLET VANE AND NO BAFFLE)

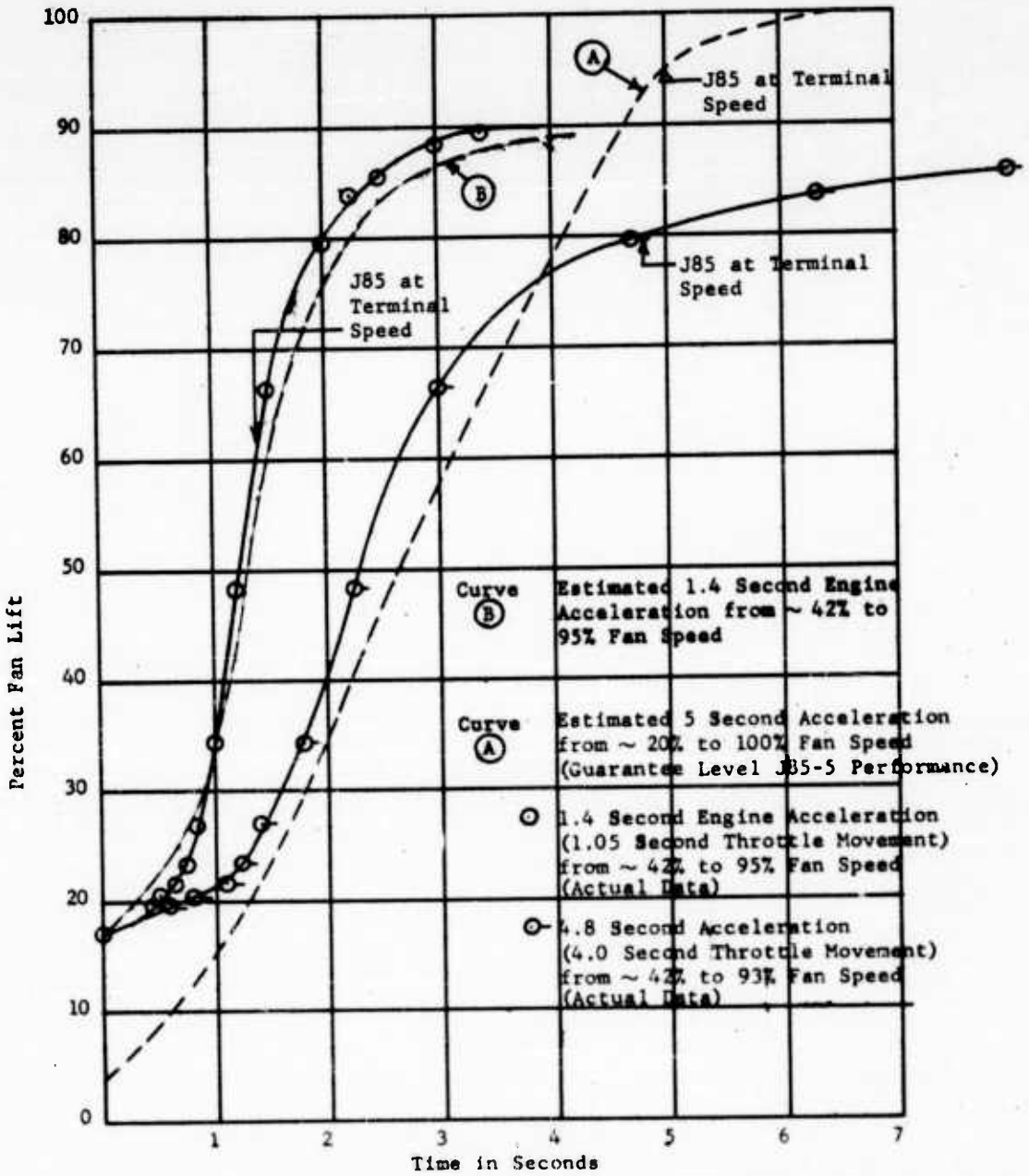

FIGURE 59 - ACTUAL AND ESTIMATED TRANSIENT PERFORMANCE, J85 ACCELERATION

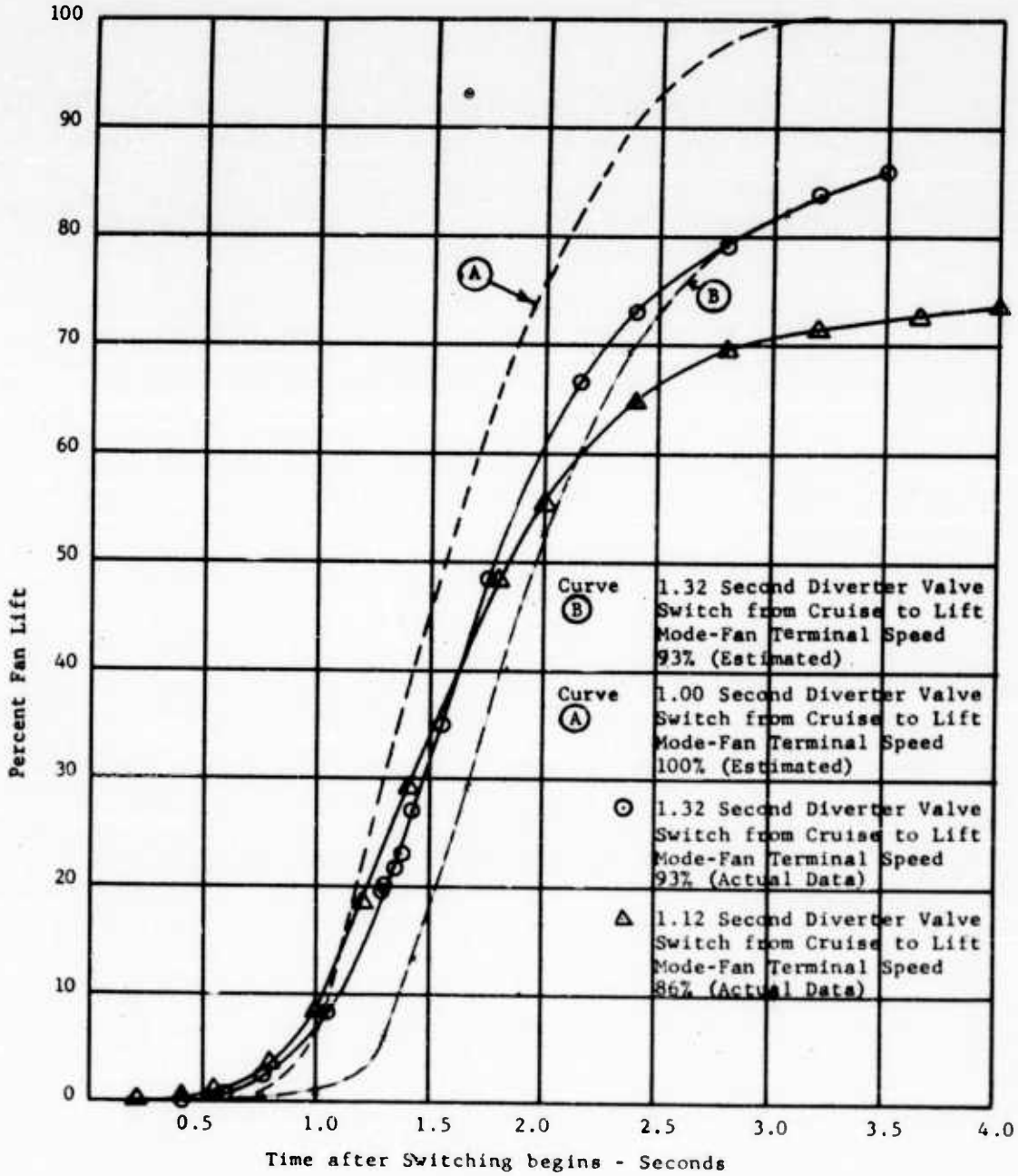

FIGURE 60 - ACTUAL AND ESTIMATED TRANSIENT PERFORMANCE, DIVERTER VALVE SWITCH FROM CRUISE MODE TO LIFT MODE

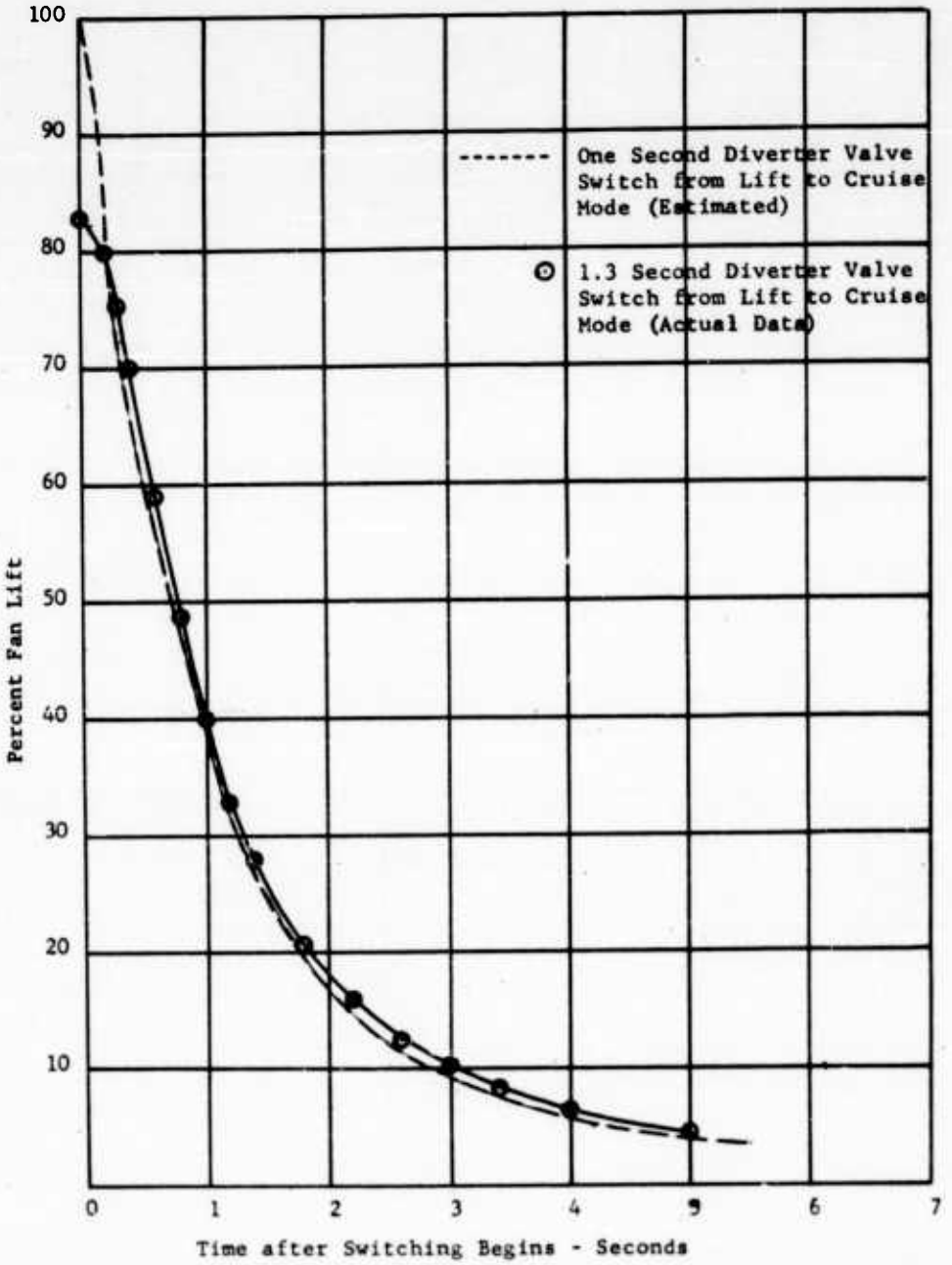

FIGURE 61 - ACTUAL AND ESTIMATED TRANSIENT PERFORMANCE, DIVERTER VALVE SWITCH FROM LIFT TO CRUISE MODE

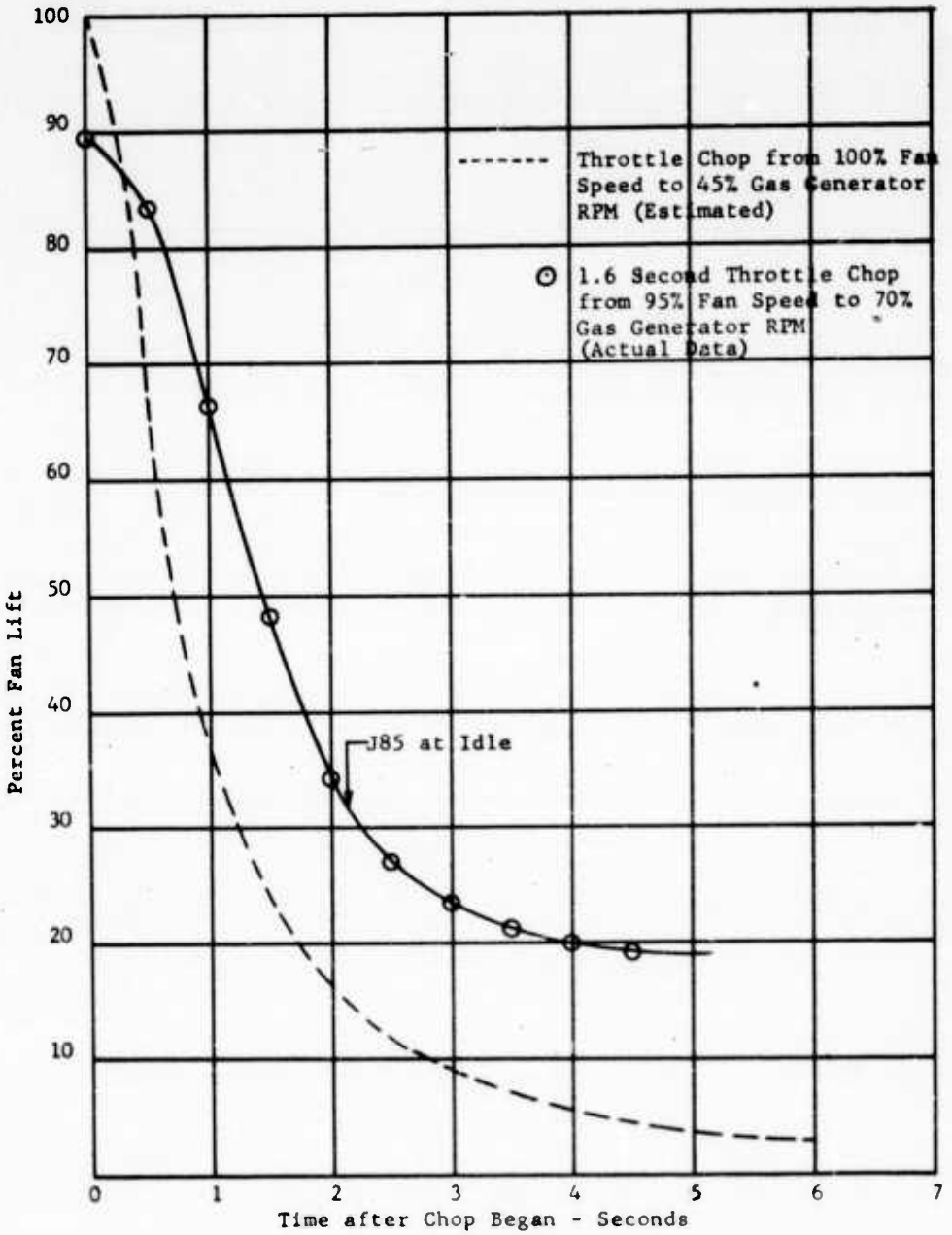

FIGURE 62 - ACTUAL AND ESTIMATED TRANSIENT PERFORMANCE, THROTTLE CHOP

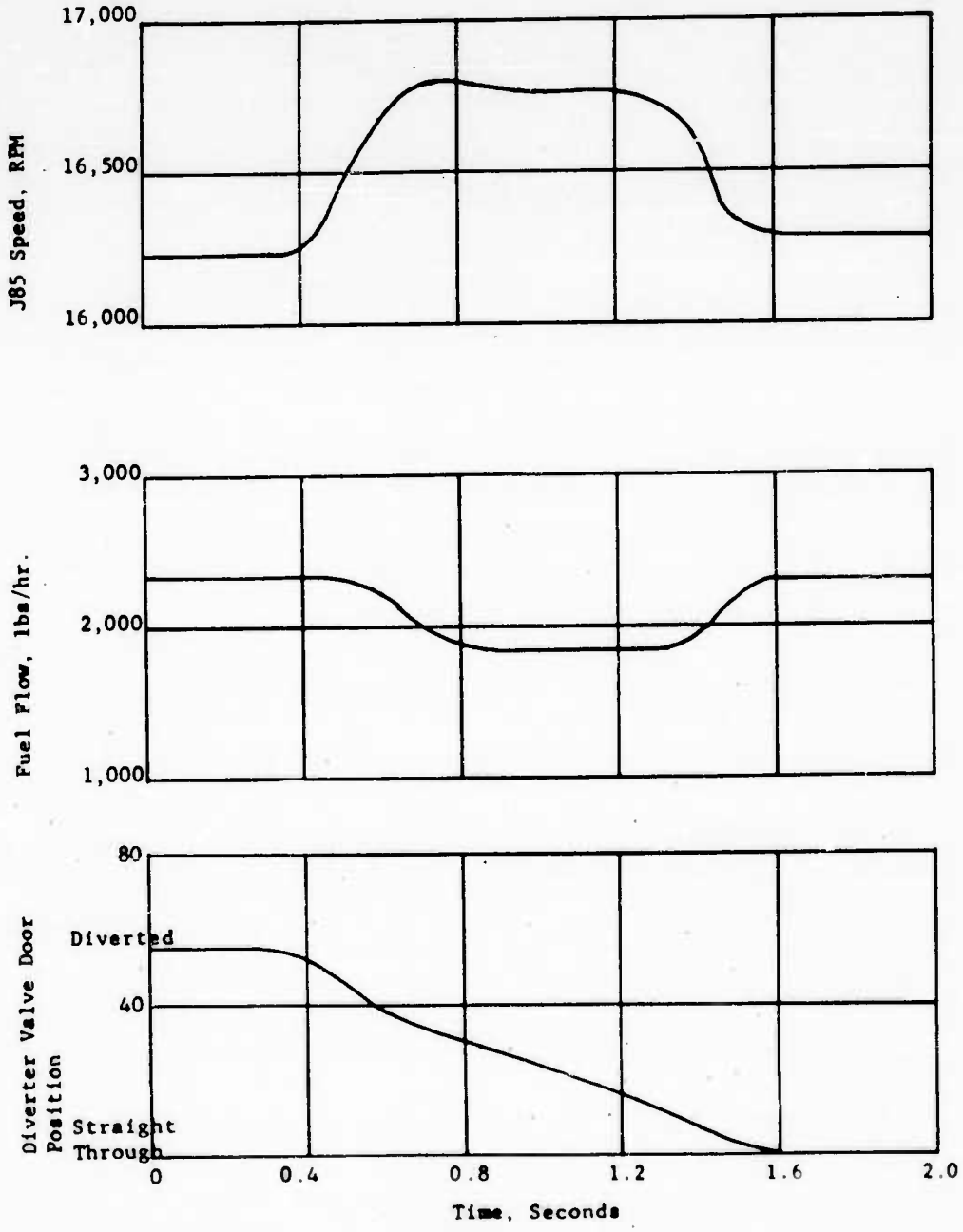

FIGURE 63 - J85 OVERSPEED

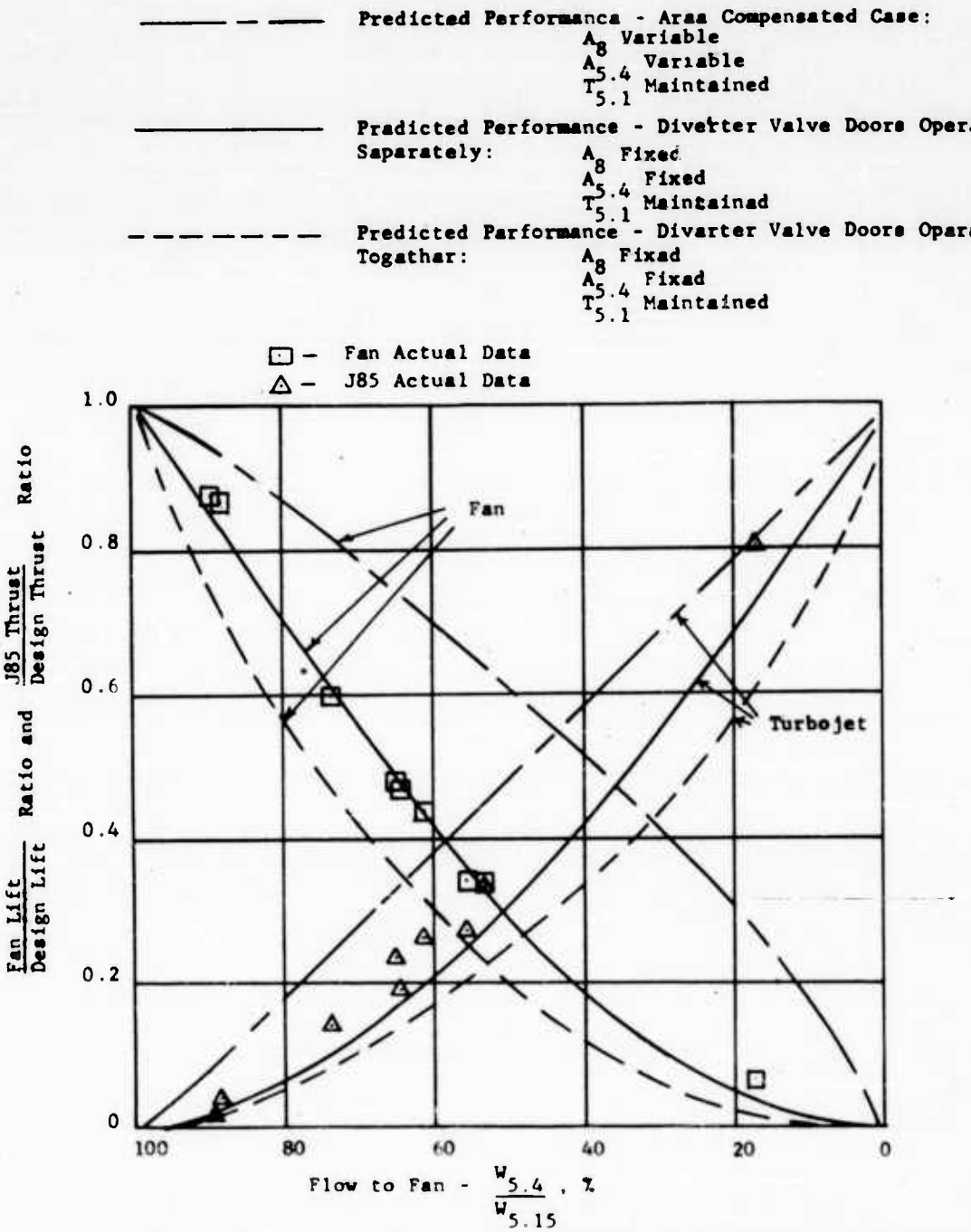

FIGURE 64 - COMPARISON - TEST RESULTS WITH DIVIDED FLOW STUDY

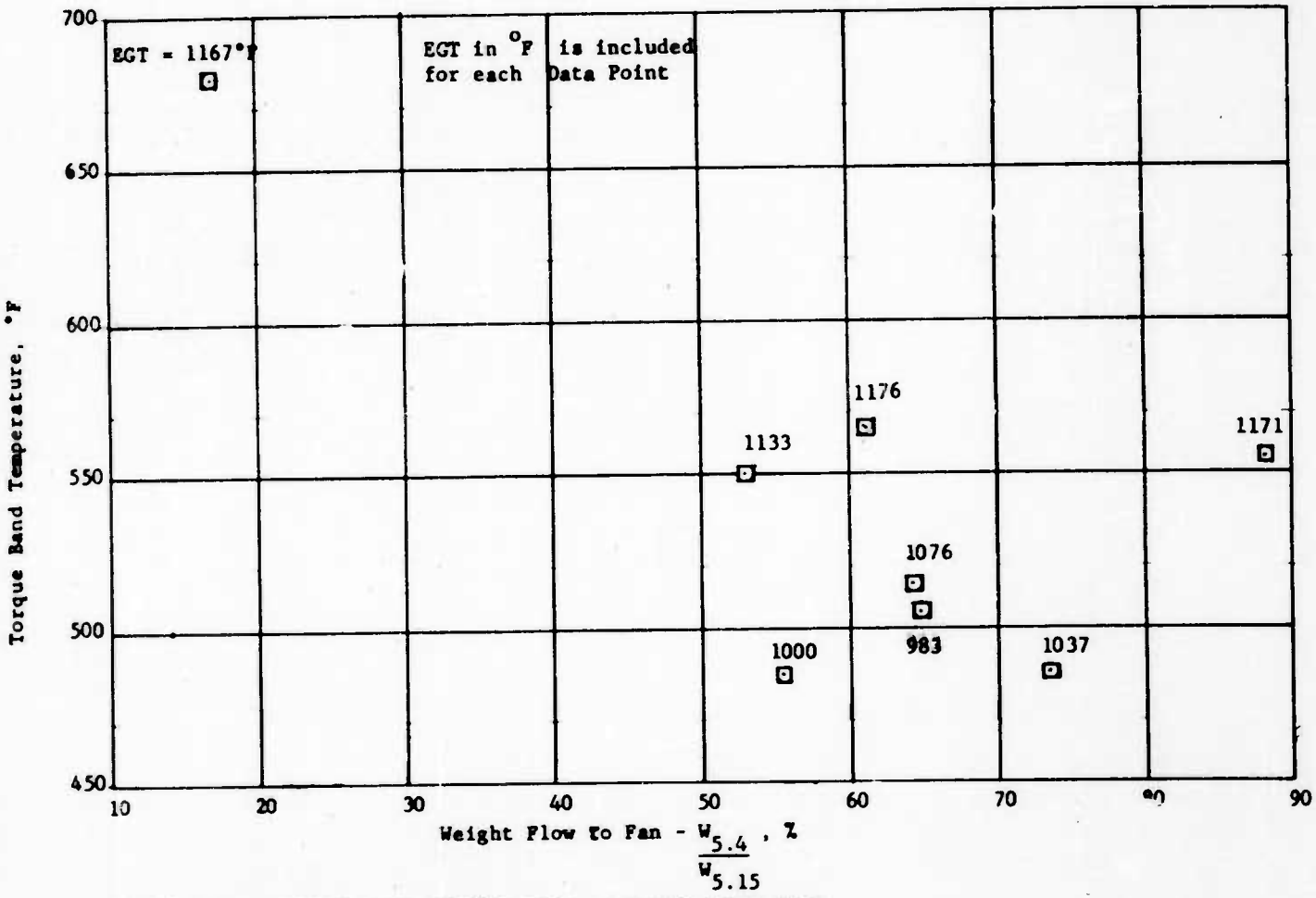

FIGURE 65 - TORQUE BAND TEMPERATURES - DIVIDED FLOW TEST

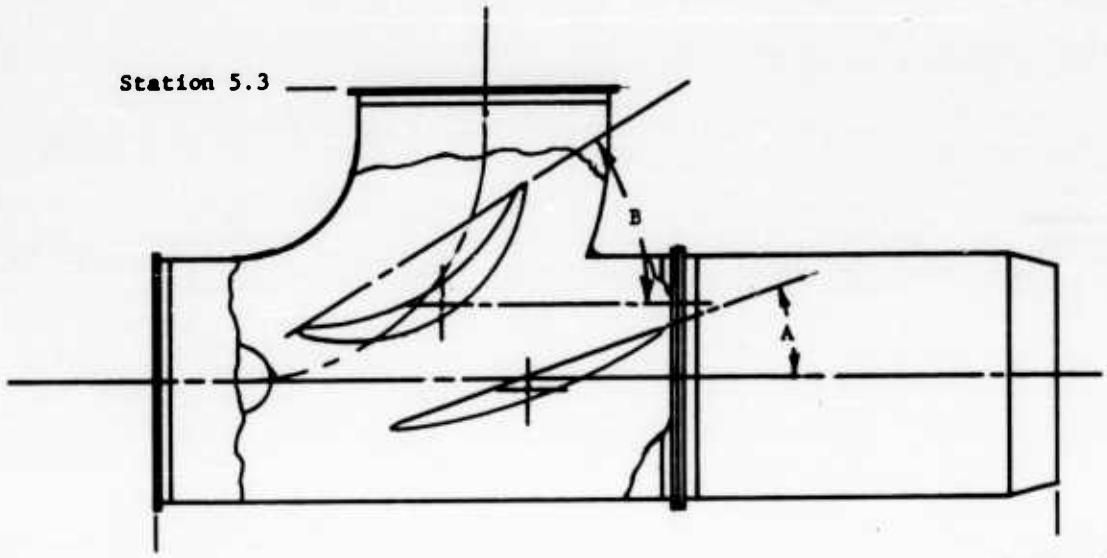

Divided Flow Test Points

Reading No.	Flat Door Position, A (Degrees)	Curved Door Position, B (Degrees)	$\frac{W_{5.4}}{W_{5.3}}$
454	50.5	53.0	
455	52.5	43.0	
456	50.0	37.0	
457	49.0	36.3	0.895
458	49.0	35.5	
459	48.5	35.0	0.883
460	50.0	50.0	
461	51.0	51.0	
462	49.0	49.0	
477	55.0	50.0	
491	0.5	1.0	
492	22.0	7.0	0.175
493	33.0	20.3	0.530
494	33.0	23.0	0.555
495	36.5	23.0	0.612
496	36.5	25.0	0.643
497	36.5	27.0	0.648
498	40.0	30.0	0.735

FIGURE 66 - SCHEMATIC OF DIVERTER VALVE POSITIONED FOR DIVIDED FLOW

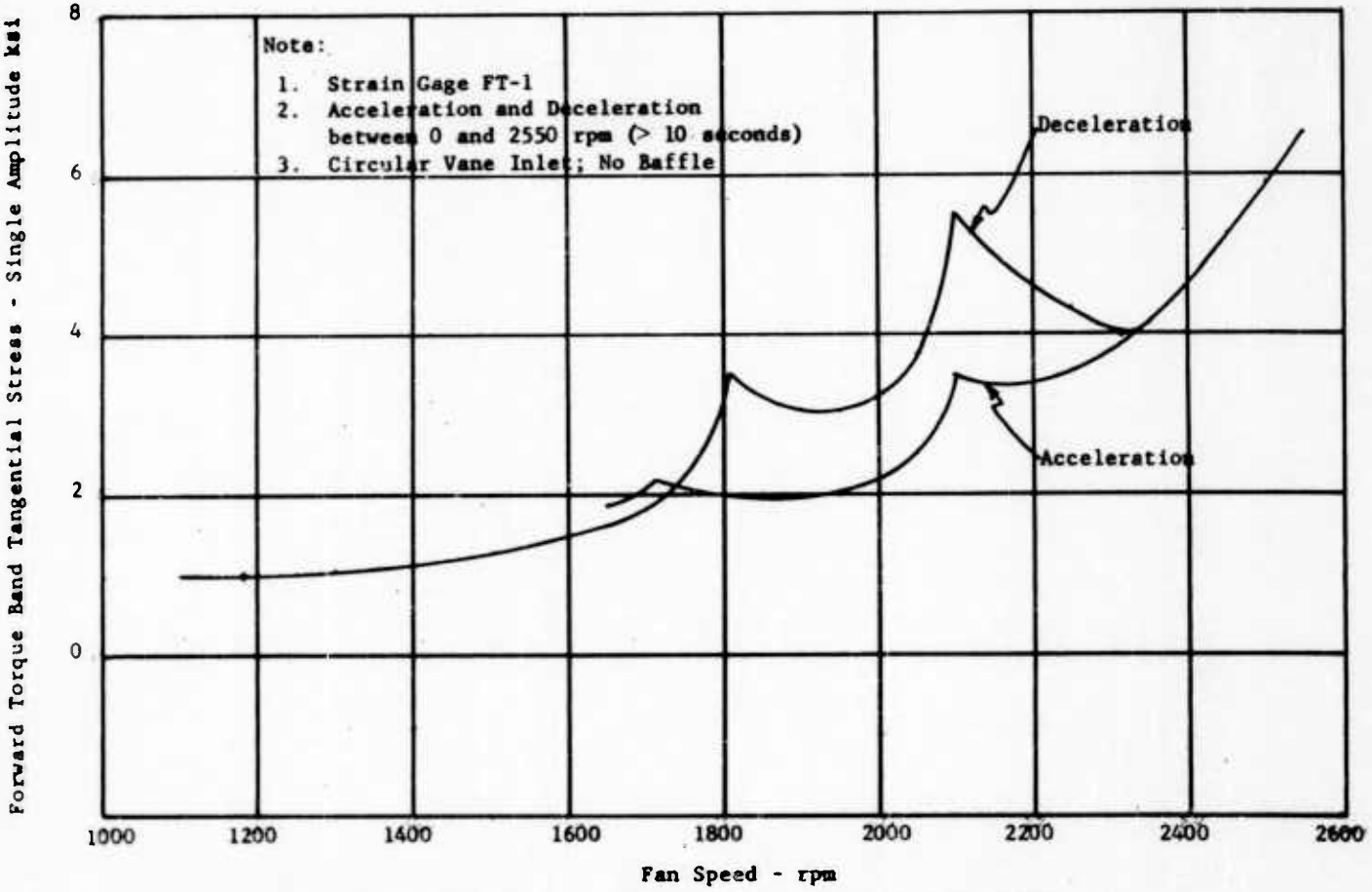

FIGURE 67 - TORQUE BAND STRESS AS A FUNCTION OF FAN SPEED (SLOW TRANSIENTS)

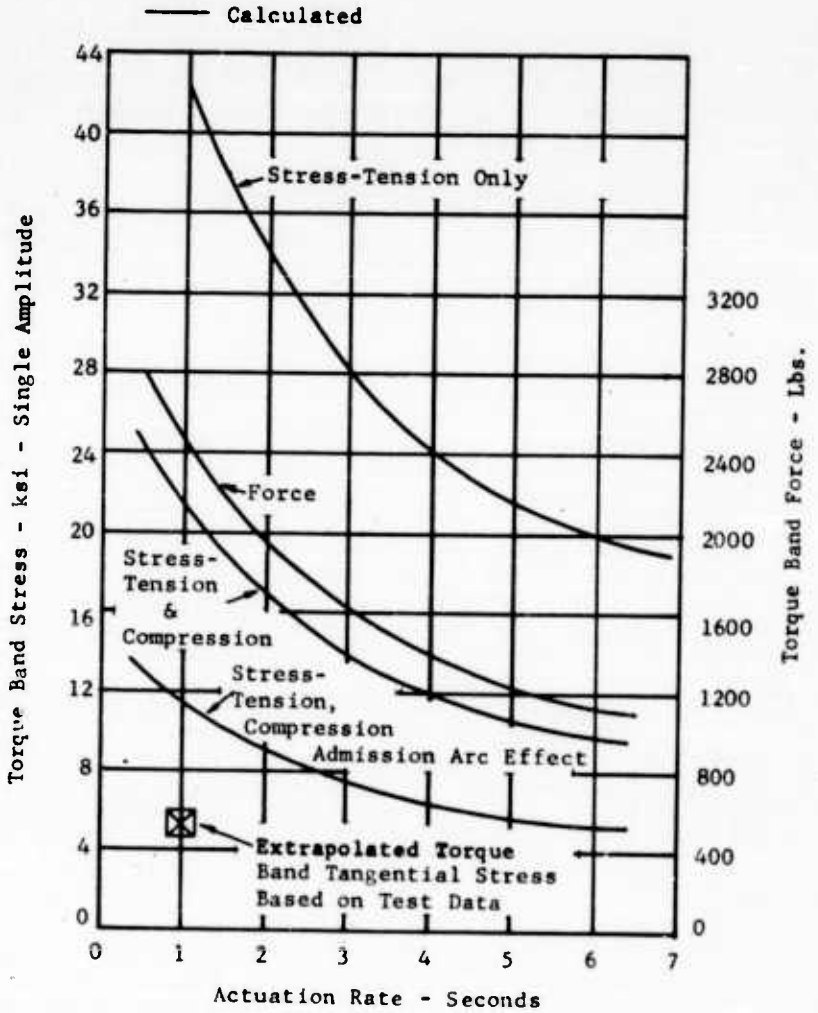

FIGURE 68 - TORQUE BAND STRESS AS A FUNCTION OF DIVERTER VALVE ACTUATION RATE

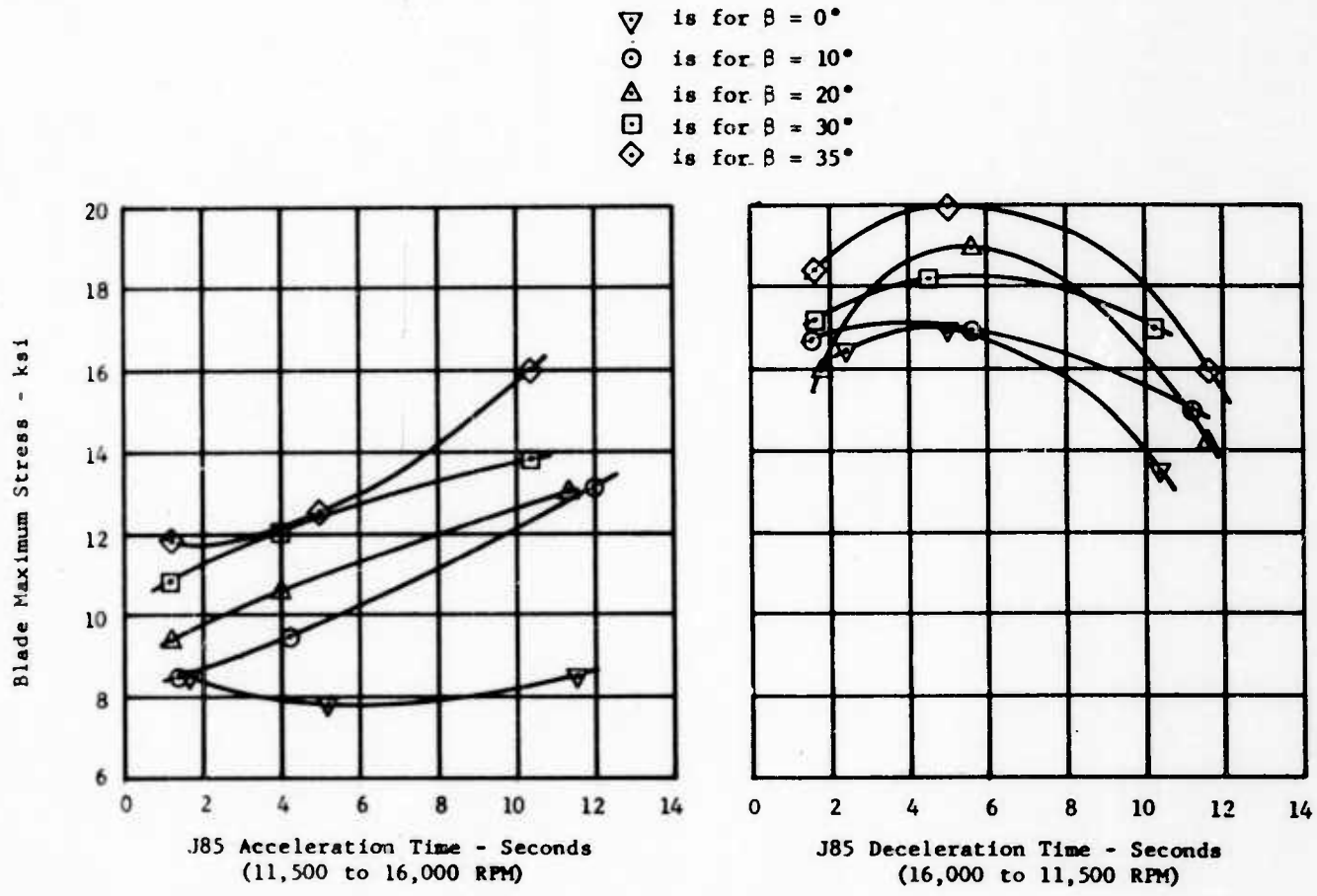

FIGURE 69 - BLADE STRESS AS A FUNCTION OF J85 THROTTLE TRANSIENTS

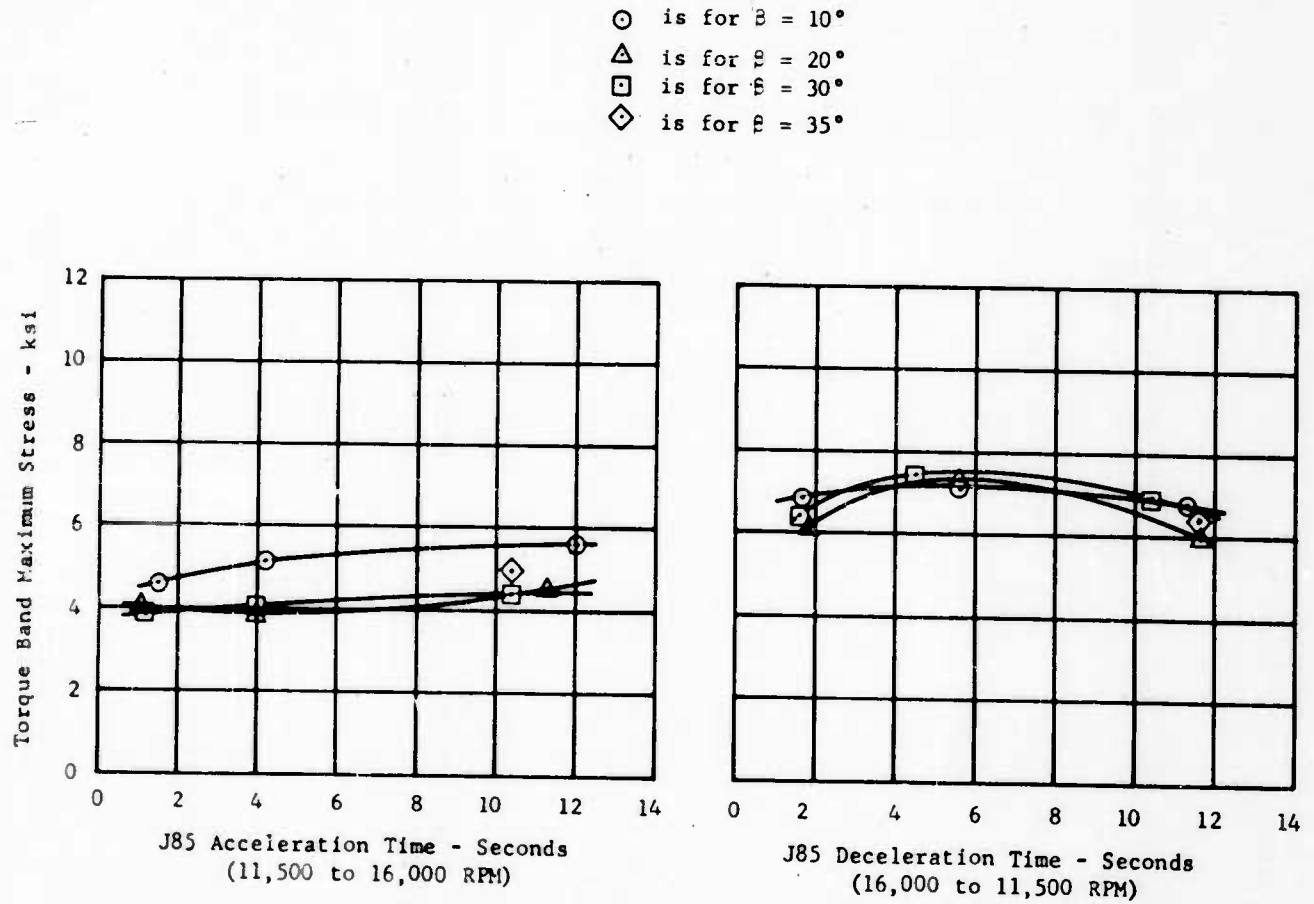

FIGURE 70 - MAXIMUM FORWARD TORQUE BAND TANG STRESS AS A FUNCTION OF J85 THROTTLE TRANSIENTS

▽ is for β = 0°
⊙ is for β = 10°
△ is for β = 20°
□ is for β = 30°
◇ is for β = 35°

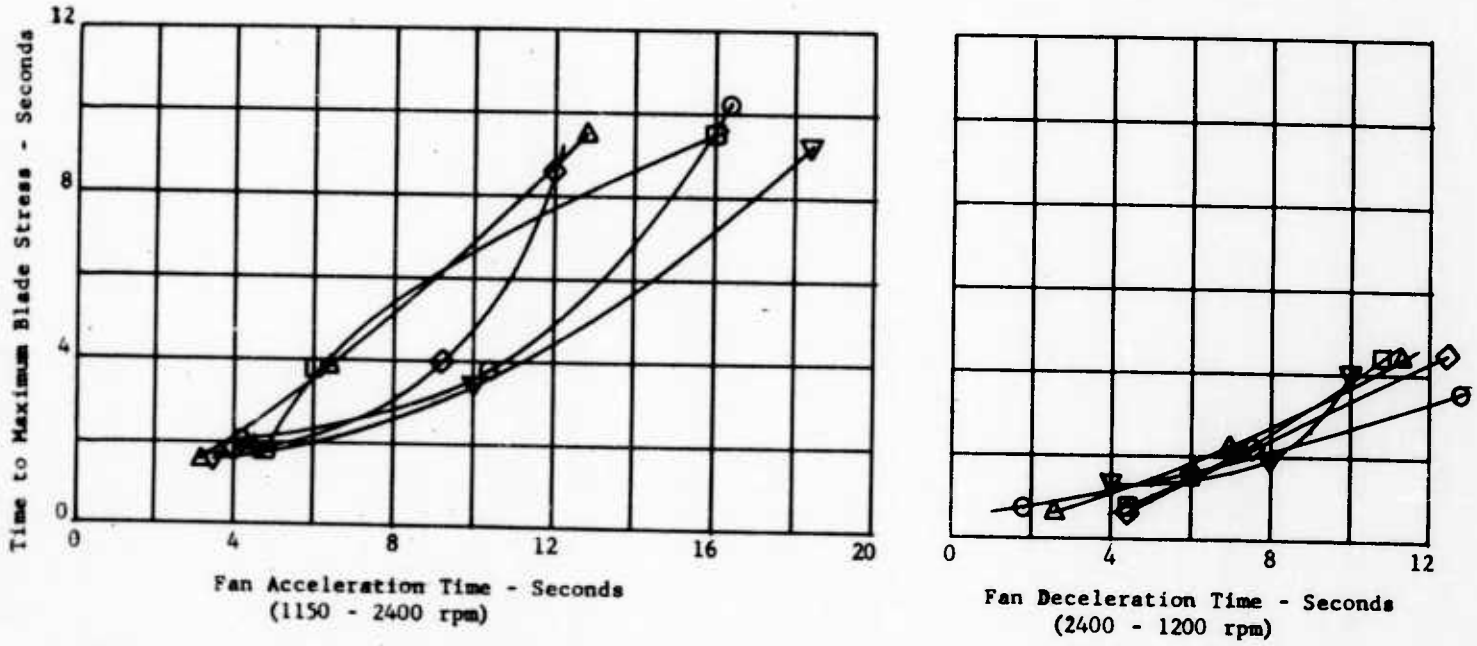

FIGURE 71 - TIME TO MAXIMUM BLADE STRESS VERSUS FAN ACCELERATION AND DECELERATION TIME

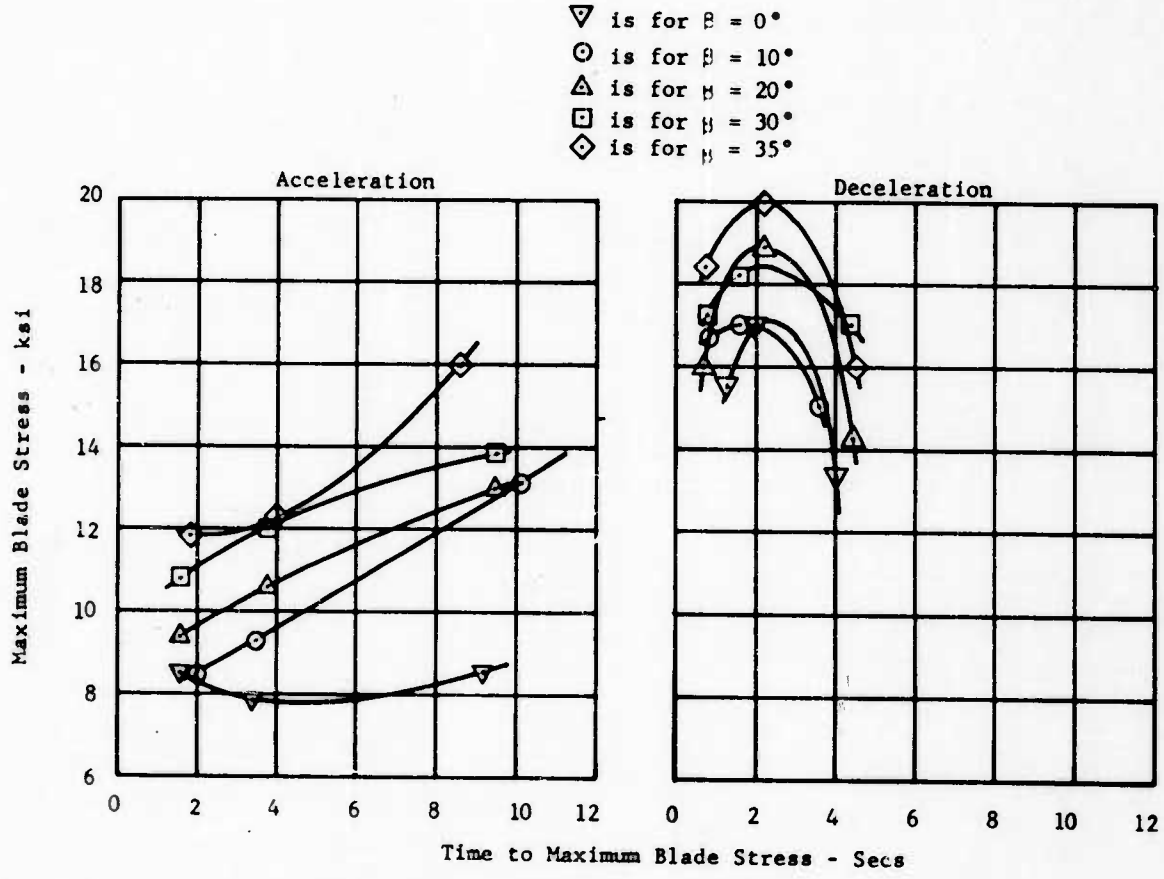

FIGURE 72 - TIME TO MAXIMUM STRESS VERSUS MAXIMUM BLADE STRESS

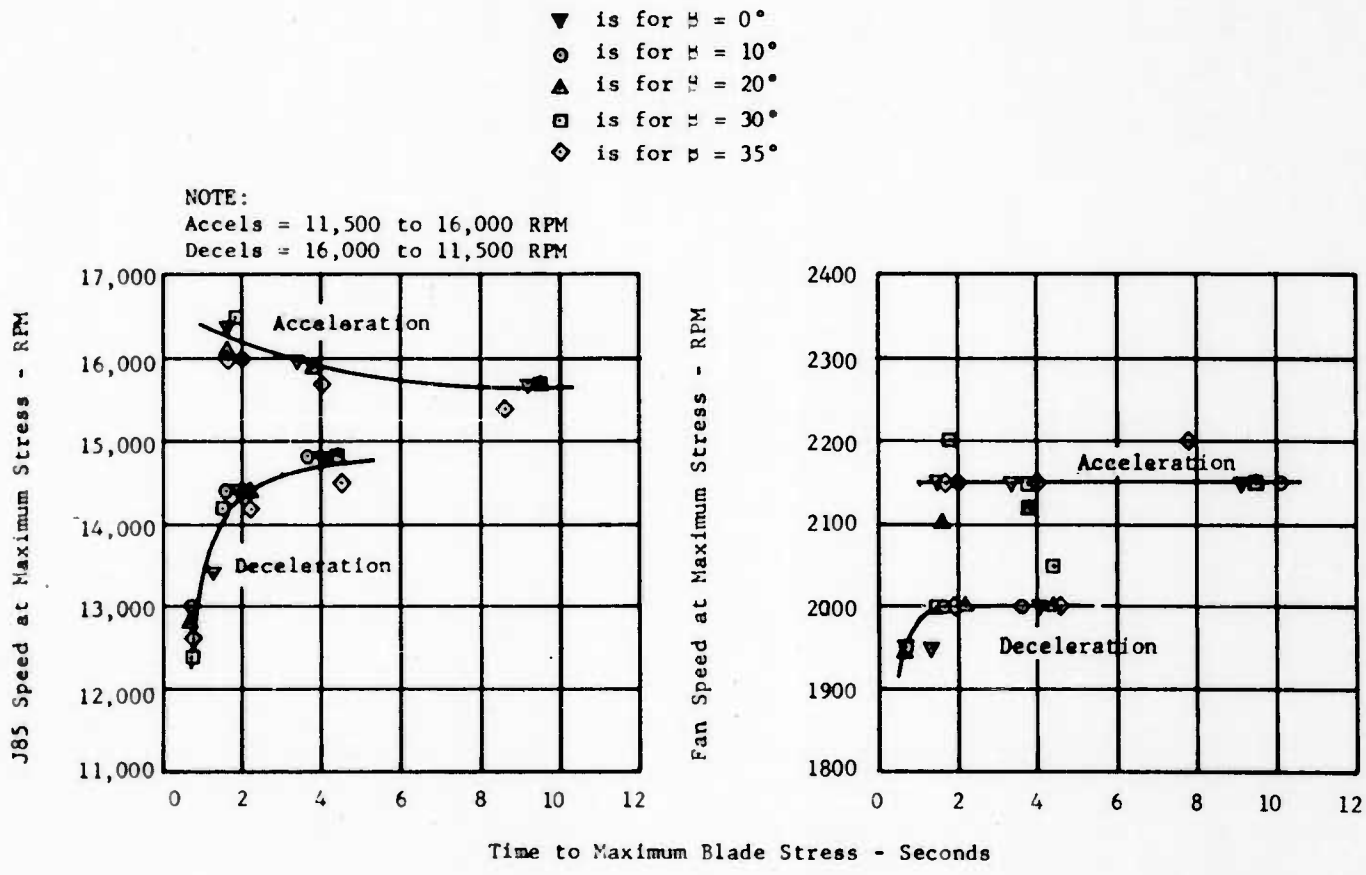

FIGURE 73 - TIME TO MAXIMUM BLADE STRESS VERSUS SPEED AT MAXIMUM BLADE STRESS (THROTTLE TRANSIENTS)

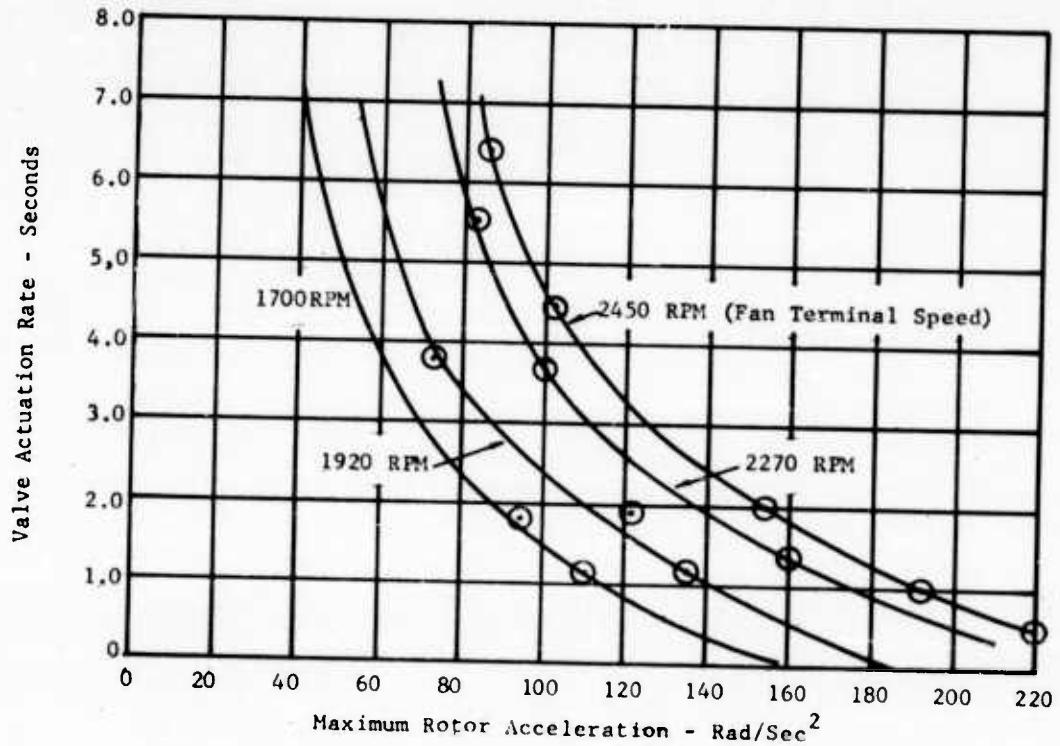

FIGURE 74 - MAXIMUM ROTOR ACCELERATION AS A FUNCTION OF SLEW RATE AND FAN TERMINAL SPEED (J85 POWER SETTING)

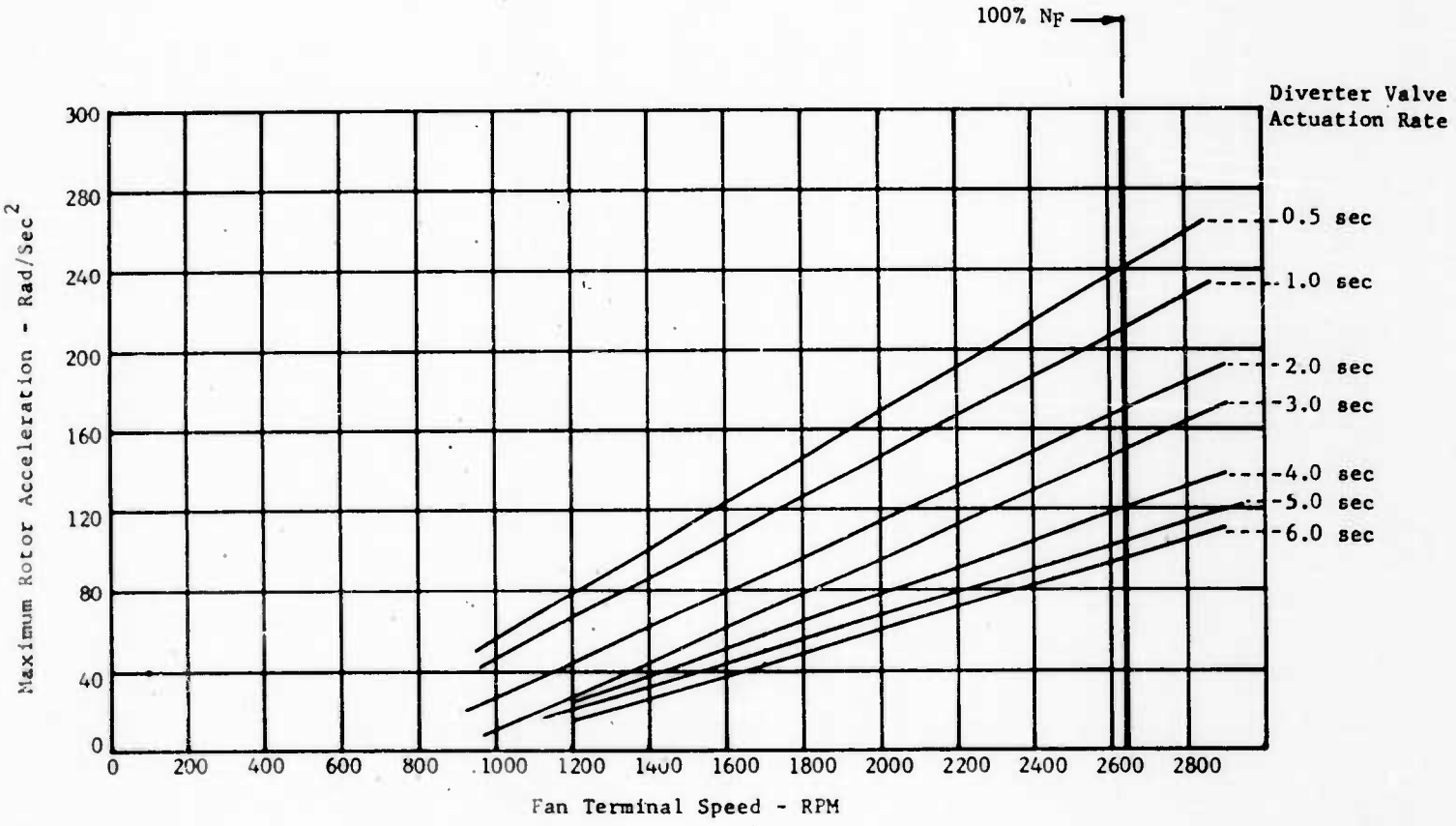

FIGURE 75 - MAXIMUM ROTOR ACCELERATION VERSUS FAN TERMINAL SPEED FOR VARIOUS SLEW RATES (DERIVED FROM TEST DATA)

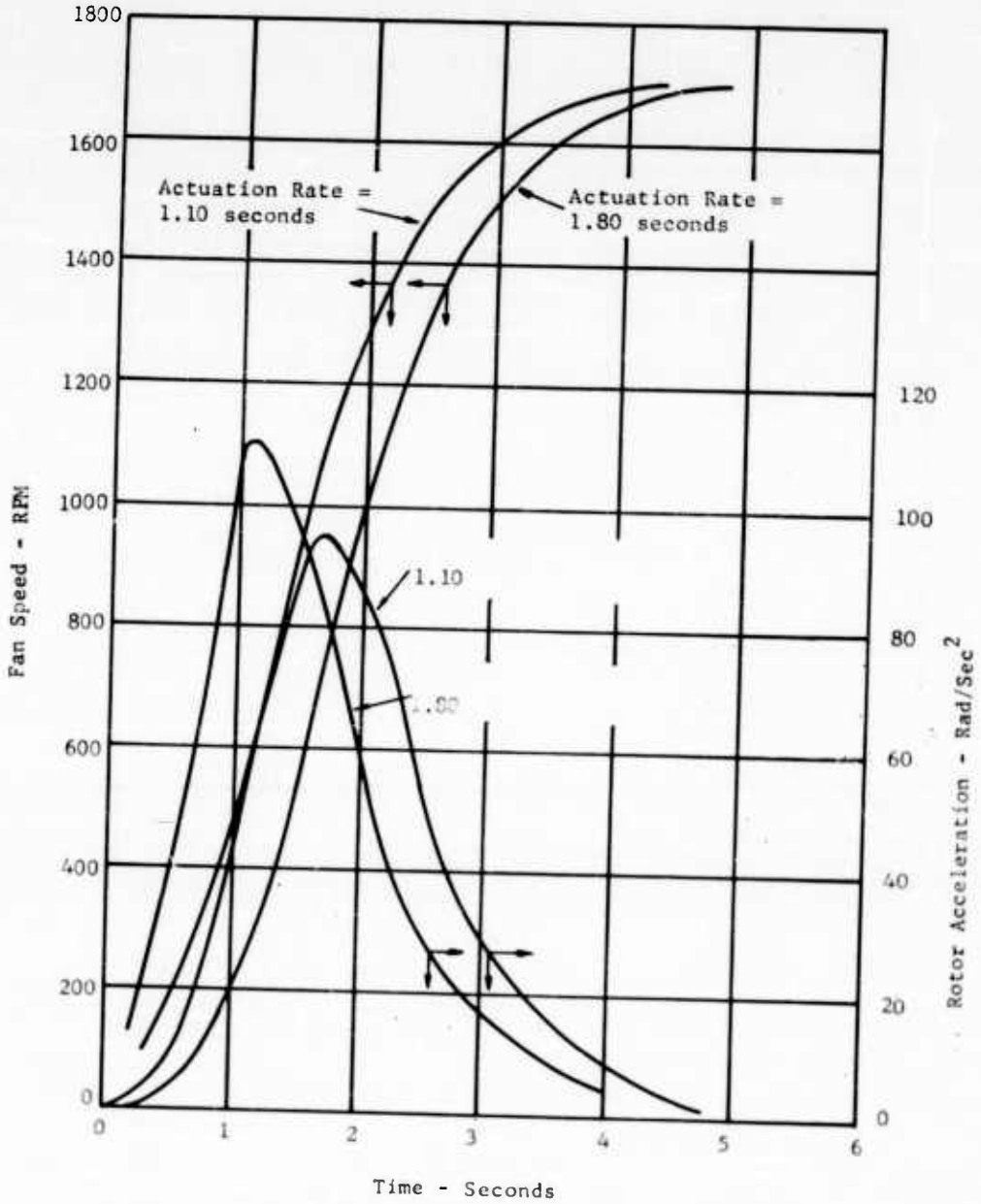

FIGURE 76 - FAN SPEED AND ROTOR ACCELERATION VERSUS TIME AS A FUNCTION OF DIVERTER VALVE ACTUATION RATE (1700 RPM FAN TERMINAL SPEED)

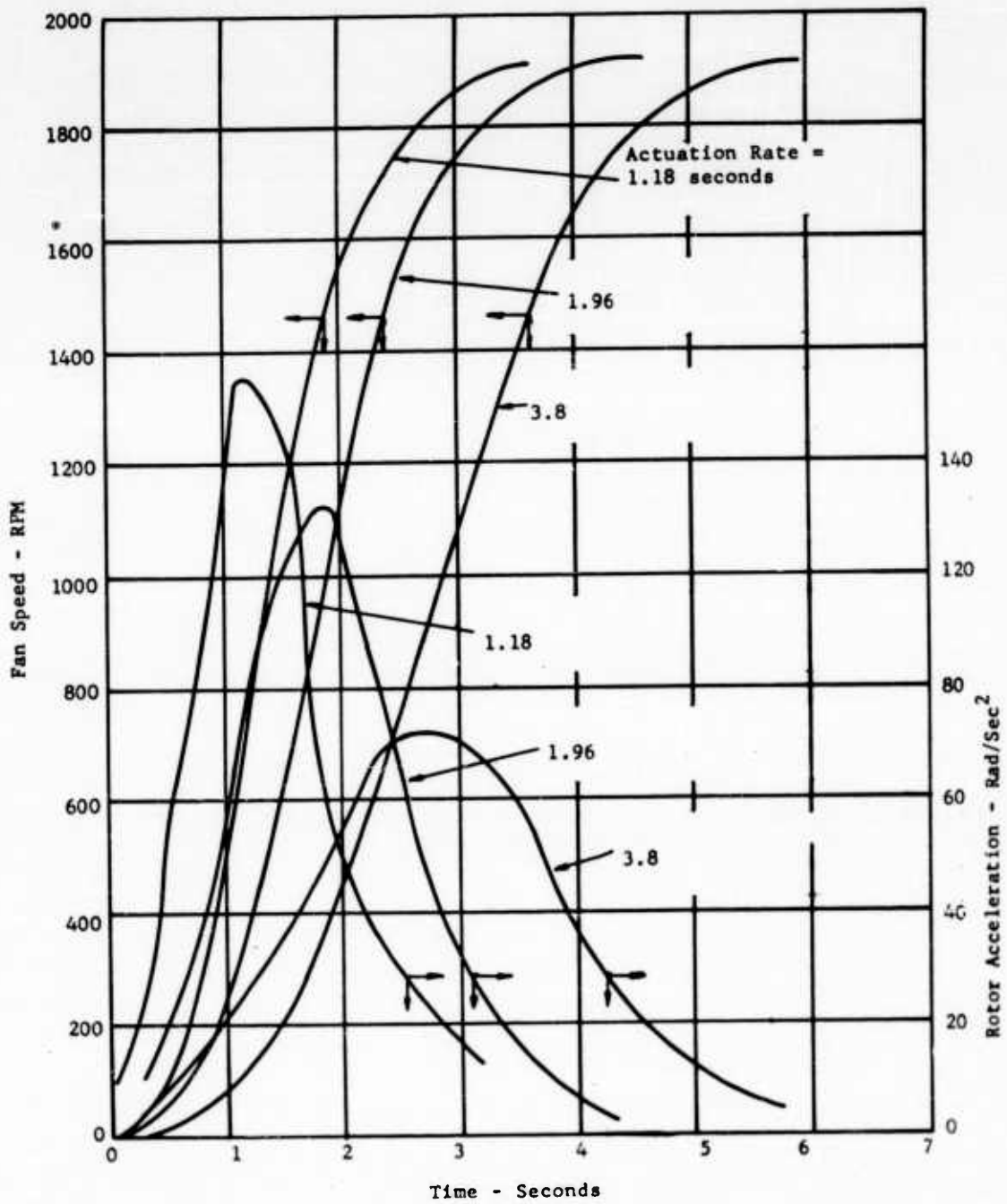

FIGURE 77 - FAN SPEED AND ROTOR ACCELERATION VERSUS TIME AS A FUNCTION OF DIVERTER VALVE ACTUATION RATE (1910 RPM FAN TERMINAL SPEED)

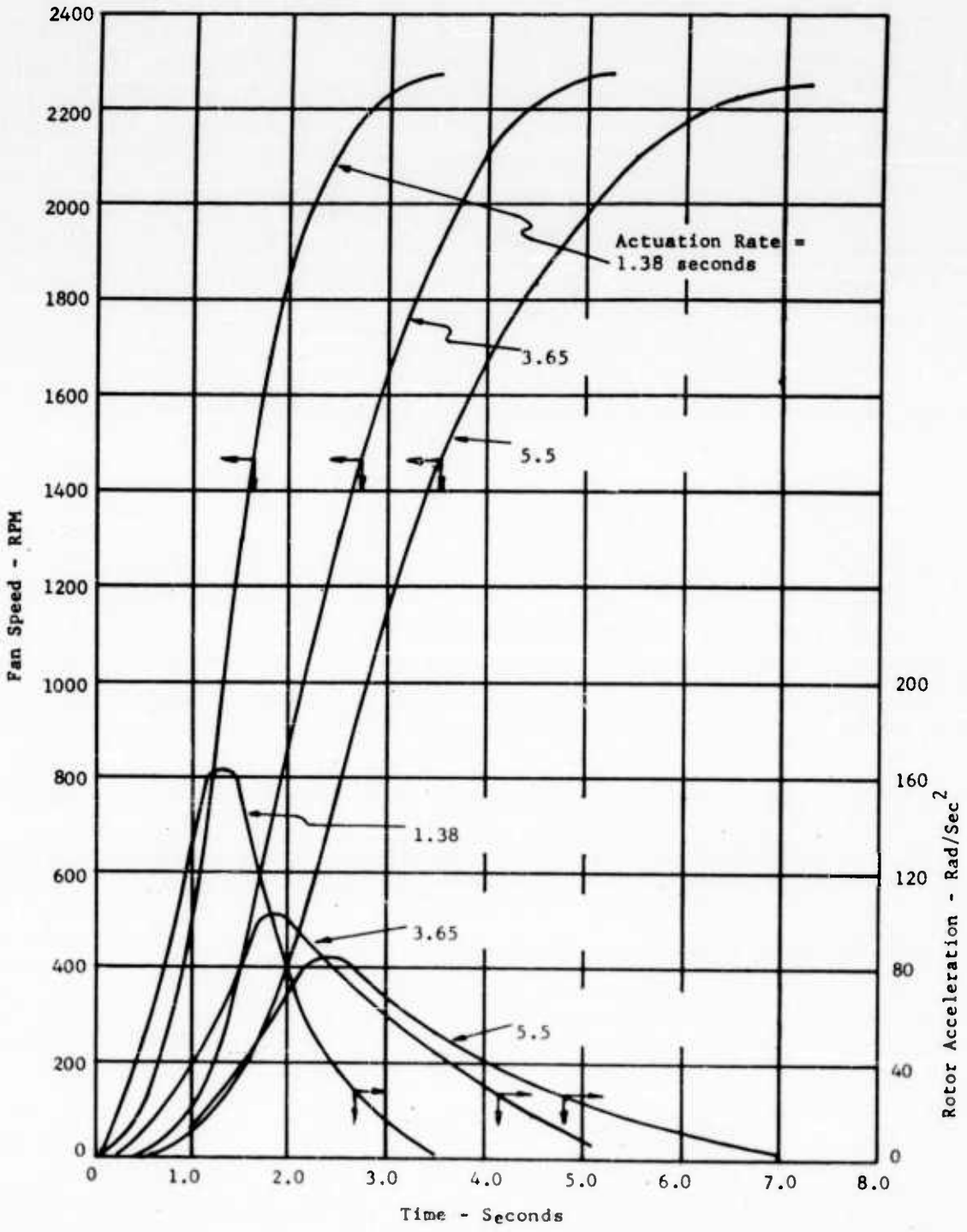

FIGURE 78 - FAN SPEED AND ROTOR ACCELERATION VERSUS TIME AS A FUNCTION OF DIVERTER VALVE ACTUATION RATE (2270 FAN TERMINAL SPEED)

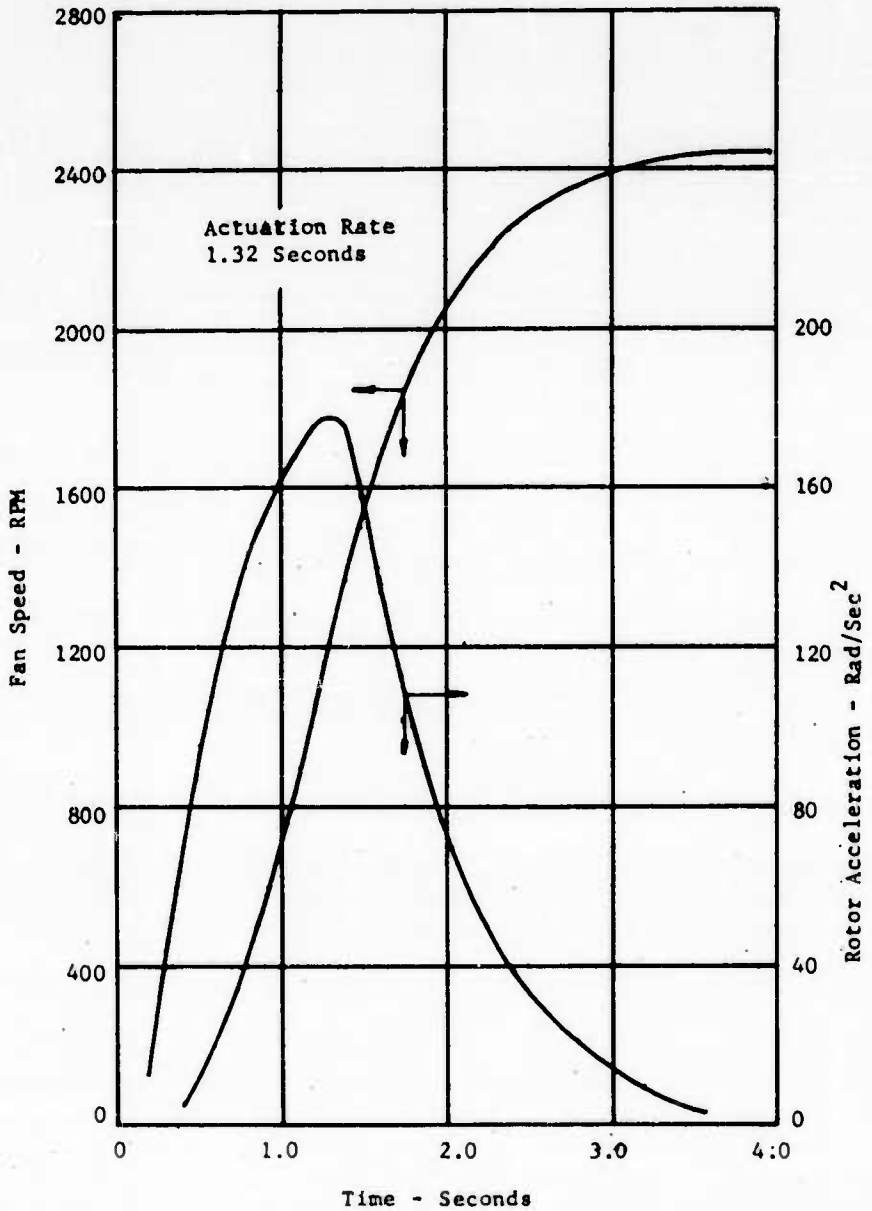

FIGURE 79 - FAN SPEED AND ROTOR ACCELERATION VERSUS TIME AS A FUNCTION OF DIVERTER VALVE ACTUATION RATE (2450 FAN TERMINAL SPEED)

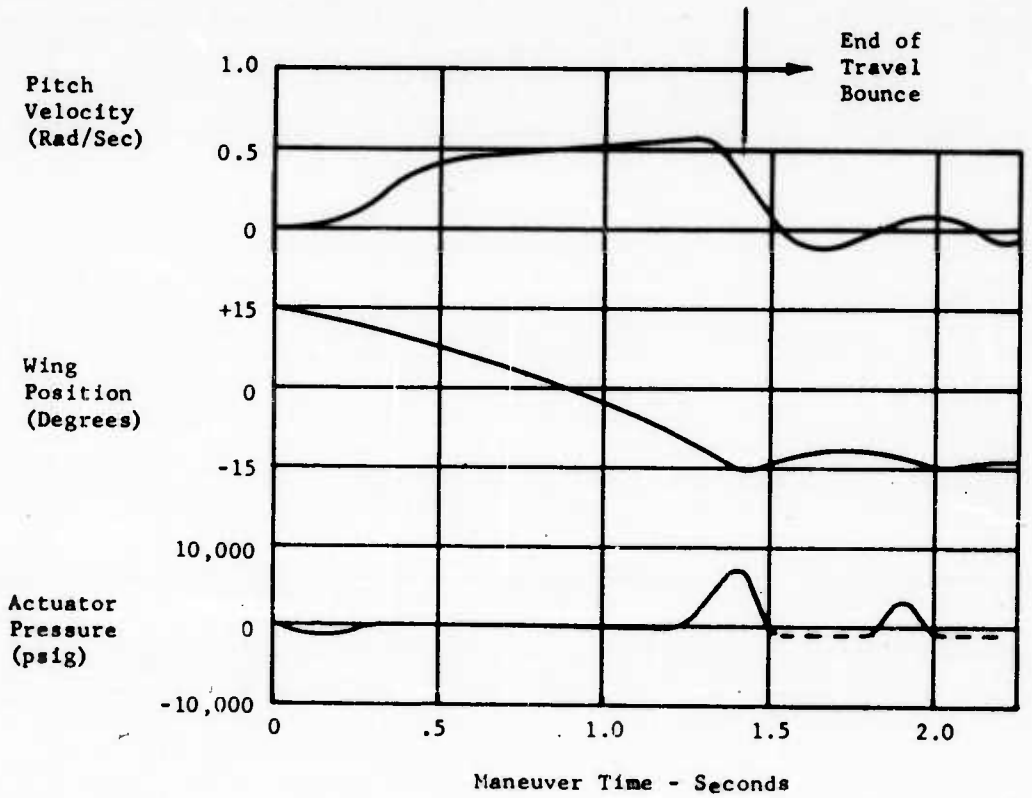

FIGURE 80 - TYPICAL PITCH MANEUVER TRANSIENTS

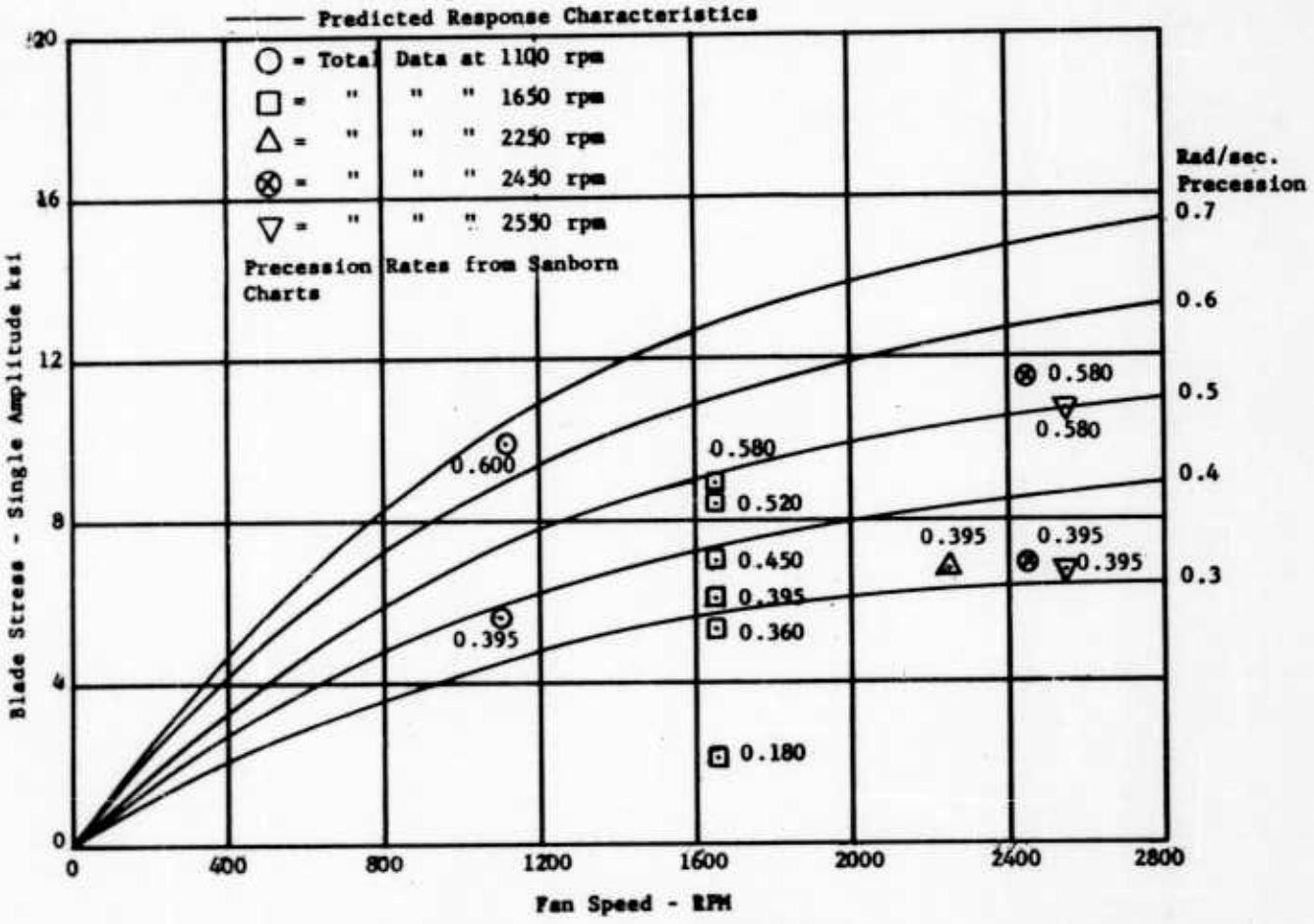

FIGURE 81 - PREDICTED AND MEASURED BLADE STRESS AS A FUNCTION OF SPEED AND PRECESSION RATE

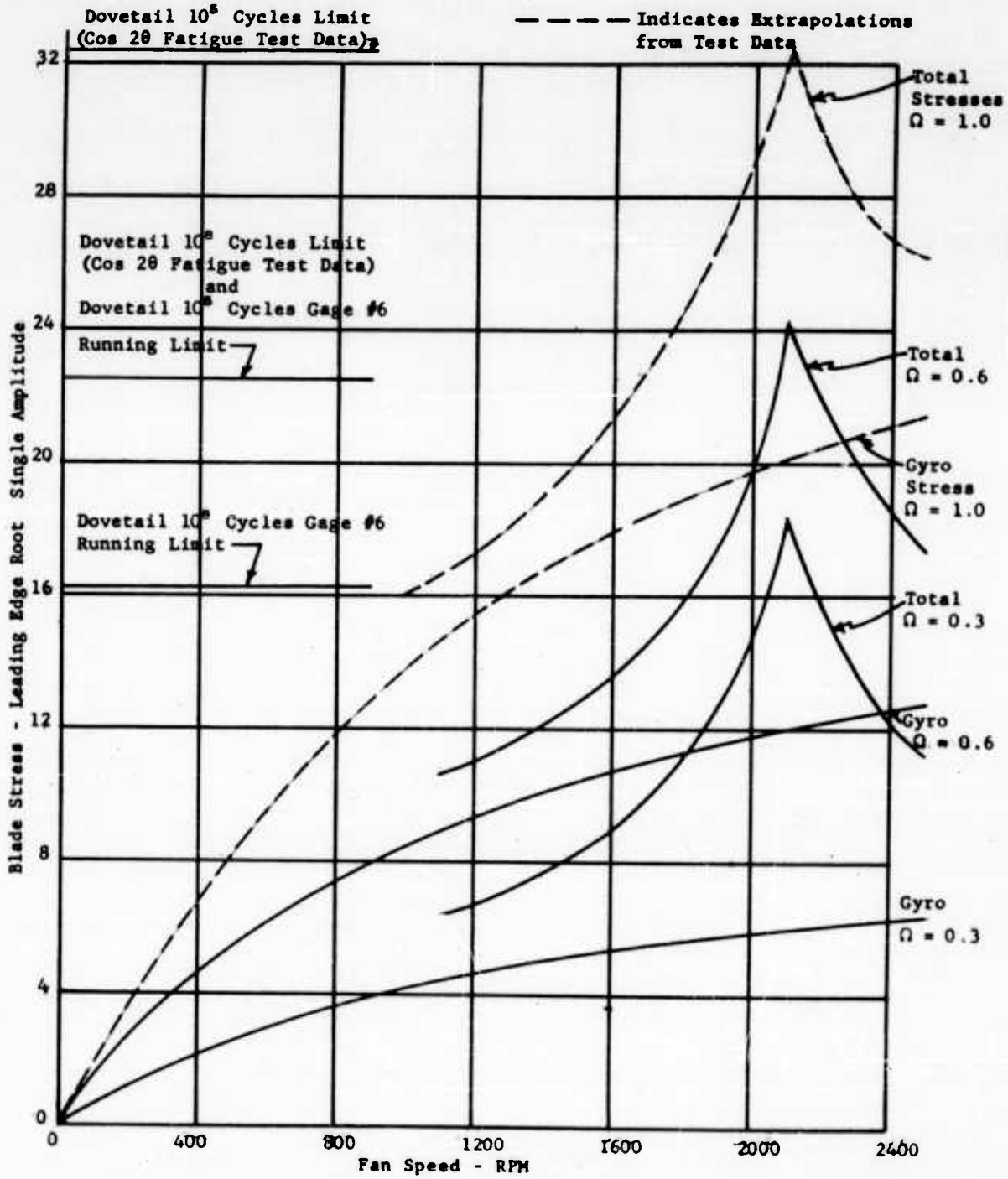

FIGURE 82 - BLADE STRESS DUE TO GYRO LOADING ONLY AND ALSO TOTAL BLADE STRESS DUE TO COMBINED LOADS AS A FUNCTION OF PRECESSION RATE

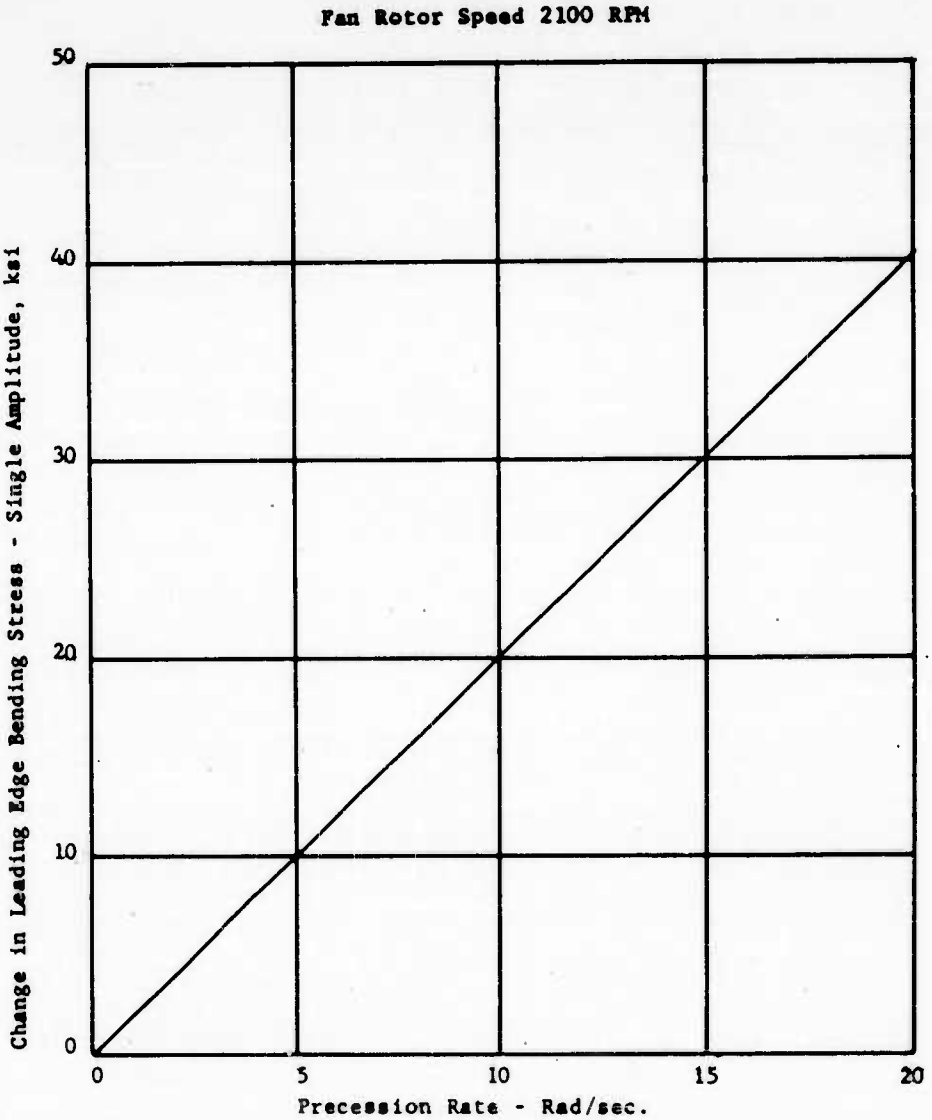

FIGURE 83 - EFFECT OF PITCH MANEUVER LOADING ON BLADE STRESS (AT CRITICAL ROTOR SPEED)

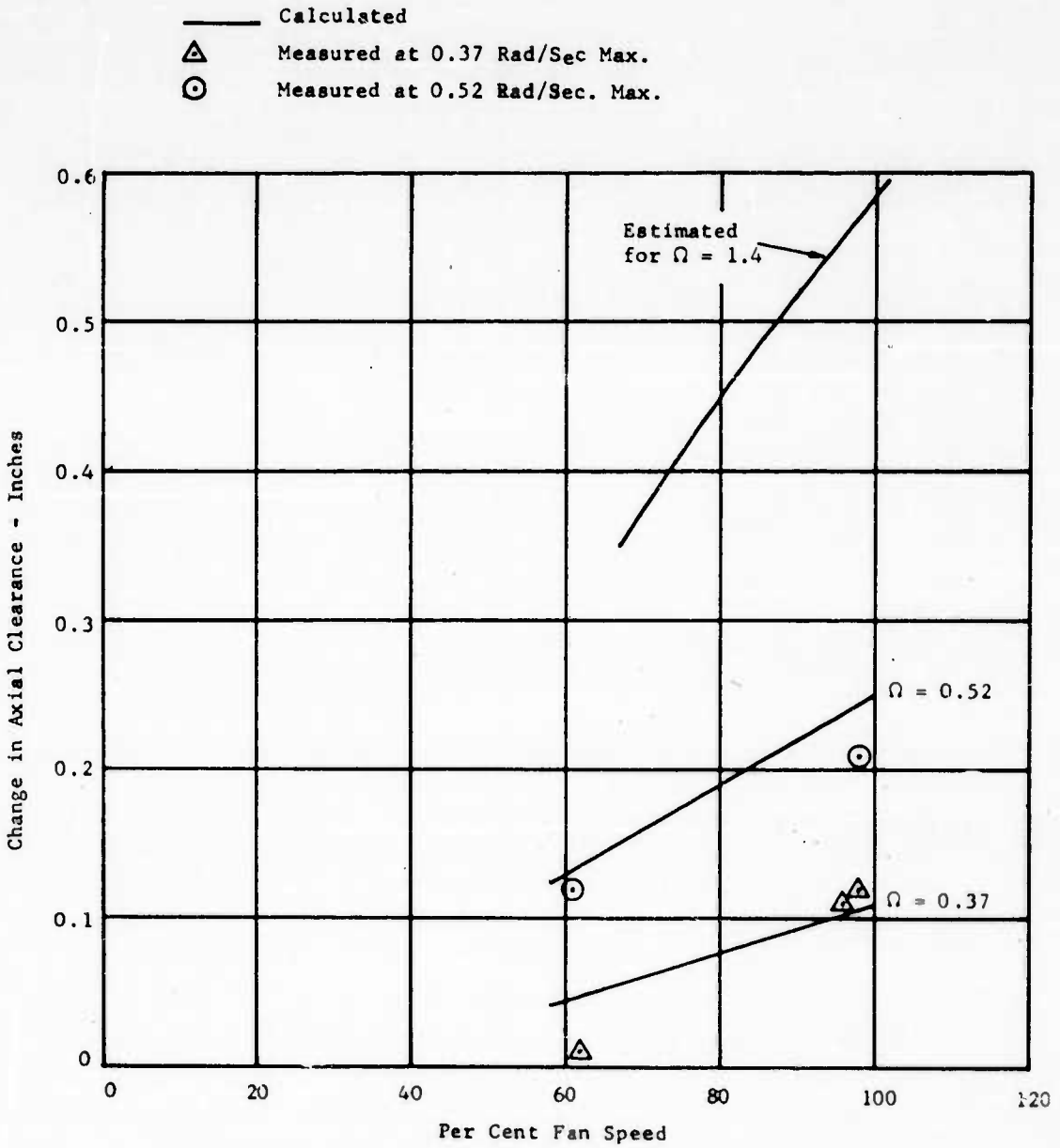

FIGURE 84 - CHANGE IN AXIAL CLEARANCE (ROTOR TO FRONT FRAME) DURING PITCH MANEUVERS (3 O'CLOCK POSITION)

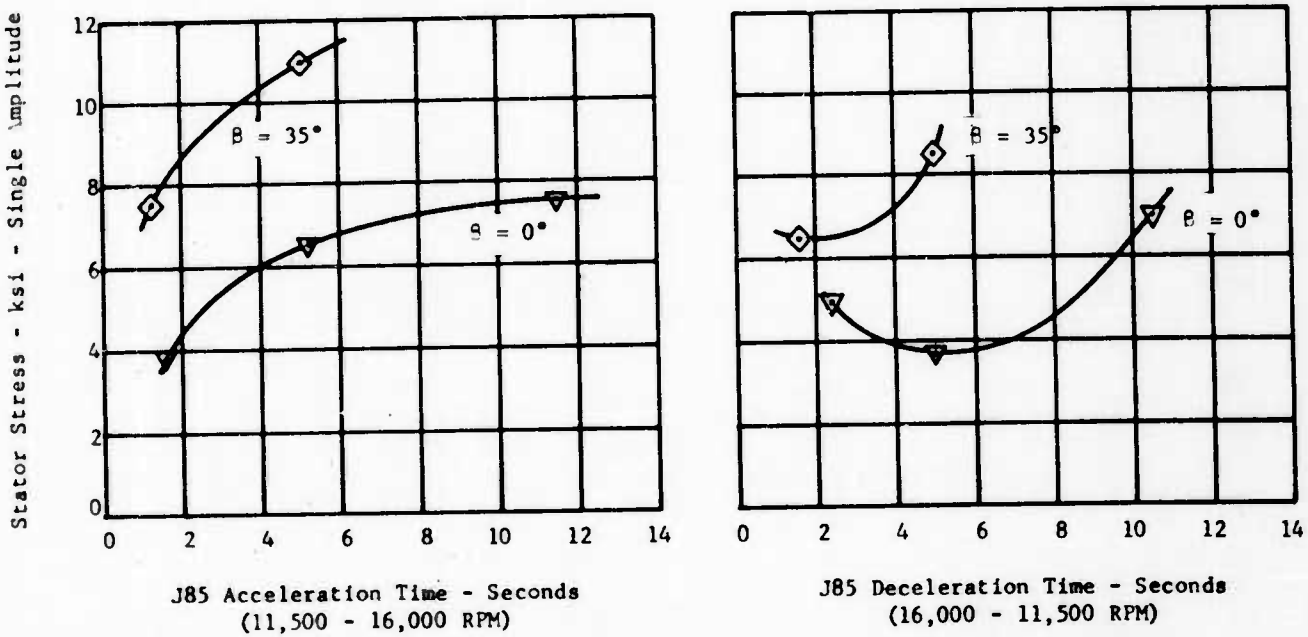

FIGURE 85 - REAR FRAME STATOR STRESS AS A FUNCTION OF J85 THROTTLE TRANSIENTS

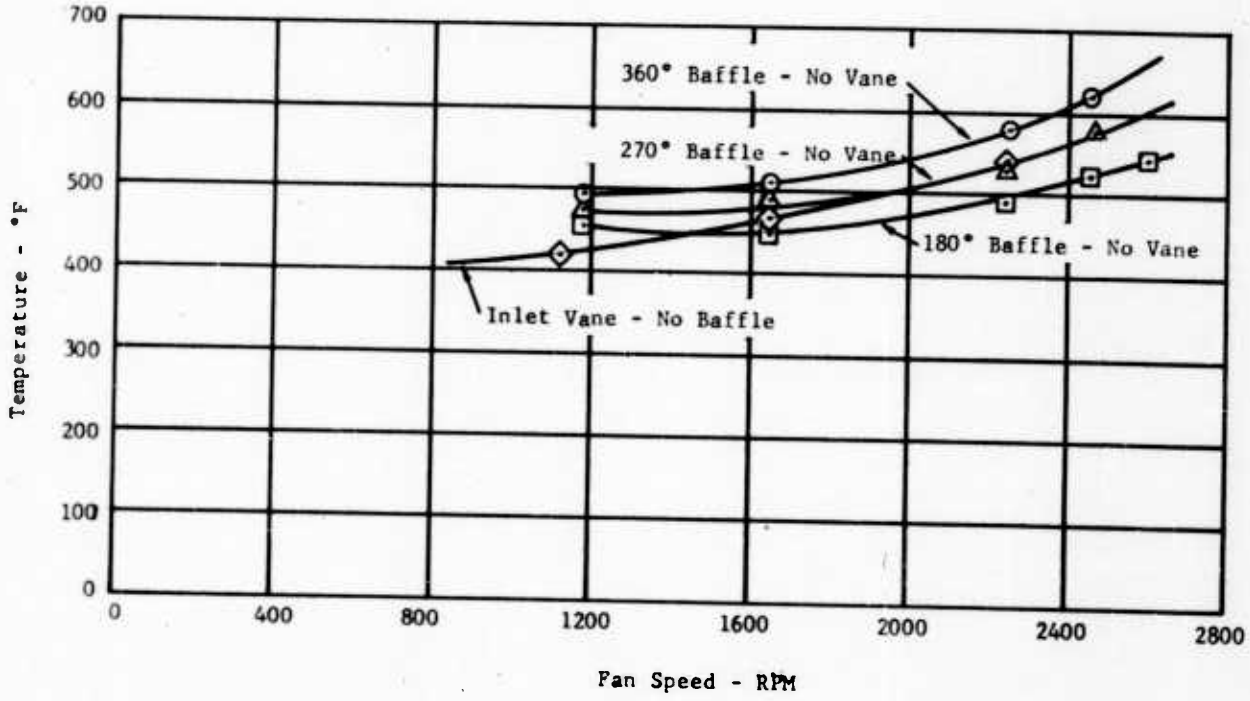

FIGURE 86 - FORWARD TORQUE BAND TEMPERATURE AS A FUNCTION OF FAN SPEED AND INLET CONFIGURATION

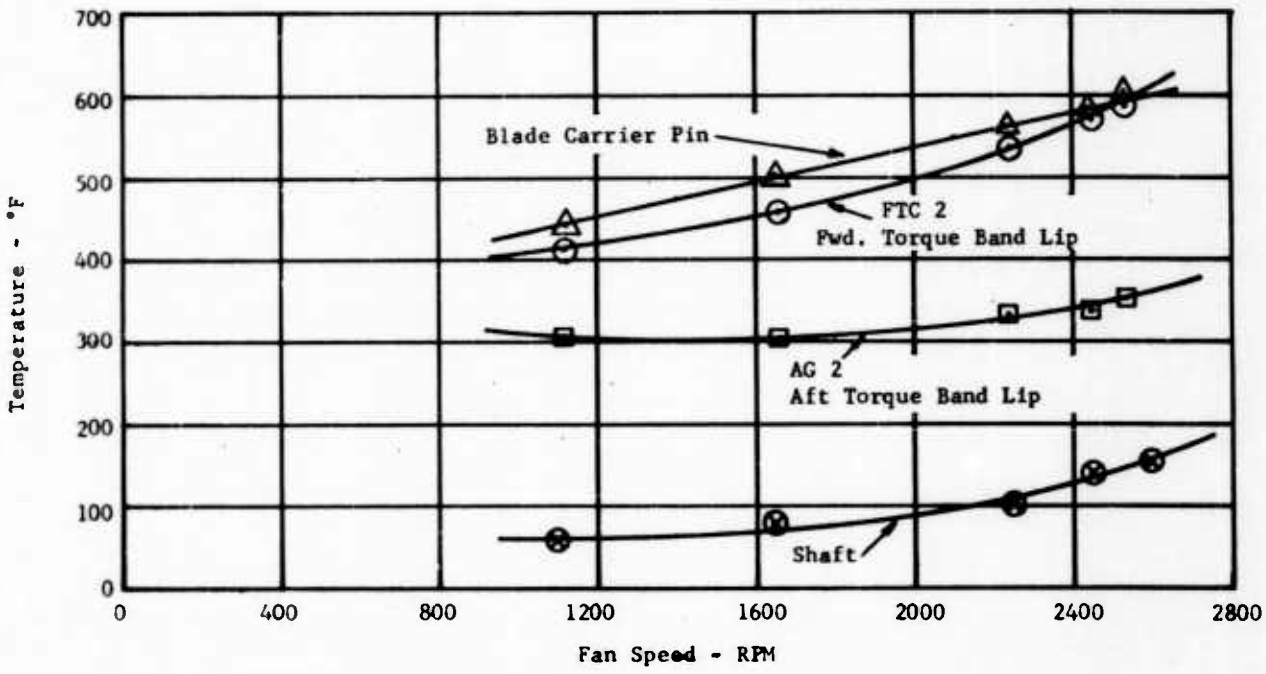

FIGURE 87 - HARDWARE TEMPERATURE AS A FUNCTION OF FAN SPEED

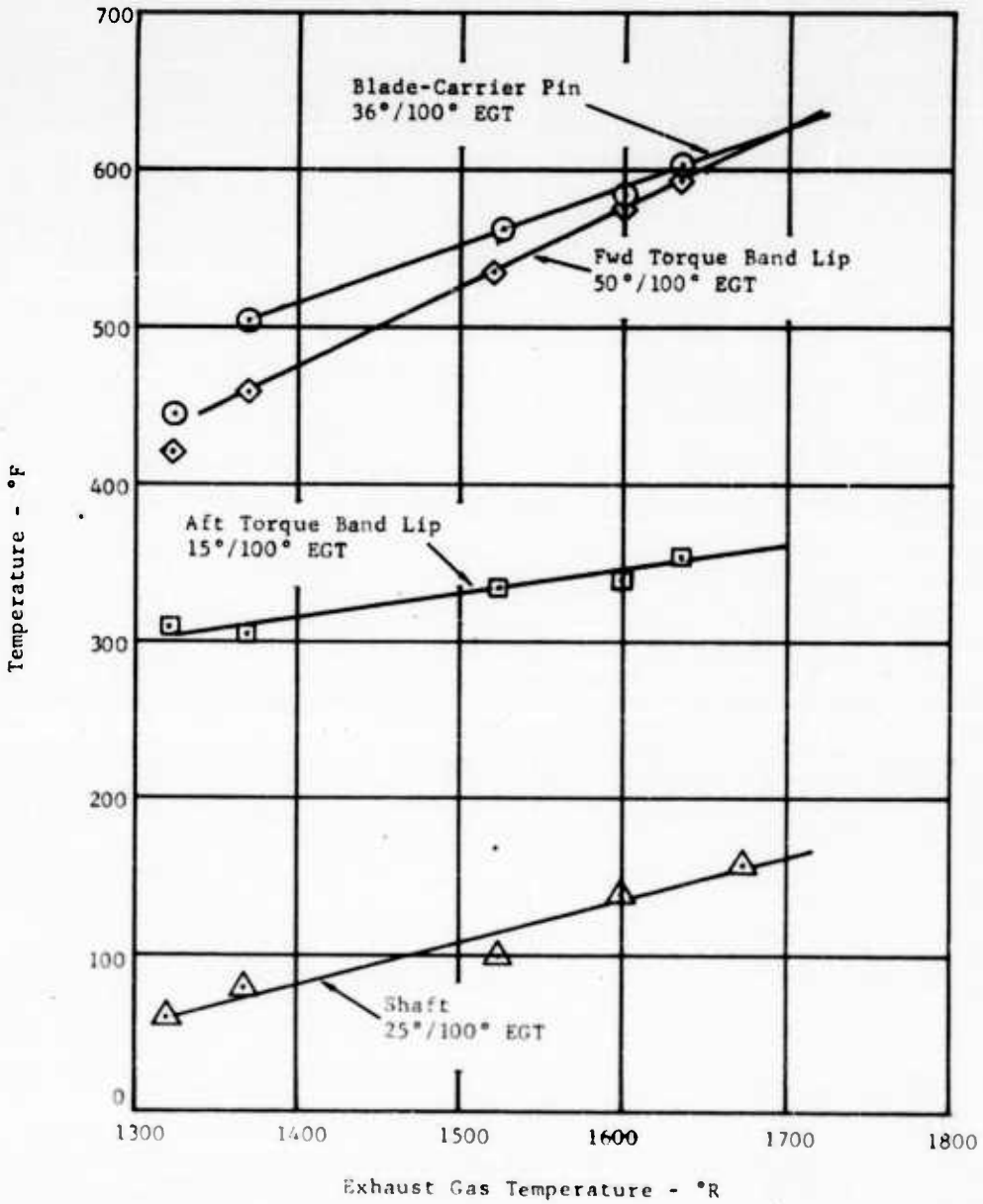

FIGURE 88 - HARDWARE TEMPERATURE AS A FUNCTION OF ENGINE EXHAUST GAS TEMPERATURE

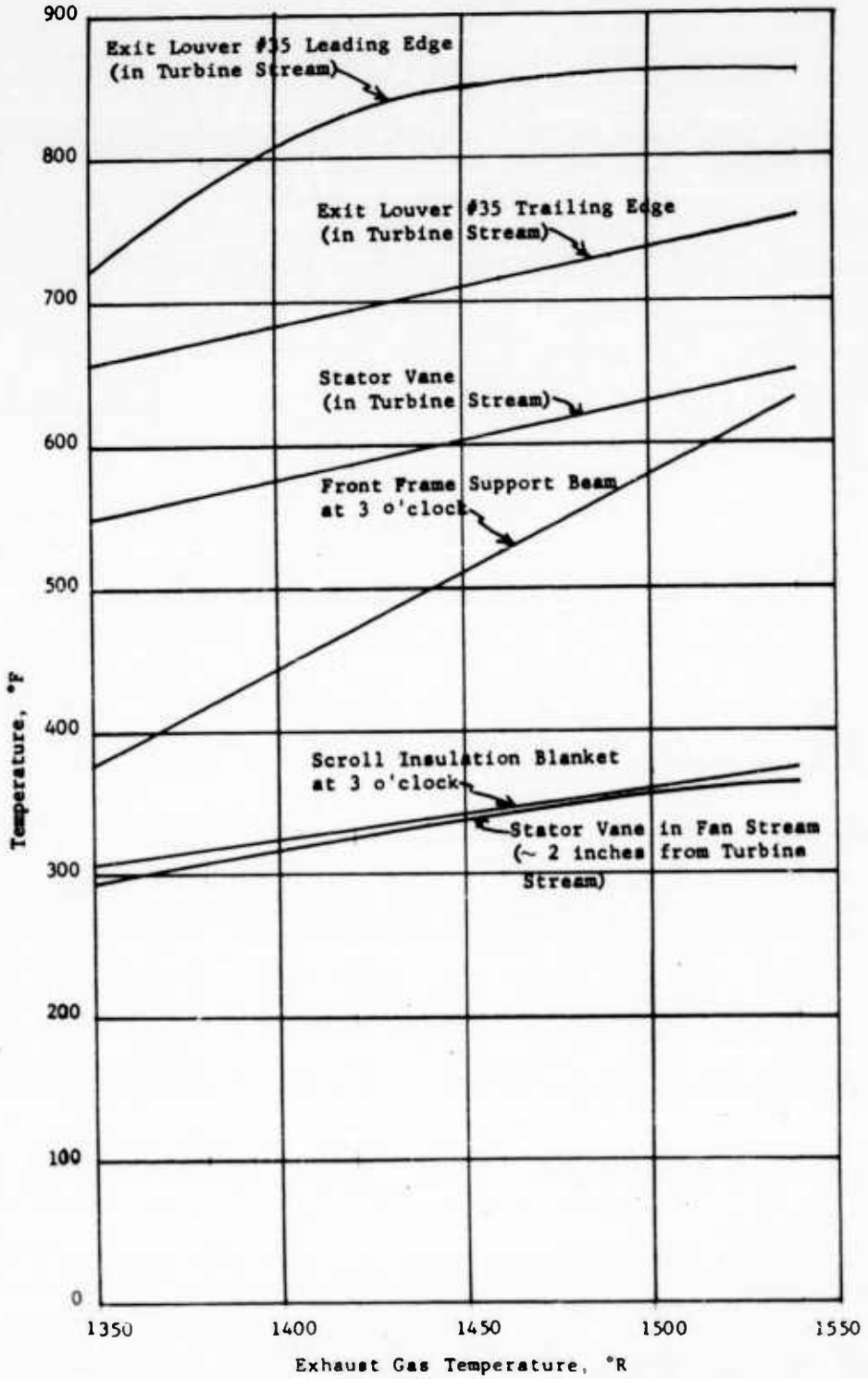

FIGURE 89 - STATIC HARDWARE TEMPERATURE AS A FUNCTION OF EXHAUST GAS TEMPERATURE

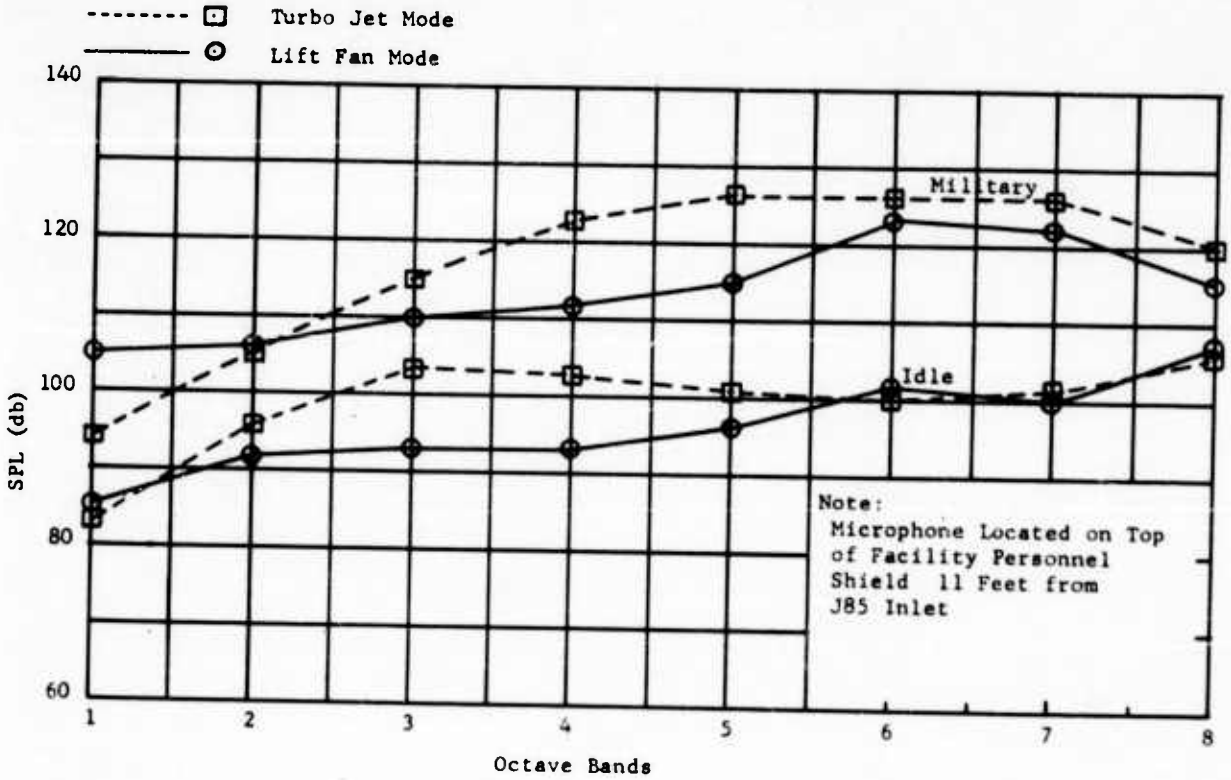

FIGURE 90 - X353-5 SOUND PRESSURE LEVEL MEASUREMENT (J85-7 GAS GENERATOR)

Circular Inlet Vane

$\beta = 0^{\circ}$

◇ Wind Velocity ~ 0 - 2 mph

⊙ Wind Velocity ~ 3 - 6 mph

⊙ Wind Velocity ~ 7 - 9 mph

△ Wind Velocity ~ 10 - 12 mph

⊡ Wind Velocity ~ 13 - 15 mph

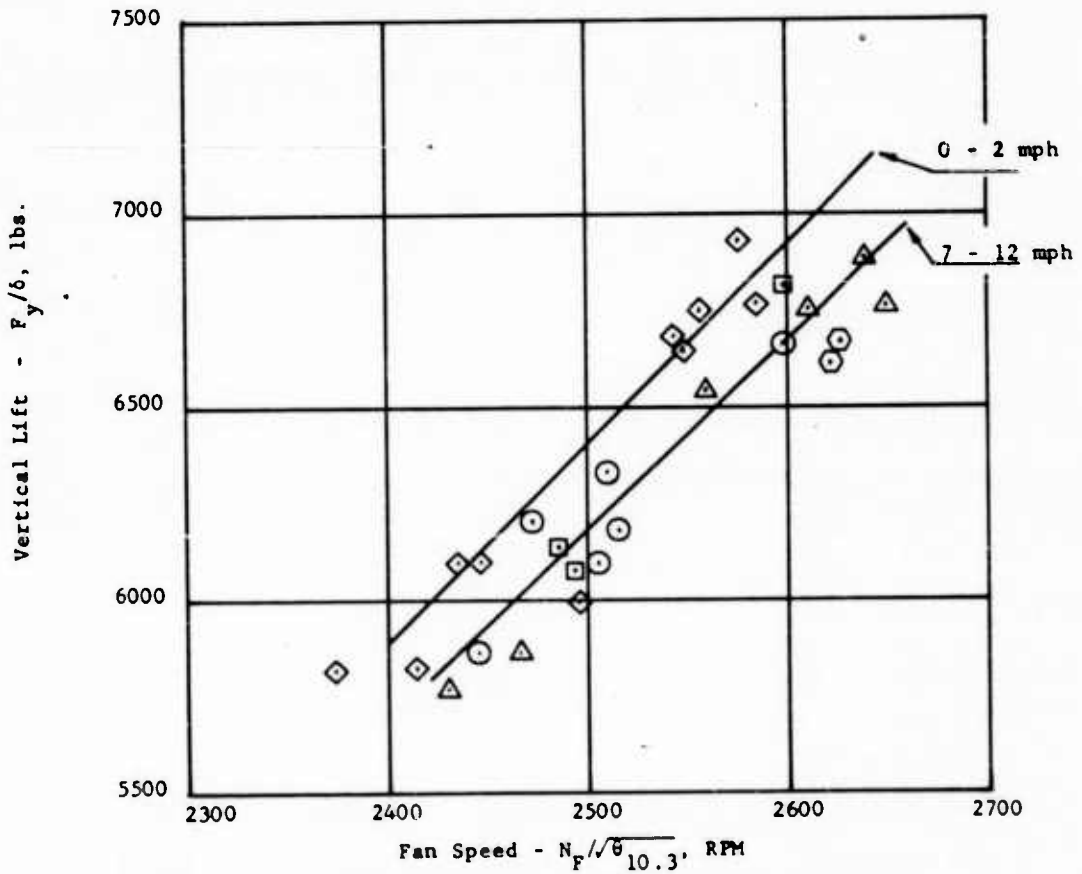

FIGURE 91 - VERTICAL LIFT AS A FUNCTION OF FAN SPEED AND WIND VELOCITY

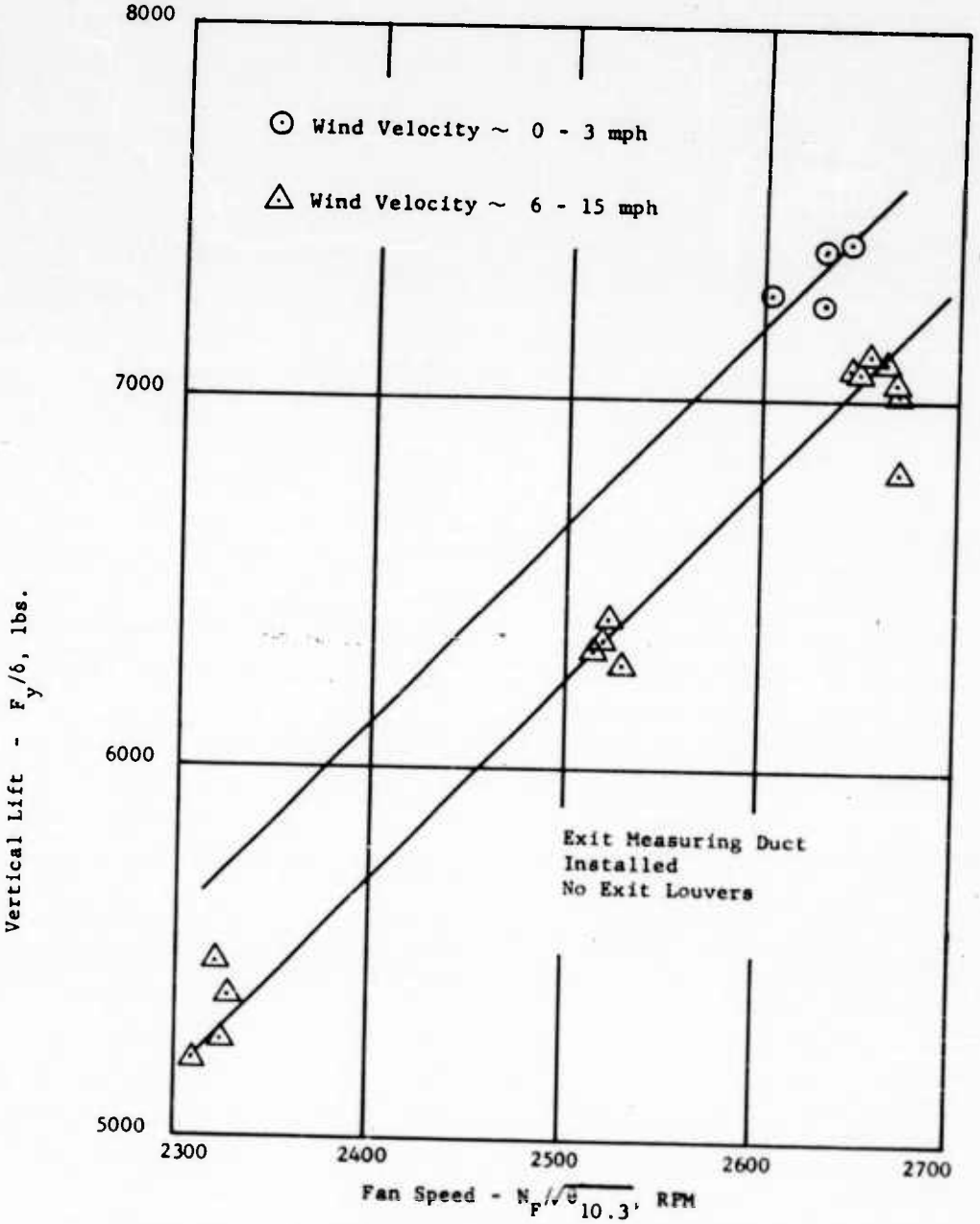

FIGURE 92 - VERTICAL LIFT AS A FUNCTION OF FAN SPEED AND WIND VELOCITY (WITHOUT EXIT LOUVERS)

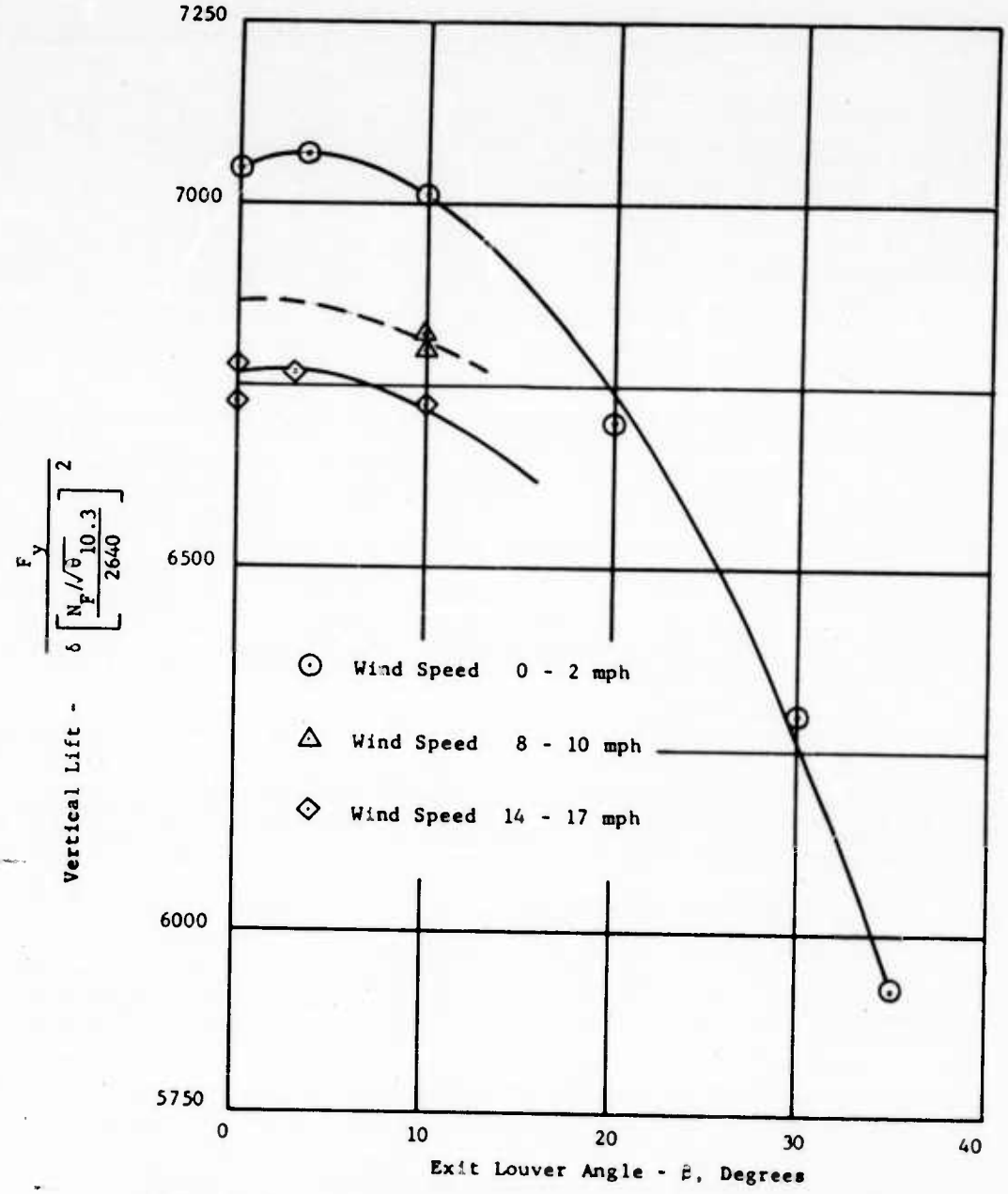

FIGURE 93 - VERTICAL LIFT AS A FUNCTION OF EXIT LOUVER ANGLE AND WIND VELOCITY

$\beta = 0^{\circ}$

$N_F/\sqrt{\theta}_{10.3} = 2577$ RPM

Reading Number 467

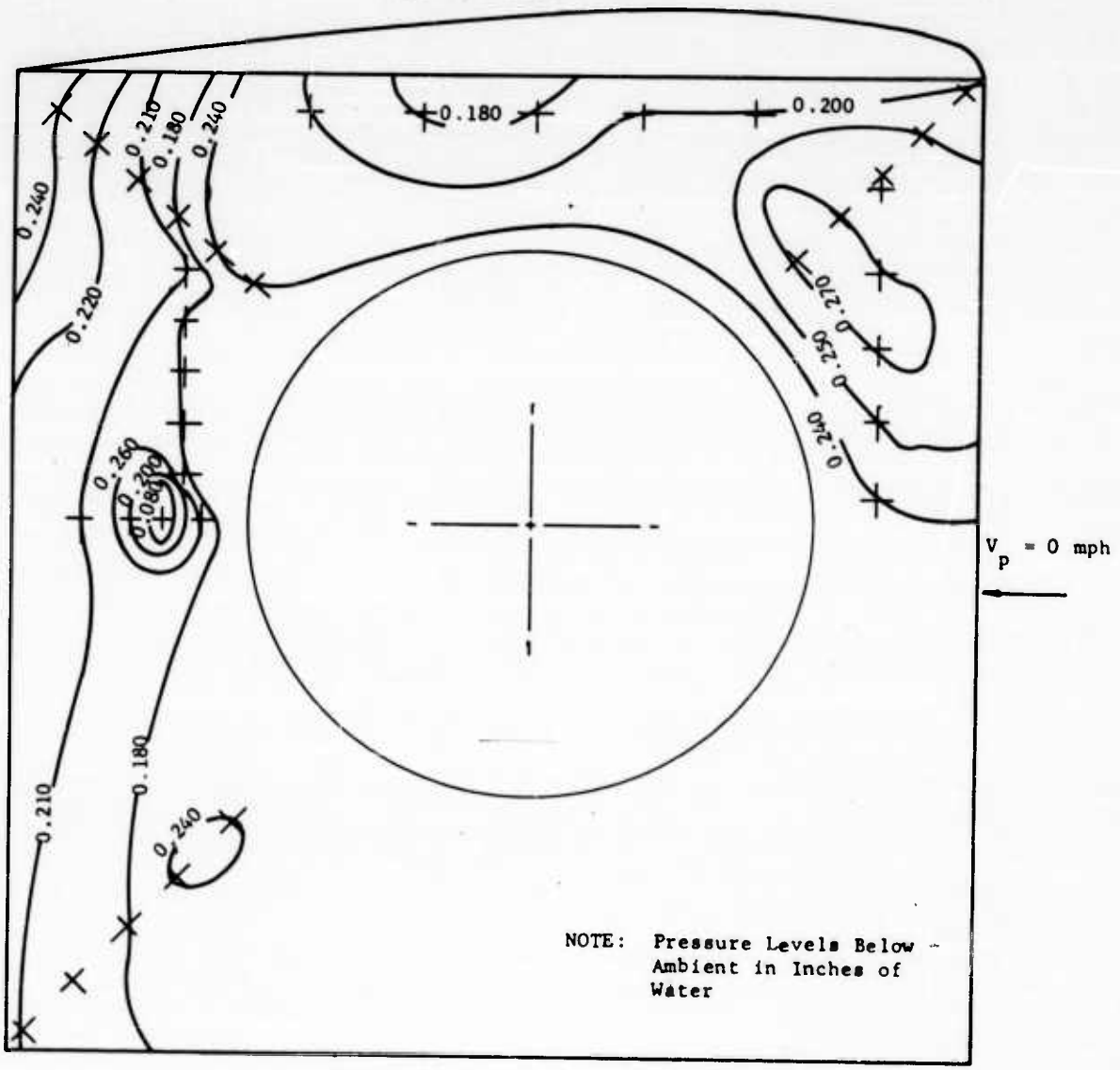

FIGURE 94a - LINES OF CONSTANT SUCTION ON THE UNDER SURFACE OF THE WING (V_p = 0 mph)

$\beta = 0^{\circ}$

$N_F/\sqrt{\theta}_{10.3} = 2611$ RPM

Reading Number 383

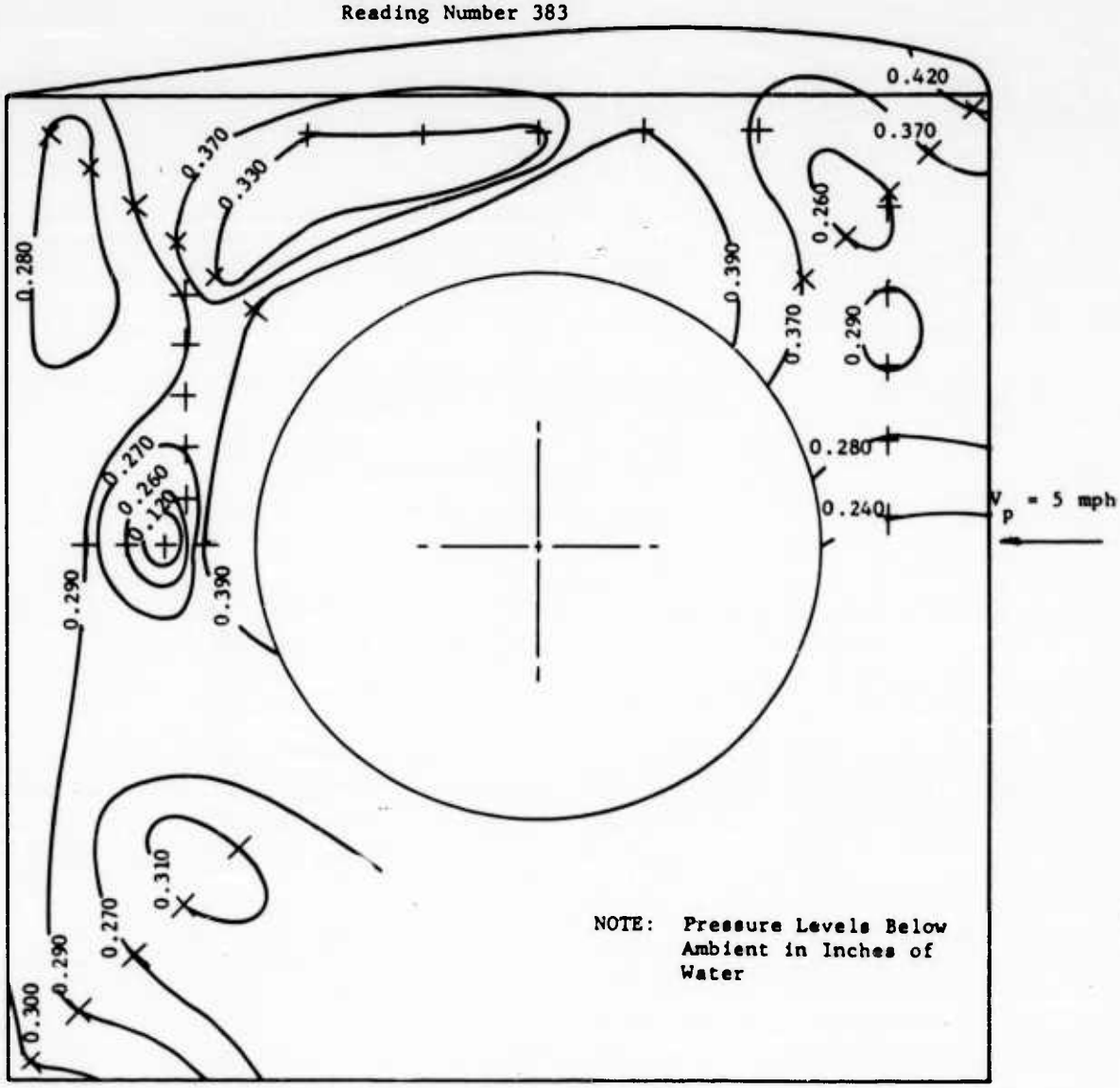

FIGURE 94b - LINES OF CONSTANT SUCTION ON THE UNDER SURFACE OF THE WING (V_p = 5 mph)

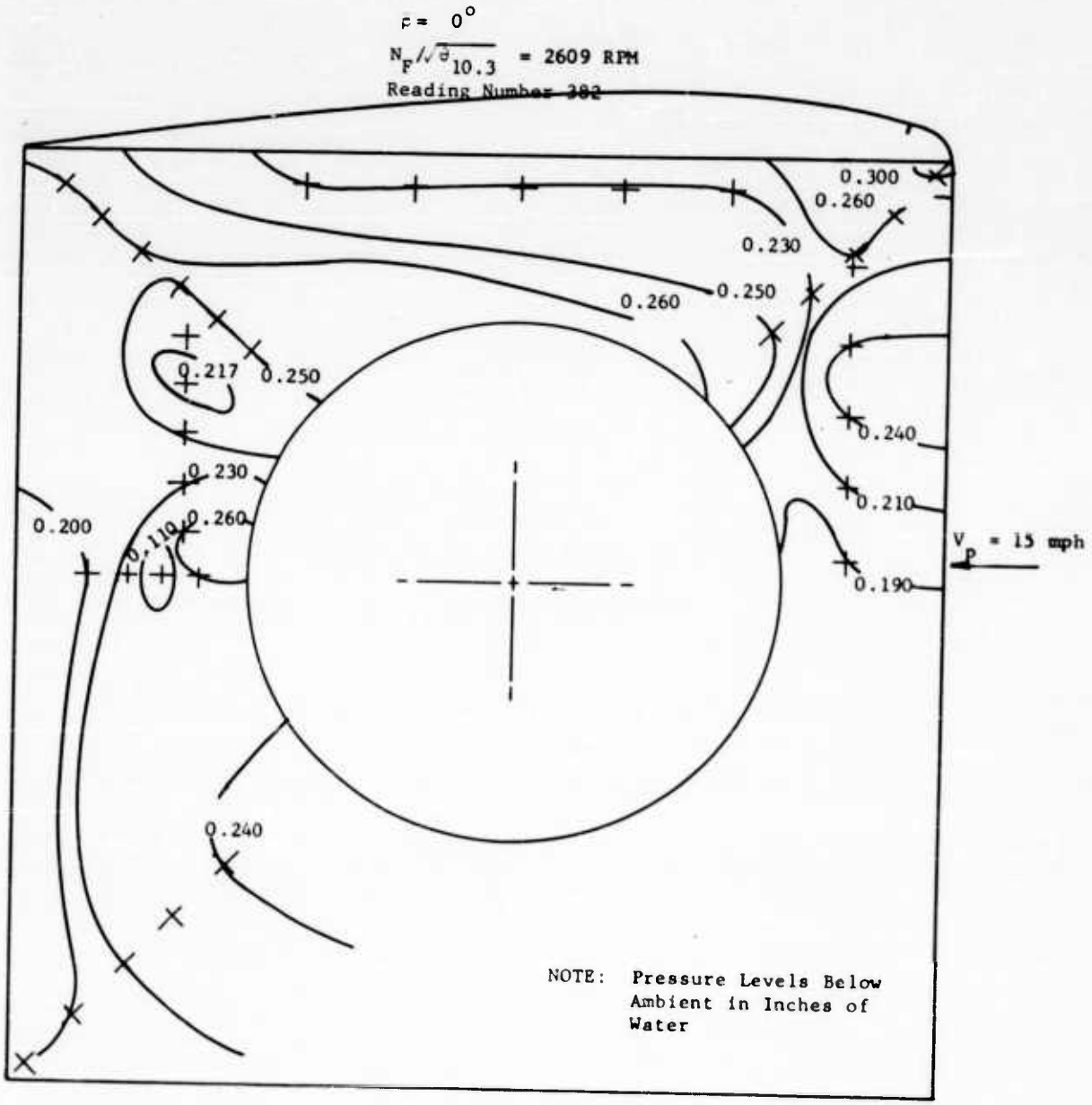

FIGURE 94c - LINES OF CONSTANT SUCTION ON THE UNDER SURFACE OF THE WING (V_p = 15 mph)

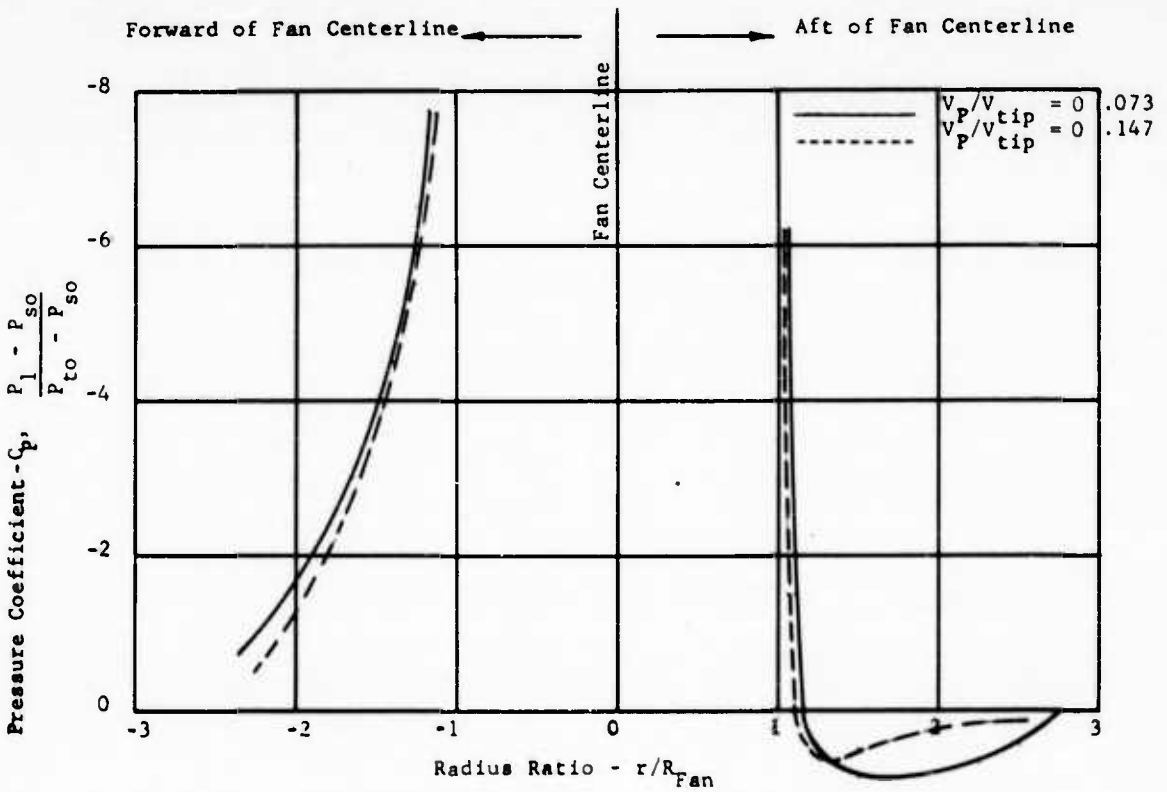

FIGURE 95 - PRESSURE DISTRIBUTION ON THE FUSELAGE UPPER SURFACE FROM FULL SCALE FAN-IN-FUSELAGE TESTING AT AMES.

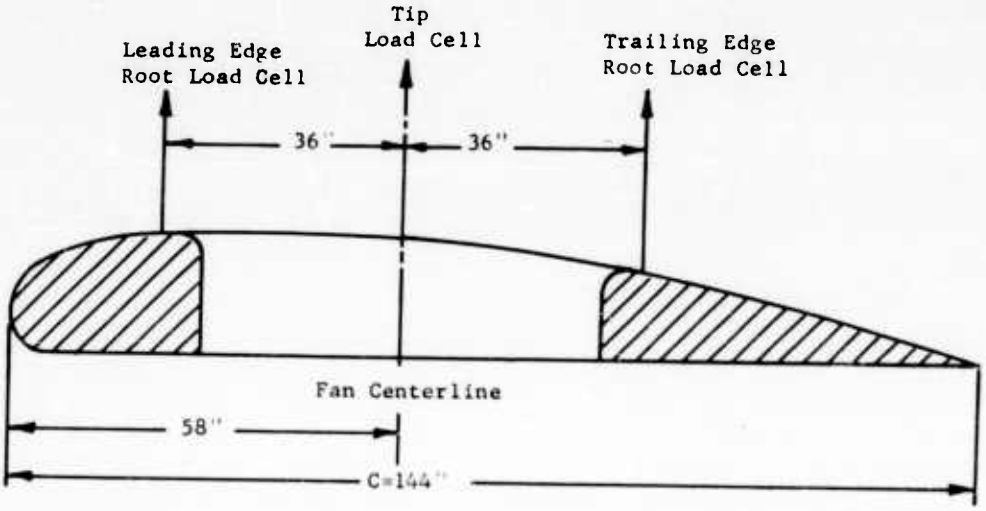

Wind Speed (mph)	(Rdg. 337) 1	(Rdg. 505) 5	(Rdg. 507) 10	(Rdg. 506) 13
Leading Edge Rdg. (lbs.)	1480	1655	1640	1660
Trailing Edge Rdg. (lbs.)	1395	1321	1201	1293
Tip Rdg. (lbs.)	3630	3909	3799	3954

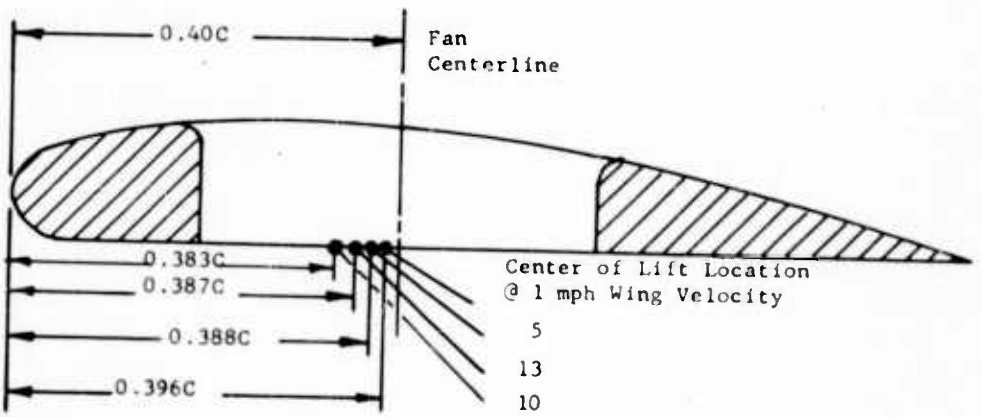

FIGURE 96 - VARIATION OF LOAD CELL READINGS AND CENTER OF LIFT WITH FORWARD SPEED.

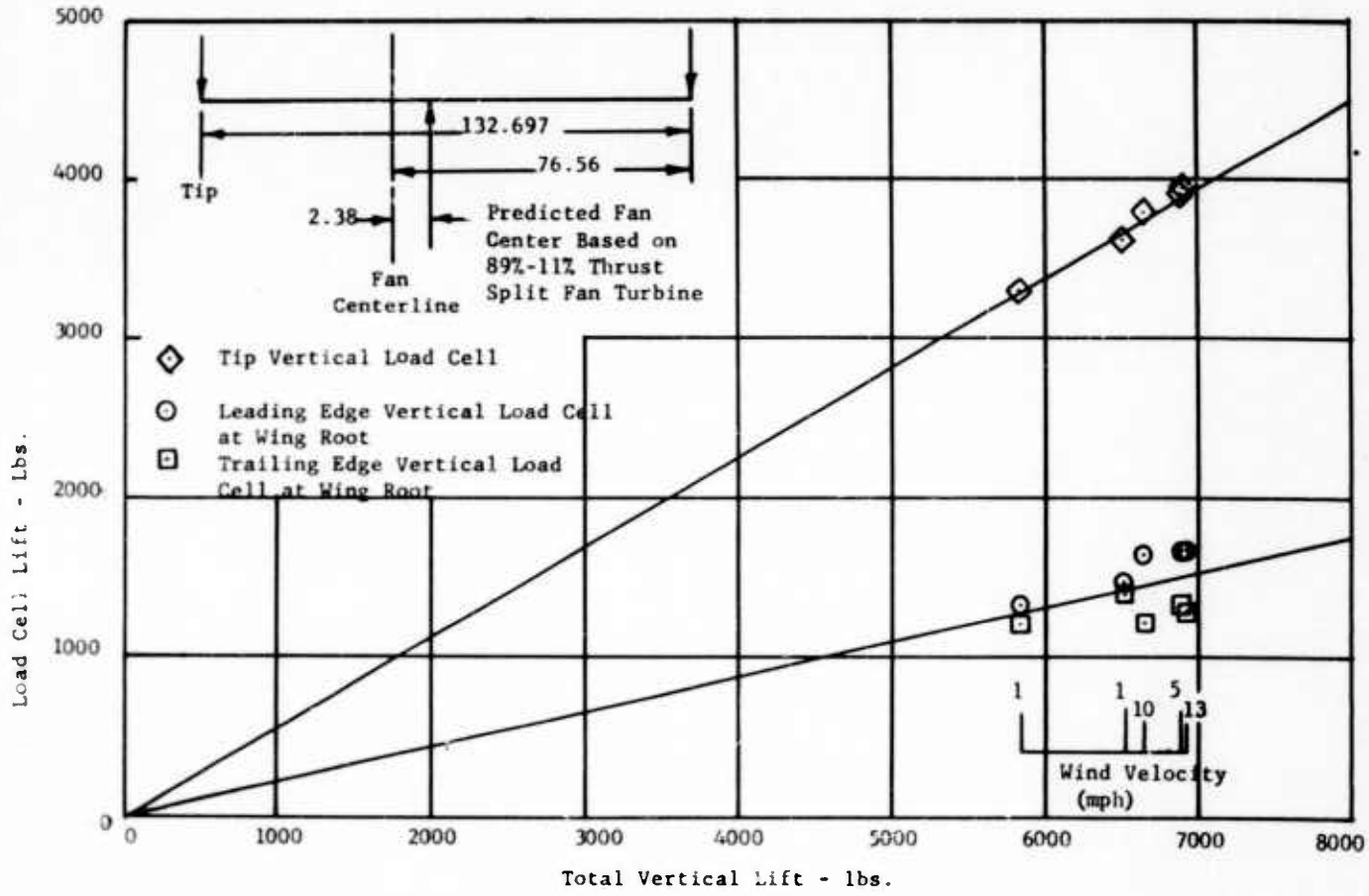

FIGURE 97 - COMPARISON OF LOAD CELL DATA WITH PREDICTED RESULTS.

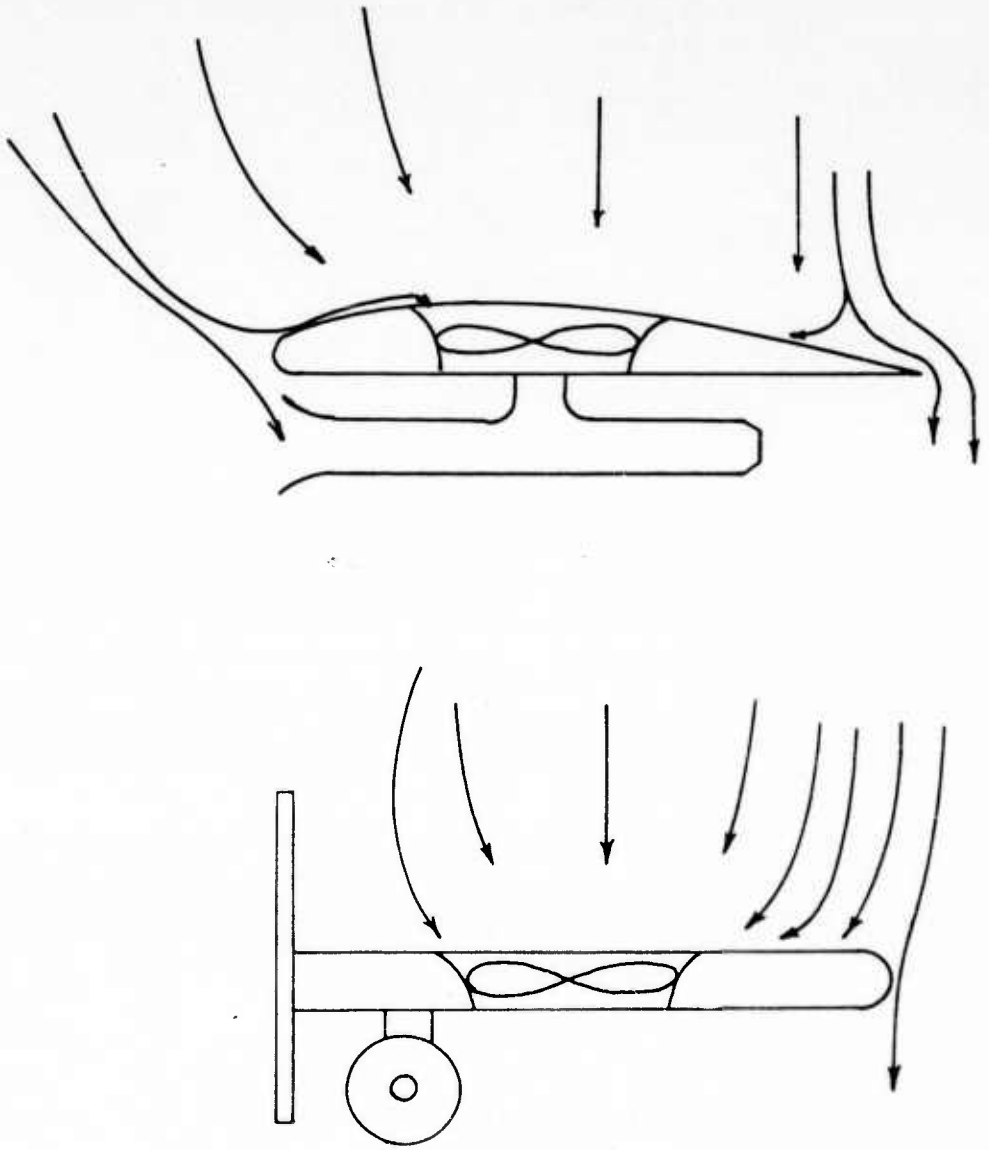

FIGURE 98 - FAN-IN-WING FLOW PATTERNS AT IDLE FAN SPEED

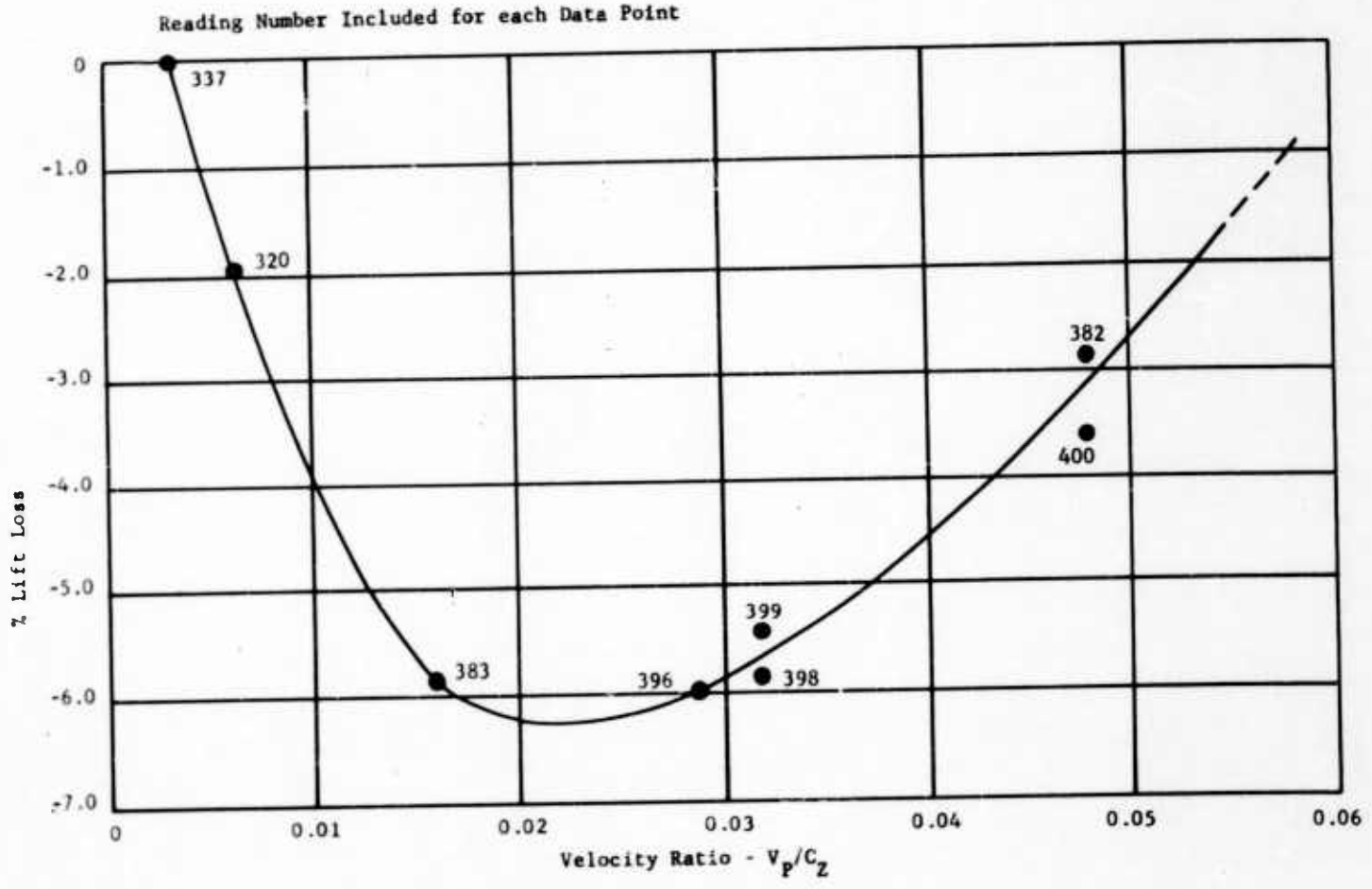

FIGURE 99 - LIFT LOSS AT LOW FLIGHT SPEED

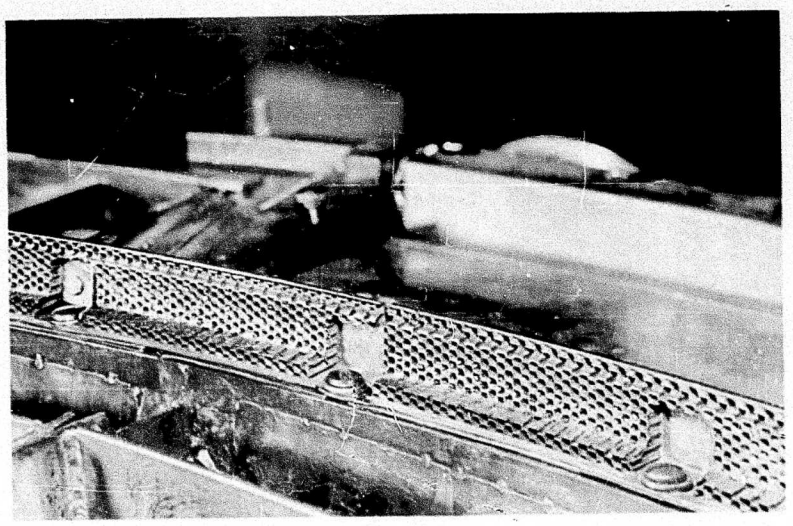

FIGURE 100a RADIAL RUB AT 12:00 O'CLOCK POSITION - FORWARD FRAME AIR SEAL

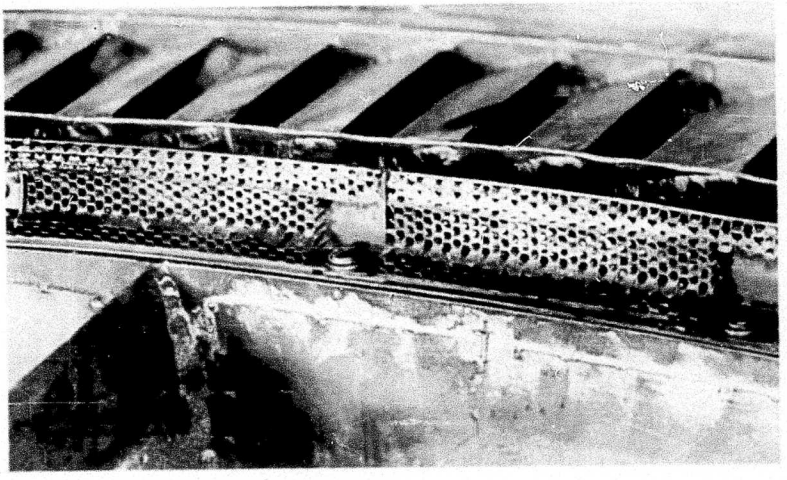

FIGURE 100b AXIAL RUB AT 3:00 O'CLOCK POSITION - FORWARD FRAME AIR SEAL

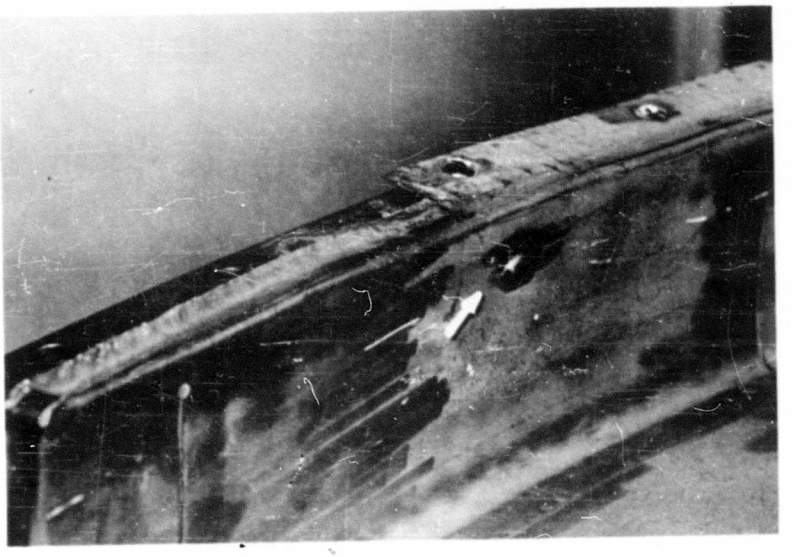

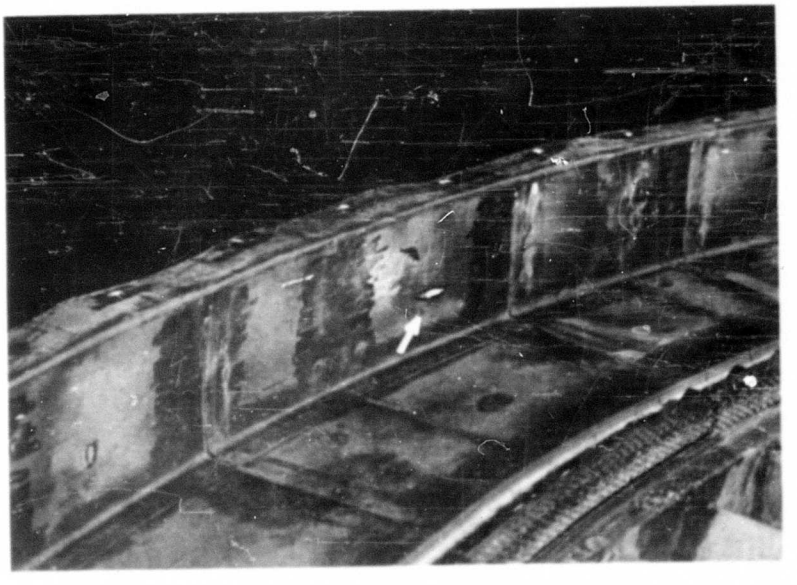

FIGURE 101 INSULATION BLANKET RUBS

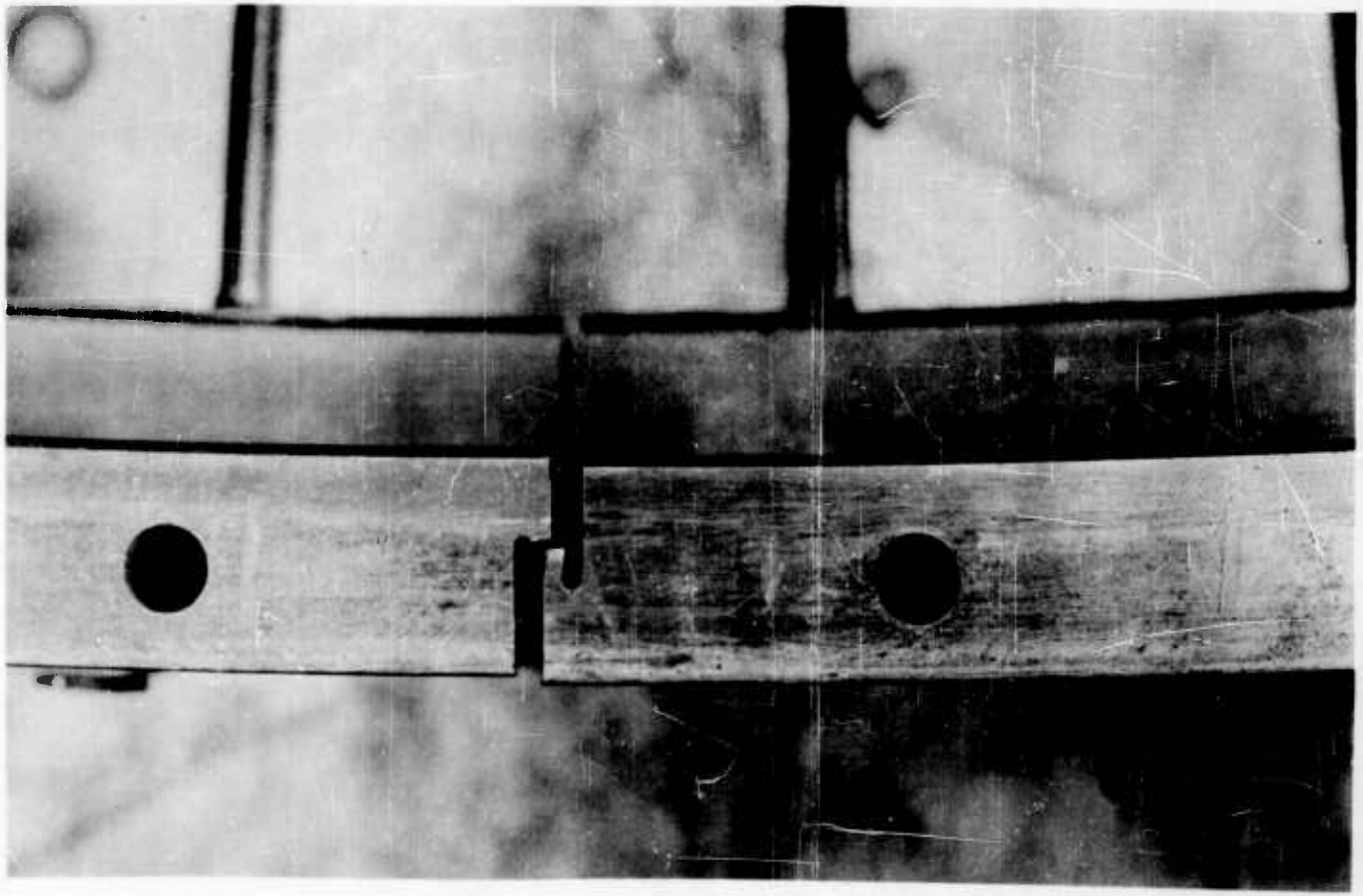

FIGURE 102 REAR FRAME SAW CUT SEPARATION

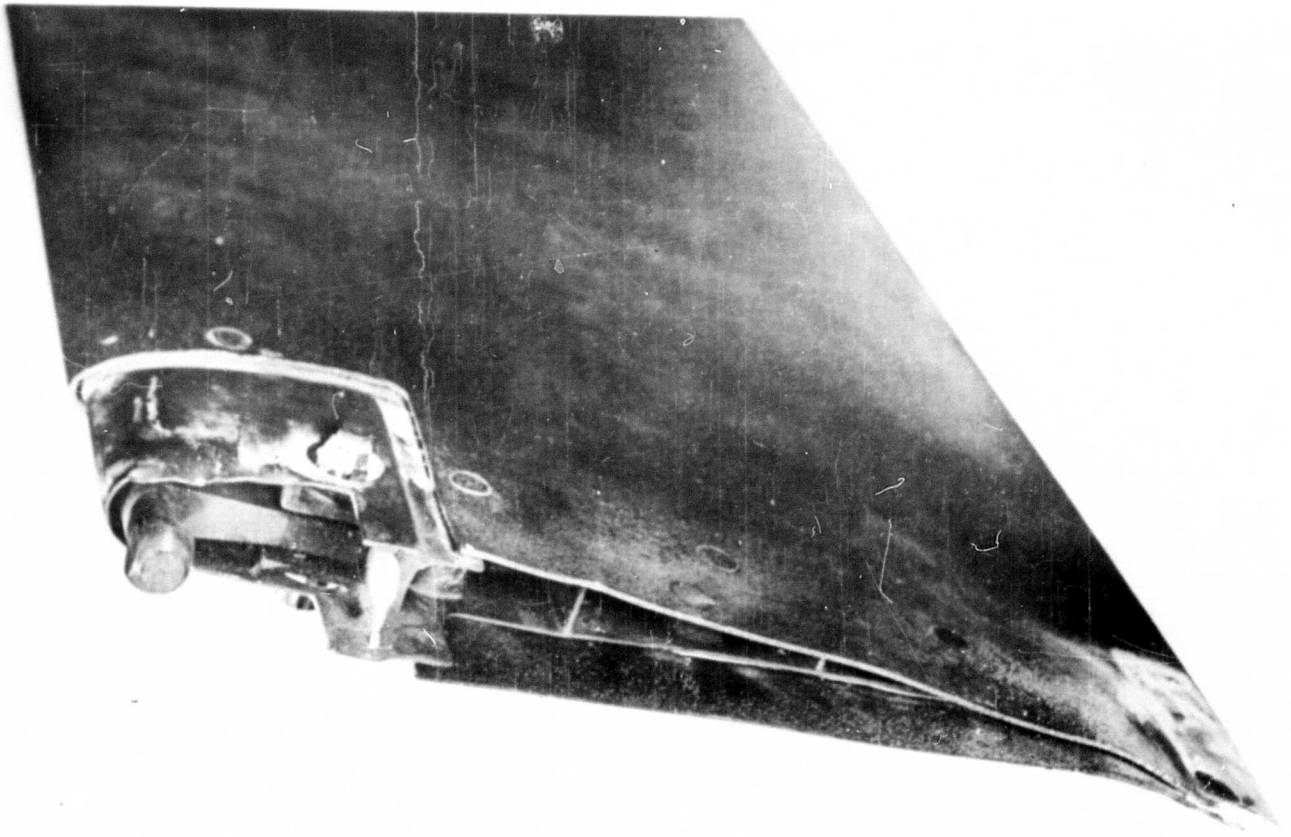

FIGURE 103 EXIT LOUVER AFTER TIP RUB

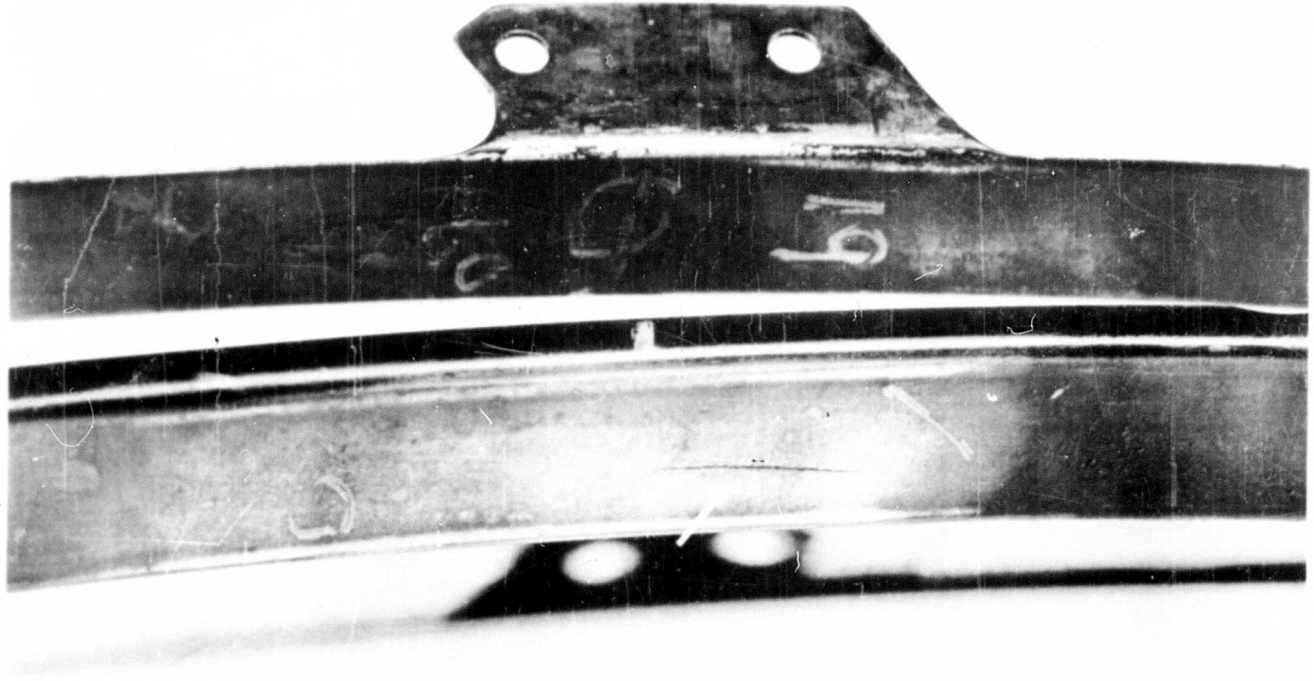

FIGURE 104 TORQUE BAND CRACK

FIGURE 105 CARRIER SIDE RAIL CRACK - 8X MAGNIFICATION

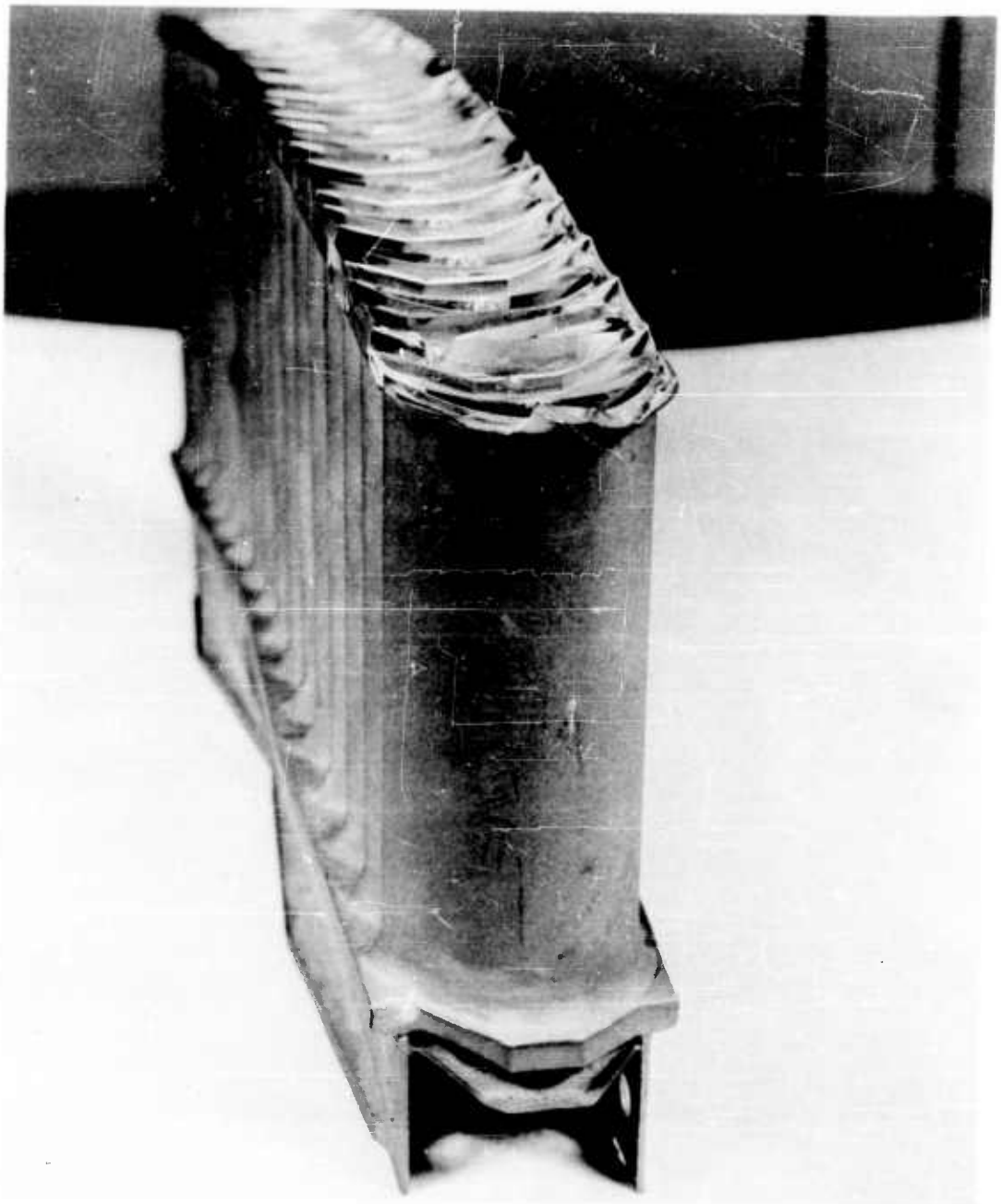

FIGURE 106 MISSING CARRIER SHROUD

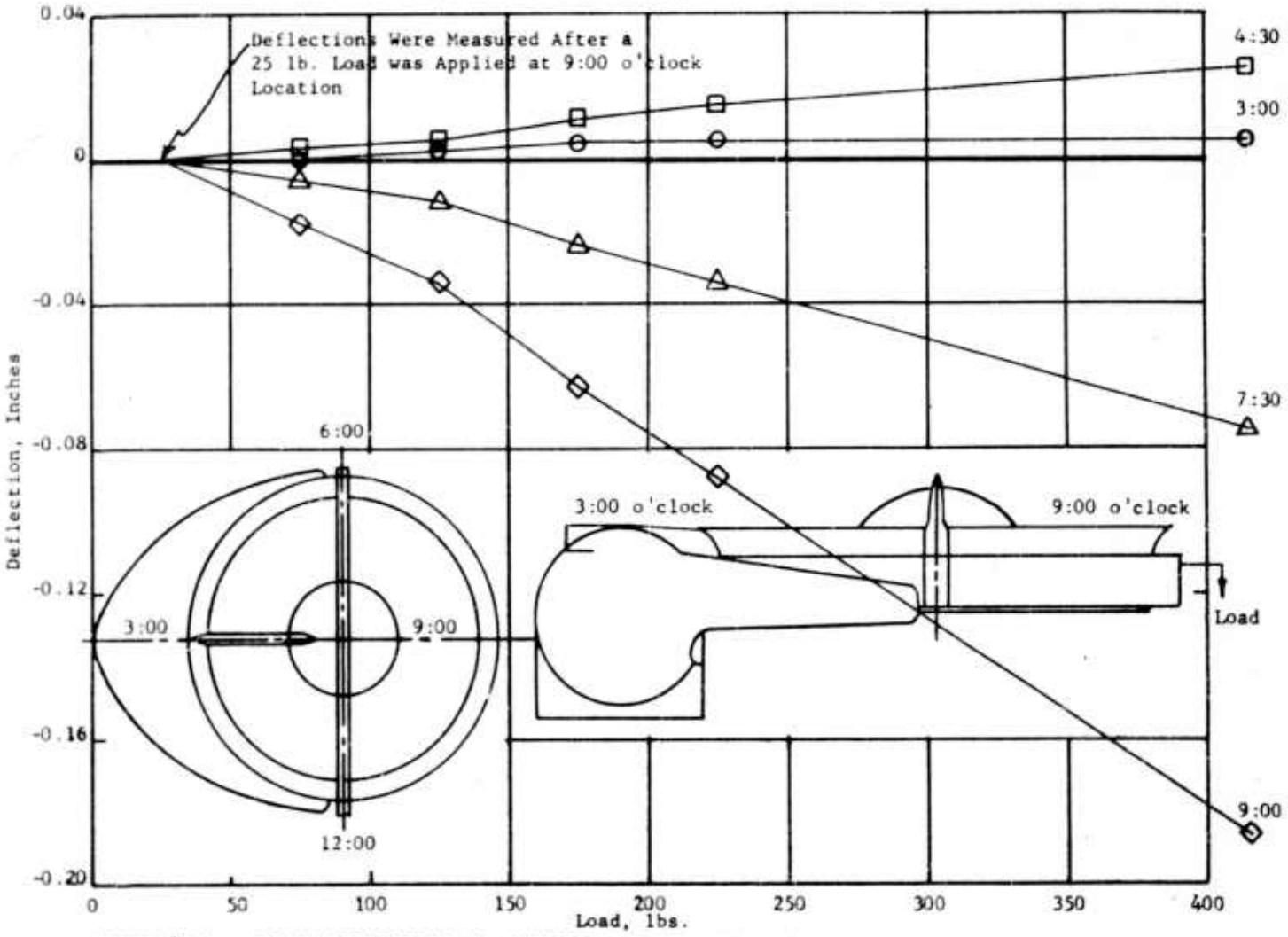

FIGURE 107 - FRAME DEFLECTION AS A FUNCTION OF RIM AXIAL LOAD

DISTRIBUTION LIST

Commanding General
United States Continental Army Command
ATTN: Materiel Developments (1)
Fort Monroe, Virginia

President
United States Army Aviation Board
ATTN: ATBG-DG (1)
Fort Rucker, Alabama

Chief of Transportation
ATTN: TCDRD (1)
ATTN: TCAFO-D (1)
Department of the Army
Washington 25, D. C.

Commander
Aeronautical Systems Division
Air Force Systems Command
ATTN: WWRMPT (2)
Wright-Patterson Air Force Base, Ohio

Commanding Officer
U. S. Army Transportation Research Command
ATTN: Research Reference Center (4)
ATTN; Aviation Directorate (1)
ATTN: Military Liaison and Advisory Office (1)
Fort Eustis, Virginia

U. S. Army Representative
Hq. AFSC (SCS-3) (1)
Andrews Air Force Base
Washington 25, D. C.

Commanding Officer and Director
David Taylor Model Basin
Aerodynamics Laboratory Library (1)
Washington 7, D. C.

Chief, Bureau of Naval Weapons (R-38)
Department of the Navy
ATTN: RAPP-14 (1)
ATTN: RAAD-32 (1)
Washington 25, D. C.

Chief of Naval Research
Code 461, Maj. L. C. Robertson (1)
Washington 25, D. C.

Director
The Research Analysis Corporation
ATTN: Library (1)
The Johns Hopkins University
6935 Arlington Road
Bethesda, Maryland

National Aeronautics and Space Administration
ATTN; Bertram A. Mulcahy
Assistant Director for Technical Information (1)
1520 H Street, N. W.
Washington 25, D. C.

Librarian (1)
Langley Research Center
National Aeronautics and Space Administration
Langley Field, Virginia

Ames Research Center
National Aeronautics and Space Administration
ATTN: Library (1)
Moffett Field, California

National Aeronautics and Space Administration
Lewis Research Center
ATTN: Library (1)
21000 Brookpark Road
Cleveland 35, Ohio

Commander
Armed Services Technical Information Agency
ATTN: TIPCR (10)
Arlington Hall Station
Arlington 12, Virginia

Office of Chief of R&D
ATTN: Air Mobility Division (1)
Department of the Army
Washington 25, D. C.

Army Research Office
Office of the Chief of Research and Development
ATTN: Research Support Division (1)
Department of the Army
Washington 25, D. C.

Commanding General
U. S. Army Transportation Materiel Command
ATTN: TCMAC-APU (1)
P. O. Box 209, Main Office
St. Louis 66, Missouri

U. S. Army Standardization Group, U. K. (1)
Box 65, U. S. Navy 100
FPO New York, New York

Office of the Senior Standardization Representative
U. S. Army Standardization Group, Canada
c/o Director of Equipment Policy (1)
Canadian Army Headquarters
Ottawa, Canada

Canadian Army Liaison Officer (3)
Liaison Group, Room 208
U. S. Army Transportation School
Fort Eustis, Virginia

British Joint Services Mission (Army Staff)
ATTN: Lt. Col. R. J. Wade, RE (3)
DAQMG (Mov & Tn)
3100 Massachusetts Avenue, N. W.
Washington 8, D. C.

Convair
Division of General Dynamics Corporation
ATTN: Library (1)
San Diego 12, California

Grumman Aircraft Engineering Corporation
ATTN: Library (1)
Bethpage, Long Island, New York

Hiller Aircraft Corporation
ATTN: Library (1)
Palo Alto, California

North American Aviation, Incorporated (1)
Columbus Division
4300 East Fifth Avenue
Columbus 16, Ohio

Republic Aviation Corporation
ATTN: Library (1)
Farmingdale, Long Island, New York

Ryan Aeronautical Company
ATTN: Library (1)
San Diego, California

Vertol Division
The Boeing Company
ATTN: Library (1)
Morton, Pennsylvania

AP_____ Accession No._____

Generel Electric Company, Cincinnati, Ohio

RESULTS OF STATIC TESTS OF A FULL SCALE, WING MOUNTED, TIP TURBINE DRIVEN LIFT FAN.

August, 1962, 249 pages - illuetratione - tebles (Contract DA 44-177-TC-584) USA TRECOM Project 9R 38-01-020-02, TREC 62-21. Unclessified Report.

This report covers 53 hours of testing conducted at the contrector's test facility et Evendale, Ohio.

Propulsion system performance, effecte of inlet configuretion, end roll-yaw control cepebility ere discussed.

Test results indicate that the Lift Fan can proceed to tha next phase of the test progrem.

UNCLASSIFIED

1. VTOL Propulsion System
2. Contract DA 44-177-TC-584

AP_____ Acceesion No._____

Generel Electric Company, Cincinnati, Ohio

RESULTS OF STATIC TESTS OF A FULL SCALE, WING MOUNTED, TIP TURBINE DRIVEN LIFT FAN.

August, 1962, 249 pages - illustrations - tables (Contract DA 44-177-TC-584) USA TRECOM Project 9R 38-01-020-02, TREC 62-21. Unclassified Report.

This report covers 53 hours of testing conducted at the contractor's test fecility at Evendale, Ohio.

Propulsion system performance, effects of inlet configuration, and roll-yew control capability ere diecussed.

Test results indicate that the Lift Fan can proceed to the next phase of the teet program.

UNCLASSIFIED

1. VTOL Propuleion System
2. Contract DA 44-177-TC-584

AP_____ Accession No._____

Generel Electric Company, Cincinnati, Ohio

RESULTS OF STATIC TESTS OF A FULL SCALE, WING MOUNTED, TIP TURBINE DRIVEN LIFT FAN.

August, 1962, 249 pages - illustrations - tables (Contract DA 44-177-TC-584) USA TRECOM Project 9R 38-01-020-02, TREC 62-21. Unclessified Report.

This report covers 53 houre of testing conducted at the contractor'e test facility et Evendale, Ohio.

Propulsion system performance, effects of inlet configuretion, and roll-yew control capability are discussad.

Test results indicete that the Lift Fan can proceed to the next phase of the tast program.

UNCLASSIFIED

1. VTOL Propulsion System
2. Contract DA 44-177-TC-584

AP_____ Accession No._____

Generel Electric Company, Cincinnati, Ohio

RESULTS OF STATIC TESTS OF A FULL SCALE, WING MOUNTED, TIP TURBINE DRIVEN LIFT FAN.

August, 1962, 249 pages - illustratione - tables (Contract DA 44-177-TC-584) USA TRECOM Project 9R 38-01-020-02, TREC 62-21. Unclaseified Report.

This report covers 53 hours of testing conducted at the contractor's test facility at Evendale, Ohio.

Propuleion eystem performance, effects of inlet configuration, and roll-yew control capability are diecuseed.

Test results indicate that the Lift Fan can proceed to the next phase of the test program.

UNCLASSIFIED

1. VTOL Propulsion Syetem
2. Contract DA 44-177-TC-584

AP_____ Accession No._____

General Electric Company, Cincinnati, Ohio

RESULTS OF STATIC TESTS OF A FULL SCALE, WING MOUNTED, TIP TURBINE DRIVEN LIFT FAN.

August, 1962, 249 pages - illustrations - tables (Contract DA 44-177-TC-584) USA TRECOM Project 9R 38-01-020-02, TREC 62-21. Unclassified Report.

This report covers 53 hours of testing conducted at the contractor's test facility at Evendale, Ohio.

Propulsion system performance, effects of inlet configuration, and roll-yaw control capability are discussed.

Test results indicate that the Lift Fan can proceed to the next phase of the test program.

UNCLASSIFIED

1. VTOL Propulsion System
2. Contract DA 44-177-TC-584

AP_____ Accession No._____

General Electric Company, Cincinnati, Ohio

RESULTS OF STATIC TESTS OF A FULL SCALE, WING MOUNTED, TIP TURBINE DRIVEN LIFT FAN.

August, 1962, 249 pages - illustrations - tables (Contract DA 44-177-TC-584) USA TRECOM Project 9R 38-01-020-02, TREC 62-21. Unclassified Report.

This report covers 53 hours of testing conducted at the contractor's test facility at Evendale, Ohio.

Propulsion system performance, effects of inlet configuration, and roll-yaw control capability are discussed.

Test results indicate that the Lift Fan can proceed to the next phase of the test program.

UNCLASSIFIED

1. VTOL Propulsion System
2. Contract DA 44-177-TC-584

AP_____ Accession No._____

General Electric Company, Cincinnati, Ohio

RESULTS OF STATIC TESTS OF A FULL SCALE, WING MOUNTED, TIP TURBINE DRIVEN LIFT FAN.

August, 1962, 249 pages - illustrations - tables (Contract DA 44-177-TC-584) USA TRECOM Project 9R 38-01-020-02, TREC 62-21. Unclassified Report.

This report covers 53 hours of testing conducted at the contractor's test facility at Evendale, Ohio.

Propulsion system performance, effects of inlet configuration, and roll-yaw control capability are discussed.

Test results indicate that the Lift Fan can proceed to the next phase of the test program.

UNCLASSIFIED

1. VTOL Propulsion System
2. Contract DA 44-177-TC-584

AP_____ Accession No._____

General Electric Company, Cincinnati, Ohio

RESULTS OF STATIC TESTS OF A FULL SCALE, WING MOUNTED, TIP TURBINE DRIVEN LIFT FAN.

August, 1962, 249 pages - illustrations - tables (Contract DA 44-177-TC-584) USA TRECOM Project 9R 38-01-020-02, TREC 62-21. Unclassified Report.

This report covers 53 hours of testing conducted at the contractor's test facility at Evendale, Ohio.

Propulsion system performance, effects of inlet configuration, and roll-yaw control capability are discussed.

Test results indicate that the Lift Fan can proceed to the next phase of the test program.

UNCLASSIFIED

1. VTOL Propulsion System
2. Contract DA 44-177-TC-584